Institute for Anatomy and Cell Biology II
Faculty of Medicine of the Justus Liebig University Giessen

Peroxisomes in endocrine pancreatic islets, possible protectors against lipotoxicity?

Inaugural Dissertation
Submitted to the
Faculty of Medicine
in partial fulfilment of the requirements
for the PhD-Degree
of the Faculties of Veterinary Medicine and Medicine
of the Justus Liebig University Giessen

by
Hermelinda del Rocío Bonilla-Martínez
of Tampico, Mexico

Giessen 2018

From the Institute of Anatomy and Cell Biology II
Division of Medical Cell Biology
of the Faculty of Medicine of the Justus Liebig University of Giessen
Director / Chairman: Prof. Dr. Eveline Baumgart-Vogt

First Supervisor and Committee Member: Prof. Dr. Eveline Baumgart-Vogt

Second Supervisor and Committee Member: PD. Dr. Elisabeth Eppler

Examination chair and Committee Member: Prof. Dr. Klaus-Dieter Schlüter

Committee Member: Prof. Dr. Christiane Herden

Date of Doctoral Defense: 28.03.2019

DECLARATION

"I declare that I have completed this dissertation single-handedly without the unauthorized help of a second party and only with the assistance acknowledged therein. I have appropriately acknowledged and referenced all text passages that are derived literally from or are based on the content of published or unpublished work of others, and all information that relates to verbal communications. I have abided by the principles of good scientific conduct laid down in the charter of the Justus Liebig University of Giessen in carrying out the investigations described in the dissertation."

Giessen, April 16, 2018 Bonilla-Martínez Rocío

INDEX OF ABBREVIATIONS

%	Percentage
µg	Microgram
µl	Microliter
µm	Micrometer
ABC	ATP-binding cassette family of transporters
ACOX	Acyl-CoA oxidase
ADP	Adenosine diphosphate
AMPK	AMP-activated protein kinase
ATP	Adenosine triphosphate
BCOX	Branched-chain acyl-CoA oxidase
Bp	Base pares
BSA	Bovine serum albumin
CAT	Catalase
cDNA	Complementary deoxyribonucleic acid
CO_2	Carbon dioxide
CPT-1	Carnitine palmitoyltransferase 1
DBP	D-bifunctional protein
DC-CoA	Dicarboxylic acids
DCFDA	Dichlorodihydrofluorescein diacetate
DHA	Docosahexaenoic acid
DHCA	3 alpha,7 alpha-dihydroxy-5 beta-cholestanoyl
DHE	Dihydroethidium
DMSO	Dimethyl sulfoxide
DNA	Deoxyribonucleic acid
EDTA	Ethylene-diamine tetraacetate
En	Endocrine
ER	Endoplasmic reticulum
Ex	Exocrine
FFA	Free fatty acid
GCG	Glucagon
GNPAT	Glyceronephosphate O-acyltransferase
h	Hour(s)
H&E	Haematoxylin and Eosin
H_2O_2	Hydrogen peroxide
HIS	Histidine
IF	Immunofluorescence
IgY	Immunoglobulin Y
InD	Intralobular ducts
INS	Insulin
IPTG	Isopropyl β-D-1-thiogalactopyranoside
IrD	Interlobular excretory duct
KANL	lysine-alanine-asparagine-leucine
kD	kilodalton
KD	Knock-down
KO	Knock-out
l	liter
LB	Luria broth
LCFA	Long-chain fatty acids
LCM	Laser capture microdissection
LD	lipid droplets
MDVs	Mitochondria-derived vesicles
mg	Milligram
min	Minute(s)
ml	Millilitre

mM	Millimolar
MTT	3-(4,5-dimethylthiazol-2-yl)-2,5-diphenyltetrazolium bromide
NADPH	Nicotinamide adenine dinucleotide phosphate
NaOH	Sodium hydroxide
ng	Nanograms
nM	Nanomolar
NZO	New Zealand Obese mice
$O2^{\cdot -}$	superoxide
ob/ob	Obese mouse
ORF	Open reading frame
ORO	Oil red o
PAX	Paired box
PBDs	Peroxisomal biogenesis disorders
PCR	Polymerase chain reaction
PDX-1	Insulin promoter factor 1 / pancreatic and duodenal homeobox 1
PEDs	Peroxisomal enzyme deficiencies
Pex	Gene encoding a peroxin (peroxisome biogenesis protein)
pH	Potential of hydrogen
PMP	Peroxisomal membrane protein
PTS	Peroxisomal targeting signal
PUFA	Polyunsaturated fatty acids
RNS	Reactive nitrogen species
ROS	Reactive oxygen species
RXR	Retinoic X receptor
s	Second(s)
SCOX	Straight-chain acyl-CoA oxidase
SCPx	Sterol carrier protein X
Scr-si	Scramble siRNA
SDS-PAGE	Sodium dodecyl sulphate polyacrylamide gel electrophoresis
siRNA	Small interfering RNA
SKL	Serine-lysine-leucine
SOD	Superoxide dismutase
VLCFA	Very long chain fatty acids
WB	Western blot
WT	Wild-type
ZS	Zellwegers syndrome

INDEX OF FIGURES

INDEX OF TABLES

TABLE OF CONTENTS

1. INTRODUCTION

1.1. Peroxisome structure, functions and biogenesis

1.1.1. Basic morphology of peroxisomes

Peroxisomes (originally called microbodies) are cell organelles present in virtually every eukaryotic cell. Discovered in 1954 by Rhodin (Rhodin 1954) and originally regarded as the garbage pail of the cell, the organelle obtained its actual name after an hydrogen peroxide-based oxidation reaction was observed by De Duve and Baudhuin in 1969 [(1)]. After this discovery, the morphological designation microbody was replaced by the more functional name peroxisome. Since then, the importance of peroxisomes for human health and development has been recognized, revealing this organelle as an active site of many vital metabolic biochemical reactions and as an essential part of the intermediate cell metabolism.

Peroxisomes (0.1-1 µm in diameter in hepatocytes) have a single-limiting membrane enclosing a fine granular matrix and are devoid of DNA [(2)] (**Figure: 1**). They are highly dynamic organelles and their functions, number and shape depend on cell type, tissue and physiological conditions [(3)].

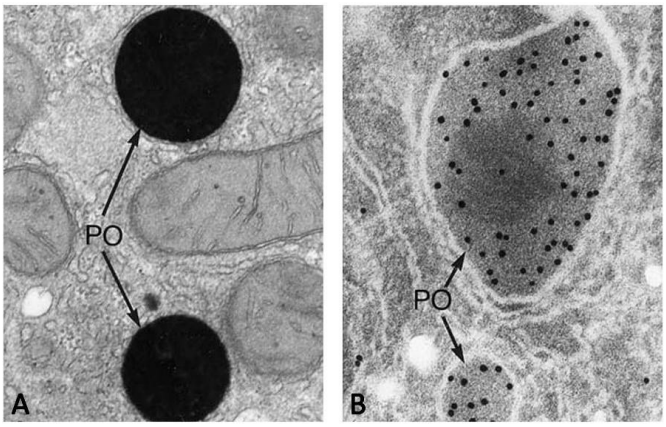

Figure 1: Localization of peroxisomes in rat liver.
A: Cytochemical localization of catalase in rat hepatic peroxisomes [(4)]. Magnification x28,600.
B: Immunocytochemical localization of catalase in rat liver using the protein A-gold technique [(5)].
Magnification x72,000. PO: peroxisome.

Currently, it is estimated that about 100 genes in humans encode for peroxisomal proteins [(6–9)]. More than half of these proteins are metabolic enzymes (around 50 in mammalian peroxisomes), while 32 proteins called peroxins (PEX) interact with each other and are required for the biogenesis and maintenance of functional peroxisomes [(2)]. The name peroxin was suggested by a unified nomenclature committee who numbered the proteins, with function in peroxisome biogenesis, according to their date of discovery independent of their intracellular localization [(10)].

1.1.2. Peroxisomal biogenesis

1.1.2.1. Import of peroxisomal membrane proteins

The current views on peroxisome biogenesis sustain that peroxisomes arise, under normal conditions, from pre-existing peroxisomes after undergoing growth and fission [11] with the subsequent import of matrix proteins. However, peroxisomes can also be formed by *de novo* synthesis from ER-associated membrane-segments as seen by the formation of the organelle in cells lacking peroxisomes (or defective for PEX3, PEX16, or PEX19) after the introduction of the defective gene [12,13]. The peroxisomes originated from the ER are pre-mature peroxisomes and only become mature organelles after the post-translational import of peroxisomal membrane and matrix proteins [14].

During the *de novo* synthesis of peroxisomes three peroxins PEX3, PEX16 and PEX19 were shown to be in charge of the post-translational import and assembly of peroxisomal membrane proteins (PMPs) into the peroxisomal envelop [15–18]. In order to be recognized, PMPs contain a membrane targeting sequence mPTS [19, 20].

In the membrane assembly process, PEX19 functions as both, a protein acceptor as well as chaperone, preventing the aggregation and degradation of PMPs [21, 22]. In the class I pathway, PEX19 forms complexes in the cytosol with newly synthesized PMPs including PEX16 and transports them to the receptor PEX3, which serves as an anchoring site in the peroxisomal membrane [14, 21]. In the class 2 pathway, PEX19 forms a complex with PEX3 and translocates it to its receptor, PEX16p [14].

In the absence of any of the peroxins in charge of the membrane biogenesis, cells lack peroxisomes and no membrane remnants are found. Both pathways constitute the initial step essential for the formation of the peroxisomal protein import machinery. Only after the peroxisomal membrane is completely assembled, the import of matrix proteins into the peroxisome can be accomplished.

1.1.2.2. Import of matrix proteins

Peroxisomes neither contain DNA nor machineries for transcription/translation. Since all peroxisomal proteins are encoded by the nuclear genome, matrix proteins and PMPs must be imported postranslationally after being synthetized on free polyribosomes in the cytosol[23]. Four consecutive steps constitute the process of peroxisomal matrix protein import: (1) targeting signal recognition by cytoplasmic receptors, (2) docking-complex

interaction, (3) cargo translocation and release, and (4) receptor release and its degradation or recycling (**Figure: 2**).

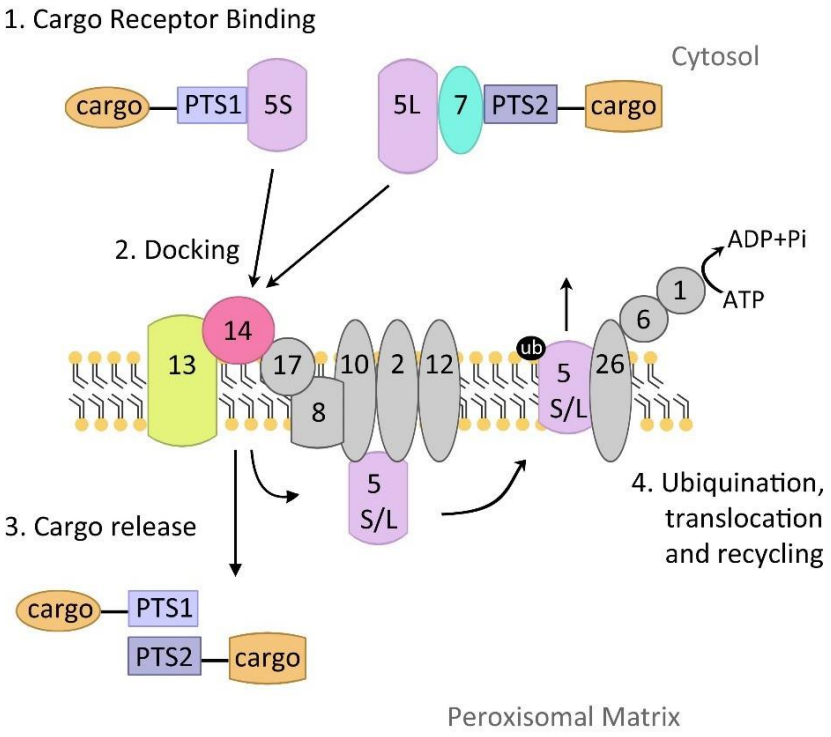

Figure 2: Peroxisomal matrix protein import. A simplified scheme for matrix protein import into mammalian peroxisomes depicting the involved peroxins, indicated by their PEX number and their interactions, is shown. The peroxisomal matrix proteins (= cargo) in the cytoplasm are recognized via peroxisomal targeting sequences PTS1 and PTS2 by their correspondent receptors PEX5 and PEX7, whereby the import of PTS2 matrix proteins is mediated by PEX7 bound to the long PEX5 isoform (1). The cargo-receptor complexes dock to PEX13/14 at the peroxisomal membrane (2). PEX14 and PEX5 interact to translocate the cargo across the peroxisomal membrane, followed by its release, involving the RING peroxins PEX2, 10, and 12. The cargo-receptors are recycled into the cytosol via an ubiquitination-dependent mechanism with the help of PEX6 and PEX1 anchored to the peroxisomal membrane by PEX26 (4). Adapted from [24].

All four processes are mediated by a unique machinery of 33 peroxins (PEX), which is in charge of the import of folded and oligomerized (or cofactor-bound) proteins into the peroxisomal matrix [25]. For their recognition and correct targeting, peroxisomal matrix proteins contain a specific targeting sequence. This is either a peroxisomal targeting signal 1 (PTS1) or 2 (PTS2). PTS1 consists of a C-terminal tripeptide ending with serine-lysine-leucine (SKL) or a related sequence [26, 27]. PTS1 binds to PEX5p, a cytosolic protein that interacts with the docking complex at the peroxisomal membrane. PTS2 is a nonapeptide located near the N-terminus [28] and is recognized by the cytosolic receptor PEX7p. The PTS2-PEX7p complex also binds the docking complex by interacting with PEX5L (a longer PEX5 isoform) [29]. The majority of the peroxisomal matrix proteins employ the PTS1-PEX5p import system, while only few peroxisomal proteins possess a PTS2 [30].

The peroxisomal docking complex contains, amongs other peroxins, PEX14 and PEX13, two important peroxisomal markers. While PEX14 functions as acceptor for the cargo-loaded receptors, the function of PEX13 is not fully clarified. It is, however, an integral membrane protein that is an essential element of the docking complex [31–33]. This peroxin is capable to interact directly with PEX14 and is involved in matrix protein import [34]. The deletion of PEX13 results in the loss of both PTS1 and PTS2 protein import leading to disrupted peroxisomal protein import and the complete dysfunction of peroxisomal metabolic pathways [35]. For this reason, proteins belonging to the PEX family are often used as target for the generation of knockout animals or knockdown cell cultures to study the effect of peroxisome deficiency in mammalian systems [36–39].

In the absence of PEX5, PEX7, or downstream binding partners (such as PEX13), peroxisomes still can be found in cells. However, they are empty and without matrix content and where described as peroxisomal membrane ghost [40].

When the process of peroxisomal matrix protein import fails for any reason, the non-imported proteins can sometimes be detected and even be still active in the cytosol (e.g. catalase) depending on their stability or whether or not they are degraded by proteases.

1.1.2.3. Peroxisome proliferation and involved nuclear receptors (PPARs)

Peroxisomes are known for their ability to adapt to cellular and environmental conditions. To cope with the cell morphological and metabolic requirements, peroxisomes proliferate by growth (e.g., elongation) and division [3, 41–43]. Both mechanisms may take place simultaneously in mammalian cells [44].

In mammals, three isoforms of PEX11 (PEX11α, PEX11β, and PEX11γ) are known to be involved in peroxisomal proliferation and regulation of the organelle abundance [41, 45–48].

Peroxisomal division and proliferation, together with the expression of many peroxisomal enzymes involved in fatty acid oxidation, can be regulated by the activation of peroxisome proliferator-activated receptors (PPARs) [49]. PPARs are ligand-activated transcription factors that regulate the expression of genes important in lipid and glucose homeostasis, cell differentiation and inflammation [50, 51]. Because of their many functions, they have been linked to the development of diabetes, hyperlipidemia, cancer and obesity [52–55]. They form a family of nuclear hormone receptors (NRs) belonging to the steroid receptor superfamily [55]. The PPAR family consists of three subtypes: PPARα, PPARβ and PPARγ, which differ from one another in their ligand specificities, tissue distribution and physiological roles [50]. After

interaction with the specific ligands, the receptors are translocated to the nucleus, where they change their structure and regulate inter alia the transcription of genes involved in glucose and fatty acid metabolism. Each member shows a distinct preference for distinct group of target genes [54, 56].

Although each member of the PPAR family has its own specific ligands, all are regulated by fatty acids and their derivatives, including VLCFA and LCFA and their CoA esters [57]. Phytanic acid [58], PUFAS and eicosanoids, which are exclusively metabolized by peroxisomes, function as natural ligands for the activation of PPARα, leading to enhanced expression levels of PPARα-regulated genes that activate peroxisomal β-oxidation. Some PPAR synthetic ligands have been used in the last decades, alone or combined, in the treatment of dyslipidemias (e.g. fibrates, PPARα activators) or diabetes mellitus type 2 (e.g. thiazolidinediones, PPARγ agonists) [52].

1.1.3. Metabolic functions of peroxisomes

Peroxisomes contain enzymes involved in different metabolic pathways that are critical for the maintenance of the cellular homeostasis and activity. A loss of peroxisomal functions is generally accompanied by the accumulation of toxic substrates and metabolic intermediates (e.g. VLCFA, phytanic acid) and a shortage of peroxisomal products (e.g. plasmalogens) with devastating consequences for human health [59, 60]. Pathways that are generally found in the peroxisomes of mammalian cells are listed in **Table 1**. In the next chapters a description of peroxisomal metabolic pathways relevant for this thesis, namely β- and α-oxidation of fatty acids, as well as ROS metabolism, will be given.

Table 1: Metabolic functions associated with peroxisomes in mammals

Metabolic pathway	Function
β-oxidation	Membrane lipid turnover; membrane breakdown in senescence [61]
β-oxidation of aromatic and cyclic compounds	Prostaglandins and leukotrienes degradation
α-oxidation of fatty acids	Breakdown of phytanic acid and other α-methyl fatty acids
Branched-chain fatty acid oxidation	Breakdown of branched-chain fatty acids such as pristanoyl-CoA, di- and tri-hydroxycholestanoyl CoA (derived from cholesterol) leading to the production of bile salts
Plasmalogen biosynthesis	Synthesis of ether-linked phospholipids (plasmalogens) which are particularly important in membranes protecting them against ROS damage. Dihydroxyacetone phosphate acyl transferase (DHAPAT) or alkyldihydroxyacetonephosphate synthase (ADHAPS) which catalyse the first 2 steps of the pathway, are peroxisomal
Isoprenoid biosynthesis	Synthesis of sterols such as cholesterol and quinones such as ubiquinone
Degradation of purines	Xanthine is converted to urate by xanthine oxidase which is peroxisomal in some species [62]

Catabolism of polyamines	Polyamine oxidases have been identified in mammals that carry putative peroxisome targeting signals [63]
Reactive oxygen metabolism	Removal of the active oxygen species produced by peroxisomal metabolism and H_2O_2 signaling [64]
Others	Viral innate immune defense [65]

1.1.3.1. β-Oxidation of fatty acids and fatty acid derivatives

The peroxisomal fatty acid β-oxidation is a process that coexists and cooperates with the mitochondrial fatty acid β-oxidation system in animal cells [24, 66, 67]. One of the main characteristics of the peroxisomal β-oxidation is that it is not involved in energy production and that it can metabolize a much broader spectrum of substrates that cannot be degraded by mitochondria. Peroxisomes catalyse the β-oxidation of very long-chain fatty acids (VLCFA) (C24:0 and C26:0), 2-methyl-branched fatty acids, pristanic acid (a product of the α-oxidation of phytanic acid), bile acid intermediates, polyunsaturated fatty acids (PUFA), eicosanoids, dicarboxylic medium-chain fatty acids and xenobiotics[68]. This capability prevents toxic or proinflammatory effects resulting from the accumulation of the bioactive lipid derivatives (e.g. eicosanoids) or precipitation of VLCFA within the cell. Long and medium-chain length fatty acids, whether saturated or unsaturated, can be substrates for both, mitochondrial and peroxisomal β-oxidation. However, even if both processes can oxidize dicarboxylic acids (DC-CoAs)[69], the reduce ability of mitochondria to activate VLCFA to their CoA derivative (via very long-chain Acyl-CoA synthetases)[70] restricts the degradation of this compounds to the peroxisome. The presence of a methyl branch at the second carbon dictates by which β-oxidation enzymes the compound will be degraded [71]. The peroxisomal β-oxidation also supplies acetyl-CoA for cholesterol and bile acid biosynthesis [72].

Peroxisomes contain at least two acyl-CoA synthetases that activate the VLCFAs to their CoA derivatives and initiate the peroxisomal β-oxidation [73]. Afterwards the FA chain is consecutively shortened by 2 carbons by a series of cyclic reactions involving four subsequent steps [74] (**Figure: 3**). The enzymes involved in this pathway present a substrate specificity, as shown in (**Table 2**).

Products of the β-oxidation include acetyl-CoA and a chain-shortened acyl-CoA. During each cycle, the fatty acid is shortened by two carbons and can then reenter the pathway[68]. After the long-chain DC-CoAs are shortened in the peroxisomal matrix (till 8 carbon atoms), the products are shifted to the mitochondrion for complete oxidation. In addition, shortened

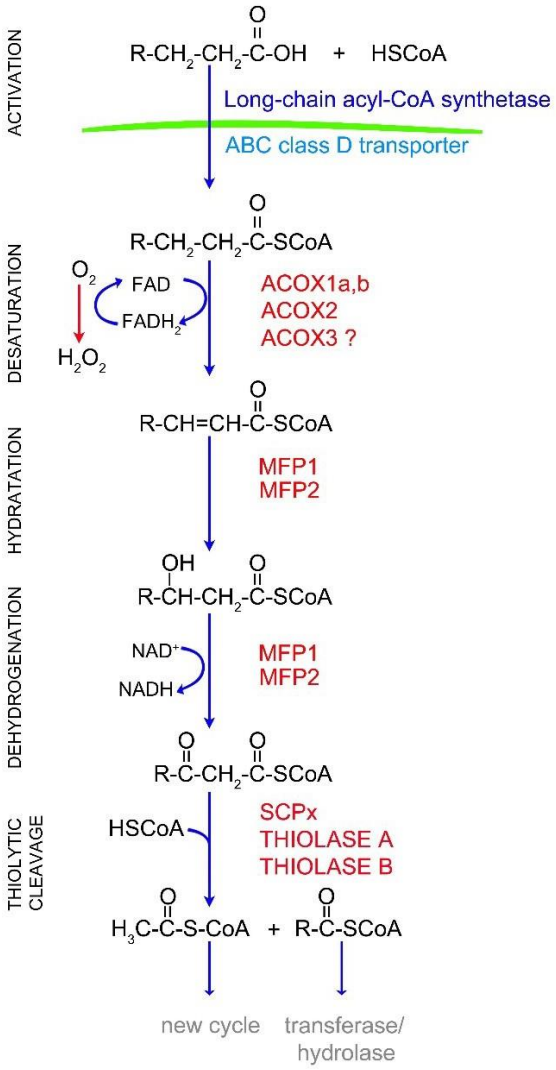

intermediates deriving from the peroxisomes also can be used for phospholipid synthesis (in the ER), whereas others can be exported to the bile or excreted via the kidneys.

Figure 3: Overview of the fatty acid β-oxidation in peroxisomes. Oxidation of fatty acids is carried out in peroxisomes following four subsequent steps. The FAs activation occurs outside the organelle involving membrane bound long-chain acyl CoA synthetases. The activated long-chain fatty acids are imported into the organelles by any of the ABCD transporters [78]. Depending on the chain length, the presence of a 2-methyl group, and structure of the acyl chain of the CoA esters, the involved enzymes will differ. The shortened acyl CoA can reenter the cycle or undergo other conversions. ACOX1-3: acyl-CoA oxidase 1-3; MFP 1-2: multifunctional protein 1-2; SCPx; sterol carrier protein x. Modified from [68, 79].

VLCFA	PUFA	Pristanic acid / bile acid intermediates	DCA	Prostanoids
ACOX1 MFP2 THIOLASE A and B SCPx	ACOX1 MFP2 THIOLASE A and B	ACOX2/3 MFP2 SCPx	ACOX1 Both MFP1/2 SCPx	ACOX1 MFP2 THIOLASE A and B

Table 2: Peroxisomal β-oxidation enzymes sorted by their substrate specificity.

Overview depicting the involvement of the different peroxisomal β-oxidation enzymes in the oxidation of VLCFAs (very long-chain fatty acids), PUFAs (polyunsaturated fatty acids), pristanic acid and bile acid intermediates, DCAs (dicarboxylic acids), and prostanoids. Adapted from [80] and [81]. Abbreviations: ACOX1-3: acyl-CoA oxidase 1-3; MFP 1-2: multifunctional protein 1-2; SCPx; sterol carrier protein x.

1.1.3.2. α-Oxidation of branched-chain fatty acids

Branched-chain fatty acids (like bile acids or phytanic acid) can arise from several different sources. In terms of quantity, non-steroidal branched-chain fatty acids are the most important ones [82]. Humans endogenously synthesize bile acids, which are oxidized

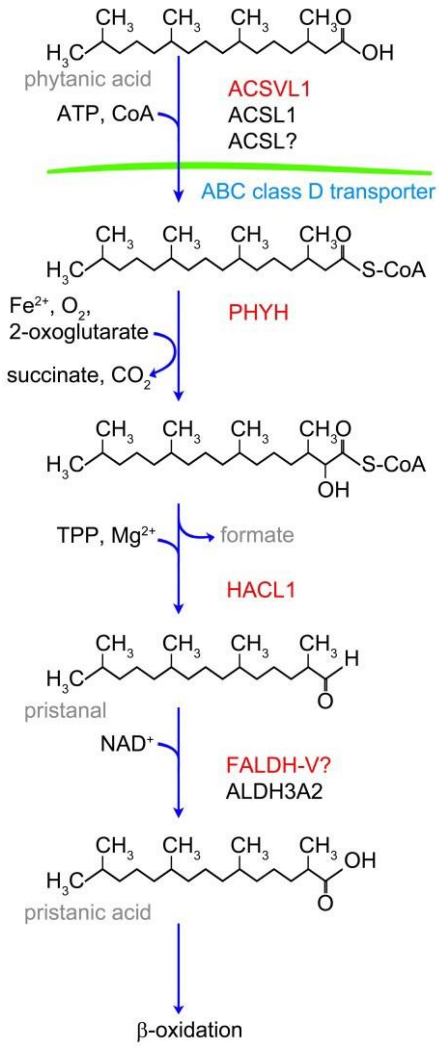

cholesterol derivatives. Phytanic acid on the other hand is a common α-oxidation substrate taken up with the meal (dairy products and beef [83, 84]). Some FAs are first metabolised via peroxisomal α-oxidation before they can enter the β-oxidation pathway. Those FAs containing a methyl group at the 3-position (e.g. phytanic acid) require a chain shortening from the carboxyl group [82] generating a one-carbon unit (formyl-CoA) instead of the two-carbon unit (acetyl- CoA) produced after β-oxidation. The pathway for the phytanic acid α-oxidation to pristanic acid comprises five steps [85] (**Figure: 4**). Pristanic acid can then enter the "normal" peroxisomal β-oxidation pathway and its end products (e.g. acetyl-CoA and propionyl-CoA) can be shifted to mitochondria to undergo full oxidation to CO_2 and H_2O [85].

Figure 4: Overview of the fatty acid α-oxidation in peroxisomes. The α oxidation pathway for phytanic acid is shown. Both phytanic acid and its precursor, phytol, are dietary lipids. ATP: adenosine triphosphate; ACSVL1: solute carrier family 27 (fatty acid transporter) member 2; ACSL: acyl-CoA synthetase long-chain family member 1; PHYH: phytanoyl-CoA α-hydroxylase; HACL1: 2-hydroxyphytanoyl-CoA lyase; FALDH-V: aldehyde dehydrogenase; TPP: thiamine pyrophosphate; Mg: magnesium; NAD: nicotinamide adenine dinucleotide. Adapted from [68].

1.1.3.3. Lipid transport across the peroxisomal membrane: ABCD transporters

As described previously, peroxisomes perform a key role in a variety of metabolic pathways for which the import of substrates into the organelle is required. Prior to β-oxidation, fatty acids are activated by thioesterification to Coenzyme A (CoA). Fatty acyl CoAs are amphipathic in nature and therefore require a transport protein to cross organellar membranes [61]. This is carried out by membrane transporters belonging to the subfamily D of the ABC superfamily of mammalian membrane-bound proteins. Three of them are localized in the peroxisomal membrane: the adrenoleukodystrophy protein (ALDP/ABCD1), the ALDP-related protein (ALDRP/ABCD2), and a 70 kD peroxisomal membrane protein (PMP70/ABCD3), showing a distinct affinity and specificity for different substrates (**Figure:**

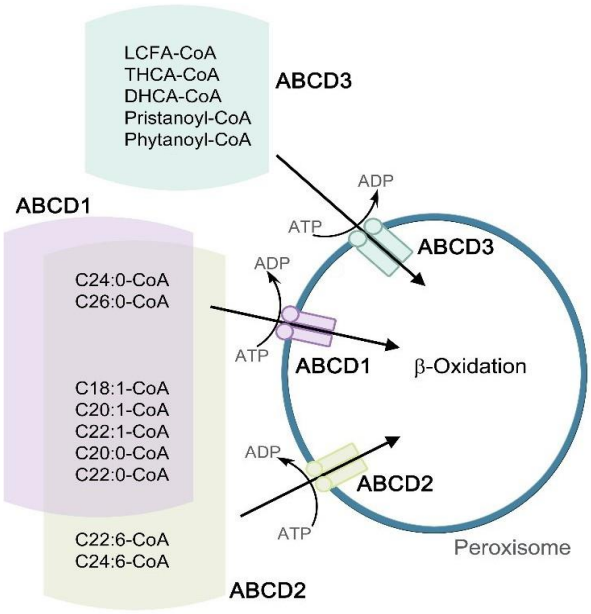

5). The fourth ABCD transporter, a PMP70 related protein (PMP70R/PMP69/ABCD4), was shown to be localized to the endoplasmic reticulum [87, 88].

Figure 5: Overview of the substrate-specificities of the ABCD membrane transporters. Three ABC proteins (ABCD1, ABCD2 and ABCD3) belonging to subfamily D are present in the peroxisomal membrane. ABCD1 and ABCD2 exhibit overlapping substrate specificities regarding saturated and monounsaturated VLCFA-CoAs, where ABCD1 has higher specificity to C24:0-CoA and C26:0-CoA than ABCD2. On the other hand, ABCD2 has an affinity for polyunsaturated VLCFA-CoAs. ABCD3 is involved in the transport of LCFA-CoA, branched-chain acyl-CoA, THCA-CoA and DHCA-CoA. VLCFA: Very long-chain fatty acid; LCFA: Long-chain fatty acid; THCA: 3 alpha, 7 alpha, 12 alpha-trihydroxy-5 beta-cholestanoic acid; DHCA: 3 alpha,7 alpha-dihydroxy-5 beta-cholestanoyl; ATP: adenosine triphosphate; ADP: adenosine diphosphate. Adapted from [88].

The ABC protein structure is highly conserved, exhibiting one transmembrane domain constituting the passageway for the substrates and one nucleotide-binding domain energizing the directional transport by cycles of ATP binding and hydrolysis (hence its name: ATP binding cassette -ABC-) [89].

1.1.3.4. Metabolism of reactive oxygen species and nitrogen species

Oxidative stress is a condition in which the production of reactive oxygen and/or nitrogen species (ROS/RNS) within the cell overwhelms the capacity of the antioxidant defense and repair mechanisms [90]. It has been extensively shown that high levels of ROS exert a toxic effect on biomolecules such as DNA, proteins, and lipids, leading to the accumulation of oxidative damage in diverse cellular compartments resulting in a wide range of pathological conditions, from atherosclerosis or hypertension, to cancer or type 2 diabetes [91]. There are many processes of intracellular ROS/RNS production taking place in different cell compartments, among which are (1) the electron transport chain in mitochondria, (2) the cytochrome P-450 enzymes in the endoplasmic reticulum (ER), (3) the NADPH oxidases at the plasma membrane, (4) the flavin oxidases inside the peroxisomes, and (5) the nitric oxide synthases (NOSs) which show different subcellular localizations [92].

As means of defense, the cell exhibits different antioxidant systems including enzymes (e.g. catalase, several superoxide dismutases, peroxiredoxins, and glutathione peroxidases) and non-enzymatic metabolites (e.g. glutathione and ascorbic acid) [92].

1.1.3.5. Peroxisomes as important sites of reactive oxygen species (ROS) production and degradation

The capacity of peroxisomes to produce ROS and RNS is well known, a characteristic that has given them their name some decades ago [1]. Since then, peroxisomes have been recognized as potential regulators of oxidative stress-related signalling pathways. Sources of ROS production within the peroxisome are the H_2O_2-producing flavin-containing oxidases (e.g. acyl-CoA oxidases) [76, 77], superoxide ($\cdot O_2^-$) generating enzymes (e.g. xanthine oxidase) [62] or those producing nitric oxide ($\cdot$NO) (e.g. iNOS, the inducible form of nitric oxide synthase) [93] (**Table 3**). The hydrogen peroxide (H_2O_2) is formed in the first step of the β-oxidation cycle where a double bond is introduced at the β position of the fatty acyl-CoA ester by FAD-containing acyl-CoA oxidases, which transfer hydrogen from metabolites to molecular oxygen [94].

Peroxisomes contain a non-selective membrane pore large enough to allow the diffusion of virtually all types of ROS/RNS that can be generated or metabolized inside the organelle [95, 96]. $\cdot$NO and H_2O_2 are membrane permeable, diffusible molecules, which are less reactive and longer lived than $ONOO^-$ and $^{\cdot}OH$ which are highly unstable, but are causing damage of the peroxisomal membrane, loss of peroxisomal functions and lipid peroxidation in a direct manner [97, 98].

Table 3: Enzymes in peroxisomes that generate ROS. Adapted from [99].

Enzyme	Substrate	ROS
Acyl-CoA oxidases		
• **Palmitoyl-CoA oxidase (ACOX1)**	Long- and very long-chain fatty acids, straight	H_2O_2
• **Pristanoyl-CoA oxidase (ACOX3)**	2-Methyl-branched fatty acids	H_2O_2
Urate oxidase (in humans is inactive)	Uric acid	H_2O_2
Xanthine oxidase	Xanthine	H_2O_2, $\cdot O_2^-$
D-amino acid oxidase	D-Proline	H_2O_2
L-pipecolate oxidase	L-pipecolic acid	H_2O_2
D-aspartate oxidase	D-aspartate, *N*-methyl-D-aspartate	H_2O_2
Sarcosine oxidase	Sarcosine, pipecolate	H_2O_2
L-hydroxy acid oxidase 1 and 2	Glycolate, lactate	H_2O_2
Polyamine oxidase	N-Acetyl spermine/ spermidine	H_2O_2
Nitric oxide synthase	L-Arginine	$\cdot$NO

H_2O_2: hydrogen peroxide; $\cdot O_2^-$: superoxide; $\cdot$NO: nitric oxide.

Due to the production of ROS/RNS peroxisomes are equipped with an efficient anti-oxidant machinery to maintain the redox homeostasis inside the organelle [100] (**Table 4**).

Peroxisomes have also the capacity to respond to oxidative stress and ROS, which have been generated in other intra- or extracellular compartments, presumably to protect the whole cell against oxidative damage [99]. Catalase, the classical marker enzyme of peroxisomes, shows an important protective function against the toxic effects of peroxides generated in peroxisomes and removes them with high efficiency [101]. Its inhibition in rat liver has been shown to suppress the peroxisomal lipid β-oxidation activity [102]. A number of other enzymes are located inside the peroxisomal matrix involved in the maintenance of the redox homeostasis. Both, catalase and glutathione peroxidase are in charge of scavenging H_2O_2, Cu,ZnSOD (SOD1) protect against $\cdot O_2^-$ by converting it to H_2O_2, peroxiredoxin 1 and 5 (PRDX1 and PRDX5) have the capacity to degrade $ONOO^-$, epoxide hydrolase 2 degrades epoxides and PRDX5 and glutathione S-transferase kappa can metabolize lipid peroxides [96]. Contrary to the previously described [103], our group has shown that SOD2 (the enzyme in charge of transforming toxic superoxide into hydrogen peroxide and oxygen) is only present in mitochondria and not in peroxisomes [104].

Table 4: Enzymes in peroxisomes that degrade ROS. Adapted from [99].

Enzyme	Substrate	PO	Enzyme also present in	References
Catalase	H_2O_2	✓	Cytosol and nucleus in some species, e.g. ginea pig and some monkeys	[4]
Glutathione peroxidase	H_2O_2	✓	All cell compartments	[105]
Cu, Zn SOD (SOD1)	$\cdot O_2^-$	✓	Cytosol	[106, 107]
Epoxide hydrolase	Epoxides	✓	ER and cytosol	[108]
Peroxiredoxin 1 (PRDX1)	H_2O_2	✓	Cytosol, nucleus, mitochondria	[109]
Peroxiredoxin 5 (PMP20)	H_2O_2, ROOH, $ONOO^-$	✓	Cytosol, nucleus, mitochondria	[110]

H_2O_2: hydrogen peroxide; $\cdot O_2^-$: superoxide; $ONOO^-$: peroxynitrite.

1.1.3.6. The response of peroxisomes to oxidative stress

Peroxisomes show an enormous plasticity regarding their response to oxidative stress. It has been shown that an elevation of environmental oxygen concentration induces an increase in the volume density of peroxisomes and their anti-oxidant enzymes up to 4-fold in CHO cells exposed to 99 % O_2 [111]. Morphological changes have also been observed in peroxisomes after exposure to oxidative stress: elongation of peroxisomes as a result of UV irradiation or direct exposure to H_2O_2 has been reported in HepG2 cells [112, 113], a response which was blocked by antioxidant treatment. PPARα agonists, that induce peroxisome proliferation accompanied by an increase in catalase activity, have been shown to prevent ROS production [114].

Furthermore, changes in peroxisomal redox metabolism sensitize cells to oxidative stress [115]. This in turn suggests that peroxisome dysfunction is not only associated with rare inborn errors of peroxisomal metabolism, but also with more common age-related diseases such as neurodegeneration, type 2 diabetes, and cancer in which an increased oxidative stress has been proven [116].

1.2. Metabolic interplay between peroxisomes and mitochondria

In order to fulfill their metabolic roles, peroxisomes rely on the interaction with other subcellular organelles. This connection is based on: (1) metabolic cooperation and cross-talk; (2) overlap in some components of the fission machinery; (3) cooperation in anti-viral signalling and defense, and (4) vesicular trafficking pathways [117]. Further, peroxisomal dysfunction can also lead to mitochondrial alterations [37].

1.2.1. Lipid homeostasis (fatty acid oxidation)

As mentioned before, both peroxisomes and mitochondria possess a β-oxidation machinery for the degradation of fatty acids. Although both mechanisms involve the same reaction steps, some important organelle-specific differences exist [118, 119]: (1) The enzymes in charge of the oxidation pathway are organelle specific differing in their molecular and catalytic properties; (2) each pathway shows specificities for different substrates (see chapters 1.1.3.1 and 1.1.3.2). As explained before in this work, peroxisomes metabolize complex fatty acids while mitochondria are in charge of the degradation of the majority of LCFA. (3) After peroxisomal β-oxidation, the resulting fatty acids products are shuttled to mitochondria for full oxidation. The export of fatty acids from peroxisomes requires a carnitine shuttle system and the involvement of membrane pores, formed by PMP22 [120, 121]. (4) In contrast to peroxisomes, mitochondria are able to produce ATP for anabolic reactions, since the mitochondrial enzymes catalyzing the first step of β-oxidation are FAD-dependent dehydrogenases, which feed their electrons into the respiratory chain [67].

1.2.2. Reactive oxygen species (ROS) homeostasis

Both, peroxisome and mitochondria are central organelles involved in the cellular redox balance and homeostasis [96] producing and scavenging ROS [97, 99]. In the mitochondria, the main site of free radical generation is the electron transport chain. Superoxide radicals can be formed at complex I (NADH-coQ reductase) and complex III (cytochrome oxidase). The damage of proteins, lipids and DNA within or outside the mitochondria results from the

conversion of the formed $\cdot O_2^-$ into H_2O_2, hydroxyl radicals or $ONOO^-$. As peroxisomes, mitochondria contain their own group of antioxidant molecules (glutathione, NADH) and enzymes (SOD2, glutathione reductase, glutathione peroxidase) to counteract the oxidative damage [122]. However, under oxidative stress conditions, the mitochondrial antioxidant machinery is often inefficient in decomposing the excess of H_2O_2 due to the limited level of glutathione (and NADPH) [122]. Peroxisomal catalase plays an important role in the maintenance of the mitochondrial function. It has been reported that in catalase deficient cells, the redox state of mitochondria was significantly increased (even under basal grow conditions) and that the reintroduction of catalase expression counteracted this effect, restoring mitochondrial integrity [123, 124]. Furthermore, an impaired catalase activity (and hence H_2O_2 metabolism) may increase mitochondrial ROS in response to fatty acids [125] and leads to their dysfunction [123].

1.3. Peroxisomes in human diseases and peroxisomal biogenesis disorders

1.3.1. Peroxisomal disorders

More than 20 inherited peroxisomal disorders have been described in the last decades, where one or more peroxisomal proteins are absent or dysfunctional [126]. This emphasizes the importance of the peroxisome in human health, especially concerning lipid metabolism and the defense against oxidative stress as described in previous chapters. Inherited peroxisomal disorders can be divided into two main subgroups: peroxisomal biogenesis disorders (PBDs) and the more frequent peroxisomal (single) enzyme deficiencies (PEDs) [81]. PBDs are caused by defects in peroxins involved in membrane biogenesis (e.g. PEX19), protein import (e.g. PEX5), or peroxisome proliferation (e.g. PEX11β) [126, 127]. In patients that are affected by PDBs, peroxisomes are either completely absent from cells, or only present as empty, non-functional membrane ghosts [40]. PBD patients suffer from severe metabolic dysfunctions, as nearly all peroxisomal metabolic pathways are affected [81]. Resulting from this is a toxic accumulation of α- and β-oxidation substrates (e.g. bile acid intermediates or VLCFA, pristanic acid, and phytanic acid) and a reduction of plasmalogen levels [81, 118, 127, 128]. Zellwegers syndrome (ZS) is the prototype and the most severe form of the PBDs. It is an autosomal recessive lethal disorder and the patients suffer from severe hypotonia, craniofacial malformations, liver and kidney problems, seizures, retinopathy and neuron migration defects and frequently die during the first year of life [126].

In the case of the single peroxisomal enzyme deficiencies, as its name implies, one enzyme (or transporter protein) in charge of a specific function in peroxisomes is absent. Depending upon which peroxisomal function is impaired, patients affected by these deficiencies may show symptoms resembling those observed in ZS patients or even be asymptomatic [126]. An example for PEDs is Refsum´s disease, which is caused by the deficiency of PHYH [129] showing an accumulation of phytanic acid in tissue lipids and in plasma [130].

Besides of the characteristic organs compromised in most peroxisomal disorders like brain, liver, kidney, testis or skeletal system also affection in the accumulation of toxic compounds that are usually degraded within the peroxisome have been shown to have a negative impact also on pancreatic tissue, exhibiting slight fibrosis and islet cell hyperplasia [131].

1.4. Overview on type 2 diabetes and structure of the pancreas

1.4.1. Structure of the pancreas and the β-cell

The adult mammalian pancreas is a complex serous gland composed mainly of acini, epithelial cells of excretory ducts, and islets of Langerhans as well as loose connective tissue. Exocrine cells (acini) constitute around 95 % of the pancreatic mass and produce digestive enzymes, which are excreted into the duodenum via the duct system. Endocrine cells are organized in globular clusters of cells known as islets of Langerhans, dispersed throughout the exocrine tissue. Each islet contains different endocrine cell types, each secreting distinct peptide hormones: α-cells produce glucagon, β-cells insulin, δ-cells somatostatin, and PP cells pancreatic polypeptide. Within the islets, β-cells make up the majority (60-80 %), forming a core around which the other cells are arranged [132].

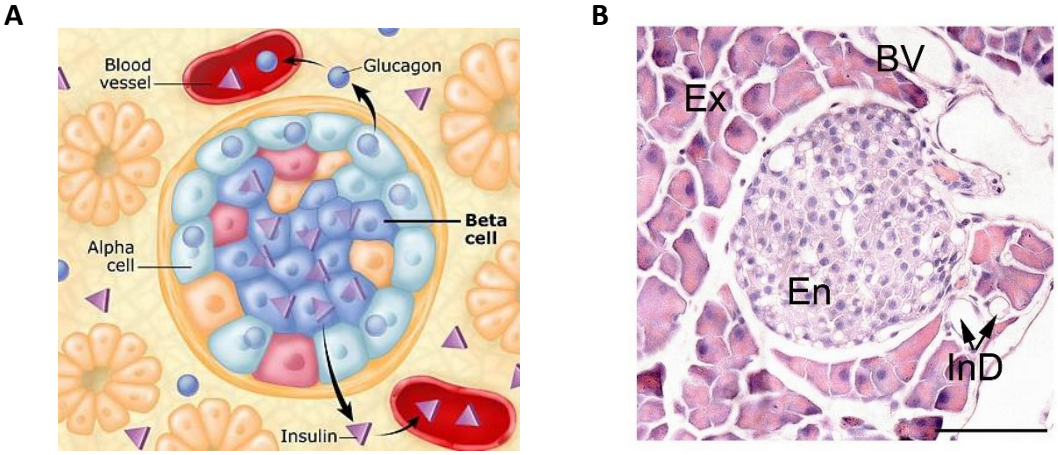

Figure 6: Representation of a murine islet of Langerhans. A: β-cells make up the core of the endocrine islet (UCSF Diabetes Education Online, https://dtc.ucsf.edu). **B:** H&E staining of a murine pancreas showing the morphology of the endocrine and exocrine part (own picture). Ex: exocrine pancreas; En: endocrine pancreas; BV: blood vessel; InD: intercalated duct. Bar = 27.5 µm.

1.4.2. Type 2 diabetes mellitus

Type 2 diabetes (T2D) is a complex metabolic disorder characterized by hyperglycaemia (a consequence of pancreatic β-cells failure) and peripheral insulin resistance. T2D affects currently more than 415 million individuals worldwide [133] and it is estimated that its prevalence will increase in the next years (642 million patients expected for 2040). With a polygenic etiology that includes genetic interaction, environmental and nutritional factors, T2D is considered a complication of the metabolic syndrome [134]. Long-term complications of T2D include retinopathy, nephropathy, neuropathy and cardiomyopathy, *inter alia*.

Two mechanisms have been suggested to cause the pathophysiological alterations of the β-cell. (1) Glucotoxicity, caused by oxidative stress, resulting in β-cell damage after hyperglycaemia due to insulin resistance [135], and (2) lipotoxicity, inducing apoptosis of β-cells as a consequence of obesity-induced ectopic fat accumulation in the pancreas [136, 137]. These mechanisms are not independent from each other and commonly their deleterious effects synergize [138-141].

1.4.3. Glucolipotoxicity in pancreas and possible involvement of peroxisomes

One important mechanism involved in β-cell glucotoxicity is glucose-induced oxidative stress. In an hyperglycaemic environment, ROS can be formed through oxidative phosphorylation, glycosylation, autoxidation, and the glucosamine pathways [142]. *In vivo*, pro-oxidant and markers for oxidative tissue damage appear constantly elevated in T2D patients. Additionally, β-cells are among the most vulnerable cells to ROS damage mainly due to the fact that they contain virtually very low levels of catalase [142]. In the scenario of ROS-induced β-cell dysfunction a defective proliferation and growth is finally followed by cell death. Thereby oxidative stress has been linked to insulin resistance resulting in impaired glucose tolerance. This in turn leads to insulin activity inhibition and secretion, promoting the onset of T2D [143].

Glucolipotoxicity implies the synergetic interaction between the toxic actions of FFAs in the context of hyperglycaemia. However, both glucose and FFAs are key modulators of insulin secretion. In a homeostatic state, glucose is the fundamental stimulator of insulin secretion with some fatty acids (e.g. palmitate) potentiating the effect of glucose [145, 146]. *In vivo*, acute infusion of FA stimulates insulin secretion in rats only in the presence of high glucose concentrations [147]. However, chronic high glucose or high FFA concentrations can exert a harmful effect on β-cells [148]. It has been shown that chronic hyperglycaemia induces

multiple β-cell defects including irreversible changes in insulin gene transcription in murine cell lines [149], changes in cell mass [150] and increase in ROS production (in both, human and rat islets) [142] accompanied by the reduction of expression and/or DNA binding capacity of PDX-1 [151]. PDX1, a transcription factor that plays a crucial role in pancreas development, β-cell differentiation, and insulin gene expression [141] is also affected during chronic hyperlipidaemia resulting in the inhibition of the insulin gene expression [152] and eventually β-cell dysfunction and death by apoptosis [139, 153, 154].

Long-chain saturated fatty acids, such as PA, are mainly oxidized by mitochondria. CPT-1, which mediates the import of long-chain saturated fatty acids into the mitochondrion, is the rate-limiting enzyme for LC-CoA oxidation and can be inhibited by an overload of glucose and PA, shifting the metabolic pathway from oxidation to lipogenesis [144]. The resulting accumulation of LC-CoAs, lipid intermediates (e.g. phosphatidic acid, diacylglycerol, lysophosphatidic acid) and ceramide synthesis play a critical role in FFA-induced toxicity [155-157]. Here, peroxisomes could sustain the degradation of excess fatty acids reducing the risk of lipotoxicity.

Palmitic acid, principal constituent of refined palm oil, is an important part of the human diet, and it can be also found in meets, cheese, butter and dairy products [158]. In a state of FA metabolic homeostasis, PA is used mainly as a cellular source of energy. However, when this homeostasis is compromised [159] the overload of PA in β-cells has detrimental effects resulting in cytotoxicity through mitochondrial dysfunction and ER stress, induced by oxidative stress [160]. It has been shown that β-cells derived from T2D murine models with hyperlipidemia exhibit elevated pro-oxidants and DNA and protein oxidation products [161, 162] apparently caused by PA lipotoxicity.

1.4.4. Models to study lipotoxicity in pancreatic cells

Although β-cells constitute the predominant cell type present within the islets of Langerhans, they comprise only about 1-2 % of the overall pancreatic cell mass. Thus, the use of primary β-cells is limited not only by its availability but also by the difficulty of isolating a homogeneous cell population. This entails the main disadvantage of the correct interpretation of the biochemical data, since the measurements will not allow the differentiation of β from non-β cells in the preparations. To overcome this particular issue, many studies of β-cell physiology, pathogenesis of diabetes and testing the effects of drugs

or chemical compounds on this specific cell type, have been carried out with clonal insulinoma cell lines. Diverse cell lines are available which are derived from multiple species.

1.4.5.1. The β-TC3 cell line

To investigate whether peroxisomes are involved in the protection of the β-cell against lipotoxicity, we have employed the β-TC3 cell-line. The β-TC3 cell line is a tumor cell line obtained from a primary culture of insulinomas developed in transgenic mice, which expressed the large T-antigen of SV40 in pancreatic islet β-cells [(163)]. This cell line resembles normal β-cells in respect to its content of insulin stored in secretory granules (3100 ± 294 ng insulin/100µg cellular protein, approximately 30 % of that of normal islets) [(164)] and remains among the most widely used rodent pancreatic β-cell lines today. Moreover, these cells respond to elevated glucose levels and to diverse secretagogues, which are used to induce insulin release in normal islets [(165)]. β-TC3 cells produce both proinsulin I and II and efficiently process each into mature insulin, making them a useful model for studying pancreatic β-cell function [(163)].

1.4.5.2. Mouse models to study diabetes mellitus

The New Zealand Obese (NZO) mouse is one of the most used models for the human metabolic syndrome and development of type 2 diabetes, presenting the main characteristics of this complex disease (insulin resistance, dyslipidemia, hypertension and early-onset obesity) [(166)]. As consequence, NZO mice develop a high fat diet-associated T2D characterized by marked hyperglycaemia and low serum insulin levels associated with β-cell failure and apoptosis [(167)].

The ob/ob (obese) mouse, the second model for obesity and diabetes used in this study, presents a mutation in the *ob* gene, coding for leptin, a hormone in charge of the appetite regulation and energy homeostasis [(168)]. The deficiency of this hormone leads to a fatty acid overload with different consequences depending of the affected tissue, from insulin resistance to β-cell dysfunction, apoptosis and diabetes (high blood sugar).

Pancreata from both animal models were kindly provided by Dr. Schürmann from the Deutsches Institut für Ernährungsforschung, Potsdam.

2. AIMS OF THE STUDY

It is well known that glucolipotoxicity, the deleterious effect of chronically elevated levels of glucose and fatty acids, adversely affects pancreatic β-cell function and thereby contribute to the deterioration of insulin secretion and cell death leading to the onset of T2D. At the cellular level, glucolipotoxicity its mainly related to alterations in intracellular energy metabolism and oxidative stress. To date both endoplasmic reticulum and mitochondria have been implicated in this phenomenon [169–171], however, scarce information is available concerning the function of peroxisomes in pancreatic β-cells. Interestingly, and contrary to the initially thought [172], our group has demonstrated significant differences in the peroxisomal abundance and enzyme composition of different pancreatic cells [173, 174], revealing a high number of peroxisomes in the endocrine region of this organ. This suggests that the metabolic function of peroxisomes might be particularly relevant to β-cell function. Since peroxisomes play an important role in the cellular β-oxidation of fatty acids and ROS homeostasis, we hypothesized that the dysfunction of this organelle should contribute to intracellular lipid accumulation and oxidative stress leading in consequence to β-cell dysfunction and decreased cell viability. Therefore, we investigated whether peroxisomes are involved in the protection of the β-cells against lipotoxicity.

To analyse the function of peroxisomes in the maintenance of normal physiology of pancreatic β-cells and reveal possible pathological alterations induced by the deficiency of peroxisomal protein import, the main aims of this project were:

- To produce and optimize an anti-mouse catalase antibody from chicken eggs (IgY) with high sensitivity by using recombinantly expressed and isolated His-tagged protein from Escherichia coli to be used for multiple Western blot experiments.
- To optimize the required conditions to obtain most sensitive immunofluorescence labelling for a large variety of peroxisomal biogenesis proteins, transporters and enzymes in murine pancreata.
- To morphologically characterize peroxisomal protein distribution in paraffin-embedded pancreatic tissue sections and their subcellular localisation in different pancreatic cell populations of wild type animals.
- To morphologically characterize the peroxisomal compartment in paraffin-embedded tissue sections of pancreata of diabetic mouse models (NZO and ob/ob)

to reveal possible peroxisomal alterations as a result of the diabetic condition induced by a high fat diet.

- To establish the appropriate conditions for the dissection of β-cells from cryosections of pancreatic tissue using the laser capture microdissection (LCM) technique for β- cell gene profiling.
- To establish optimal culture conditions to obtain a highly mature peroxisomal compartment and high insulin expression in β-TC3 cell line.
- To characterize the peroxisomal protein composition and peroxisome related gene expression under optimal conditions in β-TC3 cells.
- To establish a *Pex13* knock down model to investigate the effects of general peroxisome deficiency in β-TC3 cells induced by siRNA experiments.
- To establish an *Abcd3* knock down model to investigate the effects of a single membrane transporter deficiency in β-TC3 cells induced by siRNA experiments.
- To analyze the effect of high concentrations of palmitic acid, a fatty acid metabolized mainly in mitochondria but in access also in peroxisomes, on the survival and gene expression of normal and peroxisome-deficient β-TC3 cells.
- To analyze the effect of high concentrations of phytanic acid, a dietary fatty acid that is degraded via peroxisomal α-oxidation, on the survival and gene expression of normal and peroxisome-deficient β-TC3 cells.
- To investigate whether the induced peroxisomal defects are interfering with the cell biological function of insulin secretion and production.

3. MATERIALS AND METHODS

3.1. Materials

3.1.1. Laboratory instruments

All laboratory instruments used for the experimental section of this thesis are summarized with corresponding supplier in **Table 5** and listed in alphabetical order:

Table 5: List of the laboratory instruments used for the experiments described in this thesis.

Instrument	Company	Instrument	Company
Biocell A10 water system	Milli Q-Millipore	**Multifuge 3 centrifuge**	Heraeus
Biofuge Fresco	Heraeus	**Oven Heraeus T 5050 EKP**	Heraeus
Biofuge Pico	Heraeus	**pH meter inoLab**	WTW
Dish washing machine (G 78 83 CD)	Miele	**Pico21 centrifuge**	Heraeus
ErgoOne Pipettes	Starlab	**Pipettes**	Eppendorf
Freezer Serie 4	Bosch	**Potter-Elvehjem homogenizer**	Braun
Gel-Doc 2000 gel documentation system	Bio-Rad	**Pressure/Vacuum Autoclave FVA/3**	Fedegari
Hera cell 240 incubator	Heraeus	**Pump Drive PD 5001**	Heidolph Instruments
Hera safe, clean bench KS-12	Heraeus	**Purple Nitrile-Xtra**	Kimberly-Clark
Ice machine, Scotsman AF-100	Scotsman Ice Systems	**Rotilabo mini-centrifuge**	Carl Roth
I Cycler PCR machine MiQ2 optical module	Bio-Rad	**Shaker 3005**	GFL
Incubation Shaker	Infors	**SmartspecTM 3000 spectrophotometer**	Bio-Rad
Labquake Rotator	Barnstead-Thermo	**Sorvall Evolution RC centrifuge**	Kendro
Leica DMRD fluorescence microscope	Leica	**Sub Cell GT lectrophoresis apparatus**	Bio-Rad
Leica DC 480 camera	Leica	**TRIO-thermoblock**	Biometra
Leica TP1020 embedding machine	Leica	**Thermal Cycler C1000**	Bio-Rad
Leica TCS SP2 cofocal laser scanning microscope	Leica	**Thermomixer comfort**	Eppendorf
Leica SM 2000R rotation microtome	Leica	**Thermo plate**	Medax
Magnetic stirring hotplate MR 3001	Heidolph Instruments	**Ultra balance LA120 S**	Sartorius
Microtome water bath	Vieth	**Vasco Nitril white**	Braun
Microwave oven MB-392445	LG	**Vortex M10**	VWR International
Mini-Protean 3 cell gel chamber	Bio-Rad	**Waterbath 1002**	GFL
Mini-Protean Tetra system	Bio-Rad		

3.1.2. Chemicals

The chemicals and drugs used in this thesis are summarized with corresponding suppliers in **Table 6**.

Table 6: Lists of chemicals and drugs used in this thesis.

Chemicals	Company	Chemicals	Company
Acrylamide	Sigma-Aldrich	**Palmitate**	Sigma-Aldrich
Agarose LE	Roche	**Paraformaldehyde (PFA)**	Sigma-Aldrich
Ampicillin	Difco	**Phytanic acid**	Sigma-Aldrich
Bradford reagent	Sigma-Aldrich	**Poly-L-lysine**	Sigma-Aldrich
Bromophenol blue	Riedel-de-Haën	**Ponceau S**	Serva
Calcium chloride	Merck	**N-Propyl-gallate**	Sigma-Aldrich
Citric acid	Roth	**Protease mix**	Serva
Dimethylsulfoxide (DMSO)	Sigma-Aldrich	**RNAzol RT**	Sigma-Aldrich
Dipotassium phosphate K_2HPO_4	Merck	**RNaseZap**	Sigma-Aldrich
Disodium phospate Na_2HPO_4	Sigma-Aldrich	**Saccharose**	Roth
Ethanol	Riedel-de-Haën	**Sodium acetate**	Sigma-Aldrich
Ethidium bromide	Fluka	**Sodium carbonate**	Merck
Ethylene diamine tetraacetic acid (EDTA)	Fluka	**Sodium chloride**	Roth
Glycine	Roth	**Sodium dodecyl sulphate (SDS)**	Sigma-Aldrich
Glycerol	Sigma-Aldrich	**Sodium hydrogen carbonate**	Merck
Glycogen	Sigma-Aldrich	**Sodium hydroxide**	Merck
β-Glycerolphosphate	Sigma-Aldrich	**Sodium iodate**	Merck
Hämalaun	Sigma-Aldrich	**Tetramethylethylenediamine (TEMED)**	Roth
Hydrogen chloride	Sigma-Aldrich	**Thiazolyl blue tetrazolim bromide (MTT)**	Sigma-Aldrich
2- Isopropanol	Sigma-Aldrich	**Tissue-Tek OCT**	VWR Scientific Products
Isopropyl-β-D-thiogalactopyranosid (IPTG)	VWR Scientific Products	**Trishydroxymethylamino methane (Tris)**	Merck
Blue/orange loading dye 6x	Promega	**Trisodium citrate dihydrate**	Sigma-Aldrich
Lysozyme	Sigma-Aldrich	**Triton X-100**	Sigma-Aldrich
β-Mercaptoethanol	Roth	**Trypan blue**	Fluka
Methanol	Sigma-Aldrich		
Monopotassium phosphate KH_2PO_4	Merck	**Tween 20**	Fluka
3-N-Morpholino propanesulfonic acid (MOPS)	AppliChem	**5-bromo-4-chloro-3-indolyl-β-D-galactopyranoside (X-Gal)**	VWR Scientific Products
Mowiol 4-88	Polysciences	**Xylene**	Merck
Oil Red O	Sigma-Aldrich	**Yeast Extract Bacto**	DB

3.1.3. Culture media and enzymes

The cell culture media used for the cultivation of β-TC3 cells and the enzymes used in this thesis are listed alphabetically with notice of corresponding suppliers in **Table 7**.

Table 7: List of culture media and enzymes used in this thesis.

Culture media and enzymes	Company	Culture media and enzymes	Company
Albumin Fraction V (fatty acid-free)	Roth	**Milk powder**	Roth
Bovine serum albumin (BSA)	Roth	**dNTPmix**	5-PRIME
Calf intestinal alkaline phosphatase	Promega	**PiNK prestained protein ladder**	NIPPON Genetics

Clarity Western ECL Substrate	Bio-Rad	**Restriction enzymes**	Promega
DMEM (1x) + GlutaMAX-I, 4,5g/l D-glucose	Gibco	**RNaseOUT**	Invitrogen
DMEM (1x) + pyruvate, 1 g/l D-glucose, without L-glutamine, without phenol red	Gibco	**SsoAdvanced universal SYBR green supermix**	Bio-Rad
DMEM (1x) + L-glutamine, without D-glucose	Gibco	**Taq DNA polymerase**	5-PRIME
Dulbecco´s phosphate buffered saline 1x (PBS)	Sigma-Aldrich	**0.25 % Trypsin-EDTA (1x)**	Thermo-Fisher Scientific
Fetal calf serum heated inactivated	Thermo-Fisher Scientific	**T4 DNA ligase**	Promega
Horse serum	Sigma-Aldrich		

3.1.4. General materials and kits

General materials and kits used for the experimental section of this thesis are listed with notice of appropriate suppliers in **Table 8**.

Table 8: List of general materials and kits used in this thesis.

General materials	Company	General materials	Company
Cell culture flask 75 cm^2	Serva	**Ligation buffer**	Promega
CL-X Posure film	Thermo-Fisher Scientific	**Molecular weight marker 1kb DNA**	Promega
Cover slips 12 mm diameter	Menzel-Gläser	**Multi-well cell culture plate 12 wells**	DB Biosciences
CryoPure 1.8 ml	Serva	**m*Pex13* siRNA**	Dharmacon
Dihydroethidium (DHE)	Invitrogen	**Oligo(dT) 12-18 primer**	Invitrogen
DNA Stain G	Serva	**Readymatic developer and fixer**	Carestream
Dynabeads His-Tag isolation & pulldown	Thermo-Fisher Scientific	**Regenerated cellulose dialysis tubing Fisherbrand**	Fisher Scientific
Filter tips	Sarstedt	**RNA molecular weight marker**	Promega
FuGENE transfection reagent	Promega	**RNase out**	Invitrogen
Immobilion-P transfer membrane	Millipore	**qRT-PCR primers (see Table 13)**	Operon
INTERFERin siRNA transfection reagent	Polyplus	**ScreenFect A transfection reagent**	Wako chemicals
Kits	**Company**	**Kits**	**Company**
Amplite fluorimetric H_2O_2 assay kit	AAT Bioquest	**NucleoSpin plasmid**	Macherey-Nagel
Catalase	Cayman Chemical	**PCR purification kit QIAquick®**	Qiagen
Deoxyribonuclease I, amplification grade	Invitrogen	**RNeasy kit**	Qiagen
Gel extraction Kit QIAquick	Qiagen	**RT-PCR kit**	Invitrogen
Insulin (Mouse) ultrasensitive ELISA	DRG Diagnostics		

3.1.5. Bacterial strains, cell lines, vectors and plasmid constructs

All cell lines, bacterial strains, vectors and plasmids constructs used for the experimental section of this thesis are summarized with corresponding suppliers in **Table 9**.

Table 9: List of cell lines, bacterial strains, vectors and plasmids constructs used in this thesis.

Name	Supplier	Name	Supplier
BL21(DE3) Rosetta competent cells	Kindly provided by Prof. Frank Voncken, University of Hull, UK	**DH5α competent *E.coli***	Invitrogen
βTC-3 cells (mouse)	Deutsche Sammlung von Mikroorganismen und Zellkulturen „DSMZ“	**pET-16b**	Kindly provided by Prof. Frank Voncken, University of Hull, UK
pTrcHis A	Invitrogen	**pCMV-SPORT 6-Catalase**	Invitrogen
pGEM T-Easy	Promega		

3.1.6. Buffers and solutions

The composition of all buffers and solutions used in this thesis for the morphological and biochemical experiments as well as for immunofluorescence and molecular biology are listed in **Table 10**.

Table 10: Buffers and solutions used in this work

Immunofluorescence and morphology	
2.5 % Anti-fading agent	2.5 g N-Propyl-gallate in 50 ml 1x PBS + 50 ml glycerol
Blocking solution	PBS + 4 % BSA + 0.05 % Tween 20
Citrate buffer	1.5 % solution A + 8.5 % solution B in dH_2O; adjusted to pH 6.0
Dilution buffer	PBS + 1 % BSA + 0.05 % Tween 20
2 % Eosin stain solution	1 g Eosin Y + 1 drop glacial acetic acid in 100 ml H_2O
Fixation solution	4 % PFA (paraformaldehyde) + 58.4 mM saccharose in 1 x PBS buffer; adjusted to pH 7.4
Fixative solution	4 % PFA in 1x PBS; adjusted to pH 7.4
1 % Glycine	13.3 mM glycine in 1x PBS buffer
1 % Glycine + 0.2 % Triton X-100	0.1 ml Triton X-100 in 50 ml 1 % glycine
Hematoxylin stain solution	1 g Aluminum Hematoxylin (Hämalaun) + 0.2 g $NaJO_3$ + 50 g $KAl(SO_4)_2$ + 50 g $C_2H_3Cl_3O_2$ + 1 g citric acid; filled up with H_2O to a final volume of 1000 ml
Mounting medium	3 parts of Mowiol 4-88 + 1 part of anti-fading agent
Mowiol 4-88 solution	16.7 % Mowiol 4-88 (w/v) in 80 ml 1x PBS + 40 ml glycerol; centrifuged at 15,000 x *g* for 1 h; supernatant collected and stored at -20°C
Oil Red O stock solution	8.5 mM Oil Red O in 99 % isopropanol
10x Phosphate buffered saline (PBS) buffer	1.5 M NaCl + 131 mM K_2HPO_4 + 50 mM KH_2PO_4; adjusted to pH 7.4
Solution A (citrate buffer)	1 M $C_6H_8O_7 \cdot H_2O$ in dH_2O
Solution B (citrate buffer)	0.2 M $C_6H_5Na_3O_7 \cdot 2H_2O$ in dH_2O
TEDS buffer	250 mM sucrose + 1 mM EDTA + 10 mM Tris HCl buffer; adjusted to pH 7.2 and supplemented with protease inhibitor 1:50
Biochemistry	
10 % Amonium persulfate (APS) stock solution (w/v)	0.1 g Ammonium persulfate in 1.0 ml dH_2O
5 % Blocking buffer	5 gr dried skimmed milk in 100 ml TBST buffer
1x Cell lysis buffer	50 mM Tris + 150 mM NaCl + 1 % Triton X-100; adjusted to pH to 7.4 and supplemented with 10 % protease inhibitor
10x Electrophoresis running buffer	250 mM Tris + 2 M glycin + 1 % SDS; filled up with dH_2O to a final volume of 1,000 ml
Laemmli buffer	1.25 ml 0.5 M Tris-HCl pH 6.8 + 2.5 ml glycerol + 2 ml 10 % (w/v) sodium dodecyl sulfate (SDS) + 5 % β-Mercaptoethanol (added fresh before use) +

	1 % Bromophenol blue; filled up with dH_2O to a final volume of 9.5 ml
Resolving gel (12 %) (for 1 mm thick gel)	4 ml 30 % Acrylamide solution + 2.5 ml 1.5 M Tris-HCl (pH 8.8) + 100 µl 10 % SDS stock solution + 60 µl 10 % APS stock solution + 5 µl TEMED + 3.35 ml dH_2O
Stacking gel (4 %) (for 1 mm thick gel)	650 µl 30 % Acrylamide solution + 1.25 ml 0.5 M Tris-HCl (pH 6.8) + 50 µl 10 % SDS stock solution + 30 µl 10 % APS stock solution + 5 µl TEMED + 3 ml dH_2O
Stripping buffer	100 mM β-Mercaptoethanol + 2 % SDS + 62.5 mM Tris-HCl; adjusted to pH 6.7
10x TBS Tris buffered saline	0.2 M Trizma base + 1.4 M NaCl in dH_2O; adjusted to pH 7.6
1x TBS-Tween (TBST) buffer	0.1 % (v/v) Tween 20 in TBS buffer
0.5 M Tris-HCl	6.0 g Tris base in 1,000 ml dH_2O; adjusted to pH 6.8
1.5 M Tris-HCl	27.23 g Tris base in 150 ml dH_2O; adjusted to pH 8.8
10x Towbin buffer	25 mM Tris + 192 mM glycine + 20 % Methanol; adjusted to pH 8.3
Molecular biology	
Ampicillin	50 mg/ml in dH_2O; 1 ml per liter of media was used for a final concentration of 50 µg/ml
Binding/washing buffer	50 mM Sodium phosphate pH 8 + 300 mM NaCl + 0.01 % Tween 20
Calf intestinal alkaline phosphatase (CIAP) stop buffer	10 mM Tris-HCl pH 7.5 + 1 mM EDTA pH 7.5 + 200 mM NaCl + 0.5 % SDS
0.1 % DEPC-water	1 % Diethylpyrocarbonate in dH_2O; let set at room temperature overnight and autoclaved for 30 minutes at 121°C
Elution buffer (gel extraction)	10 mM Tris-Cl pH 8.5
5x Formaldehyde loading dye	16 µl Bromophenol blue saturated aqueous solution + 80 µl 500 mM EDTA pH 8.0 + 12.3 M formaldehyde 37 % + 3,084 µl formamide + 4 ml 10x MOPS buffer + 1 ml glycerol 100 % in DEPC water; filled up to a final volume of 10 ml
LB Agar	50 ml LB medium + 1 g Agar + 100 µg/ml Ampicillin
LB (Luria Bertani) medium	0.17 M NaCl + 1 % tryptone + 0.5 % yeast extract; adjusted to pH 7
Lysate buffer	4 ml Binding/washing buffer + 10 µl protease mix 1:100 (without EDTA) + 50 µl Lysozyme 1:100 (final concentration of 1 mg/ml) + 30 U Dnase I
10x MOPS buffer	200 mM MOPS + 50 mM $C_2H_3NaO_2$ + 10 mM EDTA in DEPC water; adjusted to pH. 7.0
TfbI buffer	30 mM CH_3CO_2K + 100 mM $RbCl_2$ + 10 mM $CaCl_2$ + 50 mM $MnCl_2 \cdot 4H_2O$ + glycerol 15 % (v/v); adjusted to pH 5.8
TfbII buffer	10 mM MOPS or Pipes + 10 mM $RbCl_2$ + 75 mM $CaCl_2$ + glycerol 15 % (v/v); adjusted to pH 6.5

3.1.7. Antibodies

The primary antibodies used for the experimental section of this thesis are summarized with corresponding supplier, host and dilution in **Table 11**.

Table 11: List of primary antibodies used in this study. All abreviations are explained below the table.

Antigen	Host	Dilution (IF)	Dilution (WB)	Supplier
ABCD3	Rabbit	1:1,000	1:500	Abcam
Alpha-tubulin	Mouse	1:20,000	1:10,000	Sigma-Aldrich
Beta-actin	Mouse		1:5,000	Sigma-Aldrich
Catalase (CAT)	Chicken		1:20,000	Self-made antibody of this thesis

				Prof. Baumgart-Vogt´s group*
Catalase (CAT)	Rabbit	1:1,000	1:30,000	Gift from Prof. Denis Crane´s group‡ [175]
Glucagon	Mouse	1:2,000		Sigma-Aldrich
GNPAT	Rabbit	1:400		Proteintech
His-Tag	Rabbit		1:10,000	Cell Signaling
Insulin + Proinsulin	Mouse	1:2,000		Abcam
MFP2	Rabbit	1:5,000		Molecular Probes
PEX3p	Rat	1:500		Prof. Baumgart-Vogt´s group* [174]
PEX13p	Rabbit	1:500	1:1,000	Gift from Prof. Crane´s group‡ [176]
PEX14p	Rabbit	1:2,000	1:30,000	Gift from Prof. Crane´s group‡ [177]
PEX19p	Rabbit	1:10,000		Prof. Baumgart-Vogt´s group* [174]
PPARα	Rabbit		1:1,000	Santa Cruz
PPARβ	Rabbit		1:1,000	Abiocode
PPARγ	Rabbit		1:1,000	Santa Cruz
SOD2	Goat		1:5,000	Everest Biotech
Thiolase	Rabbit	1:500	1:1000	Gift from Prof. Braverman´s group**

* Institute for Anatomy and Cell Biology, JLU, Gießen, GE; ‡ School of Biomolecular and Physical Sciences, Griffith Univeristy, Brisbane, Qld, AUS; **Department of Pediatrics, Faculty of Medicine, McGill University, Montreal, CA; GNPAT: glyceronephosphate O-acyltransferase; MFP2: multifunctional protein 2; PEX3, 13, 14 and 19: peroxisomal biogenesis factor 3, 13, 14 and 19; ABCD3: ATP-binding cassette transporter, sub-family D, member 3; PPARα,β,γ: peroxisome proliferator-activated receptor alpha, beta and gamma; SOD2: superoxide dismutase 2 - Mn dependent; Thiolase: 3-ketoacyl-CoA thiolase; IF: immunofluorescence; WB: Western blot

The secondary antibodies used for the experimental section of this thesis are summarized with corresponding supplier, host and dilution in **Table 12**.

Table 12: List of secondary antibodies and nuclei counterstaining used in this study.

Secondary detection system used	Host	Dilution	Supplier
Western blotting			
Anti-mouse IgG horseradish peroxidase conjugate	Donkey	1:50,000	Jackson Immuno Research
Anti-goat IgG horseradish peroxidase conjugate	Rabbit	1:10,000	Jackson Immuno Research
Anti-chicken IgY horseradish peroxidase conjugate	Goat	1:10,000	Jackson Immuno Research
Anti-rabbit IgG horseradish peroxidase conjugate	Donkey	1:10,000	Jackson Immuno Research
Immunofluorescence			
Anti-rabbit IgG Alexa Fluor 488	Donkey	1:300	Molecular Probes
Anti-mouse IgG Texas Red	Horse	1:300	Vector Laboratories
Anti-mouse IgG Alexa Fluor 555	Donkey	1:300	Molecular Probes
Anti-chicken IgY Alexa 633	Goat	1:300	Molecular Probes
Anti-rat Cy3	Donkey	1:400	Dianova
Anti-rat IgG Alexa Fluor 594	Goat	1:300	Molecular Probes
Anti-sheep IgG Alexa 555	Donkey	1:300	Molecular Probes
Counterstaining of nuclei			
TO-PRO-3 Iodide	1:750		Molecular Probes
Hoechst 33342	1:750		Sigma

3.1.8. Primers

The sequences of all primers used for the qRT-PCR and RT-PCR experiments are listed in alphabetical order in **Table 13** summarizing the annealing temperature used for the PCR and the size of the amplified product.

Table 13: Sequences of qRT-PCR and RT-PCR primers used in this study

Gene of interest	Symbol	Accession no.	Forward/reverse primers	Ann. Temp. in °C	Prod. length
Sequences of the primers used for semi-quantitative RT-PCR					
β-Actin	*Actb*	NM_007393.3	For TGCCCTGAGGCTCTTTTCCA Rev TGGACAGTGAGGCCAGGATG	60	283
Acyl-Coenzyme A oxidase 1, palmitoyl	*Acox1*	NM_015729.3	For TGAACAAGACAGAGGTCCACGAA Rev TGTAAGGGCCACACACTCACATCT	60	565
Acyl-Coenzyme A oxidase 2, branched chain	*Acox2*	NM_053115.2	For CTCTTGCACGTATGAGGGTGAGAA Rev CTGAGTATTGGCTGGGGACTTCTG	62	688
Catalase	*Cat*	NM_009804.2	For ATGGTCTGGGACTTCTGGAGTCTTC Rev GTTTCCTCTCCTCCTCGTTCAACAC	63	832
Enoyl-coenzyme A, hydratase/3-hydroxyacyl coenzyme A dehydrogenase (Ehhadh)	*Mfp1*	NM_023737.3	Rev ATGGCCAGATTTCAGGAATG For TGCCACTTTTGTTGATTTGC	55	211
17β-Hydroxysteroid dehydrogenase 4 (Hsd17b4)	*Mfp2*	NM_008292.4	Rev GAGCAGGATGGATTGGAAAA For TGACTGGTACGGTTTGGTGA	55	223
Peroxisomal biogenesis factor 13	*Pex13*	NM_023651.4	Rev GACCACGTAGTTGCAAGAGCAGAGT For CTGAGGCAGCTTGTGTGTTCTACTG	60	717
Peroxisomal biogenesis factor 14	*Pex14*	NM_019781.2	Rev CACTGGCCTCTGTCCAAGAGCTA For CTGACAGGGGAGATGTCACTGCT	60	298
Peroxisome proliferator- activator receptor β	*Ppard*	NM_011145.3	Rev CACCGAGTTCGCCAAGAACA For AGAGCCCGCAGAATGGTGTC	60	363
Peroxisome proliferator- activator receptor γ	*Pparg*	NM_001127330.1	Rev TCCGTAGAAGCCGTGCAAGA For CACCTTGGCGAACAGCTGAG	60	441
Peroxiredoxin 1	*Prdx1*	NM_011034.4	Rev TCTCTTTCAGGGGCCTTTTT For CCAAAACACAGCTCAGACCA	60	396
Peroxiredoxin 5	*Prdx5*	NM_012021.2	Rev GAAAGAAGCAGGTTGGGAGTGT For CCCAGGGACTCCAAACAAAA	55	184
Superoxide dismutase 1, (Cu, Zn-dependen)	*Sod1*	NM_011434.1	Rev AGCGGTGAACCAGTTGTGTTGT For CCACACAGGGAATGTTTACTGC	60	405
Superoxide dismutase 2, (Mn- dependent)	*Sod2*	NM_013671.3	Rev AAGTAGGTAGGGCCTGTCCGATG For CTAAGGGACCCAGACCCAACAAG	60	624
Sequences of the primers used for qRT-PCR					
Acetyl-Coenzyme A acyltransferase /13-Ketoacyl-CoA thiolase	*Acaa 1*	NM_130864.3	For CAATGAACTGAAGCGTCGTG Rev CACCACTGTGGCACTCTCTG	60	147
β-Actin	*Actb*	NM_007393.3	For GTGACGTTGACATCCGTAAAGA Rev GCCGGACTCATCCGTAAAGA	60	112
Acyl-Coenzyme A	*Acox1*	NM_0012718	For CCGCCACCTTCAATCCAGAG Rev CAAGTTCTCGATTTCTCGACGG	60	86

oxidase 1, palmitoyl		98.1			
Acyl-Coenzyme A oxidase 3, pristanoyl	*Acox3*	XM_006504200.2	For TTCTAGTGCTGATTAACTGCCTG Rev AGAAACGAAAACTGTGGTTCCA	60	98
Alpha-methylacyl-CoA racemase	*Amacr*	NM_008537.4	For CTATTTGGCTTTATCAGGCGTTC Rev TTCTCACCGCTTCTGCCAAT	60	51
ATP-binding cassette transporter, subfamily D, member 1	*Abcd1*	NM_007435.1	For ACAGTGCCATCCGCTACCTA Rev ATGAGCTACTAGACGGCTTCG	60	65
ATP-binding cassette transporter, subfamily D, member 3	*Abcd3*	NM_008991.2	For TCAGAATGGGACGCTCATTGA Rev TGGCAGCGATGAAGTTGAATAA	60	86
Catalase	*Cat*	NM_009804.2	For TGGCACACTTTGACAGAGAGC Rev CCTTTGCCTTGGAGTATCTGG	60	114
17β-Hydroxysteroid dehydrogenase 4 (Hsd17b4)	*Mfp 2*	NM_008292.4	For TTAGGAGGGGACTTCAAGGGA Rev TCGCCTGCTTCAACTGAATCG	60	119
Insulin	*Ins*	NM_008386.4	For TGGCTTCTTCTACACACCCAAG Rev ACAATGCCACGCTTCTGCC	60	132
Paired box 4	*Pax4*	NM_011038	For GACCCTGAGACCTCTTCCT Rev AGCCAACTGGCAAACTGA	60	108
Paired box 6	*Pax6*	NM_001244198	For GAGTTTGAGAGGACCCATTATCC Rev TCCATTTGGCCCTTCGATTAG	60	115
Pancreatic and duodenal homeobox 1	*Pdx1*	NM_008814.3	For TCCACCACCACCTTCCAGCTCA Rev AATTCCTTCTCCAGCTCCAG	60	250
Peroxisome biogenesis factor 13	*Pex13*	NM_023651.4	For TGGATATGGAGCCTACGGAAA Rev CGGTTAAAGCCCAAACCATTG	60	81
Peroxisome proliferator-activated receptor α	*Ppara*	NM_001113418.1	For TCCTTTCTGAATGGGCACTT Rev TTAACATTGGGCCGGTTAAG	60	125
Peroxisome proliferator- activator receptor β	*Ppard*	NM_011145.3	For GCGGGCTCTAGAATTCCATC Rev CCGTCTTCTTTAGCCACTGC	60	137
Peroxisome proliferator- activator receptor γ	*Pparg*	NM_001127330.1	For TTTTCAAGGGTGCCAGTTTC Rev ATGGACACCATACTTGAGCA	60	128
Phytanoyl-CoA hydroxylase	*Phyh*	NM_010726.2	For ACTGCCTTCTCCCCGAGATT Rev TGGGTCCAGTGAAACACTCCA	60	51
Sterol carrier protein X/2	*ScpX/2*	NM_011327.4	For TGGGTGGTGGATGTGAAGAA Rev TGAAAGAAGGCCGACTGAGG	60	140
Superoxide dismutase 1 (Cu, Zn-dependen)	*Sod1*	NM_011434.1	For GGAACCATCCACTTCGAGCA Rev CCCATGCTGGCCTTCAGTTA	60	87
Superoxide dismutase 2 (Mn- dependent)	*Sod2*	NM_013671.3	For GGGAGCACGCTTACTACCTTC Rev GAGCCTGGCACTCAATGTG	60	150

3.2. Methods

3.2.1. Culture of the murine β-TC3 cell line

β-TC3 adherent cells were cultured in Dulbecco´s MEM medium containing 4,5 g/l glucose and supplemented with 15 % (v/v) horse serum and 2,5 % (v/v) heated-inactivated fetal bovine serum. The cells were used for the experiments between passages 15–40. β-TC3 cells

were incubated at 37°C in a humidified atmosphere of 8 % CO_2 and split for subculture (1:10 dilution) every 3 days when about 90 % confluency was reached. One ml of 1x 0.25 % Trypsin-EDTA was used for 2 min to harvest the cells. β-TC3 cells were seeded out at a density of 5 x 10^4 cells into each well of a 24 well cell culture plate before each experiment.

3.2.2. Induction of insulin secretion via glucose stimulation

β-TC3 cells were seeded into appropriate culture dishes 2–3 days before the experiment and grown under the cell culture conditions mentioned above. The day of the experiment the cells were then incubated with DMEM medium without glucose for 1 h and thereafter stimulated for 12 h with DMEM medium containing 20 mM glucose.

3.2.3. Incubation with fatty acids to induce lipotoxicity

3.2.3.1. Palmitic acid (hexadecanoic acid)

To explore the role of peroxisomal metabolism during lipotoxic stress, wild type, *Pex13*- and *Abcd3*-knockdown β-TC3 cells were challenged with an overload of palmitic acid (PA). The preparation of the PA was performed as previously described [178]. Palmitate/bovine serum albumin (BSA) conjugates were prepared through soaping of PA with NaOH and then mixing with fatty acid-free BSA. A stock solution of PA (20 mM) was prepared with NaOH (0,01M) in dH_2O. Before use, the solution was incubated at 70°C for 30 min. Ten % fatty acid-free BSA in 1x PBS was combined with the fatty acid soaps in a 3:1 volume ratio. The 5 mM palmitate conjugates were freshly diluted in complete standard DMEM medium to obtain the desired final concentrations. For the experiments, the cells were treated for 48 h (unless otherwise specified) in the presence of BSA-NaOH (vehicle) as a control or with the PA-BSA complex as indicated.

3.2.3.2. Phytanic acid (3,7,11,15-tetramethyl hexadecanoic acid)

Phytanic acid was diluted 1:1,000 in DMSO to prepare a stock solution of 16.8 mM. A 250 µM PHY solution was freshly made in complete standard DMEM medium. A working solution was prepared according to the desired final concentration in DMEM medium. The amount of DMSO in the final solution treatment was not higher than 0.6 %. For the experiments, wild type, *Pex13*- and *Abcd3*-knockdown β-TC3 cells were incubated in the presence of DMSO as a control (in a comparable concentration of the final solution treatment).

3.2.4. Knockdown of *Pex13* or *Abcd3* gene expression by siRNA-mediated transfection of β-TC3 cells

To analyze peroxisomal dysfunction, transient transfection was accomplished by siRNA-mediated *Pex13*- or *Abcd3*-knockdown in β-TC3 cells via lipofection using INTERFERin siRNA transfection reagent (Polyplus). The cells were seeded the day before the transfection at a density of 5 x 10^4 cells per well (24-well plate), to reach ~40 % confluency at the time of transfection. A final siRNA concentration of 30 nM (for *Pex13*-si RNA) or 50 nM (in the case of *Abcd3*-si RNA) was diluted into 100 µl of serum-free DMEM medium. Then, 3 µl INTERFERin reagent were added and immediately homogenized for 10 s. The complex was incubated for 15 min at RT. Five hundred µl of fresh complete DMEM medium were added, subsequently 100 µl of the transfection mix was incorporated dropwise.

Table 14: List of small interfering RNA (siRNA) used in this thesis

***Pex13*-siRNA**	
Company:	Dharmacon® GE Healthcare
Reference number:	SO-2488657G
Name	mPEX13 modified siRNA
Sense Sequence	GCU AUA GCC CUU AUA GUU AUU
Antisense Sequence	UAA CUA UAA GGG CUA UAG CUU
***Abcd3*-siRNA**	
Company:	Santa Cruz Biotechnology, INC
Reference number:	sc-41148
Name	ABCD3 siRNA (m)
Sequences	Not given by the company
Control-siRNA (Scr-siRNA)	
Company:	QIAGEN, Hilden, Germany
Reference number:	1027280
Name	AllStars Negative Control siRNA
Sequences	Not given by the company

3.2.5. Cell viability tests

3.2.5.1. Methylthiazole tetrazolium (MTT) test

To determine the viability of β-TC3 cells after being exposed to different treatments, the MTT test was used. A 12 mM MTT stock solution was prepared in DMEM without phenol red and filtrated. A working solution was freshly made by diluting the stock solution 1:10 in DMEM. Subsequently, the treated cells were incubated with 500 µl of the MTT working solution and maintained at 37°C and 8 % CO_2 in a humidified chamber for 3 h. After labelling the cells with MTT, 1 ml DMSO/isopropanol (1:1) was added to each well to solubilize the newly formed formazan. The absorbance of the produced formazan was read at 570 nm

(background wavelength of 670 nm) using a spectrophotometer. The percentage of cell viability was calculated according to the formula: $(\frac{\text{A570 of the sample}}{\text{A570 of the control}}) \times 100.$

3.2.5.2. Trypan blue assay

Cell viability was also determined by the ability of β-TC3 cells to exclude trypan blue since living cells with intact cell membranes do not take the stain up. Adherent cells were brought into suspension using 0.25 % trypsin/EDTA in HBSS without Ca^{2+}/$Mg^{2+}$and then resuspended in fresh warm medium containing serum. To break up clumps the cells were gently pipetted up and down a few times. Two hundred µl of the cell suspension were removed and added to an equal volume of 0.4 % filtrated trypan blue in 1x PBS. Both sides of a haemocytometer chamber were filled with 10 µl of the cell suspension and the number of viable and non-viable cells were counted under an inverted phase contrast microscope. Eight fields and at least 200 cells not stained with trypan blue per assay condition were counted. The cell density was then calculated as follows:

$$(\frac{\text{Number of living cells}}{\text{Number of large corner squares counted}}) \times \text{Dilution factor} \times 1 \text{ x } 10^4 .$$

To obtain the number of dead cells, non-viable trypan blue-positive cells were counted and calculated as follows:

$$(\frac{\text{Number of non-viable cells}}{\text{Number of large corner squares counted}}) \times \text{Dilution factor} \times 1 \text{ x } 10^4 .$$

Finally, the percentage of viability was calculated using the next equation:

$$(\frac{\text{Number of viable cells}}{\text{Total cell number}}) \times 100.$$

3.2.6. Molecular biological experiments

3.2.6.1. Laser capture microdissection (LCM) of Langerhans islets

A protocol has been carefully established taking all the precautions aimed to avoid the activation of tissue RNases in pancreas tissue. All materials were cleaned using RnaseZap or irradiated with UV light at 254 nm for 30 min. Dissection instruments were heat sterilized at 180°C for 15 min before use and all the solutions and plastic ware were RNase free. Reagents were freshly prepared in DEPC-treated water.

An icy chamber containing chilled isopentane surrounded by dry iced and 100 % ethanol was prepared in advance. Male wild type C57BL/6J mice (3-4 months old) were killed under anaesthesia by cervical dislocation and the pancreatic tissue was quickly removed, placed into a cryomold (so that the desired cutting surface of the tissue laid flat on the bottom)

and carefully covered with cold Tissue-Tek OCT embedding compound. The mold was transferred into the cooled isopentane until the OCT completely solidified. Thereafter, the isopentane in the specimen was left to evaporate onto dry ice and the sample was wrapped tightly in aluminum foil and stored at -80°C until sectioning.

Sectioning was performed in a cryostat equilibrated at -20°C. Fourteen µm sections were cut and three of them mounted on a UV-treated membrane slide cooled inside the cutting chamber (-20°C) and thereafter stored at -80°C inside of sterile 50 ml Falcon tubes. One section out of every 5 was kept for H&E staining to evaluate the presence of islets in the tissue sections and to draw a tissue map of the islet distribution making the laser cutting procedure faster and more efficient.

Tissue dehydration and staining were performed on one slide at a time immediately after its removal from a box kept on dry ice and before the LCM session (**Figure: 7**).

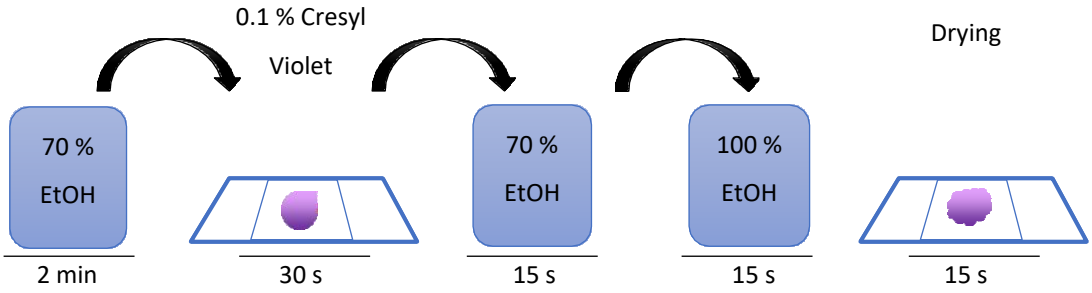

Figure: 7. Summary of the tissue dehydration and staining procedures performed before laser capture microdissection

The LCM and pressure catapulting of the sample were carried out in a PALM Robo microdissection system using a 40 x objective. Laser power and duration were kept around 35 mW and 2.5 ms respectively. To avoid possible cross contamination with other cell types, mainly the core of each islet was dissected.

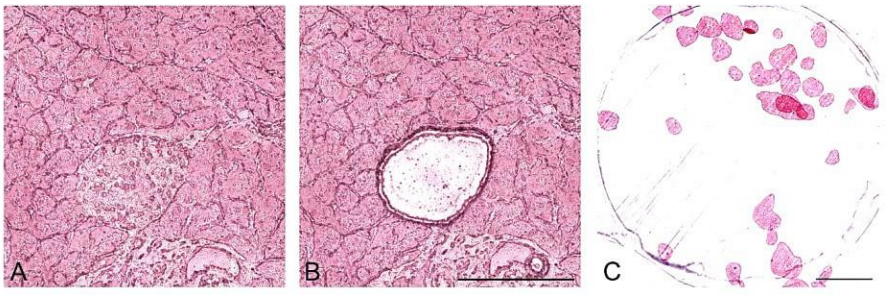

Figure 8: Tissue section of murine pancreatic tissue dehydrated and stained according to the described protocol for LCM. A: islet of Langerhans before LCM; **B**: same islet after LCM was performed; **C**: group of islets collected in a tube cap after catapulting the dissected cells at the end of the session. Scale bars in **A-B**: 150 µm, in **C**: 300 µm.

The microdissected endocrine islet cells were then catapulted into a tube cap containing 1.5 µl of mineral oil and RNA later. After collecting the dissected islets, 50 µl RNAzol plus 5 µl carrier-RNA were added to the sample, which was quickly centrifuged, and stored at -20°C for subsequent RNA extraction. The microdissection session of one objective slide with 3 frozen sections was never longer than 15 min to preserve the RNA from degradation.

3.2.6.2. RNA isolation from β-TC3 cells and reverse transcription to generate cDNA

Total RNA from β-TC3 cells was isolated using RNAzol RT reagent. The cells were lysed in 300 µl RNAzol RT containing glycogen as a carrier (250 µg/ml) and collected directly from the cell culture plate by using a cell scraper. After collection, 0.4 ml of RNase-free water per ml of RNAzol RT used were added. After vigorous shaking for 15 s, sample DNA, proteins and polysaccharides were precipitated for 15 min at RT and by centrifugation at 12,000 x *g* for 15 min at 4°C. Thereafter, the upper supernatant containing the RNA was carefully transferred into a new tube and to precipitate the RNA an equal volume of 100 % isopropanol (~400 µl) was added. After 10 min incubation, the sample was centrifuged at 12,000 x *g* for 10 min at RT. The RNA pellet was washed twice with 0.4 ml 75 % ethanol (v/v) in DEPC water per 1 ml of supernatant used for precipitation and centrifuged at 8,000 x *g for* 3 min at RT. The RNA pellet was then solubilized in 15 µl RNase-free water at a concentration of ~1 µg/µl and stored at -80°C prior to further use. The final preparation had a A_{260}/A_{280} ratio of 1.7-2.1 and a A_{260}/A_{230} ratio of 1.6-2.3 measured with a NanoDrop 2000 spectrophotometer. As a quality control the RNA was analysed on a 1.2 % formaldehyde agarose gel (see 3.2.6.3).

To eliminate any possible residual genomic DNA in the RNA sample, the digestion of single- and double-stranded DNA was performed using a Deoxyribonuclease I kit before reverse transcription. To prepare the RNA sample the following ingredients were added into a RNase-free tube on ice: 1 µg of RNA sample, 1 µl of 10x DNase I reaction buffer, 1 µl of DNase I, Amp Grade (equivalent to 1 U/µl) and adjusted to a final volume of 10 µl with DEPC-water. After 15 min incubation at RT, 1 µl of 25 mM EDTA solution was added to the reaction mixture to inactivate the DNase I. Subsequently the sample was heated for 10 min at 65°C in a Thermoblock.

First-strand cDNA was synthesized from 1-2 µg RNA. A 2x RT-master mix containing the following ingredients was prepared and kept on ice: 2 µl of 10x RT buffer, 0.8 µl of 25x dNTP

mix (equivalent to 100 nM), 2 µl of 10x RT random primers, 1 µl of MultiScribe reverse transcriptase, 1 µl of RNase OUT and 3.2 µl of DEPC-water. Ten µl of the prepared 2x master mix was added into a tube containing 10 µl of RNA (1 µg). Subsequently, the tubes were incubated at 25°C for 10 min and at 37°C for 120 min for reverse transcription. Finally, the samples were heated at 85°C for 5 min to inactivate the reaction.

3.2.6.3. RNA formaldehyde agarose gel electrophoresis

The overall quality of the isolated RNA was assessed by electrophoresis on a formaldehyde agarose gel. To prepare a 1.2 % agarose gel, 1.2 g agarose were dissolved in 90 ml DEPC water and then 10 ml 10x MOPS buffer and 1 µl ethidium bromide stock solution (10 mg/ml) were added. The gel was poured into a tray previously washed with RNase AWAY and then allowed to set at RT. Four volumes of 5x formaldehyde loading dye were added to 4 µg (~4 µl) of RNA sample. After a heat-denaturing procedure (65°C for 5 min) the sample was immediately cooled on ice and then loaded into the gel in a tank containing 1x formaldehyde running buffer. The gel was run at 60 V for 90 min and the bands visualized on a UV transilluminator. An RNA marker was loaded together with the samples and prepared according to manufacturer´s instructions. The integrity of the RNA was documented by photographing of the ethidium bromide-stained intact 28S and 18S ribosomal RNA bands.

3.2.6.4. cDNA amplification by semiquantitative polymerase chain reaction (RT-PCR) and agarose gel electrophoresis

Amplification was performed as follows: a standard PCR reaction master mix was prepared containing 1 U of Taq DNA polymerase, 500 nM of forward primer, 500 nM of revere primer, 1 µl of template cDNA, 2.5 µl of 10x PCR reaction buffer, 0.2 µl of 10 mM dNTP mix and adjusted to a final volume of 25 µl using DEPC-water. The PCR reactions were carried out in a Bio-Rad iCycler C1000 using the following parameters: 95°C for 3 min (pre-denaturation) followed by 35 cycles of amplification: 95°C for 30 s (denaturation), 50-65°C for 30 s (annealing) and 72°C for 1 min (extension) concluding with a final extension at 72°C for 5 min. To analyse the target gene expression resulting from the amplification, agarose gel electrophoresis was used to separate the RT-PCR product by size. *28S r*RNA was used as a control for the normalization of the gene expression using ImageJ software. The sequences of the primers used for the qRT-PCR are listed in **Table 13**. The specific annealing temperature for each primer pair was optimized with a temperature gradient from 55-65°C

in an iCycler basal PCR machine (without optical module) before conducting the experiments.

Gel electrophoresis was used as a standard procedure for separating DNA by size (to be used either for visualization or purification). Depending on the size of the bands needed to be separated a 1, 2 or 4 % agarose gels were prepared. For a 1 % gel, 1 gr of agarose was poured into 100 ml of 1xTAE buffer and microwaved until the agarose was completely dissolved. After cooling down the solution, 4.5 µl SERVA DNA stain G were added, mixed, and poured into a gel tray and allowed to solidify. Gels were run in a Sub-Cell GT electrophoresis cell (Bio-Rad) in 1xTAE buffer at 120 V. Before loading, 2 µl of gel loading buffer were added to each DNA sample. A 1 kb DNA ladder was loaded in parallel to detect and compare the DNA band sizes after electrophoresis. The DNA fragments were visualized with UV light using the Gel-Doc 2000 transilluminator and analysed with the Gel-Doc 2000 gel imaging system.

3.2.6.5. cDNA amplification by quantitative real-time polymerase chain reaction (qRT-PCR)

Amplification was performed using a SsoAdvanced universal SYBR green master mix on an IQ5 I cycler using the standard protocol recommended by the manufacturer. The samples were prepared in duplicates as follows: 5 µl of 2x SYBR green, 500 nM of forward primer, 500 nM of reverse primer and 1 µl of template cDNA. The reaction was adjusted to a final volume of 10 µl with DEPC-water. The polymerase activation and DNA denaturation were performed at 95°C for 3 min followed by 40 cycles at 95°C for 15 s (denaturation), T_m 60°C for 30 s (annealing), and 72°C for 1 min (extension). The average threshold (Ct) values of at least three independent experiments were used to calculate the relative amounts of mRNA using the 2-ΔΔ CT method and normalized to β-actin values. For the sequences of the primers used for the qRT-PCR refer to **Table 13**. The specificity and efficacy of all primers were validated before use. For each primer set, a standard curve was generated from cDNA stepwise diluted from 10-fold to 10,000-fold to investigate the efficiency of all primer pairs used.

3.2.6.6. Western blot analysis

3.2.6.6.1. Isolation of protein from whole cell lysates

Western blot analysis was used for the visualization and relative quantification of proteins. Protein samples were collected from cells grown on cell culture dishes on ice by using a rubber policeman in cold cell lysis buffer containing a protease inhibitor cocktail (1:100). The collected samples were subjected to 3 cycles of cooling for 10 min on ice and vigorous vortexing thereafter for 5 s. Subsequently, they were centrifuged at 2,500 x *g* for 10 min at 4°C. After centrifugation, the supernatants were collected for further use. All samples were kept on ice during the procedure to minimize protease activity. Protein concentration was determined according to Bradford [179] using BSA as a standard. The average of three independent measurements of each sample was used to calculate the protein concentration.

3.2.6.6.2. Isolation of peroxisome-enriched fractions from pancreas and liver

To isolate peroxisome-enriched fractions from mouse pancreata and liver, male wild type C57BL/6J mice (3-4 months old) were killed under anaesthesia by cervical dislocation and immediately perfused with 1x PBS buffer injected through the left ventricle. Liver and pancreas were quickly removed and ~50 mg of tissue were resuspended in 2 ml TEDS buffer on ice. After mincing the tissue into small pieces, it was shredded with the help of an ultraturrax. The resulting lysate was homogenized with a Dounce homogenizer using 30 manual up and down strokes always keeping the sample on ice. A first centrifugation step (1,000 x *g* at 4°C for 10 min) was carried out to obtain the nuclear fraction. The resulting supernatant was centrifuged at 5,000 x *g* at 4°C for 10 min to remove the large mitochondrial fraction and later centrifuged again at 30,000 x *g* at 4°C for 30 min with the purpose to isolate the peroxisome-enriched and cytoplasmic fraction. The peroxisomal pellet was resuspended in 200 µl buffer containing Tris (50 mM) pH 8.0, NaCl (150 mM) and 0.1 % Triton X-100. Samples were stored at -20°C until used.

3.2.6.6.3. Polyacrylamide gel electrophoresis (PAGE)

Prior to SDS-PAGE, sample solubilisation was carried out in Laemmli buffer containing SDS and 2-β-mercaptoethanol. After addition of the sample buffer, the samples were incubated at 95°C for 5 min and subsequently kept on ice for another 5 min. Ten to 20 µg of total protein were loaded in a 12 % SDS polyacrylamide gel in 1x electrophoresis running buffer

for separation. The electrophoresis was performed using a Mini-PROTEAN chamber (Bio-Rad) for 40 min at 200 V. A precision plus protein dual color (Bio-Rad) ladder was used as recombinant standard.

3.2.6.6.4. Electrophoretic transfer and immunodetection of specific proteins

For the protein transfer onto a polyvinylidene fluoride membrane (Immobilion-P transfer membrane) a tank blotting procedure was performed. The transfer was carried out for 1 h at 100 V in cooled Towbin buffer. Non-specific protein-binding sites on the membrane were blocked using a blocking solution for at least 1 h at RT with gentle agitation. After washing the membrane in TBST buffer for 5 min, the blots were incubated for 1 h at RT with the primary antibody at the optimized dilution (refer to **Table 11**) in blocking solution with gentle agitation. Thereafter the membrane was washed 3 times (15, 5 and 5 min) in TBST buffer before incubation with a secondary antibody (see **Table 12**) diluted in blocking solution for 1 h at RT. A final washing procedure for 15 min and 2x for 5 min prior to blot development was performed. The chemiluminiscence detection of HRP activity was achieved by incubating the membrane for 5 min with the Clarity Western ECL Substrate (Bio-Rad). The blot was exposed to a CL-X Posure film (Thermo Scientific) and developed with Readymatic developer and fixer (Carestream). The transferred membranes were stripped and re-probed not more than 3 times to detect different target proteins. Except for the detection of thiolase (due to antibody shortage), all Western blot analyses were performed in triplicates.

3.2.6.6.5. Total protein detection

3.2.6.6.5.1. Ponceau S staining

After transfer, the membrane was immersed in Ponceau S Stain solution and incubated for 2 min to visualize pattern of the transferred proteins was satisfactory. Afterwards, the membrane was destained in dH_2O until complete cleaning of the dye. Subsequently, the membrane was rinsed in TBST buffer for 5 min with gentle agitation and a standard immunodetection procedure was carried out.

3.2.6.6.5.2. Coomassie staining

After washing the gel or/and the membrane 3 times (5 min each) in dH_2O to remove excess of SDS and to minimize background staining, the gel/membrane was incubated with Coomassie brilliant blue stain for 1 h at RT with gentle agitation. Subsequently, the

gel/membrane was rinsed 3 times (5 min each) in dH_2O and only in the case of membrane staining, once more in 30 % methanol until the desired resolution was attained.

3.2.6.6.6. Membrane stripping and re-probing

Due to shortage of pancreatic protein samples, Western blot membranes were re-probed. After incubation in stripping buffer for 10 min at 60°C on a roller, the membranes were washed 2 times (10 min each) at RT using large volumes of TBST buffer. Subsequently, the membranes were immersed in 5 % (w/v) blocking solution in TBST buffer for 1 h at RT before performing the next immunodetection.

3.2.7. Morphological experiments

3.2.7.1. Hematoxylin and Eosin (H&E) staining

One to 2 µm tissue sections were first deparaffinized with Xylene 3 times (5 min each) and then hydrated in alcohol in a downstream dilution series (99 %, 99 %, 96 %, 80 %, 70 %, 50 %) 3 min each. The samples on objective slides were rinsed in dH_2O for 3 min and incubated in Mayer´s hematoxylin solution for 2 min. The slides were rinsed in running tap water (10 min), placed in dH_2O for some seconds and counterstained with Eosin Y solution containing 0.2 % glacial acetic acid for 30 s. Samples were rinsed shortly in dH_2O followed by sample dehydration and clearance by immersion in 50, 70, and 80 % EtOH (each 1 min), 96 % EtOH (3 min), and 99 % EtOH (2 times 3 min each). Finally, the slides were immersed in Xylene (3 times for 5 min each), allowed to dry and mounted in DEPEX.

3.2.7.2. Oil red O staining (ORO)

Oil red O (ORO) staining was used to analyse lipid droplet appearance. After treatment, β-TC3 cells were gently rinsed with 1x PBS and then fixed with 10 % formalin for 10 min. The formalin was removed and fresh 10 % formalin was added for 1 h more. After gently rinsing twice with dH_2O, 60 % isopropanol was added and allowed to stand for 5 min with the purpose of preventing the carrying of dH_2O into the ORO solution. The cells were then stained with freshly diluted oil red O solution (5.1 mM) for 10 min. Thereafter, the stain was removed and the cells were washed four times with tap water until the water appeared clear. As counterstain, the samples were incubated for 2 min with 10 % hematoxylin. The slides were mounted in Mowiol 4-88 solution. All the procedures were performed at RT.

3.2.7.3. Indirect immunofluorescence staining of cultured β-TC3 cell line

β-TC3 cells were grown on poly-L-lysine coated coverslips before staining. After washing the cells with 1x PBS buffer for 2 min, they were fixed with 4 % PFA + 2 % saccharose in PBS at RT for 20 min. Thereafter, the cells were rinsed 3 times with 1x PBS for 10 min each. The samples were incubated first with fresh prepared 1 % glycine solution in 1x PBS for 10 min and thereafter in 1 % Glycine containing 0.2 % triton X-100 for 25 min for permeabilization. After washing the cells 3 times (10 min each) with PBS, the blocking of the nonspecific antibody-binding sites was achieved by 45 min incubation in blocking solution. Subsequently, the samples were incubated in diluted antibody (in blocking buffer) at the optimized dilution (refer to **Table 11**) overnight at 4°C in a light-tight box. The next day, the samples were washed 3 times in 1x PBS (5 min each) and incubated with the secondary antibody diluted in blocking buffer for 1 h at 4°C in the dark. As a counterstaining, Hoechst 33342 (2µg/ml) in 1x PBS was used for a 10 min incubation. After rinsing the samples one more time with 1x PBS the coverslips were mounted with a drop of Mowiol/n-propyl-gallate (3:1) on super frost plus slides. Slides were stored in the dark at 4°C.

3.2.7.3.1. Coating of coverslips for cell culture

A 0.1 % solution of poly-L-lysine was prepared in a 1:1 (v/v) solution of 1.91 % borax buffer and 1.25 % boric acid buffer and filtrated. Twelve mm diameter autoclaved coverslips placed in a 24-well plate were coated with the poly-L-lysine solution and incubated overnight at RT. The next day the solution was removed, and the coverslips were rinsed 2 times with autoclaved dH_2O and allowed to rest for 5 h. Thereafter, the coverslips were rinsed 2 times with autoclaved dH_2O with an incubation time of 20 min in between. Finally, the coated coverslips were allowed to dry completely and stored at 4°C. All procedures were performed under sterile conditions.

3.2.7.4. Indirect immunofluorescence staining of paraformaldehyde-fixed paraffin-embedded mouse pancreata

Male wild type C57BL/6J mice (3-4 months old) were used for the immunofluorescence-based detection and the precise localization of peroxisomal antigens in pancreata. The animals were killed under anaesthesia via cervical dislocation and perfused-fixed with 4 % paraformaldehyde (PFA) containing 2 % saccharose in PBS (pH 7.4) injected through the left ventricle. After a second fixation procedure by immersing the dissected tissue in PFA

overnight, the fixed samples were paraffin-embedded using a Leica TP 1020 automated vacuum infiltration tissue processor. Using a Leica RM2135 rotation microtome, sections of 1-2 µm were cut and mounted on super frost plus slides and stored at RT until needed.

An indirect immunofluorescence protocol was established for immunolabeling of mouse pancreatic paraffin sections. A first deparaffinization step was carried out in an oven at 50°C overnight. After a second deparaffinization procedure by immersing the slides in Xylene 3 times for 10 min each, the sections were rehydrated in a series of ethanol at different dilutions (99 %, 99 %, 96 %, 80 %, 70 %, 50 %) 3 min each and rinsed in dH_2O for 2 min. For antigen retrieval the samples were treated with trypsin (0.01 %) in 1x PBS for 8 min at 37°C followed by microwave irradiation. Before microwaving, the samples were washed 3 times in 1x PBS (5 min each) and once in dH_2O. Thereafter, microwaving was carried out for 3x5 min in 10 mM sodium citrate buffer at pH 6. The samples were allowed to cool slowly for refolding of proteins. Thereafter, they were washed, once shortly in dH_2O and 3 times for 5 min in PBS. Nonspecific binding sites were blocked with blocking solution for 2 h at RT in a light-tight box. The sections were washed in PBS and finally incubated with the primary antibodies at the optimized dilution (see **Table 11**) in dilution buffer overnight. The next day the specimen were rinsed 3 times in 1x PBS 5 min each and incubated in fluorochrome-conjugated secondary antibodies in dilution buffer for 2 h in the dark. The slides were rinsed 3 times in 1x PBS for 5 min each and incubated for 10 min with TO-PRO-3 iodide and/or Hoechst 33342 diluted in 1x PBS (1:750) to visualize nuclei. Finally, coverslips were mounted with Mowiol 4-88 and n-propylgallate as an antifading agent at a 3:1 dilution and allowed to cure overnight at RT protected from light. Negative controls were processed in parallel by addition of dilution buffer instead of the primary antibody and washed separately. To be able to examine the co-distribution of 2 different antigens in the same sample, a double immunofluorescence procedure was simultaneously carried out if necessary. In that case 2 antibodies from different species were chosen and appropriate secondary antibodies selected that were not cross-reacting with each other.

3.2.8. Insulin enzyme-linked immunosorbent assay (ELISA)

An insulin ultrasensitive ELISA assay was used for the quantitative determination of insulin secretion and cellular insulin storage. After cell treatment (see 3.2.3.) and to determinate the insulin secretion, the medium was collected from the samples and centrifuged for

10 min at 4°C and 2,000 x *g*. In parallel, total protein was isolated from the cells with the cell lysis buffer and used for insulin storage determination by ELISA. Twenty-five µl of each sample or the calibrators were incorporated to a 96-wells plate. Thereafter, 100 µl of the enzyme conjugate 1x solution were added and incubated on a plate shaker (700 rpm) for 2 h at RT. The wells were washed 6 times with 350 µl washing buffer 1x solution per well. Subsequently, 200 µl of substrate TMB were added to each well and allowed to stand for 15 min. After the addition of 50 µl stop solution, the optical density was read at 450 nm and the results were calculated against the absorbance values obtained for the calibrators using a data analysis software (www.elisaanalysis.com). The results were normalized to the total protein concentration, measured by Bradford assay.

3.2.9. Cellular reactive oxygen species detection

3.2.9.1. 2´,7´-Dichlorofluorescein diacetate (DCFDA) detection of H_2O_2 generation

Intracellular generation of ROS (hydroxyl and peroxyl) was detected with the 2´,7´-dichlorofluorescein diacetate (DCFDA) dye. This dye diffuses into the cell where it is deacetylated by cellular esterases to a non-fluorescent compound. Subsequently DCFDA dye can be oxidized by ROS into 2´, 7´-dichlorofluorescein (DCF) which is highly fluorescent. Transfected and attached β-TC3 cells were removed from the cell culture plates and brought into suspension by trypsinization for 2 min. Thereafter, the reaction was stopped by addition of fresh medium and the cells were centrifuged for 5 min at 500 x *g* at RT. The cells were resuspended and stained with 20 µM DCFDA in prewarmed DMEM medium without phenol red supplemented with 10 % foetal calf serum and EDTA (2 nM) at 37°C in a humidified atmosphere of 8 % CO_2 for 30 min. Thereafter, the medium containing DCFDA dye was removed via centrifugation and the cells treated with palmitic or phytanic acid for 6 h. The result was examined on a LEICA DMRD microscope (equipped with a LEICA CD480 camera) at excitation / emission spectra of 485 nm and 535 nm respectively. The fluorescence change was determined as percentage after background subtraction. A 30 min treatment with antimycin A (65 µM) was used as a positive control due to its capacity to induce ROS production via inhibition of the mitochondrial electron transport chain complex III.

3.2.9.2. Dihydroethidium (DHE) detection of superoxide generation

To detect superoxide generation in living cells, the oxidizable fluorescent probe dihydroethidium (DHE) was used. This compound is dehydrogenated to ethidium in the

presence of superoxide once internalized into the cells. Sample cells were incubated in a 10 µM DHE solution in standard complete DMEM medium at 37°C and 8 % CO_2 for 30 min. After a washing procedure with 1x PBS (2 times, 5 min each) the cells were fixed with 4 % PFA for 20 min at RT. Thereafter, the samples were washed 3 times (10 min each) in 1x PBS. Subsequently, nuclei were counterstained with Hoechst 33342 (1:750 in 1x PBS) for 10 min. After rinsing 2 times for 5 min each with 1x PBS, the coverslips were mounted with a drop or Mowiol 4-88 on super frost plus slides. Fluorescence emission was detected with a LEICA DMRD microscope (equipped with a LEICA CD480 camera) with maximum excitation and emission spectra of 530 nm and 600 nm respectively.

3.2.10. Catalase activity assay

The enzymatic activity of catalase was determined based on its peroxidatic function. The formaldehyde produced in the reaction of catalase with methanol in the presence of an optimal concentration of H_2O_2 was measured spectrophotometrically using a catalase assay kit. The cells were harvested using a rubber scraper and then homogenized on ice in 2 ml cold buffer containing 50 mM potassium phosphate and 1 mM EDTA (pH 7.0). After centrifugation at 10,000 x *g* for 15 min at 4°C the supernatant was removed and kept on ice. In individual wells of a 96-wells plate, 100 µl of diluted assay buffer, 30 µl of methanol, and 20 µl of each sample supernatant were loaded. Thereafter, 20 µl of diluted H_2O_2 were added to each well and then incubated on a shaker for 20 min at RT in the dark. To terminate the reaction, 30 µl of diluted potassium hydroxide and 30 µl of catalase purpald were incorporated to each well and incubated for 10 min on a shaker. Finally, 10 µl of catalase potassium periodate were added and after a 5 min incubation the absorbance was monitored at 540 nm using a plate reader. Results were normalized to total protein concentration measured by Bradford assay.

3.2.11. Catalase expression for antibody generation

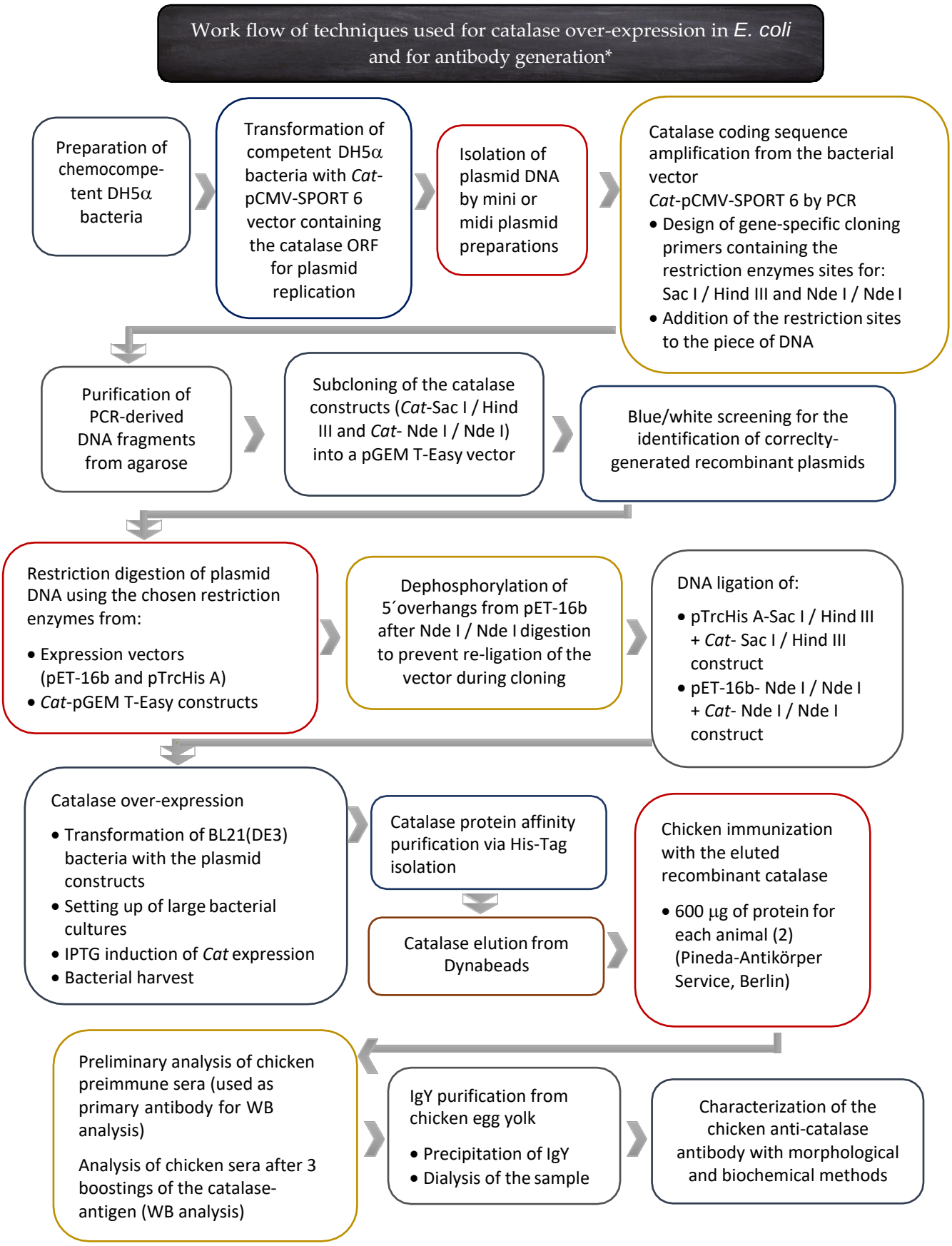

*All techniques and plasmid maps are described in detail in the **Appendix**.

4. STATISTICAL ANALYSIS

Statistical analysis was performed by either two-way ANOVA or by the Student-*t*-test for paired values calculated with the software Prism 6 from GraphPad Software (USA). Values are presented as means ± SD (standard deviation). Results are representatives of at least three experiments (unless otherwise specified). Significance levels were set for *p*-values < 0.05 (*), 0.01 (**), 0.001 (***) and 0.0001(****).

5. RESULTS

Catalase was the typical marker enzyme located in the peroxisomal matrix. This important enzyme inactivates hydrogen peroxide (H_2O_2), which is produced by a variety of oxidases inside the peroxisomal matrix, providing the fundaments for the "peroxisome concept" by De Duve and Baudhuin [(1)]. Therefore, catalase plays a central role in the defense against oxidative damage by reactive oxygen species (ROS). For many years, this protein has been *the* marker enzyme for the morphological or biochemical study of peroxisomes. Given the importance of catalase activity for the peroxisome-related research continuous improvement of the detection methods was required leading to the production of a variety of different antibodies against catalase.

5.1. Recombinant catalase expression for antibody generation

In general, antibodies are essential for the structural and functional study of cells and organelles. One of the main drawbacks of antibody generation is the limited availability of properly purified antigens. To further investigate the catalase expression, distribution and its alterations under different experimental conditions used in this study, we required an anti-catalase antibody i) in sufficiently high amounts to be used for further investigations independent from company supply, ii) sensitive enough to detect the low quantity of pancreatic catalase, iii) able to detect catalase in all the tissues that we are currently investigating in our laboratory and iv) that was usable for double-labeling in Western blots and immunofluorescence studies with all rabbit or mouse antibodies against other peroxisomal proteins present in our laboratory. For these reasons, we decided to generate our own anti-catalase antibody by recombinant overexpression technology in *Escherichia coli* to obtain high amounts of protein and to use chicken as a host for antibody production and isolation in eggs.

For catalase overexpression, two prokaryotic recombinant expression vectors, *Cat*-pTrcHis A and *Cat*-pET-16b, were first constructed and then used for the expression of catalase in *E. coli* BL21 (DE3). The catalase protein was enriched by His-tag-based isolation and 600 μg of the recombinant protein were used for the immunization of chickens to generate an IgY antibody. Subsequently, the effectiveness of the antibody was assessed by Western blot and immunofluorescence analysis.

5.1.1. Construction of the expression vectors and expression of recombinant catalase

pCMV-SPORT 6 vector containing the full-length open reading frame (ORF) encoding mouse catalase was transformed into DH5α competent bacteria for replication. After plasmid isolation, the presence of the correct catalase cDNA was verified by DNA-sequencing (Seqlab, Göttingen) using specific primers for the T7 (5´-TAATACGACTCACTATAGGGAGA-3´) and the Sp6 (5´-AGCTATTTAGGTGACACTATAG-3´) polymerase promoter regions located inside the vector and flanking the catalase ORF.

The open reading frame (ORF) of mouse catalase was amplified by PCR using gene-specific cloning primers (see **Appendix 1** for a full description) located at the start (32-mer forward primer) and the stop (31-mer reverse primer) codon region of the ORF (**Figure: 9**).

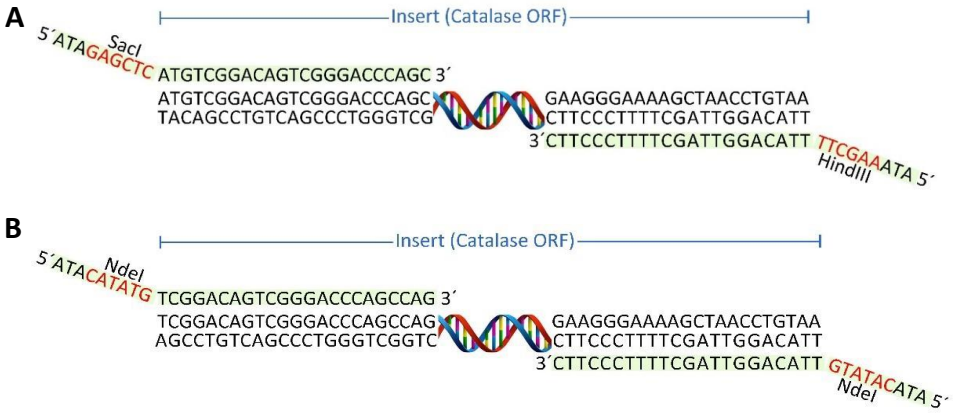

Figure: 9. Designed primers used for the amplification of the catalase ORF via PCR adding restriction sites for (A) Sac I at the 5´end and Hind III at the 3´end and (B) Nde I at both 5´and 3´ends.

The primers either contained the restriction enzymes sites for Sac I (forward primer) and Hind III (reverse primer) for cloning of the catalase ORF into pTrcHis A or Nde I (forward and reverse primer) for cloning into pET-16b. This procedure introduces the chosen restriction sites into the catalase ORF for the further cloning procedure (**Figure: 10**). PCR analysis showed an expected 1,584 bp band corresponding to catalase proving the right size of the PCR product without any additional non-specific bands.

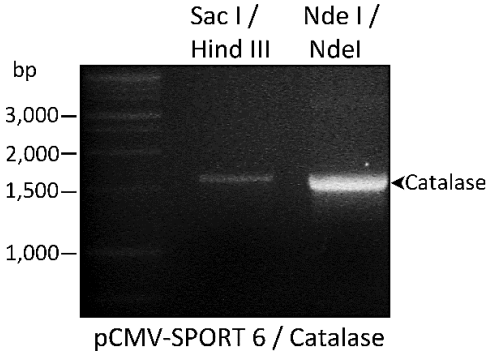

Figure: 10. Catalase ORF amplification by PCR using specific primers including the restriction enzymes Sac I / Hind III and Nde I / Nde I. After the PCR amplification 5µl of the obtained product were loaded on a 2% Agarose gel to determine whether the size of the obtained fragment was correct (1,584 bp). No additional, unspecific bands were visualized.

After assessing that we obtained only one PCR product of the expected size, the remainder of the PCR reaction (45 µl) was used for gel band purification. After purification of the PCR products, both catalase inserts (containing Sac I/Hind III or Nde I/Nde I restriction enzymes sites) were sub-cloned into the pGEM-T Easy vector for T/A cloning with high efficiency for ligations. Since the multiple cloning site present in the pGEM-T easy vector is flanked by the coding region of the enzyme β-galactosidase (enzyme that hydrolyzes galactose), successful cloning of the insert into the vector was assessed by blue/white screening (data not shown). Ten white, positive clones were double checked by colony PCR prior to the setup of miniprep cultures for plasmid multiplication (**Figure: 11**). The obtained PCR products were visualised on an agarose gel. For the *Cat*-Sac I/Hind III + pGEM-T Easy construct 9 out of 10 clones were positive showing a single band around 1,584 bp corresponding to catalase. Clone 1, 3, and 4 with highest DNA content were chosen for subsequent replication and purification. The colony PCR analysis for the *Cat*-Nde I/Nde I + pGEM-T Easy construct confirmed 6 positive clones out of 10. Clones 1, 5, and 10 with highest DNA amount were selected for further cloning.

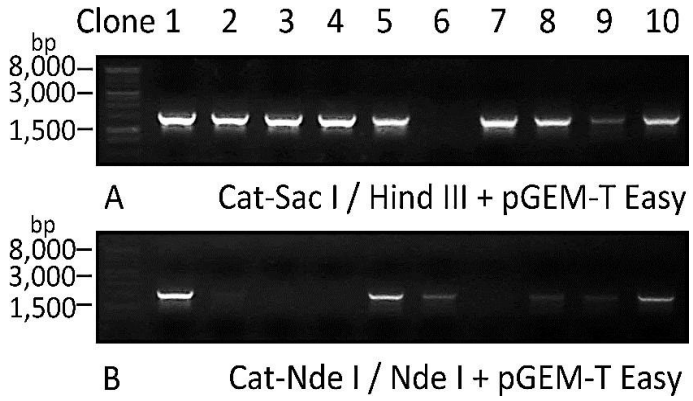

Figure: 11. PCR screening of positive clones after pGEM-T Easy sub-cloning. Gene specific primers including the restriction enzymes sites were used for the screening and the PCR reaction amplified 35 cycles. Fifty µl of each PCR product were loaded on a 1 % Agarose gel. Note that for the *Cat*-Sac I / Hind III + pGEM-T Easy construct **(A)** only the clone number 6 resulted negative whereas for the *Cat*-Nde I / Nde I + pGEM-T Easy construct **(B)** clones (3, 4, and 7) gave no visible band.

To excise catalase from the replicated and purified pGEM-T Easy constructs, a restriction enzyme digestion using Sac I / Hind III or Nde I / Nde I was carried out and the fragments were loaded on a 1 % agarose gel to purify and extract the digested DNA. At the same time, the final target expression vectors pTrcHis A and pET-16b, were replicated, purified and digested using the same restriction enzymes as for the inserts. Additionally, pET-16b underwent a dephosphorylation step before purification in order to prevent recircularization and re-ligation of the Nde I-linearized DNA.

Thereafter, the specifically digested expression vectors and appropriate catalase inserts were ligated and ligations were transformed into *E. coli*. As negative controls for the

transformation “vector alone + ligase” and the “insert alone + ligase” were used. As before, white positive clones were confirmed by colony PCR analysis.

Two positive clones in which the catalase sequence was successfully integrated into the pTrcHis A vector (**Figure: 12**) and three into the pET-16b vector (figure not shown) were selected, propagated and the plasmid DNA isolated.

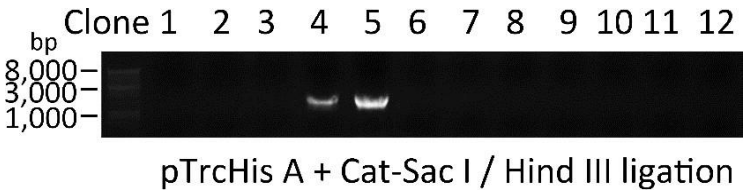

Figure: 12. Agarose gel electrophoresis analysis after colony PCR amplification of pTrcHis A + *Cat*-Sac I /Hind III construct. 12 positive clones were selected and collected for PCR screening. Specific primers including the restriction enzymes sequences were used. Similar results were obtained for the pET-16b constructs. Fifty µl of each PCR product were loaded on a 1 % Agarose gel.

To ensure that the catalase insert was indeed present, the purified plasmids were first digested using both restriction enzymes and then analysed by agarose gel electrophoresis (**Figure: 13**). The release of a 1,600 bp target fragment corresponding to the amplified catalase ORF was assessed in the analysed clones by agarose gel electrophoresis. Both digests (pTrcHis A using Sac I and Hind III and pET-16b with Nde I) displayed the expected band of 1,584 bp corresponding to the catalase insert. Additionally, the digest of pTrcHis A showed a clear 4,400 bp band while the one of pET-16b a 5,711 bp one. These bands correspond to the pure linearized plasmids. The larger band of approximately 6,000 bp visible in clone 5 of pTRC-His-A corresponds to the digested linearized plasmid with the catalase ORF (most probably cut only with one enzyme).

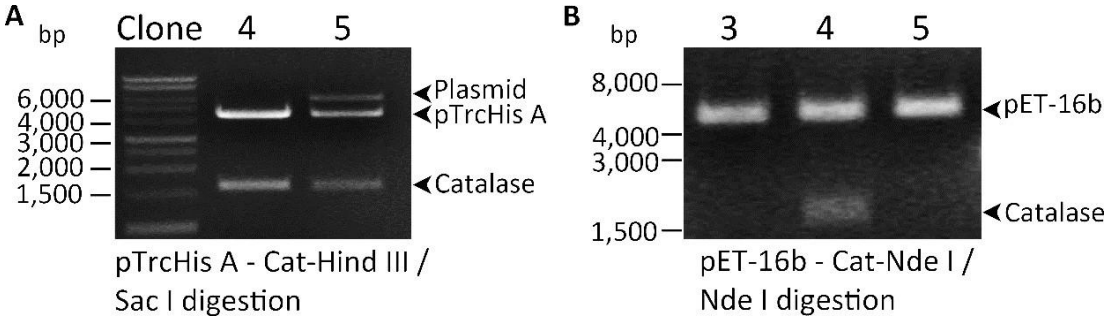

Figure: 13. Agarose gel electrophoresis analysis after digestion of pTrcHis-A + *Cat*-Sac I /Hind III construct and pET-16b + *Cat*-Nde I / Nde I construct. A: Note the release of a 1,600 bp target fragment corresponding to catalase and a 6,000 bp band of a not completely digested linearize vector (clone 5). **B**: Note that only the clone number 4 gave 2 distinctive bands: one for pET-16b (5,711 bp) and one for catalase (1,600 bp). The lack of bands from the other 2 clones (3 and 5) could be due to an incomplete phosphorylation with a consequent re-ligation of the vector (empty vector).

Positive recombinant plasmids were sequenced to verity that the cloned ORF sequence was identical to the original catalase ORF (without any base exchanges) and was positioned in frame with the appended His-Tag and start-codon contained in the plasmids. The sequencing results showed no Taq-polymerase amplification mistakes and confirmed that the His-tag (used for future affinity purification of the protein) was in frame with the start-codon.

5.1.2. Expression optimization of the recombinant catalase

The purpose of designing two different expression vectors was to use the more efficient one for the expression in *E. coli*. The two protein expression vectors used in this study contain a polyhistidine (6xHis) region at the N-terminus to allow the purification of the recombinant catalase by affinity purification with magnetic Dynabeads. The expression of the His-tagged catalase recombinant protein could be initiated using the Isopropyl β-D-1-thiogalactopyranoside (IPTG) inducible T7 promoter located upstream of the His-tag.

To express catalase, the constructed vectors pTrcHis A + *Cat* and pET-16b + *Cat* were transformed into *E. coli* BL21 (DE3) Rosetta and the resistant clones cultured at 37°C in Luria broth (LB) medium containing 100 µg/ml ampicillin overnight. The next day, the starting culture was used to set-up a large liquid culture at 1:50 dilution in medium. When the absorbance of the bacterial culture reached 0.45 at 600 nm, IPTG (1 mM) was added to induce the expression of the recombinant protein. To optimize the expression conditions, the bacteria were cultured with different media (Terrific broth and/or Luria broth), different temperatures of induction (16, 20, and 37°C), and three different dilutions of the starting culture for inoculation (1:20, 1:50, and 1:100). Samples were collected every 30 min after induction during the first 3 h, and after 4 and 5 h and analyzed by 12 % SDS-PAGE. The gel was subjected to Coomassie blue staining in order to visualize the protein bands (**Figure: 14, A-B** and **figure: 15, A-B**) and to Western blot analysis using an anti His-Tag primary antibody (**Figure: 14, C-D** and **figure: 15 C-D**). Western blot analysis of total bacterial lysate transformed with the pTrcHis A + *Cat* construct after IPTG induction showed maximum catalase expression levels under slow bacterial growth conditions at 20°C and after 120-150 min. After this time point, the catalase expression tended to decline, possibly due to the bacterial culture saturation with a concomitant decrease of nutritional elements necessary for bacterial growth. No improvement regarding the protein expression was found using

16°C as the culture temperature. Much less amount of catalase was expressed when bacteria were maintained at 37°C in comparison to 20°C during the same period of time (data not shown). Using the pET-16b + *Cat* construct, the expression of catalase reached its maximum peak after 150 min of induction at a starting dilution of 1:50 and after 120 min at a starting dilution of 1:100. The pTrcHis A + *Cat* construct proved to be more efficient than the pET-16 b + *Cat* construct for the catalase expression, whence we decided to continue only with the first one for the purpose of expressing larger amounts of the protein. The optimal conditions for the expression of the His-tagged recombinant catalase using the pTrcHis A + *Cat* construct were expression time of 150 min for a 1:50 starting dilution, maintained in Luria broth medium at 20°C (after induction).

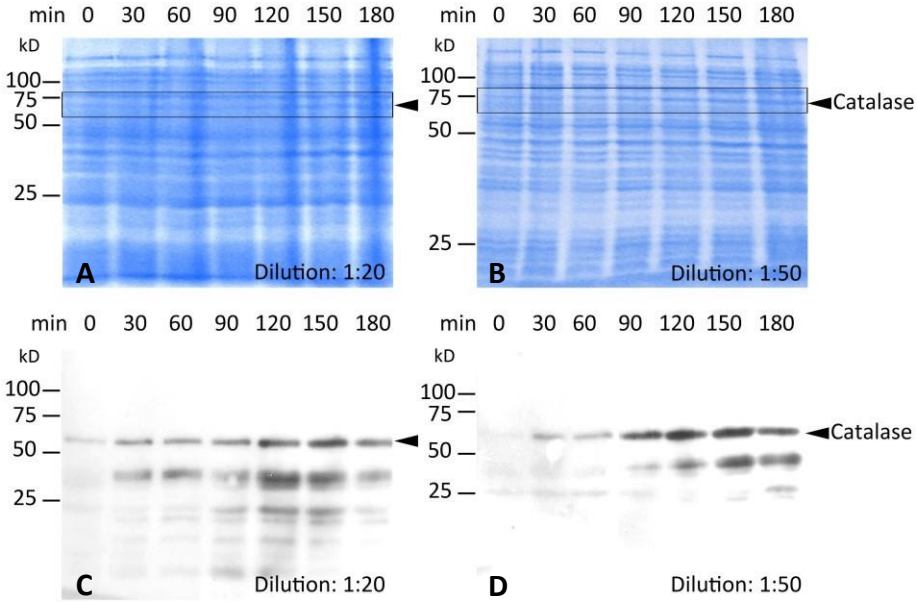

Figure: 14. Coomassie brilliant blue staining and SDS-PAGE analysis of the induction of recombinant catalase using the construct pTrcHis A + *Cat*. Optimization of the recombinant protein induction. **A-B**: Total bacteria lysate of recombinant *E. coli* BL21 (DE3) at different time points after induction with IPTG using pTrCHis A + *Cat*. 1:20 and 1:50 dilutions from the starter culture were used. **C-D**: Corresponding SDS-PAGE analysis using anti His-Tag as a primary antibody for the detection of the recombinant catalase. Note that the catalase expression was higher around 120-150 minutes after induction (with a subsequent decline) and at a starting dilution of 1:50. IPTG: isopropylb-D-thiogalactopyranoside.

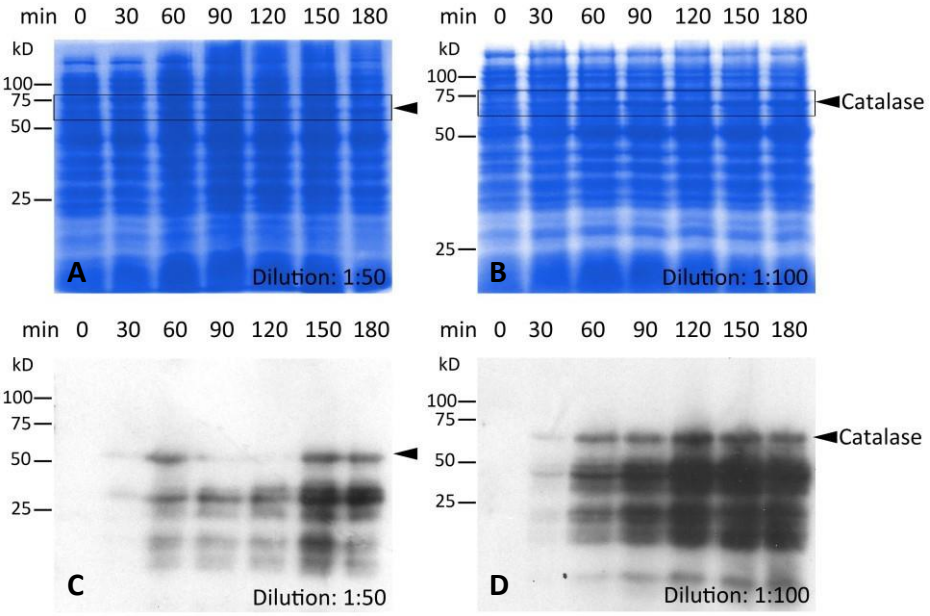

Figure: 15. Coomassie brilliant blue staining and SDS-PAGE analysis of the induction of recombinant catalase using the construct pET-16b + *Cat* (see figure on page 62). Optimization of the recombinant protein induction. **A-B**: Total bacteria lysate of recombinant *E. coli* BL21 (DE3) at different time points after induction with IPTG using pET-16b + *Cat*. 1:50 and 1:100 dilutions from starter culture were used. **C-D**: Corresponding Western blot analysis using anti His-Tag as a primary antibody for the detection of the recombinant catalase. Note that the catalase expression was higher at 150 min post induction and a starting dilution of 1:100, however, the expression of His-tagged catalase with the pET-16b vector resulted in less complete catalase expression product and a higher amount of lower molecular weight bands. IPTG: isopropylb-D-thiogalactopyranoside.

5.1.3. Affinity purification of recombinant catalase

To isolate the expressed recombinant catalase, affinity purification using Dynabeads was performed taking advantage of the histidine-tagged protein. The incubation of the bacterial lysate containing catalase with the Dynabeads allowed the binding of the histidine to the cobalt beads. Thereafter, the bound catalase was subjected to an elution process using three different molarities of the imidazole elution buffer (100, 250, and 500 mM). The purity and the size of the eluted recombinant catalase protein was analyzed by SDS-PAGE and Coomassie brilliant blue staining. The lysate before and after the Dynabeads incubation, the supernatant resulting from each washing step, the eluted protein, and the used beads were loaded onto a 12 % SDS-gel (**Figure: 16**) and the membrane was probed using anti His-Tag as primary antibody.

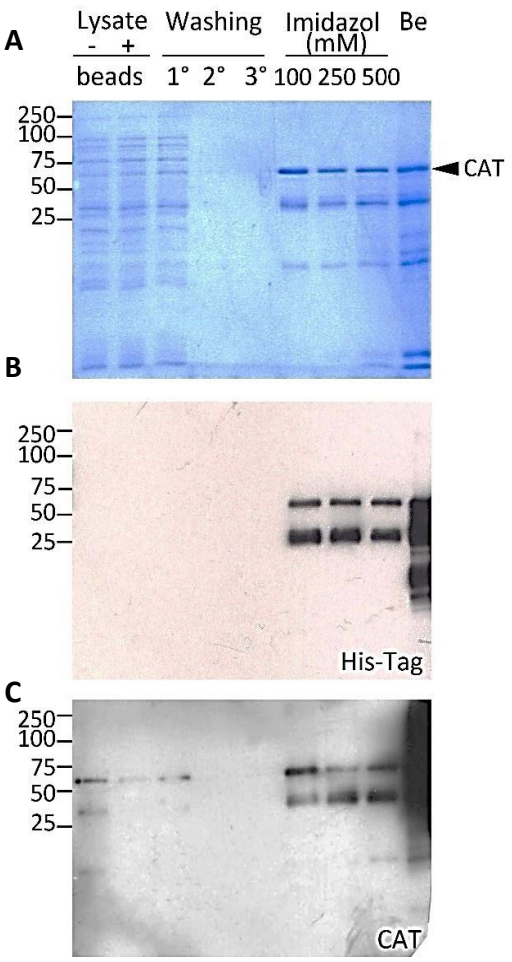

Figure: 16. Detection of the recombinant catalase by SDS-PAGE after Imidazole-elution. A: Coomassie brilliant blue staining of protein samples from the different steps of catalase purification after SDS-PAGE. The first two lanes correspond to the total bacterial lysate before and after being incubated with the Dynabeads. Lanes 3-5 show the flow-through collected after 3 subsequent washing steps; lanes 6-8 represent the recombinant catalase eluted from the beads using different imidazole concentrations. The last lane shows the beads (Be) after elution. The same volume (10 µl) was loaded for each sample. **B**: Corresponding Western blot analysis using an anti His-Tag antibody for the detection of the tagged recombinant catalase. **C**: Western blot analysis of the eluted protein detected by an anti-catalase antibody. The predicted molecular weight of approximately 58 kD for the recombinant catalase plus one band of ~30 kD were labelled with both antibodies, whereas a smaller band of ~10 kD was only present in the Cat blot, suggesting that this was the cleaved C-terminal part of the catalase protein.

Two clear bands were identified in the eluted sample corresponding to 58 kD and ~30 kD respectively (**Figure: 16B**). To verify the identity of the bands, the same membrane was stripped and re-probed using a commercially available anti-catalase antibody. The efficiency of the stripping procedure was confirmed prior to the analysis by incubation with the secondary antibody alone (data not shown). Both bands obtained after the catalase labeling corresponded to those observed previously using the anti-His-Tag antibody (**Figure: 16C**).

Even though imidazole eluted part of the recombinant catalase from the Dynabeads, the SDS- PAGE results showed that a significant amount of the protein was still bound to the beads after elution. Therefore, different elution buffers, differing in the detergent composition and imidazole concentration (**Table: 15**), were tested and the eluted protein and the beads were analyzed by SDS-PAGE.

Table: 15. Buffers used in this work for the optimization of the recombinant catalase elution from the Dynabeads.

EB #	PB (mM)	NaCl	Tween 20 (%)	Triton X100 (%)	Triton X114 (%)	SDS (%)	Imidazol (mM)	pH
1	50	2M	0.01	-	-	-	100	8
2	50	2M	0.01	-	-	-	500	
3	50	300 mM	-	0.5	-	-	100	
4	50	300 mM	-	0.5	-	-	500	
5	50	300 mM	-	-	0.5	-	100	
6	50	300 mM	-	-	0.5	-	500	
7	50	300 mM	-	-	-	0.5	100	
8	50	300 mM	-	-	-	0.5	500	

EB: elution buffer; PB: phosphate buffer

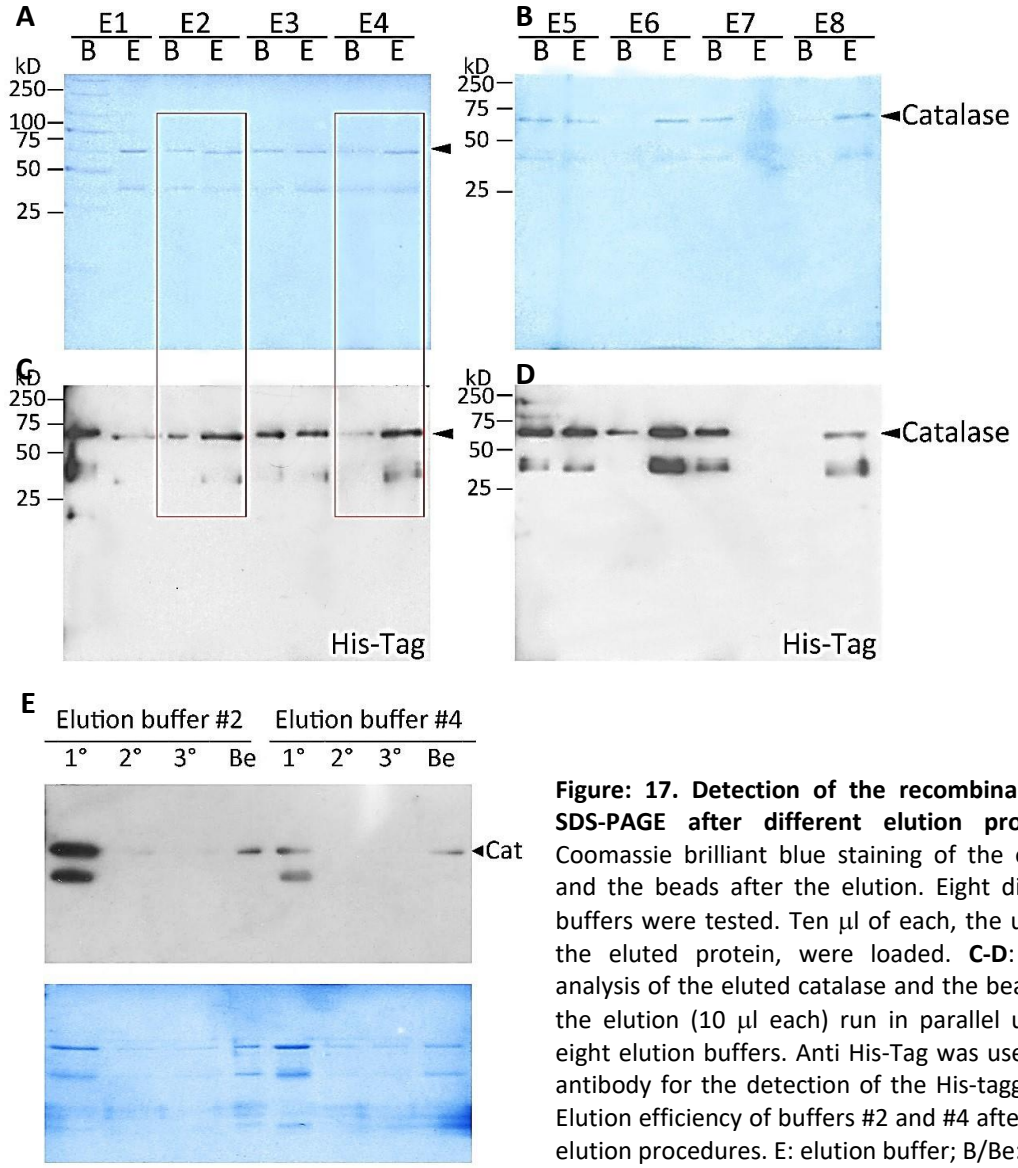

Figure: 17. Detection of the recombinant catalase by SDS-PAGE after different elution procedures. A-B: Coomassie brilliant blue staining of the eluted catalase and the beads after the elution. Eight different elution buffers were tested. Ten µl of each, the used beads and the eluted protein, were loaded. **C-D**: Western blot analysis of the eluted catalase and the beads subsequent the elution (10 µl each) run in parallel using the same eight elution buffers. Anti His-Tag was used as a primary antibody for the detection of the His-tagged catalase. **E:** Elution efficiency of buffers #2 and #4 after 3 consecutive elution procedures. E: elution buffer; B/Be: beads.

After Western blot analysis, we could conclude that the highest amount of catalase was eluted from the Dynabeads using buffers 2, 4, 6 and 8. We opted for the use of buffer

number 2 containing Tween 20 as a detergent agent and buffer number 4 with Triton X100 both containing high imidazole concentrations (500 mM) (**Figure: 17**), because Triton X100 and Tween20 are milder detergents than Triton X114 or even SDS (E8 from figure: 18). In subsequent experiments the elution obtained using the buffer containing Tween 20 (E2 from figure: 18) showed higher elution efficiency (**Figure: 17E**) and therefore we decided to use this elution buffer as standard for the rest of the experiments.

5.1.4. Preparation, purification and characterization of the antibody against catalase

We decided to use the eluted recombinant catalase (600 μg of protein for each animal) to immunize two chickens. The animals were chosen after several preliminary experiments analyzing the chicken preimmune sera as primary antibody on Western blots using 2 different sera dilutions (1:1,000 and 1:10,000) and an anti-chicken secondary antibody. Homogenate protein (10 and 25 μg) obtained from mouse liver and the β-TC3 tumor cell line were used as test-samples for the Western blot analysis (**Figure: 18**). Those chickens were chosen, whose preimmune serum did not result in the detection of protein bands in the Western blot procedure (chicken no. 1 and 3).

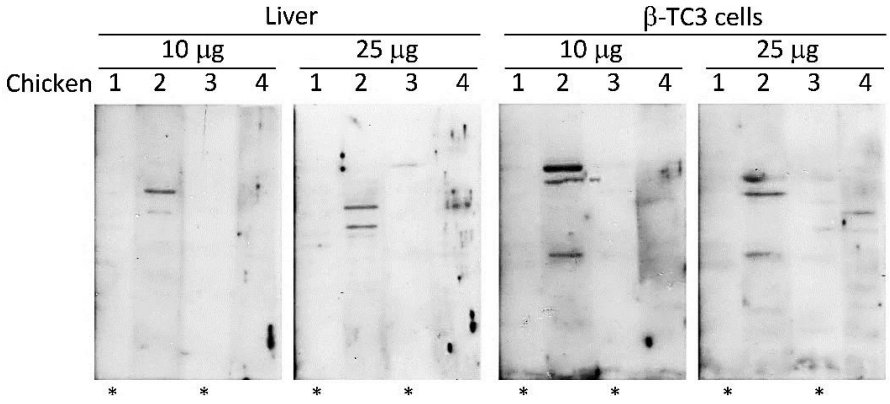

Figure: 18. Selection of chickens after the analysis of the preimmune sera as primary antibody on Western blot. Sera from 4 chickens were collected before the catalase immunization and used at 1:10,000 dilution on Western blot analysis of liver and β-TC3 protein homogenates. The membranes were probed with an HRP-labelled anti-chicken at 1:30,000 dilution. Note that in the animals 1 and 3 (marked with a *) none (using 10 μg of protein either from liver of from β-TC3 cells) or a considerable less amount of bands (in the case of 25 μg of protein used) were detected in comparison with the chicken number 2 and 4.

The animal immunization was carried out by Pineda Antikörper-Service, Berlin (www.pineda-abservice.de). After the 3rd boosting (repeated injection of the catalase antigen), the sera were collected from the chickens and tested by Western blot analysis of protein samples derived from liver, pancreas and β-TC3 cells (data not shown). Additionally, IgY was precipitated and purified also from the obtained egg yolks and the specificity of the

antibody against catalase was verified by Western blot analysis of the same samples as mentioned before. In all three samples catalase could be successfully detected using the sera as a primary antibody.

Twenty µg of protein homogenate from β-TC3 cells were used to test different antibody dilutions (1:2,000; 1:5,000; 1:10,000 and 1:20,000) in order to estimate the best concentration to use for the detection of catalase by Western blot analysis. Subsequently, the membrane was probed with HRP-conjugated anti-chicken IgY antibody (**Figure: 19**). The highest dilution used for this experiment revealed a single band at the expected kD range (~58 kD) and minimal background indicating the monospecificity and high sensitivity of the catalase antibody.

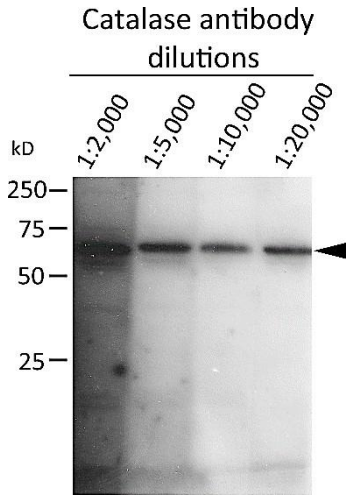

Figure: 19. Characterization of the chicken anti-catalase antibody. Western blot analysis of catalase expression using the IgY anti-catalase antibody purified from egg yolk. The antibody detected catalase in 20 µg protein homogenate from β-TC3 cells at different dilutions. 1:20,000 resulted in a clear band around the expected 58 kDa with minimal background. The membrane was probed with HRP-labelled anti-chicken IgY antibody.

Based on the above-mentioned results, we chose to further determine the antibody specificity by Western blot analysis at 1: 20,000 dilution using total protein homogenates of different mouse tissues (**Figure: 20**). Western blot analysis showed that a band of the expected molecular weight of 58 kDa was present in most analysed tissues except for muscle and brain (which showed one single band of lower molecular weight). As expected, in all analysed tissues more than one band could be detected after overexposure. The phenomenon of different band sizes could be due to the presence of different isoforms of catalase o protein degradation (since the samples were frozen and thawed repeatedly prior to this experiment for another purposes). As shown before in this work, the detection of catalase using our antibody in protein homogenates from β-TC3 cells resulted consistently in one single 58 kDa band (**Figure:19**). After the antibody was isolated, all detections of

catalase for Western blotting in the experimental work of this thesis were performed using this antibody.

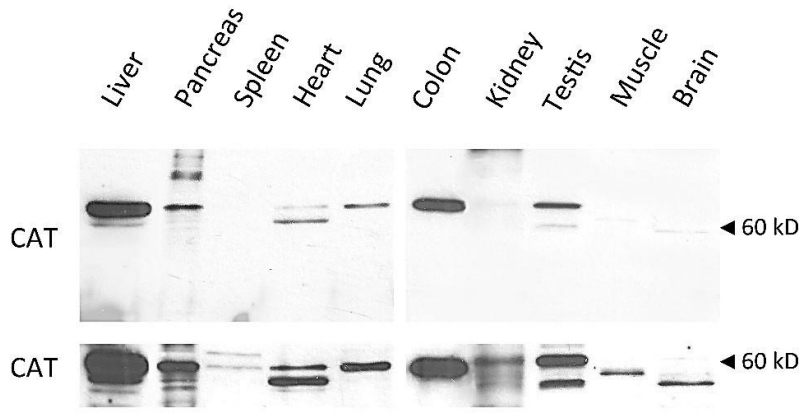

Figure: 20. Antibody specificity against catalase analysed in different murine tissues. Western blot analysis of the purified polyclonal IgY anti-catalase antibody. Twenty μg of total protein from different murine tissues were analysed by SDS-PAGE. Upper panel: obtained after 1 minute of exposure. Lower panel: prolonged exposure to observe the appearance of additional specific bands.

5.2. Characterization of peroxisomes in pancreatic tissue

5.2.1. Peroxisomal gene expression in pancreatic β-cells

Peroxisome-related gene expression profiling is a useful tool for studying the role of peroxisomes in β-cells either in normal or pathological conditions. However, isolated islets undergo changes in gene expression as a result of the cell exposure to the trauma of ischemia during their isolation [(180)]. This problem can be overcome by dissecting the β-cells from the pancreatic tissue directly by laser capture microdissection (LCM). Employing this technic on pancreata is particularly challenging due to the high RNase activity found in this tissue (total RNase activity is a 181,000-fold higher than in brain) [(181)]. Therefore, a LCM protocol was developed to obtain non-degraded, high quality RNA required to analyze the peroxisome-related gene expression by semi-quantitative RT-PCR in pancreatic β -cells. In rodents, unlike in humans, the insulin producing cells are the main cell type located in the core of the islets, therefore only this portion was dissected to minimize the possibility of contamination with other islet cell types. Different tissue treatments including staining and dehydration methods, temperature adjustments, RNase-control measurements, and general handling time shortening were extensively tested to achieve reliable β-cell total RNA isolation. The integrity of the isolated RNA was validated prior to cDNA synthesis by electrophoresis on a denaturing formaldehyde-agarose gel and the RNA bands on the gel were visualized on a UV transilluminator. Due to the relatively small sample size collected

from LCM (2 μg from ~250 dissected pancreatic islets) not more than 0.5 μg RNA was loaded on the gel (**Figure: 21**, lane 1 and 2). Clear but faint *28S* and *18S* rRNA bands were observed for the total RNA sample isolated from LCM β-cells using the optimized protocol (explained under *Material and Methods,* chapter 3.2.6.1.) (lane 1) with a 28S:18S ratio of 1.5:1. An example of a completely degraded RNA corresponding to the β-cells isolated before the optimization of the LCM protocol is shown in the second lane with the appearance of a very low molecular weight smear. As comparison 2 μg RNA isolated from cultured β-TC3 cells are shown in lanes 3 and 4 where the *28S* band appeared twice as intense as the *18S r*RNA band. The presence of sharp bands with a 2:1 ratio is a good indication of the RNA integrity. In conclusion, using the newly developed protocol we were able to drastically reduce RNA degradation during the isolation from pancreatic tissue and to obtain high quality RNA suitable for downstream qPCR analysis.

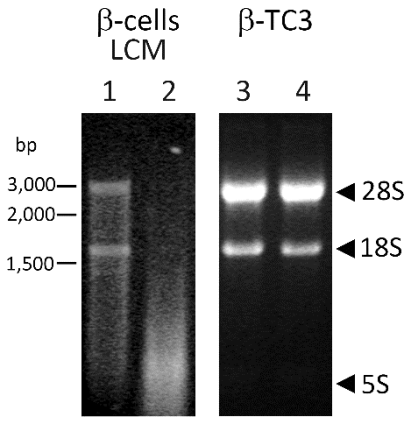

Figure: 21. Formaldehyde-agarose gel analysis to determine the integrity of the LCM isolated RNA. 0.5 μg RNA isolated from pancreatic islets using LCM or 2 μg total RNA obtained from cell culture samples were run on a 1.5 % denaturing agarose gel. Note the maintained RNA integrity of the 28S and 18S rRNA bands after isolating RNA from LCM β-cells using our newly developed protocol (lane 1) in comparison with the standard LCM protocol (lane 2). Lane 3 and 4 represent RNA isolated from cultured β-TC3 cells as control.

Once the RNA quality was assessed, semi-quantitative RT-PCR was used to analyse the steady-state levels of the mRNA encoding peroxisomal proteins in pancreatic β-cells (**Figure: 22**).

Insulin 1 and 2 (*Ins1* and *2*) gene expression were also confirmed in in the isolated β-cells (**Figure: 22G**). As control, glucagon (*Gcg*) gene expression was analyzed. Since this hormone is produced by the α-cells located in the outer rim of the islets of Langerhans, the absence of a band (**Figure: 22G**) denotes the purity of the sample where just the β-cell-enriched central core of the islet was dissected. Some peroxisomal genes such as the membrane lipid transporter *Abcd3* (**Figure: 22C**), the rate-limiting enzyme of the β-oxidation pathway *Acox1* (**Figure: 22D**), *ScpX/Scp2* and *Hsd17β4* (**Figure:22E**) encoding for the sterol carrier protein X (SCPx) /sterol carrier protein 2 (SCP2) and the multifunctional protein 2, respectively,

exhibited a strong expression in β-cells (*ScpX* > *Abcd3* = *Acox1* > *Hsd17β4*). *Pex14* (**Figure: 22B**), *Abcd2* (**Figure: 22C**), *Acca1* (**Figure: 22D**), and *Acox3* (**Figure: 22D**) mRNA were also expressed (*Pex14* > *Acox3* > *Abcd2* > *Acca1*). In comparison, the mRNA expression of the biogenesis peroxin *Pex13* (**Figure: 22B**) was weakly expressed and the mRNA for the lipid transporter *Abcd1* (**Figure: 22C**), and for the β-oxidation enzymes *Ehhadh* and *Acox2* (**Figure: 22D, E**) were almost absent. As expected, *Cat* (**Figure: 22F**) encoding for the antioxidative enzyme Catalase, was extremely low abundant exhibiting only a faint band. In contrast, *Sod1* (**Figure: 22F**) encoding for superoxide dismutase 1, a cytoplasmic antioxidant enzyme, was clearly expressed, however the SOD1 protein possesses a dual localization in the cell with the greatest part in the cytosol and less SOD1 protein in peroxisomes.

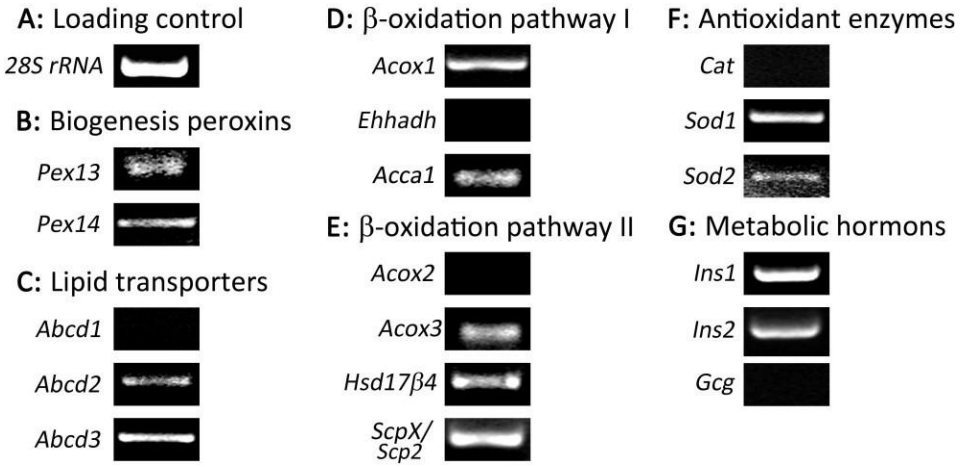

Figure: 22. Semiquantitative RT-PCR analysis of cDNA prepared from total RNA of pancreatic β-cells obtained by laser capture microdissection (LCM). A: *28S rRNA* as internal control; **B:** Gene expression for the peroxisomal biogenesis genes *Pex13* and *Pex14*; **C:** Gene expression for the peroxisomal Abcd-transporters *Abcd1-3*; **D:** Gene expression for the enzymes of the β-oxidation pathway 1, *Acox1*: acyl-CoA oxidase I, *Ehhadh*: multifunctional protein 1, *Acca1*: 3-Ketoacyl-CoA thiolase; **E:** Gene expression for the enzymes of the β-oxidation pathway 2, *Acox2* and *3*: acly-CoA oxidase 2 ad 3, *Hsd17β4*: multifunctional protein 2 and *ScpX/Scp2*: sterol carrier protein X / sterol carrier protein 2; **F:** Gene expression for the peroxisomal antioxidant enzyme *Cat*: catalase, cytosolic/peroxisomal antioxidant enzyme *Sod1*: superoxide dismutase 1, and mitochondrial *Sod2*; **G:** Gene expression for *Ins1* and *2*: Insulin 1 and 2 and *Gcg*: Glucagon.

5.2.2. Peroxisomal proteins are heterogeneously distributed in different cell types of the mouse pancreas

Our group has already described the best conditions for the immunofluorescence-based detection and the precise localization of peroxisomal antigens in diverse tissues [173, 174, 182]. However, murine pancreas presents its own challenges mainly because some antigens used as islet markers (e.g. glucagon) need special experimental conditions in order to be correctly detected. Therefore, the IF technique was optimized in a series of preliminary experiments

(**Figure: 23**) with the purpose of obtaining the ideal conditions for the localization of both, peroxisomal and islet markers. The best antibody concentrations to obtain optimal double-staining patterns for peroxisomal and islet cell markers used for each IF analysis in this work were determined for all antibodies in a set of serial dilution stainings. Samples were exposed to different boiling times (0, 5, 10, and 15 min) in citrate buffer to improve antigen retrieval. The incubation of the samples in non-boiling citrate buffer resulted in a good detection of glucagon but no PEX14 signal (**Figure: 23A**). The gradual increase of the boiling time (5 and 10 min) caused an improvement of the PEX14 signal intensity without compromising the glucagon staining (**Figure: 23B** and **C**). The best results with excellent staining for peroxisomal proteins and still acceptable glucagon stain were achieved by the incubation of the tissue sample in citrate buffer for 15 min (**Figure: 23D**).

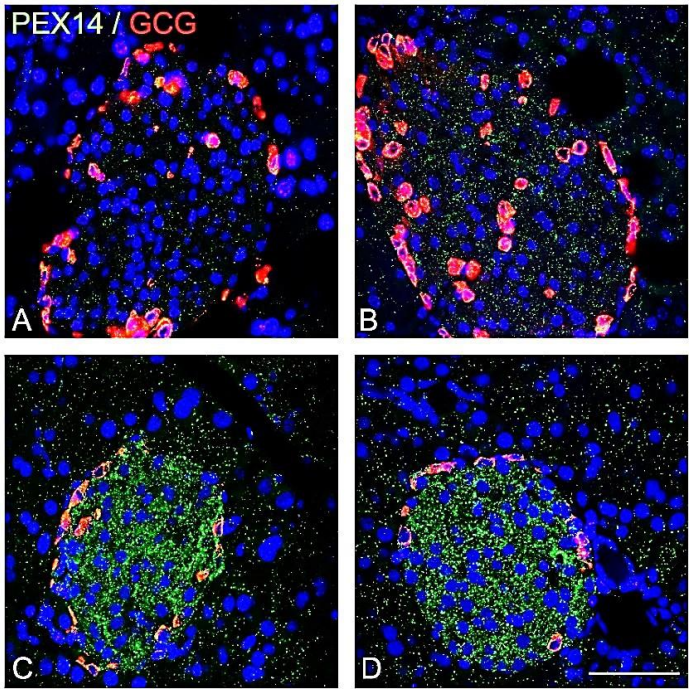

Figure: 23. Optimization of the immunofluorescence (IF) technique to establish the best conditions for the localization of peroxisomal and islet cell markers in mouse pancreata.
IF analysis of paraffin sections of WT C57BL/6J mice against the peroxisomal membrane associated protein PEX14 and Glucagon (GCG). Sections were incubated in citrate buffer **A:** for 15 min without microwaving; **B:** 5 min; **C:** 10 min and **D:** 15 min, in boiling citrate buffer. Nuclei were counterstained with Hoechst 33342 dye. Note the improvement of PEX14 staining with the increase of the microwaving time conserving a good GCG signal. Scale bar = 52 µm.

Using immunofluorescence to detect peroxisomal antigens we could evaluate the distribution of the two peroxisomal biogenesis proteins PEX14 and PEX13 within the different regions of a WT C57BL/6J murine pancreas. PEX14 was detected in both the endocrine (En) and the exocrine (Ex) pancreas showing a less intense signal in the last one. Besides the characteristic punctuate peroxisomal staining pattern, tubular peroxisomes could also be identified, appearing evenly distributed through all the exocrine and

endocrine tissue. In the epithelium of the interlobular excretory duct (IrD) PEX14-labelled peroxisomes were much less numerous (**Figure: 24D-F**).

With regard to PEX13, a markedly overall weaker signal compared to that seen with PEX14 was observed displaying poor labeling of the islets of Langerhans and the exocrine acini showing a similar intracellular distribution of peroxisomes as in PEX14 staining (**Figure: 24G-I**). Furthermore, the IF signal intensity varied in the different pancreatic cell types. Intralobular ducts (InD) were stronger labeled suggesting a higher abundance of PEX13. Generally, PEX13 IF was particularly difficult to perform mainly due to the low expression of this protein in pancreas and because of the autofluorescence of the pancreatic tissue. Similar results have been found for PEX13 staining with the same antibody in an earlier study [173, 183] in which PEX13 labeling was hardly visible in liver or lung tissue, but stained excellently the germ cells in the testis [184]. This suggests that the antibody is specific and reliable, but stains mainly tissues with high PEX13 abundance (e.g. testis).

Two peroxins required for the assembly of the peroxisomal membrane were also analysed by immunofluorescence: PEX3 and PEX19. The PEX3 staining revealed an even distribution of peroxisomes in the basal part of the acini (**Figure: 24J-L**). This pattern composed by dotted structures, was similar to the one observed for ABCD3 but with a difference in the signal intensity. As catalase, PEX3 was clearly detectable in the exocrine part while the endocrine cells were weakly stained. The PEX3 staining for the epithelium of the interlobular excretory duct (IrD) was hardly visible when exposed to the same microscopy settings used for the exocrine part.

Figure: 24. Immunofluorescence localization of peroxisomal proteins PEX14, PEX13, PEX3, and PEX19 in distinct pancreatic regions (see figure on page 60). IF analysis of paraffin sections of WT C57BL/6J mice against: **A-F:** the membrane peroxisomal biogenesis protein PEX14; **G-I:** the membrane peroxisomal biogenesis protein PEX13; **J-L:** the peroxisomal biogenesis factor PEX3; and **M-O:** the peroxisomal biogenesis factor PEX19. Nuclei were counterstained with Hoechst 33342 dye. **A, D, G, J, and M:** Representative picture of a pancreatic islet of Langerhans; **B, E, H, K, and N:** acini clusters; **C, F, I, L, and O:** Interlobular duct lined by a single layer of cubic cells. **A-C:** corresponding phase contrast microscopic analysis of the PEX14 stained pancreatic regions. En: endocrine pancreas; Ex: exocrine pancreas; IrD: interlobular duct. Scale bar = 20 µm.

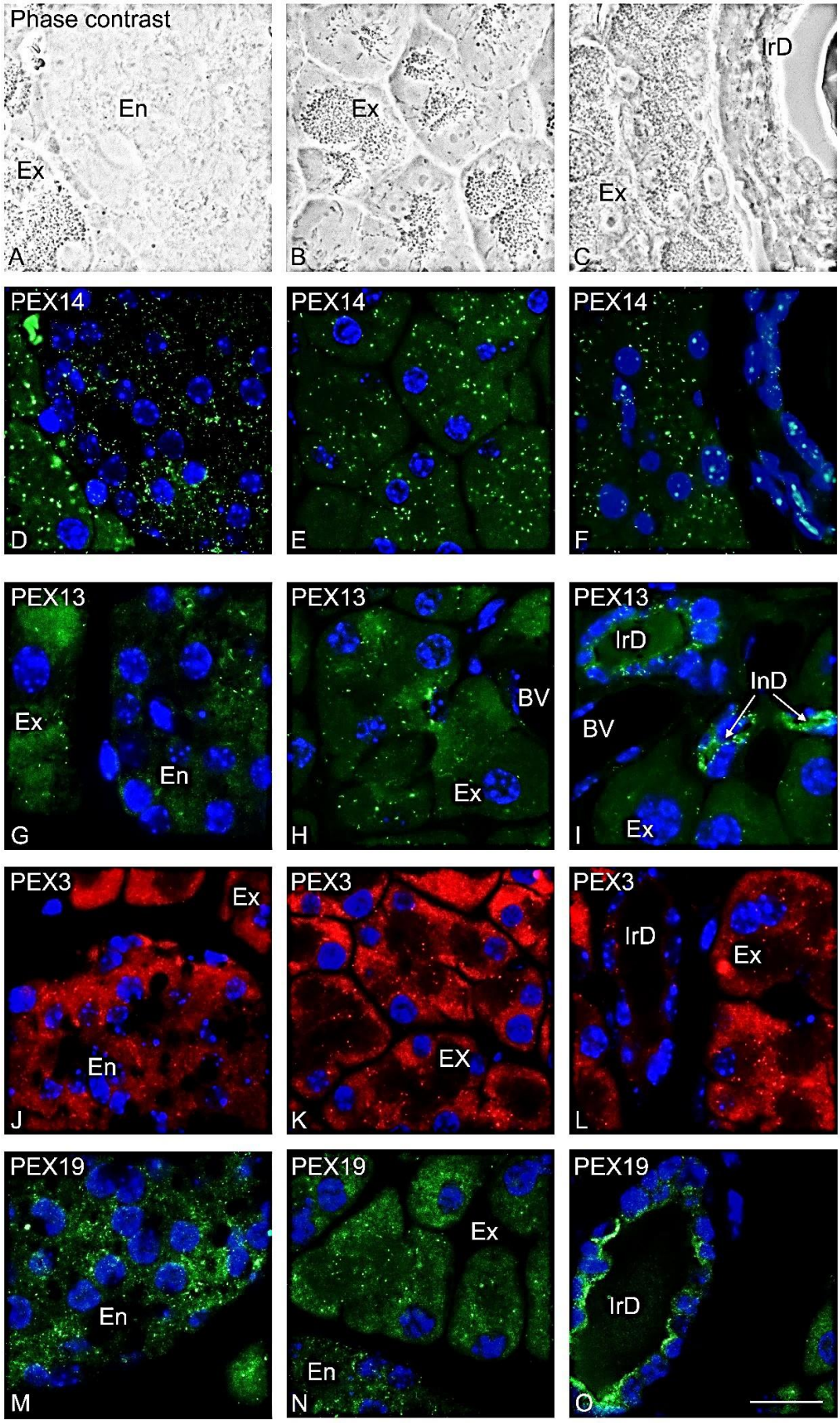
Phase contrast
En
Ex
A
Ex
B
IrD
Ex
C
PEX14
D
PEX14
E
PEX14
F
PEX13
Ex
En
G
PEX13
BV
Ex
H
PEX13
IrD
InD
BV
Ex
I
PEX3
Ex
En
J
PEX3
EX
K
PEX3
IrD
Ex
L
PEX19
En
M
PEX19
Ex
En
N
PEX19
IrD
O

PEX19 is a cytoplasmic receptor that binds PMPs and targets them to the peroxisome by binding to PEX3. It therefore exhibits a double subcellular localisation, which is particularly noticeable in the acini of the exocrine pancreas. In comparison, the PEX19 staining of the islet of Langerhans was not particularly strong (**Figure: 24M** and **N**). In contrast to PEX3 and PEX14, PEX19 exhibited, like catalase, a strong perinuclear staining in the excretory duct (**Figure: 24O**).

The sub-cellular localization of catalase (CAT) differed considerably across the different sections of the tissue. In pancreatic endocrine cells the peroxisomal staining for CAT was almost absent as shown by the low intensity of the immunofluorescence signal localized to the islets of Langerhans (**Figure: 25G** and **H**). The enzyme was mainly detected in peroxisomes of endothelial cells within the islet. In contrast the epithelial cells of the acini showed a defined and uniformly distributed peroxisomal signal exhibiting a punctuated staining pattern. A higher abundance of peroxisomes positive for CAT was noted in the interlobular ducts (IrD) where a perinuclear distribution was observed (**Figure: 25I**).

ABCD3, one of the highest abundant peroxisomal membrane proteins involved in the transport of branched and long-chain acyl-CoAs, and frequently used as a peroxisomal marker, was abundantly expressed in pancreatic cells showing the highest intensity in the endocrine portion (**Figure: 25D** and **E**). Similar to the pattern observed for PEX14, a fine punctuated staining as well as tubular structures could be identified in the exocrine (Ex) pancreas. However, the peroxisomal staining was not evenly distributed across the exocrine portion; here the most apical part of the acinar cells containing zymogen granules showed an absence of immunofluorescence signal. ABCD3 positive peroxisomes were mainly located in the lower apical part of the cells between the nucleus and the secretory granules (**Figure:25F**).

Insulin and glucagon, both peptide hormones produced in the islets of Langerhans, were used as marker proteins for the visualisation of respectively pancreatic β- and α- cells by immunofluorescence analysis. The insulin staining showed the characteristic punctuate pattern associated with this protein, which is stored in secretory granules distributed throughout the cytoplasm of the β-cells (**Figure: 25J**). The α-cells, which are mainly located in the outer rim of the islets, showed an intense fluorescence signal resulting from the detection of glucagon (**Figure: 25K**).

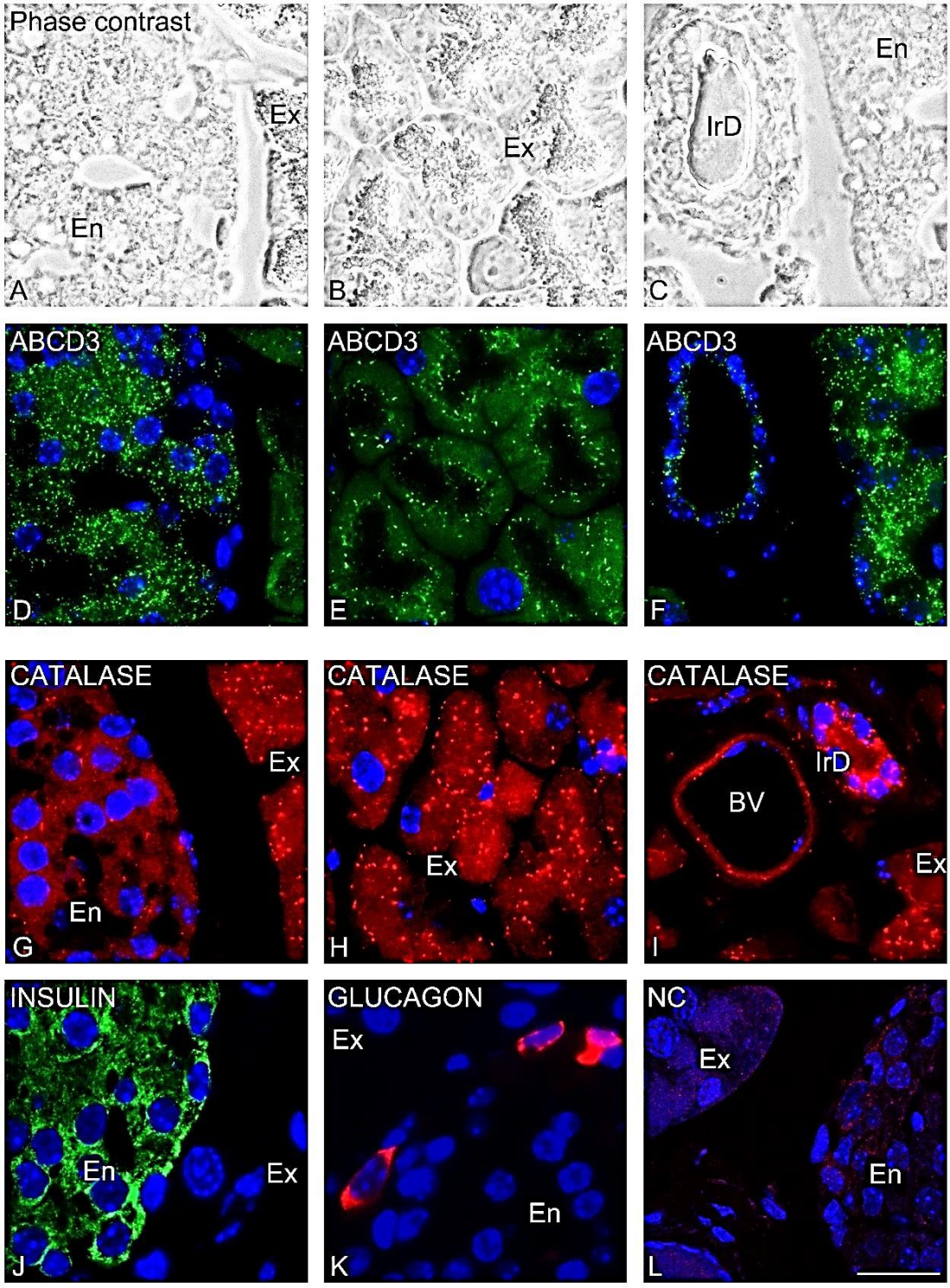

Figure: 25. Immunofluorescence localization of ABCD3, catalase, insulin and glucagon in distinct pancreatic regions. IF analysis of paraffin sections of WT C57BL/6J mice against **D-F:** the peroxisomal membrane lipid transporter ABCD3; **G-I:** the peroxisomal antioxidant enzyme catalase; **J:** Insulin, a hormone produced by β-cells and **K:** Glucagon, produced by α-cells. **L:** Secondary antibody control. Nuclei were counterstained with Hoechst 33342 dye. **A, D, G, J and K:** Representative picture of a pancreatic islet of Langerhans; **B, E, H:** acini of the exocrine pancreas; **C, F, I:** Interlobular duct lined by a single layer of cubic cells. **A-C:** Phase contrast microscopic analysis of the section stained for ABCD3. En: endocrine pancreas; Ex: exocrine pancreas; IrD: interlobular duct; BV: blood vessel. Scale bar = 20 µm.

5.2.3. Protein abundance of PEX13, ACOX1, ABCD3 and CAT present in enriched peroxisomal fraction from pancreata in comparison with liver

Liver is widely used as a standard tissue for the detection of peroxisomes due to the high amount of the organelle found in it. To compare the peroxisomal protein abundance between pancreas and liver Western blot analysis was performed using a peroxisomal enriched fraction isolated from both tissues. All peroxisomal proteins detected, including PEX13, ACOX1, ABCD3 and CAT were less abundant in pancreas in comparison with liver, particularly the β-oxidation rate-limiting enzyme ACOX1 (**Figure: 26**).

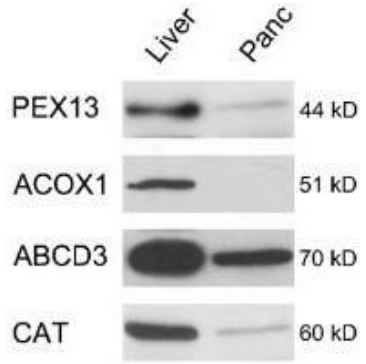

Figure 26: Western blot analysis of enriched peroxisomal fractions isolated from adult mouse pancreas and liver. Pancreatic and liver tissue were isolated from a WT C57BL/6J mice. Proteins (40 µg) were subjected to Western blot analysis and probed sequentially with antibodies against PEX13, ACOX1, ABCD3 and CAT. The autoradiographic signal was visualized as described under *Material and Methods*. The equal loading of liver and pancreas fractions was controlled via Ponceau staining before Western blot incubation with the antibodies against peroxisomal marker proteins. PEX13: peroxisomal biogenesis factor 13; ACOX1: acyl-coenzyme A oxidase 1; ABCD3: ATP- binding cassette transporter, subfamily D, member 3; CAT: catalase.

5.2.4. Alteration of peroxisomal protein abundance in paraffin-embedded pancreas tissue of diabetic animal models

To the best of our knowledge, little information is available concerning the impact that diabetes has on enzyme composition and functionality of peroxisomes. Also, the potential involvement of this organelle during the pathogenesis of diabetes has not been investigated so far. To analyze the alterations of peroxisomal abundance and proteome that might result from the type 2 diabetes (T2D) condition, pancreata from 2 animal models were analyzed by IF: i) The ob/ob mice and ii) The New Zealand Obese (NZO) mice maintained under a high-fat diet. The paraffin-blocks of the diabetic animal models and appropriate control tissue was kindly provided by Dr. Schürmann (Deutsches Institut für Ernährungsforschung, Potsdam).

Paraffin embedded pancreata from these mice were thin sectioned (1µm) for comparative IF analysis using different peroxisomal markers and the α- and β- cell markers glucagon and insulin respectively. The thickness of all sections was determined by xzy-scans (vertical scans) with a CLSM (pinhole: airy 1, objective: 63 x, zoom: 8) to corroborate that the obtained sections displayed the same thickness.

The detection of PEX14, the optimal peroxisomal marker, allowed the evaluation of this organelle distribution and abundance in the analysed sections. Control animals displayed the same IF staining pattern as already observed in this thesis for WT C57BL/6J animals. Punctuated peroxisomal staining and elongated tubular peroxisomes were identified in the endocrine part and in the exocrine portion of the tissue, albeit the staining of the exocrine part was weaker (**Figure: 27A**). In comparison to WT mice pancreata the IF analysis of the NZO diabetic animals kept under a high-fat diet, displayed a much stronger PEX14 immunoreactivity as well as a higher number of peroxisomes ($p \leq 0.03$) and peroxisomal clusters in the endocrine islets suggesting peroxisomal proliferation (**Figure: 27B**).

Further, the abundance of ABCD3 (the most abundant peroxisomal lipid transporter in pancreas) and MFP2 (involved in the peroxisomal β-oxidation pathway 2) were analysed (**Figure: 27C-F**). For this series of experiments, we used a different antibody than for the WT C57BL/6J animals, due to the antibody availability at that time. In a series of preliminary experiments different antibody concentrations were tested and the best one was used for the identification of ABCD3. In the control animals, a peroxisomal staining was clearly visible in the endocrine cells whereas a very low signal was observed in the exocrine region, however, being detectable after longer exposure times (**Figure: 27C**). In the contrary to what we observed for PEX14, the labelling intensity of ABCD3 in the islets of the NZO diabetic animals was drastically decreased in comparison with the one for the control animals (**Figure: 27D**).

Whit regard to MFP2 (multifunctional protein 2 of the fatty acid β-oxidation 2) a slight reduction of immunoreactivity was observed in the NZO diabetic animals in comparison to the controls. In both groups, a peroxisomal signal was observed in the pancreatic endocrine region heterogeneously distributed between distinct cells. As observed also for ABCD3, only a very faint staining was present for MFP2 in the acini showing no changes between control and NZO diabetic tissue (**Figure: 27E** and **F**).

We further detected insulin in the pancreatic islets from the control and the NZO diabetic animals. As expected, a punctuate pattern of high intensity was observed in the control group, representing the insulin stored in secretory granules present inside the β-cells. Numerous clusters of granules were observed (**Figure: 27G**). Insulin was barely detectable in the β-cells from the NZO diabetic samples, leading to the hypoinsulinemia commonly found in this animal model (**Figure: 27H**).

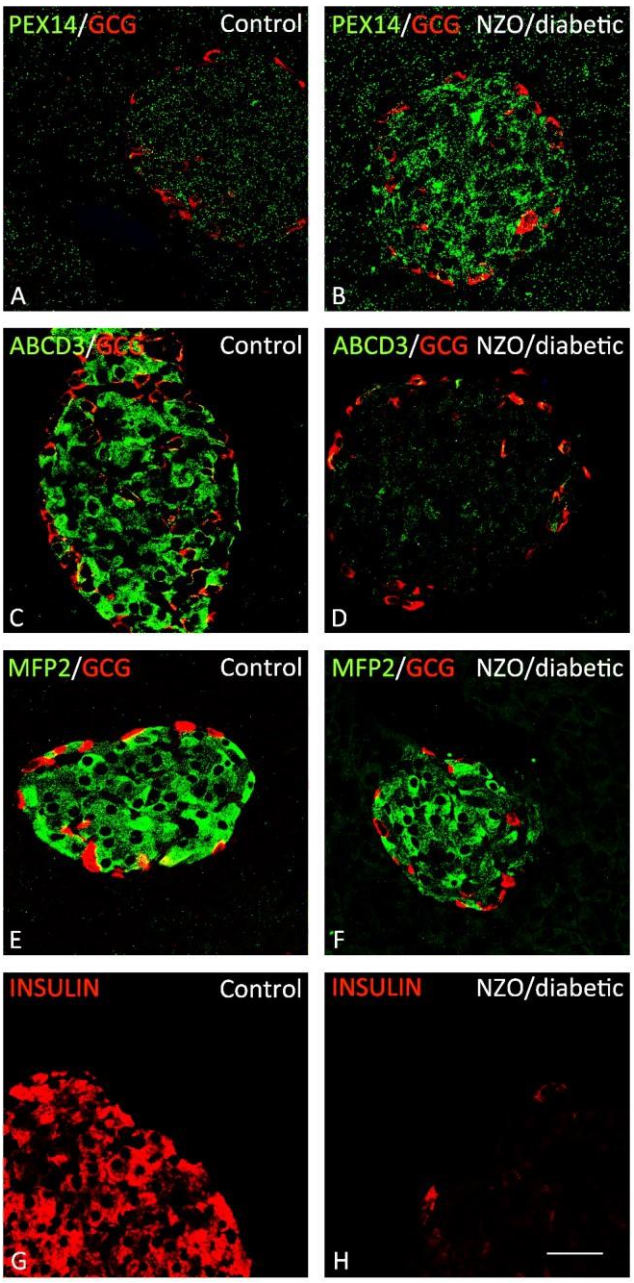

Figure: 27. Double-immunofluorescence analysis of peroxisomal proteins with glucagon signal and for insulin in pancreata of NZO diabetic and control animals. IF analysis of 1 µm sections of paraffin-embedded pancreata. **A-B:** The membrane-associated peroxisomal biogenesis protein PEX14 and the α-cell hormone glucagon (red) were labelled. The abundance of PEX14 in the NZO diabetic islets was higher than in the controls. **C-D:** The IF analysis of ABCD3 showed opposite alterations compared to PEX14: the expression of the lipid transporter was considerably decreased in the islets of the NZO diabetic animals. **E-F:** A slight reduction was observed after MFP2 labelling in the NZO diabetic animals. **G-H:** Insulin (INS) staining exhibiting a clear signal localized to β-cells corresponding to secretory granules of control animals in comparison to the almost absent staining found in the pancreas of NZO diabetic mice. Bar = 52 µm.

In the ob/ob mice fed with a high-fat diet, the expression of PEX14, which was strongly up-regulated in the endocrine pancreas of NZO diabetic animals, was scarcely increased in comparison to the controls (**Figure: 28A** and **B**). PEX14 exhibited a defined and uniformly distributed fluorescent signal showing a punctuated pattern with some elongated peroxisomes and peroxisomal clusters in the islets. In the exocrine part of the pancreas the PEX14 staining was less intense and sparsely distributed. The ABCD3 staining revealed a strong down-regulation of the peroxisomal labelling in the ob/ob high-fat diet mouse (**Figure: 28C** and **D**). As before, a strong peroxisomal staining pattern with empty nuclear regions was observed in the islet cells of the control group.

MFP2-positive stained peroxisomes were found in both, the ob/ob control and the high-fat maintained group. However, while the signal was low but more less distributed through the islet in the control group, a punctate pattern with some clusters distributed heterogeneously across the endocrine region of the ob/ob animals fed with a high-fat diet, was observed (Figure: 29E and F).

Opposite to the findings in the NZO animals, the INS immunoreactivity in both ob/ob groups showed a strong signal with a punctuated, cytoplasmic pattern (**Figure: 28G** and **H**) suggesting healthy β-cells. This result was expected since the T2D-like characteristics found in this animal model are due to a leptin mutation and the obesity developed thereafter and not due to a β-cell dysfunction. Taken together, these results indicate alterations in a subset of peroxisomal proteins as a result of the high-fat diet induced diabetic condition.

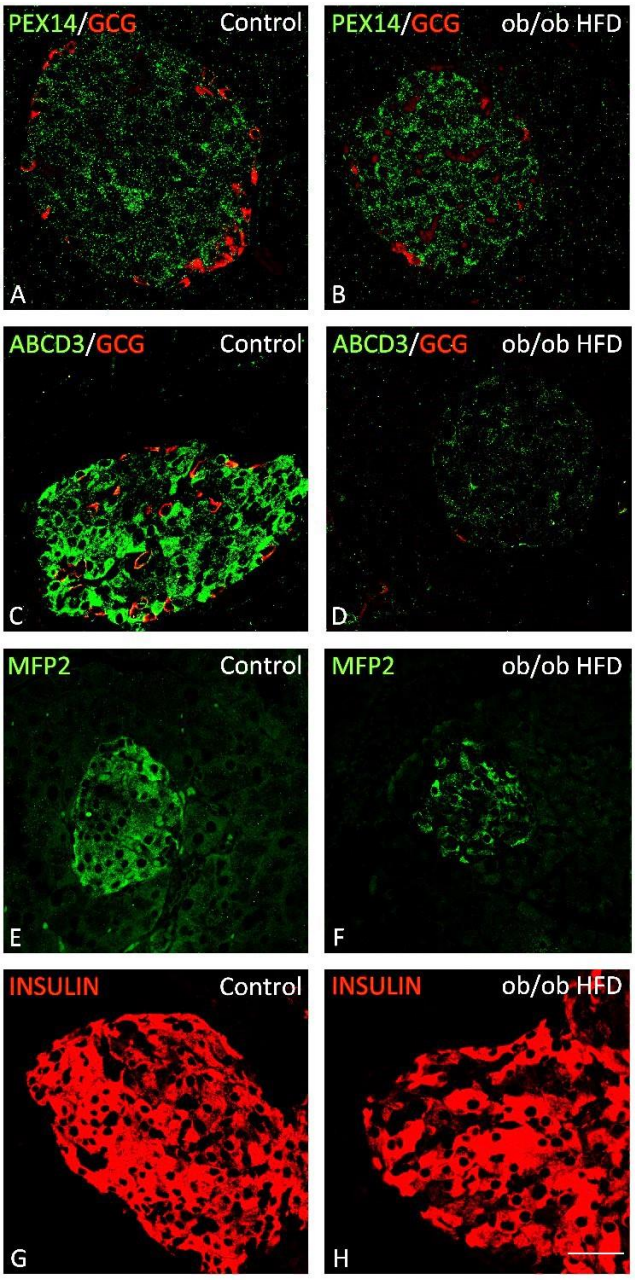

Figure: 28. Double-immunofluorescence analysis of the localization of peroxisomal proteins with glucagon and single staining of insulin in pancreata of ob/ob diabetic animals and its controls. IF analysis of 1 µm sections of paraffin embedded pancreata. **A-B:** The membrane-associated peroxisomal biogenesis protein PEX14 and the α-cell hormone glucagon (red) were labelled. The expression of PEX14 in the ob/ob diabetic islets was slightly higher than in the controls. **C-D:** The IF analysis of ABCD3 showed a considerably decreased abundance of the lipid transporter in the islets of the ob/ob diabetic animals. **E-F:** A MFP2 labelling heterogeneously distributed in some cells of the islets was observed in the ob/ob HFD diabetic-sections in comparison to the control. **G-H:** Insulin (INS) staining exhibiting a clear signal localized to β-cells corresponding to healthy β-cells. HFD: high fat diet. Bar = 52 µm.

5.2.5. Characterization of β-TC3 cell line as a suitable model for the study of β-cell function and peroxisome physiology

To investigate the possible roles of the peroxisome in β-cell dysfunction, the murine line β-TC3 was chosen as a model for the analysis of pancreatic β-cell function. We were first interested to determine whether this cell line could represent a genuine model for the study of the peroxisomal function and dysfunction in pancreas and to ensure its resemblance to normal β-cells. For this purpose β-TC3 cells were exposed to different culture conditions and their mRNA expression profile and morphology were characterized. Our first aim was to determine the optimal CO_2 concentration for cell culture, mainly due to a discrepancy in the recommended parameters given by the supplier and those found in the literature. Two CO_2 concentrations (5 and 8 %) were tested and the abundance of mRNAs for some peroxisomal markers and genes encoding for various antioxidative enzymes were analysed by semi-quantitative RT-PCR (**Figure: 29**). The increase in CO_2 concentration led to a significant increase of the expression of the *Abcd1* and *Abcd2* (1.9- and 2.2-fold higher), genes encoding for membrane lipid transporters in charge of the transport of different very long-chain acyl-CoA. Similarly, the mRNA levels of the β-oxidation pathway 2 enzymes *Hsd17 β4* (also known as *Mfp2*) and *Acox3* showed an up regulation (2.5- and 1.6-fold) under 8 % of CO_2 in comparison with low CO_2 conditions. In contrast, the mRNAs for β-oxidation enzymes *Acox1*, *Acox2*, and *Acca1,* showed a down-regulation (34, 62, and 40 %) when exposed to 8 % CO_2. *Pex13*, *Pex14*, *Abcd3*, and *Cat* mRNA levels were unaffected by the different CO_2 concentrations. The mRNA for *Ehhadh* could not be amplified with the primer pairs and conditions used in this work, suggesting that its expression level in pancreas is too low for being visualised. Interestingly, the three superoxide dismutase antioxidative enzymes showed changes in their gene expression as well. *Sod1* mRNA level decreased (45 %) while the level of *Sod2* and *Sod3* exhibited a minor but clear up-regulation when maintained at 8 % CO_2 (1.2- and 1.5-fold respectively). Since many peroxisomal genes showed higher expression levels in β-TC3 cells cultured with high CO_2 concentration, we decided to carry out our experiments keeping the cells under this culture condition.

This analysis also revealed some differences in the peroxisome-related and antioxidative gene expression of the β-TC3 cells and the LCM-isolated β-cells. *Pex13*, *Abcd1* and *Cat*, all showing next to no mRNA expression in LCM isolated β-cells were expressed at higher levels in the β-TC3 cell line. In the case of *Abcd1* a strong expression was observed in β-TC3 cells,

especially after 8 % CO_2 incubation, contrary to what we observed for the LCM cells. Likewise, *Sod2* a gene encoding for the mitochondrial antioxidative enzyme superoxide dismutase 2, was clearly expressed in the β-TC3 cell line whereas it was very low expressed in LCM isolated β-cells. However, several resemblances were also found: in both the microdissected β-cells and the β-TC3 cells the mRNA level of the β-oxidation enzymes *Ehhadh* and *Acox2* were low abundant while the other peroxisomal genes analysed, including genes encoding for biogenesis proteins, lipid transporters and β-oxidation enzymes were clearly expressed.

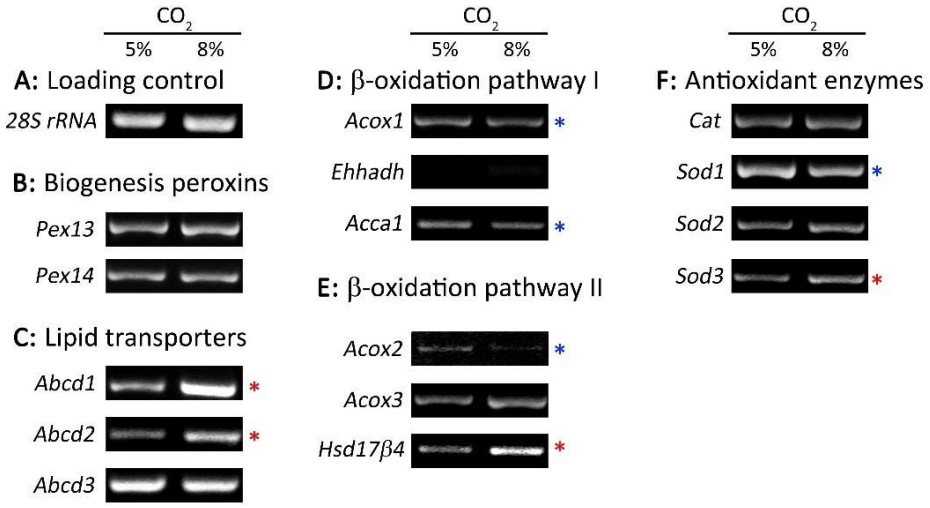

Figure: 29. Semiquantitative RT-PCR analysis of cDNAs prepared from total RNA of β-TC3 cells maintained under different CO_2 conditions. β-TC3 cells were incubated in complete DMEM medium and maintained in two different CO_2 conditions. One µg of RNA was used for semiquantitative RT-PCR analysis. **A:** *28S r*RNA was used as internal control; **B:** Peroxisomal biogenesis genes *Pex13* and *Pex14*; **C:** Peroxisomal ABC-transporters *Abcd 1-3*; **D:** *Acox1*: acyl-CoA oxidase 1, *Ehhadh*: multifunctional protein 1, *Acaa1*: 3-ketoacyl-CoA thiolase; **E:** *Acox2-3*: acyl-CoA oxidase 2-3, *Hsd17β4*: multifunctional protein 2; **F:** Peroxisomal and mitochondrial anti- oxidative enzymes, *Cat*: catalase; *sod 1-3*: superoxide dismutase 1-3. Red stars (*) indicate those genes in which the RNA expression levels increased after the exposure to 8 % CO_2. Blue stars (*) show those genes with a down-regulation after changing CO_2conditions.

A prominent feature of the β-TC3 cell line is its capacity to respond to glucose, the major physiological stimulus of insulin secretion from normal β-cells, hence we tested the effect of different glucose concentrations and length of exposure to determine the best conditions for the stimulation of insulin production and secretion. For this purpose, cells cultured for 48 h in standard DMEM medium (containing 20 mM glucose) were exposed to medium lacking glucose for 30 min, 1, 3, 6, 12 and 24 h and subsequently stimulated for 6 or 12 h with the re-introduction of 20 mM glucose. Controls were kept under standard conditions during the progression of the experiment. Semi-quantitative RT-PCR analysis was carried out to determine the mRNA expression of Insulin 1 (*Ins I*) and Insulin 2 (*Ins II*). Unlike in humans,

rodents possess two insulin genes that are structurally similar but non-allelic. Both genes are functional, but *Ins I* has been shown to be selectively glucose responsive while *Ins II* is responsible of the basal secretion of the hormone [185]. The highest expression of the *Ins I* mRNA levels was obtained using the experimental condition of 0 mM/l glucose for 1 h followed by 12 h of exposure to 20 mM glucose (**Figure: 30**). As expected, *Ins II* expression levels were not affected by the glucose exposure.

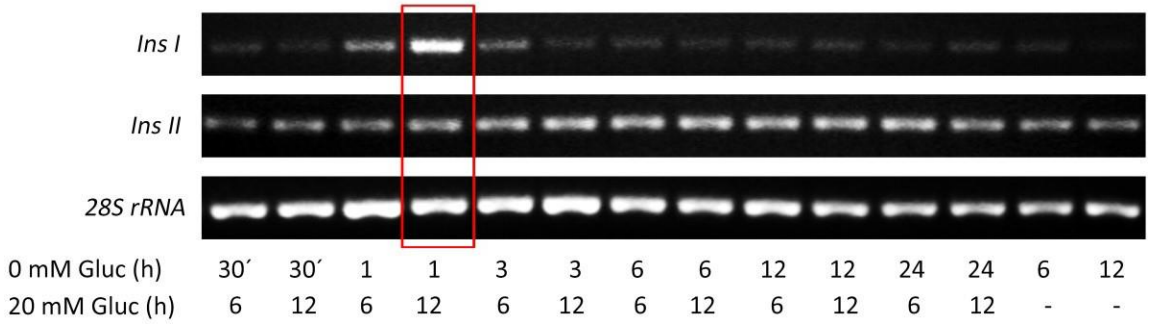

Figure: 30. Semiquantitative RT-PCR analysis of cDNAs prepared from total RNA of β-TC3 cells stimulated with glucose. β-TC3 cells were incubated in DMEM medium containing 0 mM/l of glucose for different time periods and then stimulated with 20 mM/l glucose as described under *Material and Methods*. One µg of RNA was used for semiquantitative RT-PCR analysis. Insulin 1 (*Ins I*) mRNA levels showed an evident up-regulation after the cells were cultured for 1 h in 0 mM/l glucose followed by 12 h 20 mM/l glucose exposure. Insulin 2 (*Ins 2*) showed no changes after treatment. 28S rRNA was used as internal control.

After establishing the best condition for the stimulation of the *Ins I* gene expression, we assessed the capability of the β-TC3 cells to release and store insulin after glucose stimulation using ELISA. Cells cultured with 20 mM glucose for 48 h exhibited low basal (~15µm/l) insulin secretion and responded with a 3-fold stimulation when challenged with 20 mM/l glucose after 1 h in the absence of glucose (**Figure: 31**). The cellular insulin content after glucose stimulation showed a more than two-fold increase compared to those cells maintained at all time with 20 mM glucose (control). β-TC3 cells responded to glucose stimulation releasing and producing insulin resembling normal β-cells.

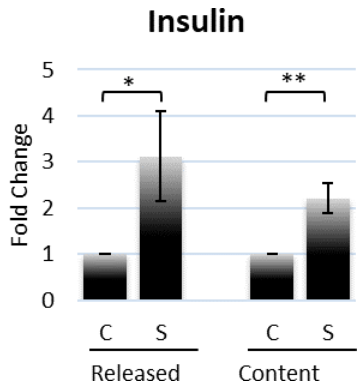

Figure: 31. Insulin released and content in β-TC3 after glucose stimulation. β-TC3 cells were cultured in DMEM lacking glucose for 1 h and then stimulated with 20 mM/l glucose for 12 h. Insulin release was measured by ELISA in the harvested supernatant and corrected for protein concentration. For the calculation of insulin content cells were collected for insulin assay and protein determination. A total protein homogenate was used to determine the protein content via Bradford assay. Values ±SEM represent the insulin fold change levels relative to control sample normalized to total protein from three independent experiments. C: control, S: stimulated. Statistics: Student´s *t-test* for paired values: * = $p \leq 0.05$; ** = $p \leq 0.01$.

To further characterize the β-TC3 cell line, we analysed peroxisomal marker proteins in cells kept under standard conditions (containing 20 mM glucose continuously) (**Figure: 32**) by immunofluorescence staining. The peroxisomal biogenesis proteins PEX14 and PEX13 were detected in punctuate structures representing peroxisomes. However, the abundance of the two proteins was different. The PEX14 signal was intense with some peroxisomal clusters distributed evenly throughout the cytoplasm, whereas the staining for PEX13 was fainter. PEX3 was detectable in β-TC3 cells with very low peroxisomal staining, exhibiting a higher cytoplasmic background than other "peroxisomal" IF-staining. This PEX3 staining pattern is certainly due to its very low protein abundance and the high antibody concentration used. Similarly to PEX14, THIOLASE A (THIO), the terminal enzyme of the β-oxidation pathway I, could be nicely visualized, exhibiting the characteristic peroxisomal staining pattern. Opposite to the findings previously described in this thesis for the detection of CAT in pancreatic islets as well as in LCM-isolated β-cells, β-TC3 cells display a higher content of this antioxidative enzyme. The IF analysis for ABCD3 showed large and strongly immunoreactive tubular as well as some round individual peroxisomes side by side.

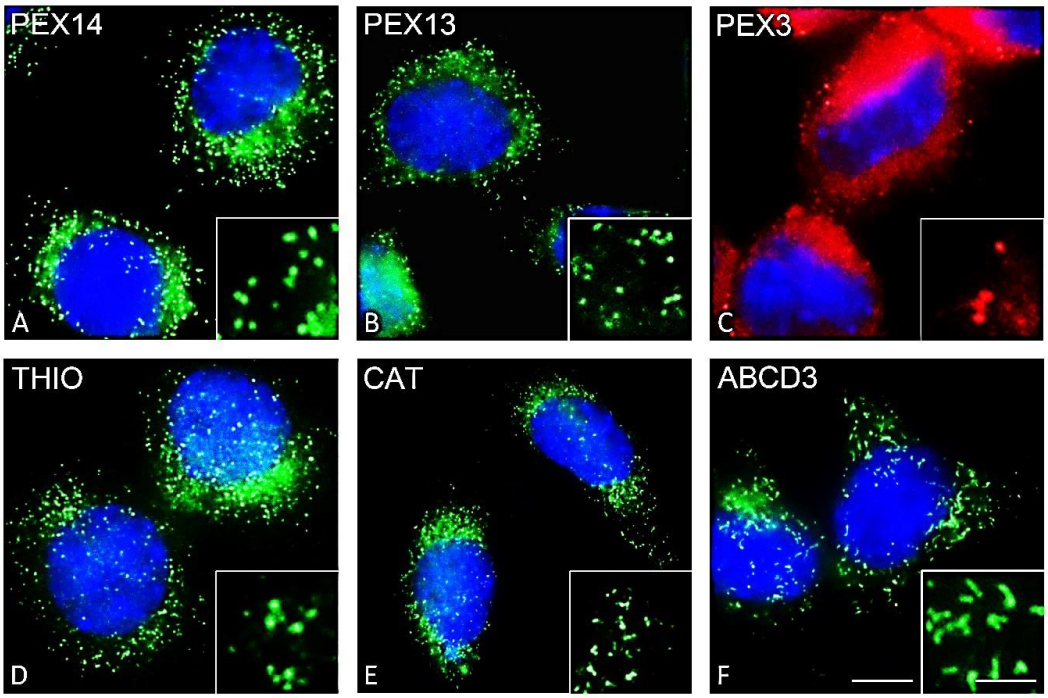

Figure: 32. Immunofluorescence localization of peroxisomal proteins in β-TC3 cells. IF-staining for: **A and B:** the peroxisomal biogenesis proteins PEX14 and PEX13; **C:** PEX3, the peroxin required for the assembly of peroxisomal membrane proteins; **D:** THIOLASE enzyme, part of the peroxisomal β-oxidation pathway 1; **E:** the antioxidative enzyme CATALASE and **F:** the lipid transporter ABCD3.

Taken all together, these results provide good evidence suggesting that the β-TC3 cell line used under the established cell culture conditions, constitutes a useful *in vitro* model for the investigation of both pancreatic β-cell function and also peroxisomal physiology and pathology.

5.3. *Pex13* down-regulation induced peroxisomal deficiency

To better understand the specific role of peroxisomes in pancreatic β-cell physiology, we developed a peroxisome-deficient β-TC3 cell line model. It has been shown that mutations and deficiencies in peroxisomal biogenesis proteins lead to severe peroxisomal biogenesis disorders [68, 81, 186]. The peroxin PEX13 is one of the components of the peroxisomal translocation machinery. It functions as a membrane docking factor for the cytoplasmic PTS1 receptor and is involved in the import of PTS1 and PTS2 proteins into the peroxisomal matrix. To simulate a peroxisomal defect in pancreas, we decided to generate a PEX13 knockdown in β-TC3 cells by using small interfering RNA (siRNA) directed against the *Pex13* mRNA. For this purpose, different transfection methods were tested in a set of preliminary experiments including physical and chemical approaches e.g. microporation and lipofection, respectively. Even though the microporation technique resulted in 85-90 % PEX13 protein down-regulation (data not shown) and catalase mistargeting into the cytoplasm (a characteristic phenotype observed in conditions of peroxisomal deficiency) (**Figure: 33**), this result was not reproducible and the cell viability was seriously affected by the procedure itself.

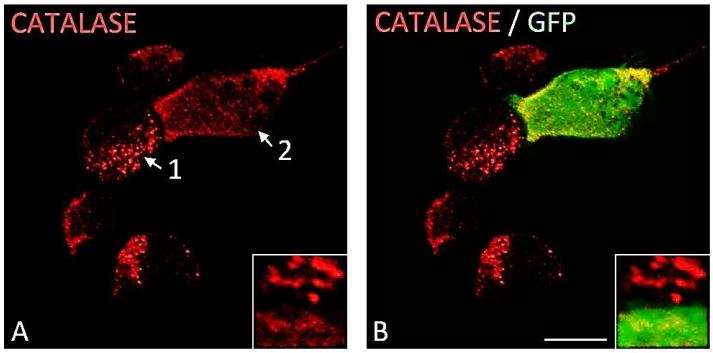

Figure: 33. Immunofluorescence analysis of catalase in β-TC3 cells after *Pex13* knockdown using microporation as a transfection method. Forty-eight hours post transfection, β-TC3 cells were fixed, permeabilized and used for IF analysis. **A:** The peroxisomal antioxidative enzyme, catalase, was detected in those cells not transfected, as punctuate structures representing peroxisomes (1). The mistargeting of catalase into the cytoplasm in β-TC3 cells after the knockdown of *Pex13* (2) demonstrates the disruption of the peroxisomal matrix proteins import. **B:** The microporated plasmid for *Pex13* shRNA contain the gene encoding the green fluorescent protein (GFP) for fluorescence microscopy-based observation of transfected cells. Scale bar = 32 μm.

As an alternative method to introduce the *Pex13*-siRNA into the β-TC3 cells, transfection via lipofection was therefore chosen and optimized. Diverse reagents, time points, and siRNA concentrations were tested to obtain the optimal conditions for *Pex13* mRNA and PEX13 protein down-regulation. As a control, we performed all the transfection experiments in parallel with the corresponding scrambled siRNA (*Scr*-si) that did not result in the down-regulation of the PEX13 protein abundance. Protein samples from the transfected β-TC3 cells were subjected to Western blot analysis 48 h after transfection. Neither the use of ScreenFect A (Wako Chemicals, USA) nor FuGENE (Promega, USA) reagent in combination with 15 or 30 nM *Pex13* siRNA resulted in a significant PEX13 down-regulation (**Figure: 34A**). By using Interferin (Polyplus, FR) as a transfection reagent in combination with 15 nM siRNA we could achieve a ~66 % down-regulation of the PEX13 protein and further improved this result to achieve ~80 % down-regulation of PEX13 protein by employing 30 nM siRNA.

Once the best transfection reagent and siRNA concentration were determined, different time periods of transfection were tested to analyze the duration and stability of the gene silencing and accordingly establish the best conditions for the further experiments using RT-qPCR analysis and Western blotting (**Figure: 34B-C**). Transient transfection of *Pex13* siRNA led to a significant decrease (up to a maximum 85 %) of *Pex13* mRNA expression ($p \leq 0.0001$) compared with the *Scr*-si control group after 48 h of transfection (**Figure: 34C**) and the decrease of PEX13 abundance was stable up to 96 h (**Figure: 34B**), time after which the protein level increased gradually (data not shown).

Figure: 34. siRNA-mediated *Pex13* knockdown in β-TC3 cells as a means of inducing peroxisomal dysfunction (see figure on page 73). A: Different transfection reagents and si-RNA concentrations (15 and 30 nM) were used to establish the right conditions for β-TC3 cell transfection via lipofection. The cells were transfected with *Pex13*-si or *Scr*-siRNA and 48 h after transfection total protein was isolated, 20 µg protein were subjected to SDS-page and Western blot analysis and probed sequentially with antibodies against PEX13 and α-Tubulin. Alpha tubulin was used as a loading control and for normalization. The autoradiographic signals were visualized and quantified as described under *Material and Methods*. **B-C:** β-TC3 cells were transfected with *Pex13*-si (30 nM) or *Scr*-siRNA via lipofection. **B:** Representative immunoblotting showing the reduction of PEX13 in β-TC3 cells after *Pex13*-si transfection at different time-points post transfection. **C:** After 48 h total RNA was isolated and analysed by real-time RT-PCR analysis using the primers for *Pex13* and *Actb*. The average threshold (Ct) values of at least three independent experiments were used to calculate the relative amounts of mRNA using the 2-ΔΔ CT method and normalized to *Actb* values. Values ±SEM represent the *Pex13* expression levels relative to the *Scr*-si transfected sample. Actb: β-actin. Statistics: Student´s *t-test* for paired values: ****: $p \leq 0.0001$.

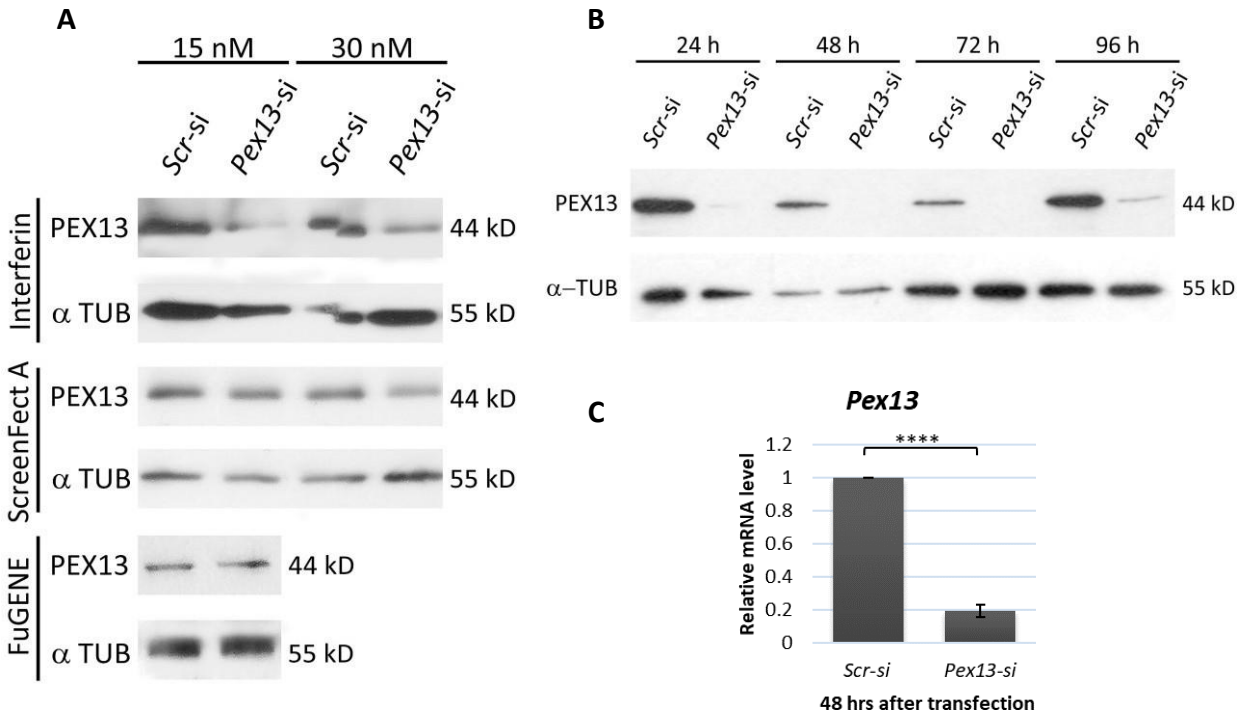

Figure: 34. For figure legend refer to page 72.

5.4. The knockdown of *Pex13* did not affect β-TC3 viability

To determine whether the knockdown of PEX13 affected β-TC3 cell survival, cell viability was assessed using the Trypan blue exclusion test at different time points (48, 72, 96 h) after transfection (**Figure: 35**). Cell survival remained almost unchanged in both groups showing no lethality upon *Pex13* gene silencing.

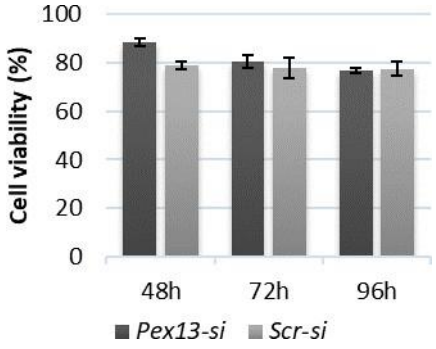

Figure: 35. β-TC3 cell viability was not affected by the down-regulation of *Pex13*. Cells were transfected with *Pex13*-si or *Scr*-siRNA as a control using Interferin transfection reagent. After 48, 72 and 96 h, the Trypan blue exclusion test was used to determine cell viability. The number of intact cells, which exhibited no blue staining, was determined (eight fields per experiment) and percentage of live cells in relation to untreated control is depicted.

5.5. The knockdown of *Pex13* altered peroxisome-related gene expression and protein abundance in β-TC3 cells

To further examine the possible effects of the *Pex13* down-regulation we analyzed the expression level of some key peroxisomal genes involved in lipid transport, β-oxidation and reactive oxygen species (ROS) regulation as well as the transcription factors of the *Ppar*

family (*Ppar* α, β, γ) by standard semiquantitative RT-PCR (**Figure: 36**). The silencing of *Pex13* in β-TC3 cells resulted in a significant increase (1.5-fold) of *Ppar*γ mRNA levels 48 h post transfection. No significant alteration was seen for PPARβ mRNA whereas the PPARα mRNA could not be amplified with two different primer pairs used, even though these primers were successfully used from other doctoral candidates for total RNA of other organs. By contrast, *Abcd3, Cat* and *Acox1* showed a decrease in their mRNA levels (64 %, 86 %, and 77 % respectively). For the calculation of the differences in the mRNA expression levels, the PCR band intensities of peroxisome-related genes and *Ppar*s were normalized for the band intensity of the *28S r*RNA of the same cDNA preparation.

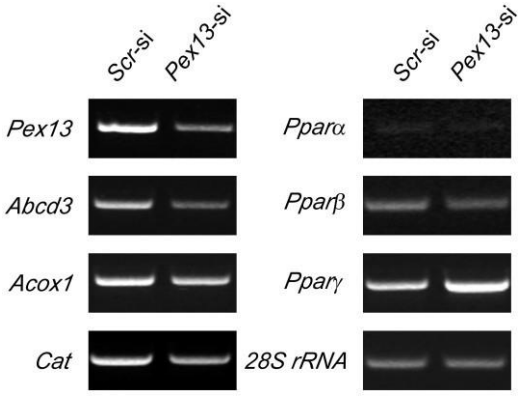

Figure: 36. Semiquantitative RT-PCR analysis on cDNAs prepared from total RNA from β-TC3 cells after *Pex13* down-regulation. Cells were transfected with *Pex13*-si or *Scr*-siRNA and 48h post transfection, total RNA was isolated and 1 µg was reverse transcribed and used for semiquantitative RT-PCR analysis. mRNAs for: *Pex13*: Peroxin 13; *Abcd3*: ATP-binding cassette, subfamily D (ALD), member 3; *Acox1:* acyl-CoA oxidase 1; *Cat*: Catalase; *Ppar*α, β, γ: Peroxisome proliferator-activated receptors α, β and γ; *28S rRNA* as internal control.

Once evaluated the peroxisomal gene expression on the *Pex13* knockdown background, the effect of the *Pex13* silencing on the abundance of PEX13, PEX14, CAT, and ABCD3 was assessed by immunofluorescence analyses. After PEX13 labelling *Scr*-si transfected cells showed a clear punctuate peroxisomal pattern with some cytoplasmic background (**Figure: 37A**). PEX13 staining in *Pex13*-si transfected cells was almost absent, showing only very few individual peroxisomes evenly distributed throughout the cell (**Figure: 37B**). This corresponds well to the results obtained by Western blot analysis showing that approximately 20 % of the protein was still present in the cells. PEX14, which is a part of the docking complex in the peroxisomal membrane and binding partner of PEX13, was detected in the *Scr*-siRNA transfected cells as small dots as well as larger aggregates, which were identified as single peroxisomes as well as peroxisomal clusters (**Figure: 37C**). Interestingly, the down-regulation of PEX13 resulted in a change of peroxisomal morphology and intracellular distribution of PEX14, however, with no change in the signal intensity. In comparison to cells transfected with *Scr*-si, peroxisomes did not appear as single dots and aggregates but in the majority as tubular structures (**Figure: 37D**).

As explained previously, PEX13 is essential for the proper import of peroxisomal matrix proteins and its depletion leads to the mistargeting of peroxisomal matrix proteins to the cytosol where they might be degraded or not. As expected, instead of the usual peroxisomal pattern (observed in the *Scr*-si transfected cells) *Pex13*-siRNA transfected β-TC3 cells labeled with an anti-catalase antibody showed a faint nuclear staining (even after prolonged exposure times), most likely due the mistargeting of the protein (**Figure: 37E** and **F**).

The immunofluorescence analysis of ABCD3 in the *Scr*-si transfected cells showed many positive-stained peroxisomes, with clear dots as well as many tubular structures. However, in contrast to the results observed for the *Abcd3* mRNA levels, the silencing of *Pex13* resulted in an increase of the ABCD3 immunofluorescence signal (**Figure: 37G** and **H**), the molecular mechanisms of which has to be elucidated in future studies.

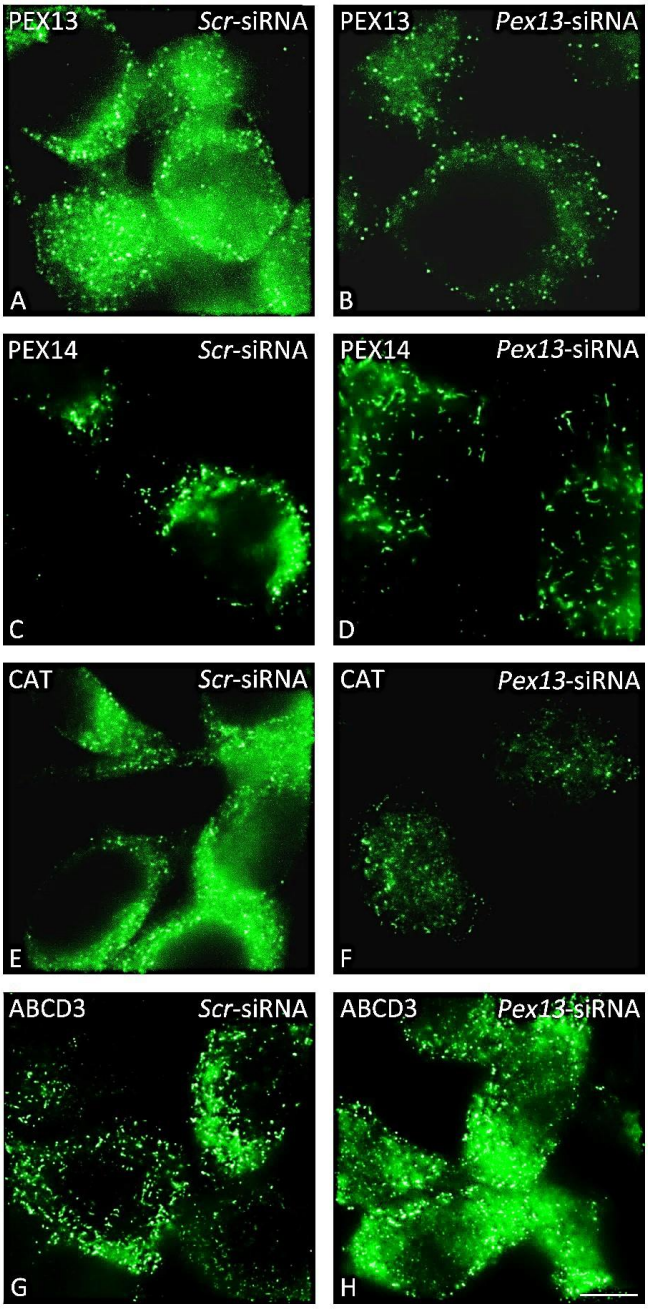

Figure: 37. Immunofluorescence analysis of PEX13, PEX14, CAT, and ABCD3 after *Pex13* silencing in β-TC3 cells. 48h after the siRNA treatment, the cells were fixed, permeabilized and used for IF analysis. **A-B:** IF staining for PEX13 localization in (**A**) control cells transfected with *Scr*-siRNA and (**B**) cells transfected with *Pex13*-siRNA; **C-D:** IF analysis for PEX14 localization in (**C**) *Scr*-siRNA and (**D**) *Pex13*-si transfected cells; **E-F:** IF analysis of Catalase localization in (**E**) *Scr*-siRNA and (**F**) *Pex13*-siRNA transfected cells. **G-H:** ABCD3 IF staining in Control *Scr*-siRNA and *Pex13*-si transfected cells respectively.
Scale bar = 15μm.

5.6. Reactive oxygen species (ROS) production in β-TC3 cells after *Pex13* down-regulation

Since the knockdown of *Pex13* leads to the mislocalization of catalase to the cytosol, an enzyme playing a central role in the oxidative stress management of the cells, its effects on the accumulation of ROS in comparison to wild type (WT) and *Scr*-si transfected cells were examined. Two fluorescent dyes, dihydroethidium (DHE) and dichlorodihydrofluorescein diacetate (H2-DCFDA) were used to detect superoxide and hydrogen peroxide (H_2O_2) production, respectively. These experiments revealed that in *Scr*-siRNA treated cells the amount of superoxide was significantly increased ($p \leq 0.0001$) in comparison with the non-treated cells (WT) as shown by the DHE staining (**Figure: 38A, B** and **G**). Interestingly, after *Pex13*-siRNA transfection, the signal intensity of the DHE staining was significantly lower ($p \leq 0.0001$) than the one observed in the *Scr*-siRNA transfected cells (**Figure: 38B, C** and **G**), nearly reaching the WT levels again.

On the other hand, the silencing of *Pex13* led to a notable increase in the H_2O_2 levels in comparison with to the *Scr*-si transfected cells ($p \leq 0.0001$) (2.5-fold) (**Figure: 38E, F** and **H**) as well as with the WT control group (5-fold) (**Figure: 38D-F** and **H**) as shown by the DCFDA staining. The fluorescence signal in β-TC3 cells after *Scr*-siRNA treatment revealed a weak but significant increase in its intensity in comparison to the WT control group.

Next to testing the amount of oxidative stress generated after the down-regulation of PEX13, we also analysed whether the abundance of key enzymes of the oxidative stress management were affected. Western blot analysis of the peroxisomal antioxidative enzyme catalase showed slightly reduced protein levels in *Pex13* KD cells after 48 h of transfection, whereas no significant changes were observed 24 h post-transfection (**Figure: 38I**), despite the fact that the protein was mistargeted to the cytoplasm (**Figure: 37E** and **F**). Moreover, the abundance of the mitochondrial antioxidative enzyme superoxide dismutase 2 (SOD2) was slightly increased by the *Pex13*-siRNA transfection after 48 h, which could explain the shift of O^{2-} to H_2O_2 production (**Figure:38I**).

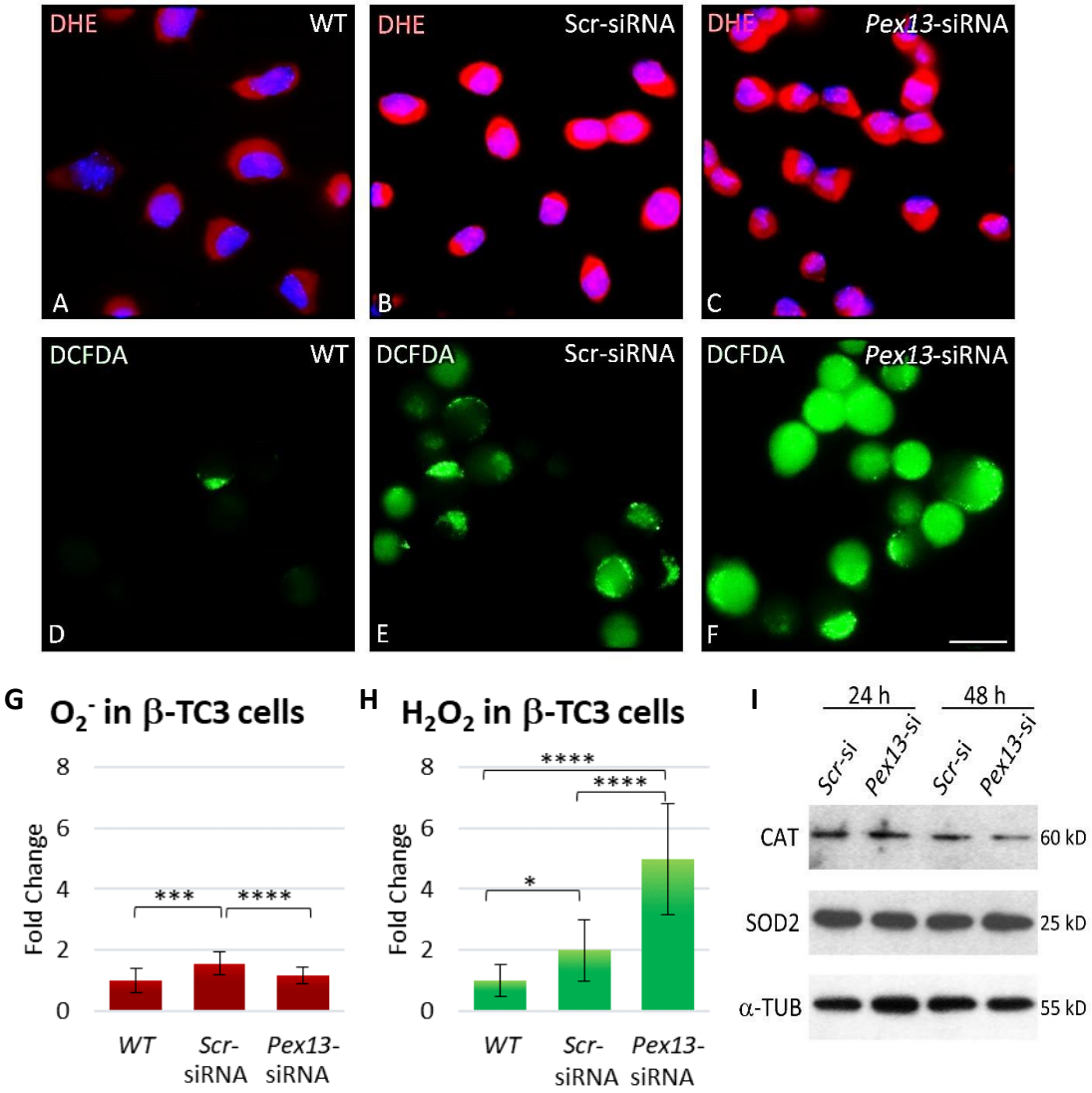

Figure: 38. Measurements of superoxide and hydrogen peroxide levels by relative quantification of DHE and DCFDA fluorescent signals and Western blot analysis of antioxidative enzymes in β-TC3 cells after *Pex13*-siRNA transfection. β-TC3 cells were transfected with *Pex13*-siRNA and *Scr*-siRNA. Wild type cells were used as control. After 48 h the cells were stained with DHE or DCFDA as indicated in *Material and Methods*. **A-C:** WT-control, *Scr*-siRNA and *Pex13*-siRNA transfected cells stained with DHE to detect superoxide production. **D-F:** Control, *Scr*-siRNA and *Pex13*-siRNA transfected cells stained with DCFDA to analyze H_2O_2 levels as an indicator of ROS. **G:** Relative quantification of superoxide generation. At least 100 cells from 3 independent experiments were used for the measurements. **H:** Relative quantification of H_2O_2 production. Only 30 cells could be photographed to measure the fluorescence intensity due to the short-lived stability of the DCFDA staining (light susceptible and rapidly metabolized in living cells). The quantification of the fluorescence intensity was done with the ImageJ software (National Institutes of Health, Bethesda, MD, USA). Statistics: Student´s *t-test* for paired values: *: $p \leq 0.05$; ****: $p \leq 0.0001$. **I:** Western blot analyses of catalase (CAT) (60kD) and superoxide dismutase 2 (SOD2) (25kD) after 24h or 48h *Pex13*-siRNA transfection. Scale bar = 32 µm for all figures.

5.7. Impaired peroxisomal lipid transport after *Abcd3* knockdown

As we were interested in the role of peroxisomes in pancreatic β-cells under lipotoxicity, we decided to study the effect of the down-regulation of ABCD3 in β-TC3 cells. The peroxisomal lipid transporter ABCD3, which is one of the most abundant integral membrane proteins of peroxisomes in pancreatic β-cells, is involved in the transport of branched- and long-chain

acyl-CoAs into the organelle. The model system to study the peroxisomal lipid transport dysfunction was accomplished via siRNA-mediated *Abcd3* knockdown in β-TC3 cells. Preliminary experiments were set up to optimize the conditions of the transfection. Different *Abcd3*-si RNA concentrations were tested (15, 30, 40, 50, and 60 nM) achieving the highest percentage (~82 %) of mRNA down-regulation with 50 nM *Abcd3*-siRNA after 48 h transfection as shown by qPCR analysis (**Figure: 39A**). Having decided on the best *Abcd3*-si RNA concentration to use, the *Abcd3* gene expression was analyzed by qPCR at different time-points after transfection (24, 48, 72, and 96 h) to analyze the duration and stability of the gene silencing. As expected, we observed that the *Abcd3*-si RNA treatment caused a time-dependent decrease of the *Abcd3* mRNA levels to 20 % of the expression level observed in *Scr*-si RNA transfected cells at 96 h post-transfection (**Figure: 39B**).

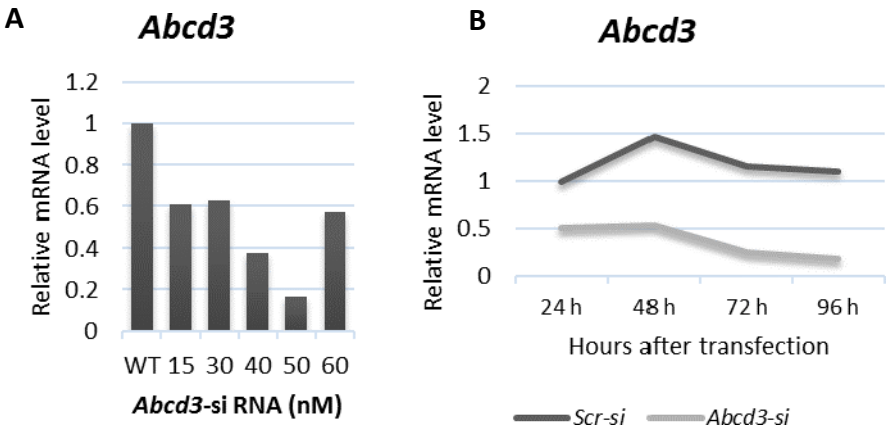

Figure: 39. Optimization of the conditions for *Abcd3* knockdown in β-TC3 cells by siRNA-mediated transfection. A: β-TC3 cells were transfected with *Abcd3*-si RNA via lipofection using different RNA concentrations (15, 30, 40, 50 and 60 nM). After 48 h, the expression of *Abcd3* was analyzed by qRT-PCR, ensuring the efficiency of the down-regulation. One µg total RNA was used for the analysis and *Abcd3* and *Actb* (β-Actin) expression levels were examined as described in *Materials and Methods*. The relative amounts of mRNAs were calculated using the threshold (Ct) values by the 2-ΔΔ CT method and normalized to *Actb*. **B:** β-TC3 cells were transfected with 50nM *Abcd3*-si or *Scr*-si RNA. Different time points were used to ensure the efficiency of the down-regulation. The average threshold (Ct) values of at least three independent experiments were used to calculate the relative amounts of mRNA. Values were normalized to *Actb*.

The reduction of the *Abcd3* mRNA levels after *Abcd3* silencing was corroborated by the decrease in the ABCD3 protein abundance after 24, 48, 72, and 96 h of transfection as assessed by immunoblot analysis (**Figure:40C**). Of the two bands observed after the analysis using an antibody against ABCD3 the lower one of ~65 kDA corresponds to ABCD3 as shown by the knockdown (**Figure:40C**). It is currently not clear what the additional band with molecular weight of ~70 kDa represents. The down-regulation of ABCD3 was confirmed by immunofluorescence analysis conducted 96 h after transfection (**Figure: 40A** and **B**). In the

Scr-siRNA transfected cells round and strongly stained peroxisomes, evenly distributed across the cell, were detected. On the other hand, the silencing of *Abcd3* resulted in next to no detectable ABCD3 staining. The future experiments and treatments were therefore all conducted at 96 h post transfection.

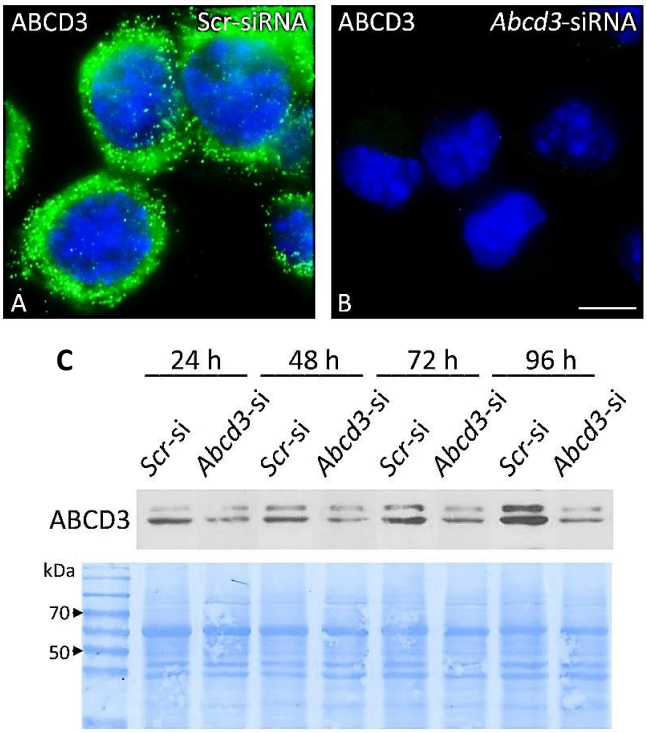

Figure: 40. ABCD3 protein abundance after siRNA-mediated *Abcd3* silencing in β-TC3. β-TC3 cells were transfected with *Abcd3*-si (50 nM) or *Scr*-si RNA via lipofection. **A-B:** After 96 h ABCD3 was detected with an antibody against ABCD3 as described in *Materials and Methods*. The nuclei were counterstained with Hoechst 33342 dye. Scale bar = 12µm. **C:** Representative immunoblot showing the down-regulation of ABCD3 in β-TC3 cells after *Abcd3*-si transfection at different time points. Total protein (20 µg) was subjected to Western blot analysis and probed with an antibody against ABCD3. Autoradiographic signals were visualized as described under *Material and Methods*. As loading control, membranes were stained with Coomassie Blue Stain (Invitrogen).

5.8. Stimulation of lipotoxicity by palmitic and phytanic acid in β-TC3 cells

Fatty acids have been reported to influence β-cell function and viability. A short exposure (acute) of β-cells to fatty acids can stimulate the release of insulin [187, 188]. This acute exposure is not toxic to the β-cells if the fatty acids are properly metabolized within the cells[189]. However, prolonged (chronic) exposure of β-cells to increased levels of fatty acids results in lipid accumulation, β-cell dysfunction and finally apoptosis (lipotoxic effect) [136, 155]. Moreover, changes in β-cell gene expression are commonly observed during the progression of lipotoxicity [190]. Since peroxisomes play an important role in the oxidation of fatty acids, we decided to treat *Pex13* KD β-TC3 cells with the saturated fatty acid palmitic acid (PA) or the branched- chain fatty acid phytanic acid (PHY) as a means to stimulate lipotoxicity. With this set-up, we intended to investigate whether β-cells lacking functional peroxisomes were more susceptible to lipotoxicity, whereas PA can be oxidized in mitochondria (and peroxisomes), PHY is only oxidized by peroxisomes.

A preliminar viability experiment was conducted to establish the right fatty acid concentration (LD50) needed to exert cell toxicity on β-TC3 cells. To determine cell viability, we used the dye Trypan blue, which is only staining dead cells.

Palmitic acid was prepared according to Choi et al. [178]: complexes of fatty acids were formed with albumin prior the incubation. Solubilized palmitic acid was added at different concentration freshly to the cell culture every 24 h over a period of 2 days. The results of this experiment showed that cell death was induced by PA in a concentration and time dependent manner (**Figure: 41A**). At 0.1 mM only 10-15 % cells were affected after 2 days of treatment, while the exposure to 0.5 mM showed toxicity already after 24 h and was sufficient to increase cell death by 4-fold after 2 days. With 1 mM PA more than 95 % of the cells died at the end of the experiment.

As with PA, the exposure of β-TC3 cells to PHY resulted in a time and concentration-dependent cytotoxicity (**Figure: 41B**). One, 10 and 20 µM PHY were not enough to cause cell death, however, using 50 µM PHY, a toxic effect was detected after only 12 h treatment with 60 % cell death reaching a nadir (~90 %) after 2 days. The highest PHY concentration (100 µM) used in this experiment proved to be extremely toxic for the cells even after 24 h, time after which no cell survived. Parallel incubations were performed to determine the toxicity of the BSA-NaOH complex (vehicle) and dimethyl sulfoxide (DMSO), both used for PA and PHY respectively. Neither solvents showed toxic effect when used at the same concentrations and time-points as in the PA or PHY suspensions (data not shown) thus corroborating that the toxicity was only due to the fatty acids. For future experiments in this study we decided to expose the cells to 0.2 mM PA or to 40 / 60 µM PHY.

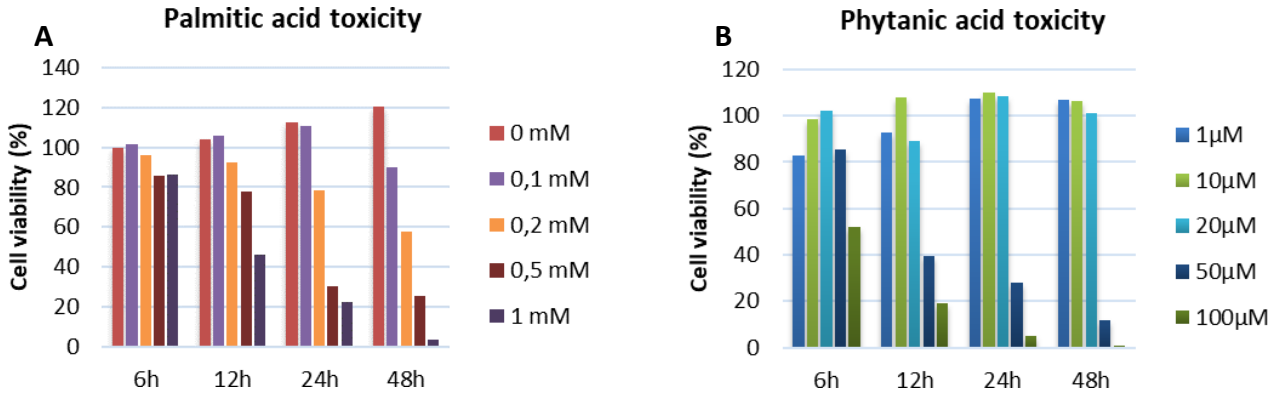

Figure: 41. Increased β-TC3 cell death after different fatty acid treatments. A: Cells were incubated with DMEM medium containing different concentration of palmitic acid (0, 0.1, 0.2, 0.5 and 1 mM) for 6, 12, 24 and 48 h. The cell viability was evaluated by Trypan blue exclusion test. The number of intact cells, which exhibited no blue staining, was determined (eight fields per experiment) and percentage of live cells in relation to

untreated control is given. **B:** An incubation with DMEM medium containing different concentration of phytanic acid (1, 10, 20, 50, and 100 µM) was carried out for 6, 12, 24, and 48h.

5.9. Elevated glucose concentrations enhance palmitate cytotoxicity in β-TC3 cells

It has been shown that free fatty acids together with high glucose (hyperglycaemia) synergize causing islet β-cell damage due to the inhibition of fatty acid oxidation and therefore of lipid detoxification [189, 191]. To analyse the interaction of PA with glucose during cell death, β-TC3 cells were treated for 24, 48, and 72 h with different concentrations of PA (0, 0.2, and 0.5 mM) in the background of hyperglycaemia (20 mM glucose) or low glucose concentration (5 mM) (**Figure: 42**).

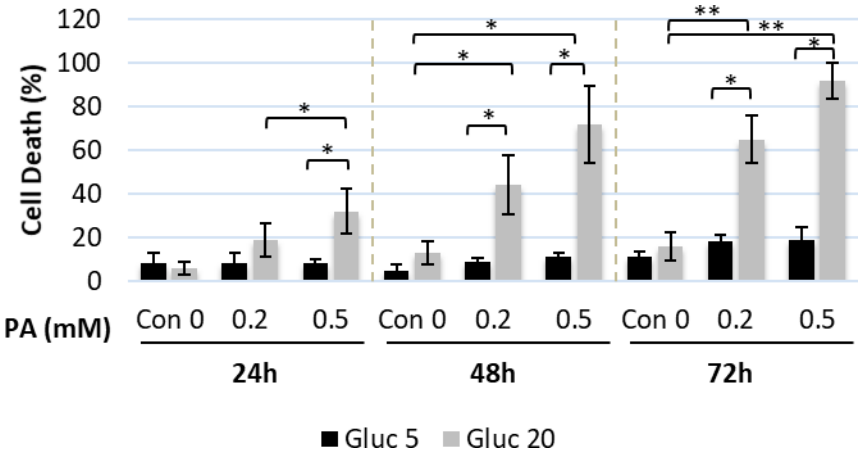

Figure: 42. Induction of cell damage caused by the synergistic effect of elevated concentrations of glucose and palmitic acid. β-TC3 cells were incubated in DMEM medium at 5 (Gluc 5) and 20 (Gluc 20) mM glucose in the absence (control) or presence of 0.2 and 0.5 mM palmitic acid (PA) during 24, 48 and 72h. The Trypan blue exclusion test was carried out for the determination of cell viability. The number of intact cells, which showed no blue staining, was determined (eight fields per experiment) and percentage of death cells in relation to living cells per group is given. Gluc: glucose (in mM); PA: palmitic acid. Statistics: ANOVA test for multi-paired values. * $p \leq 0.05$; ** $p \leq 0.01$.

In the presence of 5 mM glucose, none of the PA concentrations displayed a significant change in cell viability throughout the duration of the experiment. Remarkably, cell exposure to low glucose (5 mM) along with high physiological PA concentrations (0.5 mM) resulted in minimal toxicity (less than 20 % after 72 h) in comparison to the control (0 mM PA) (~16 % cell death after 72 h) or the 0.2 mM PA treated group (~18 % cell death after 72 h). In contrast, in the cells incubated with 20 mM glucose, the PA toxicity was markedly increased in a time and concentration dependent manner, showing a reduction in the cell number after only 24 h of treatment, where the exposure to 0.2 mM and 0.5 mM resulted in 19 % and 32 % of cell death respectively, compared to the group exposed to 0 mM of PA. At the end of the experiment ~65 % of the cells incubated in high glucose medium

supplemented with 0.2 mM PA died, while this toxic effect increased to 90 % when cells were exposed to 0.5 mM PA. Taken together, these results support the glucolipotoxicity hypothesis of β-cell death, which suggests that elevated fatty acids (in this case, PA) are particularly toxic in the context of hyperglycaemia.

5.10. Intracellular lipid accumulation of palmitic acid and phytanic acid in β-TC3 cells

Since one of our aims was to better define the role that peroxisomes play during lipotoxicity in β-cells, we decided to verify the fatty acid uptake and/or accumulation in our cell model using PA and PHY at different concentrations. Intracellular lipid accumulation was analyzed by light microscopy after staining the cells with Oil red O as described in *Materials and Methods*. When β-cells take up free fatty acids (FFA), they convert them to triglycerides or cholesterol ester for intracellular storage in form of lipid droplets within the cytoplasm. If the storage capability of the cells is exceeded, excessive FFA may impair insulin secretion and induce apoptosis [(192)]. The exposure of β-TC3 cells to PA showed an increase in the amount of intracellular lipid accumulation in form of Oil red O stained lipid droplets in a concentration dependent manner (0, 0.1, 0.2, 0.4, 0.5, and 1 mM). The droplets, clearly observed in the control group as small and circular structures scattered across the cytoplasm of some cells (**Figure: 43A**), became more prominent, numerous, and larger as the PA concentration increased, appearing as well-defined large round structures occupying very large parts of the cytoplasm (**Figure: 43D**). Higher PA concentrations (0,5 and 1 mM) were also analyzed, however, due to their high toxicity and resulting cell damage it was not possible to obtain a representative picture.

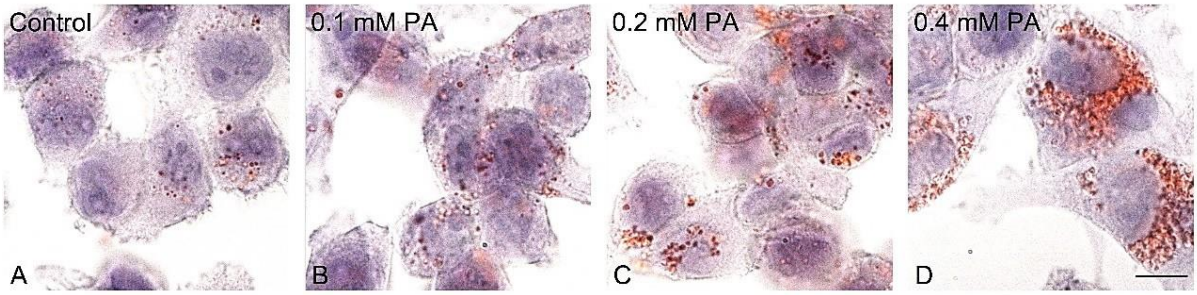

Figure: 43. Effect of palmitic acid treatment on the cellular lipid storage in wild type β-TC3 cells. A: β-TC3 cells were maintained in DMEM medium supplemented with serum without PA as control. **B-D:** β-TC3 cells treated with PA at different concentrations (0.1, 0.2, and 0.4 mM) for 48 h, time after which the appearance of lipid droplets was observed by Oil red O staining. Nuclei were stained with hematoxylin providing better cell visualization and identification. The results were examined using a phase contrast microscope (LEICA DMRD equipped with a LEICA CD480 camera). PA: palmitic acid. Scale bar = 26 µm for all images.

In comparison with PA, PHY, which is exclusively metabolized in peroxisomes, showed a similar but less intense Oil red O staining. While the staining of control cells resulted in sporadically distributed, very small round structures (**Figure: 44A**), the exposure to PHY led to the formation of larger, strongly stained droplets, the number of which increased with increasing PHY concentration (**Figure:44D**). A high percentage of cell death was observed after 48 h of treatment with 60 µM PHY, yet enough cells could be obtained for the analysis. Interestingly, the number of lipid droplets observed after the treatment with PHY at a toxic concentration, was clearly lower than that found for PA at toxic concentration. In other words, for PA a higher accumulation of intracellular lipid droplets could be achieved than for PHY using similar toxic conditions.

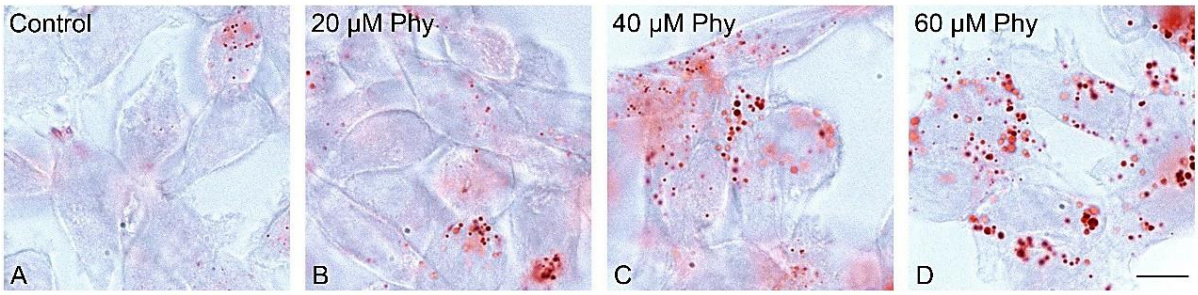

Figure: 44. Effect of phytanic acid treatment on the cellular lipid storage in wild type β-TC3 cells. A: Cells were maintained in DMEM medium without PHY as control. **B-D:** β-TC3 treated with serum supplemented with PHY at different concentrations (20, 40, and 60 µM) for 48 h, time after which the appearance of lipid droplets was observed by Oil red O staining. The results were examined using a phase contrast microscope (LEICA DMRD equipped with a LEICA CD480 camera). Phy: phytanic acid. Scale bar = 26 µm for all images.

5.11. The peroxisomal lipid transporter ABCD3 showed an opposite regulation in β–TC3 cells treated with palmitic and phytanic acid

As observed previously, the cell exposure to palmitic and phytanic acid resulted in the increase of cytoplasmic lipid droplet formation. We were further interested in analyzing this effect on the ABCD3 protein amount since this membrane lipid transporter is in charge of the peroxisomal lipid transport. Interestingly, the treatment of β-TC3 cells with increasing PA concentrations resulted in an inversely proportional ABCD3 IF staining intensity. A very strong IF signal was observed in the untreated control group (0 mM PA) displaying round peroxisomes forming clusters throughout the cytoplasm (**Figure: 45A**). The addition of 0.2 mM PA into the culture medium resulted in a strong decrease of the ABCD3 IF signal intensity. Individual peroxisomes were evenly distributed throughout the cell and still weakly positive for ABCD3 (**Figure: 45B**). A further increase of the PA concentration to

0.4 mM resulted in an even weaker signal, revealing only faintly stained granular structures (**Figure: 45C**).

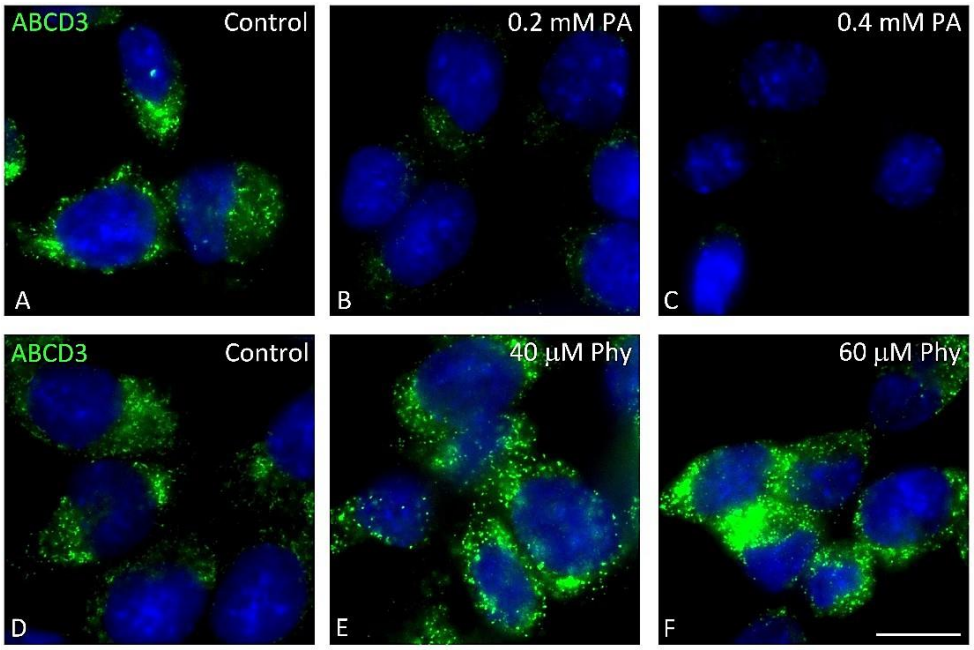

Figure: 45. Effect of palmitic and phytanic acid treatment on the peroxisomal lipid transporter ABCD3 in β-TC3 cells. A-C: IF analysis of β-TC3 cells after PA treatment. The cells were incubated with PA at two different concentrations: 0.2 (**B**) and 0.4 (**C**) mM for 48 h to observe the effect of the saturated fatty acid on the abundance of the peroxisomal membrane lipid transporter ABCD3. **D-F:** β-TC3 cells were incubated with PHY at two different concentrations: 40 (**E**) and 60 (**F**) µM for 48 h. Cells were subjected to IF staining using an ABCD3 antibody at a dilution of 1:500 and nuclei were visualized with Hoechst 33342 dye as described in *Materials and Methods*. PA: palmitic acid; Phy: phytanic acid. Scale bar = 20 µm for all images.

Contrary to the results observed after the PA treatment, the exposure to PHY resulted in an increase in the abundance of ABCD3. IF analysis of β-TC3 cells maintained in medium lacking PHY (control) revealed a peroxisomal pattern composed of punctuate structures evenly distributed across the cytoplasm as well as some tubular peroxisomes (**Figure: 45D**). In comparison with the non-treated cells, the exposure to 40 µM PHY produced an increase in the ABCD3 staining intensity depicted as big round peroxisomes (**Figure: 45E**). Moreover, rising the PHY concentration to highly toxic 60 µM resulted in an even stronger signal with large peroxisomes clustering in patches across the cytosol (**Figure: 45F**).

To ensure the ABCD3 down-regulation observed in β-TC3 cells exposed to the PA treatment, RT-qPCR analysis for *Abcd3* mRNA levels was carried out. Interestingly, the exposure to 0.2 mM PA led to a 4-fold increase of *Abcd3* mRNA levels after 6 h (**Figure: 46**). This effect decreased after 12 h of incubation, where the *Abcd3* mRNA level after the PA treatment did not show a variation in comparison with the control group. The analysis of later time-points

revealed, as expected, a decrease in the *Abcd3* expression after 24 h of PA exposure, reaching a 50 % suppression after 48 h, in agreement with the results observed by IF analysis.

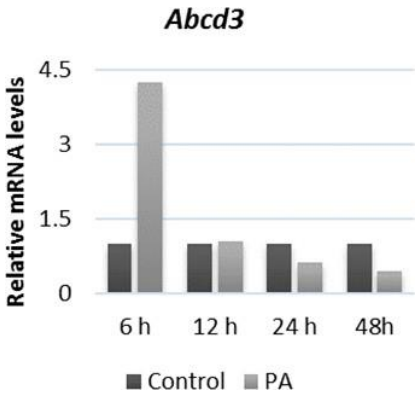

Figure: 46. Effect of palmitic acid treatment on *Abcd3* mRNA levels in β-TC3 cells. Real-time RT-PCR analysis of *Abcd3* at 6, 12, 24, and 48 h after 0.2 mM PA treatment in β-TC3 cells compared with the control group. The primers for *Abcd3* and *Actb* (β-Actin) were used as described in *Materials and Methods*. The relative amount of mRNA was calculated using the 2-ΔΔ CT method and data was normalized to *Actb* values. The graphic shows the result of a single experiment.

5.12. Reactive oxygen species (ROS) production in βTC3 cells after their exposure to palmitic acid

It was suggested in the literature that intracellular accumulation of ROS produced by some metabolites of PA (such as diglycerol) [(193)] can result in β-cell apoptosis and decrease of insulin secretion, thereby impairing the function and reducing the number of β-cells [(194)]. Since β-cells are poorly protected against oxidative stress due to their low content of antioxidative enzymes [(195)] it was of our interest to investigate the cellular levels of ROS along with the activity and mRNA expression of catalase in response to PA exposure in β-TC3 cells. Interestingly, as determined by DHE staining, a significant ($p \leq 0.01$) decrease in the fluorescence signal intensity corresponding with lowered intracellular superoxide levels was observed in those cells exposed to 0.2 mM PA for 48 h in comparison with the non-treated cells (**Figure: 47A, B** and **E**).

Since the DCFDA staining has a relatively short-time stability mainly due to its light susceptibility and metabolism in living cells, only a 6h PA exposure was used to assess the H_2O_2 production. The cell exposure to high PA concentration (2 mM) resulted in a significant ($p \leq 0.001$) 2.8-fold increase in the DCFDA staining an indication for the presence of elevated hydrogen peroxide levels (**Figure: 47C, D** and **F**).

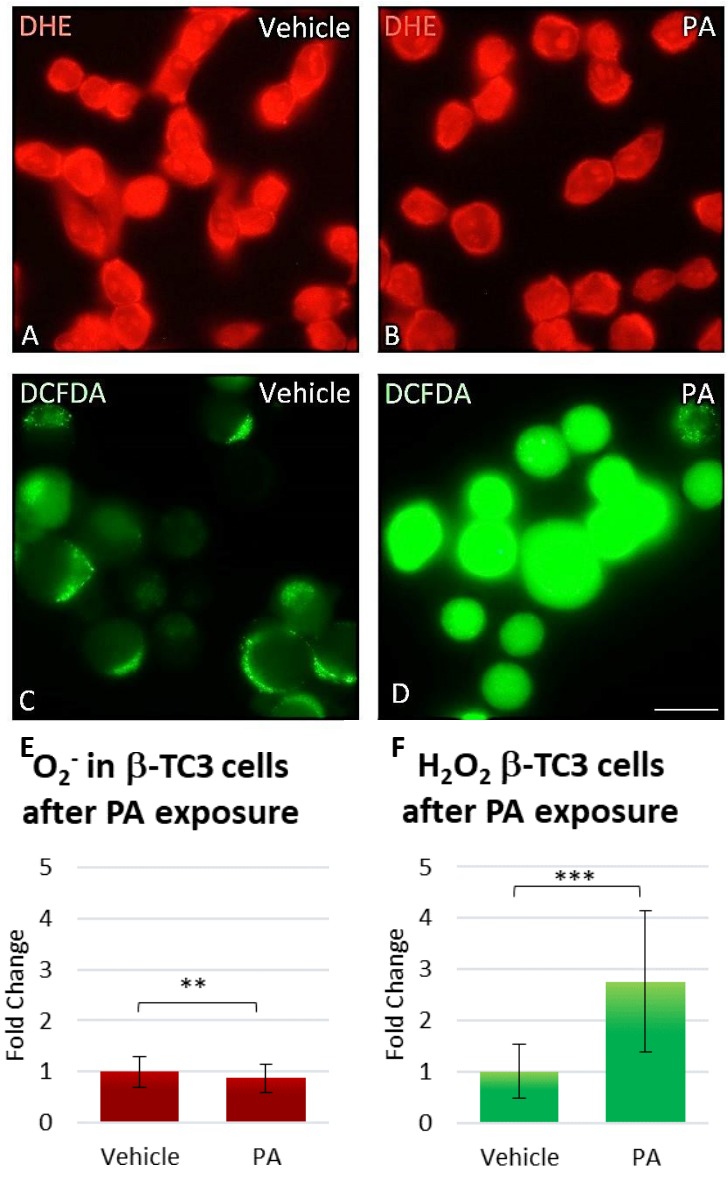

Figure: 47. Palmitic acid treatment induces H_2O_2 but decreases superoxide levels in β-TC3 cells. A-B: Control and PA (0.2 mM) treated β-TC3 cells stained with DHE to analyze superoxide presence and general ROS production. **C-D:** DCFDA staining showing a stronger fluorescence signal resulting from the increase in H_2O_2 levels after PA (2 mM) exposure in comparison with the control group. The fluorescence measurement was done 6 h after treatment. **E:** Relative quantification of superoxide levels. At least 100 cells from 3 different experiments were used for the measurements. **F:** Quantification of H_2O_2 production. Only 30 cells could be photographed to measure the fluorescence intensity due to the short-lived stability of the DCFDA staining (light susceptible and rapidly metabolized in living cells). The quantification of the fluorescence intensity was done with the ImageJ software. Statistics: Student´s *t-test* for paired values: **: $p \leq 0.01$; ***: $p \leq 0.001$. Scale bar = 32 µm.

Since the peroxisomal antioxidative enzyme catalase and the mitochondrial enzyme superoxide dismutase 2 (SOD2) play an important role in the degradation of H_2O_2 and superoxide, we investigated their protein abundance by Western blot and immunofluorescence analysis after 48 h of PA exposure (0.2 mM). When compared with the non-treated cells, the PA treatment produced a notorious increase in the catalase staining intensity (**Figure: 48A, B**) sustained by the 1.6-fold rise in the catalase amount as shown by the Western blot analysis. No significant changes were found in SOD2 protein amount (**Figure: 48**).

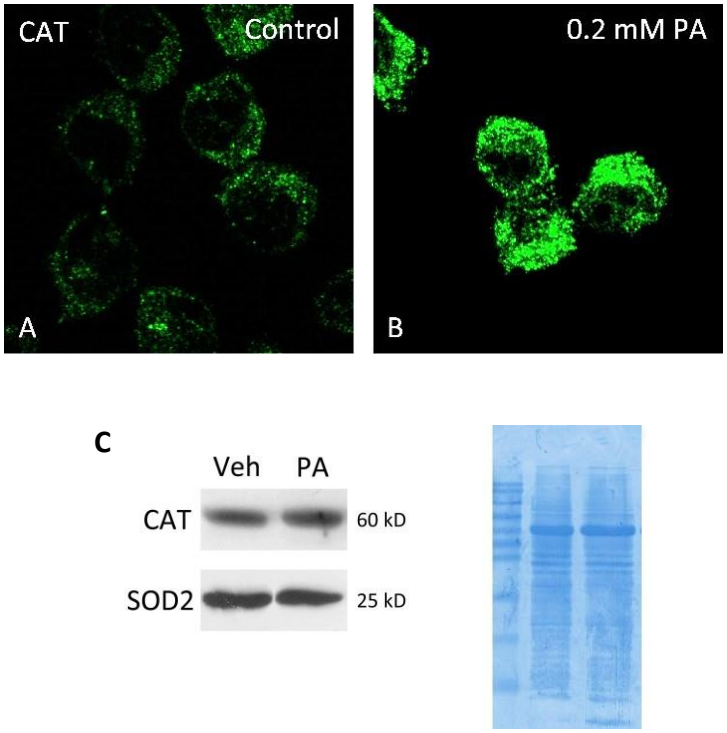

Figure: 48. Catalase and SOD2 analysis in β-TC3 cells after palmitic acid treatment. A-B: IF analysis of β-TC3 cells after PA treatment. The cells were incubated with vehicle **(A)** or 0.2 mM PA (**B**) for 48 h to observe the effect of the saturated fatty acid on the abundance of catalase. Cells were subjected to IF staining using a CAT antibody at a dilution of 1:200. Scale bar = 20 µm. **C:** Western blot analysis of catalase (CAT) and superoxide dismutase 2 (SOD2) after 48 h of PA (0.2 mM) treatment. Total protein (20 µg) was subjected to Western blot analysis and was sequentially probed with antibodies against catalase and SOD2. As loading control, membranes were stained with Simply Blue Stain (Invitrogen).

Furthermore, the treatment with PA led to a biphasic induction of the catalase mRNA expression, showing the first peak after 6 h of exposure (3-fold) followed by a decline (1.5-fold after 12 h) and a gradual time-dependent rise in the following time points (24 and 48 h) up to a slightest higher level (3.2-fold), as revealed by RT-qPCR analysis (**Figure: 49A**). To further assess the functional consequences of the PA exposure, we analyze the enzymatic activity of catalase after 48 h of treatment. Despite catalase showing a protein and mRNA level up-regulation after the fatty acid exposure, this did not result in a statistically significant increase in its enzymatic activity (**Figure: 49B**).

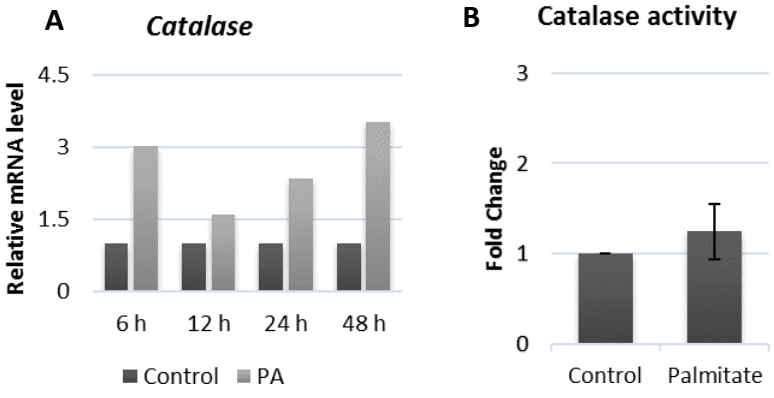

Figure: 49. *Catalase* mRNA levels and enzymatic activity after PA treatment in β-TC3 cells. A: RT qPCR analysis of *catalase* at different time points after 0.2 mM PA treatment in β-TC3 cells. The relative amount of mRNA was calculated using the 2-ΔΔ CT method and data was normalized to *Actb* values. **B:** β-TC3 cells were treated with 0.2 mM PA for 48 h and the peroxidatic function of the enzyme Catalase was determined.
Data were normalized to sample protein concentrations.
PA: palmitic acid.

5.13. Increased hydrogen peroxide production in β-TC3 cells exposed to phytanic acid

As with PA, we also analysed the effect of PHY in the production of ROS (superoxide and hydrogen peroxide) in β-TC3 cells. No changes were observed in the amount of superoxide generated after the treatment with 60 μM PHY for 48 h, as shown by the DHE staining (**Figure: 50A, B** and **E**). Opposite to this, the introduction of high concentrations of PHY (60 μM) to the culture medium led to significant ($p \leq 0.0001$) increase of H_2O_2 accumulation (4.2-fold) observed as a rise in the DCFDA fluorescence signal intensity (**Figure: 50C, D** and **F**).

The exposure of β-TC3 cells to 60 μM PHY for 48 h further led to a minor but clear increase of 1.3-fold in CAT protein amount whereas SOD2 showed a 0.6-fold decrease (**Figure: 51**).

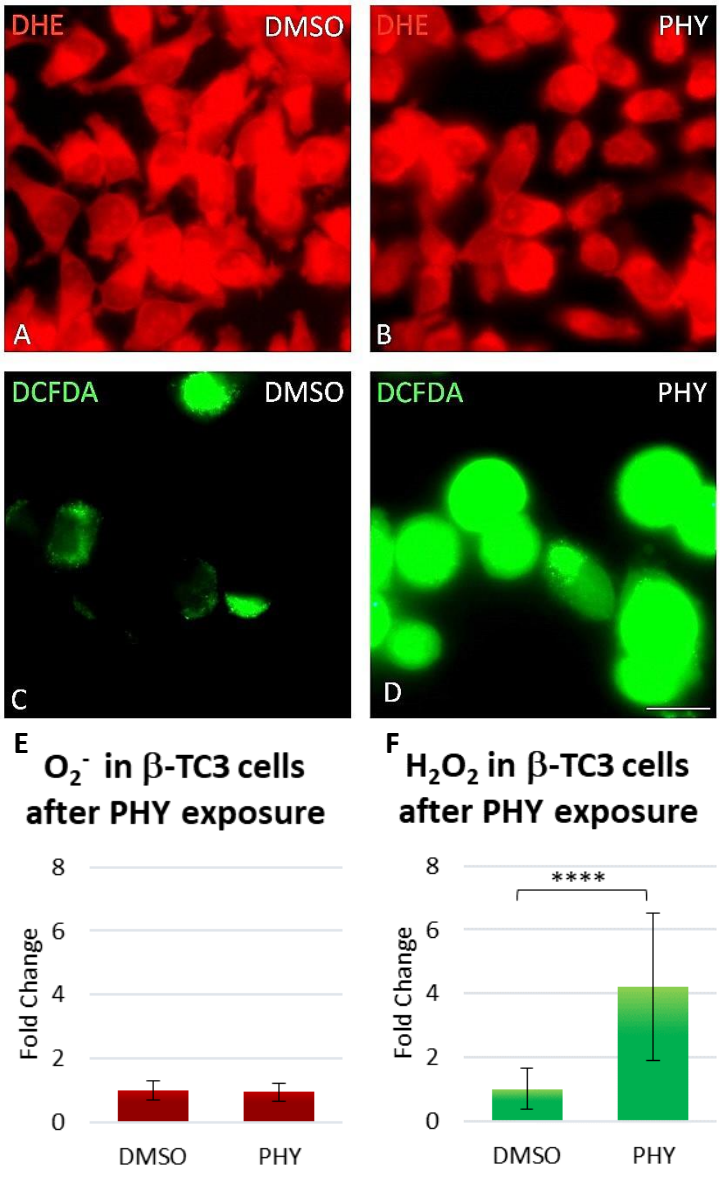

Figure: 50. Phytanic acid treatment induces H_2O_2 production in β-TC3 cells. A-B: Control and PHY (60 μM) treated β-TC3 cells stained with DHE to analyze superoxide presence and general ROS production. **C-D:** DCFDA staining showing a stronger fluorescence signal resulting from the increase in H_2O_2 levels after PHY (60 μM) exposure in comparison with the control group. The fluorescence measurement was realized 6 h after treatment. **E:** Relative quantification of superoxide levels. At least 100 cells from 3 different experiments were used for the measurements. **F:** Quantification of H_2O_2 production. Only 40 cells could be photographed to measure the fluorescence intensity due to the short-lived stability of the DCFDA staining (light susceptible and rapidly metabolized in living cells). The quantification of the fluorescence intensity was done with the ImageJ software. Statistics: Student´s *t-test* for paired values: ****: $p \leq 0.0001$. Scale bar = 32 μm for all IF-images.

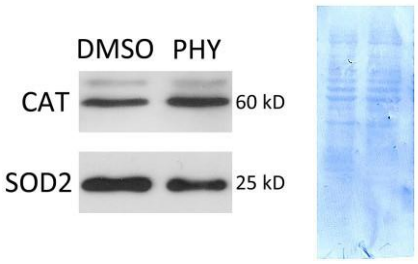

Figure: 51. Phytanic acid treatment increases the catalase protein amount in β-TC3 cells. Western blot analysis of catalase (CAT) and superoxide dismutase 2 (SOD2) after 48 h of PHY (60 μM) treatment. Total protein (20 μg) was subjected to SDS-PAGE and Western blot analysis and was sequentially probed with antibodies against Catalase and SOD2. As loading control, membranes were stained with Simply Blue Stain (Invitrogen).

5.14. Influence of palmitic acid exposure in β-TC3 cells displaying a *Pex13*-KD

5.14.1. The down-regulation of *Pex13* did not result in an increased lethality in β-TC3 cells after palmitic acid exposure

To investigate whether β-cells displaying a peroxisome-deficiency were more susceptible to lipotoxicity, our β-TC3 cell *Pex13* knockdown model was exposed to toxic concentrations of PA. Since our results showed that glucose plays an important role in cell death caused by elevated PA concentrations, our experiments were conducted in the background of hyperglycaemia (20 mM). The cell lethality was analyzed using the Trypan blue exclusion test. At a high PA concentration (0.5 mM) we observed that transfected cells (*Scr*-si and *Pex13*-si) were generally more susceptible to the fatty acid exposure compared to similarly treated WT cells (data not shown). For this reason, we decided to carry out our further experiments using a lower but still toxic PA concentration (0.2 mM). Since we wanted to mimic chronic PA exposure in our *Pex13* knockdown cell-culture model, we started the cell treatment 24 h after transfection adding the solubilized PA freshly every 24 h over a period of maximum 2 days to make sure that the PEX13 knockdown was still present. Vehicle (BSA-NaOH complex) was used as a control treatment. Our experiments showed that both control (*Scr*-siRNA) and *Pex13* knockdown cells were more susceptible to the PA treatment than the cells that were treated with vehicle only (**Figure: 52**). However, no significant difference was observed between *Scr*-si and *Pex13*-si transfected groups.

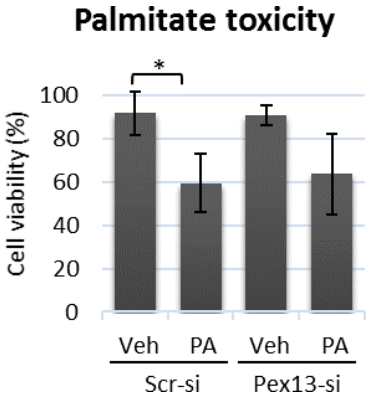

Figure: 52. Increased β-TC3 cell dead after PA treatment. Transfected cells were incubated with DMEM medium containing 0.2 mM palmitic acid (PA) for 48 h. Trypan blue exclusion test was carried out for the determination of cell viability. The number of intact cells, which exhibited no blue staining, was determined (eight fields per experiment) and percentage of living cells per group is given. Statistics: ANOVA test for multi-paired values. * $p \leq 0.05$. Veh: vehicle; PA: palmitic acid.

5.14.2. The silencing of *Pex13* in β-TC3 cells resulted in an increased intracellular lipid accumulation after the exposure to palmitic acid

To investigate whether there was an increase in intracellular lipid accumulation after the *Pex13* knockdown in βTC3-cells exposed to PA, we analyzed the appearance of lipid droplets by light microscopy using the Oil red O staining method. Oil red O stains mainly neutral lipids (such as triglycerides or cholesterol) synthesized *de novo* after PA exposure and stored in lipid droplets within the cytoplasm. The silencing of *Pex13* led to a minor increase in the lipid droplet abundance compared with the *Scr*-si transfected cells (both groups treated with vehicle only). The cells display small and round droplets, scattered across the cytoplasm (**Figure: 53A** and **C**).

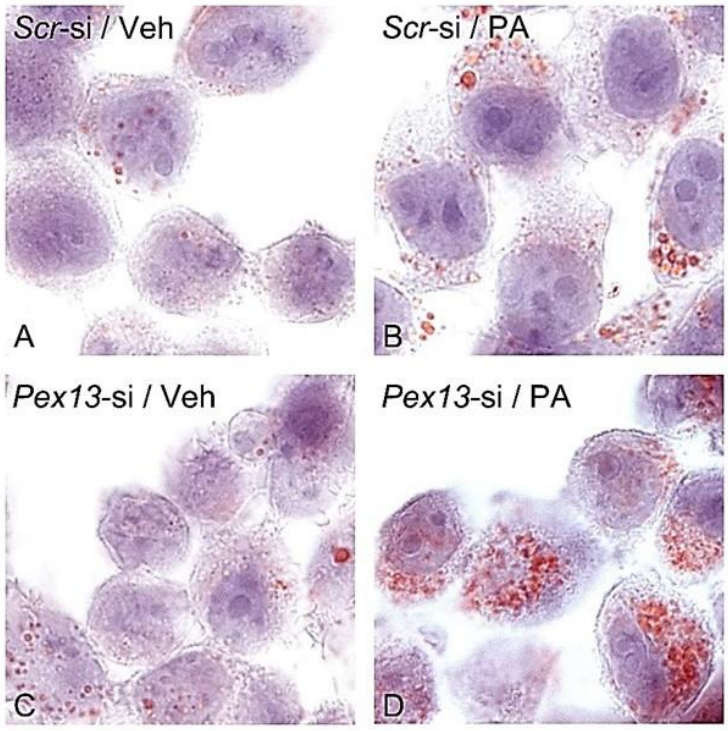

Figure: 53. Oil red O staining for detection of lipid droplet accumulation in β-TC3 cells. β-TC3 cells were transfected with *Pex13*-si and *Scr*-siRNA for 24 h before being exposed to PA (0.2 mM) for 48 h. BSA-NaOH complex (Veh) was used as a control treatment. The appearance of lipid droplets was observed after Oil red O staining. **A-B:** *Scr*-siRNA treated cells exposed to vehicle (**A**) and PA (**B**); **C-D:** *Pex13*-si transfected cells exposed to vehicle (**C**) or PA (**D**). Nucleoli were stained with hematoxylin. Results were examined using phase contrast (LEICA DMRD equipped with a LEICA CD480 camera). Scale bar = 26 μm.

When cells were treated with 0.2 mM PA for 48 h, a clear increase in the number and size of the lipid droplets was found (**Figure: 53A** and **B**). This effect was much more prominent in the *Pex13* knockdown than in the *Scr*-si transfected cells (**Figure: 53B** and **D**).

5.14.3. ABCD3 regulation after *Pex13* silencing in β-TC3 cells exposed to palmitic acid

We observed an increased lipid droplet accumulation in *Pex13*-si transfected cells caused by the lack of functional peroxisomes. To investigate whether the import of fatty acids into the peroxisomes was disturbed we investigated the expression of ABCD3, the most abundant

peroxisomal lipid transporter, under the same experimental setting. For this purpose, we investigated the *Abcd3* mRNA expression as well as the ABCD3 protein abundance by qRT-PCR and Western blotting respectively. Our experiments showed that the treatment with PA significantly increased the mRNA expression of *Abcd3* in both, the *Scr*-si and the *Pex13*-si transfected cells (a fold change of 0.8 and 1.4) (**Figure: 54A**). Further, in both control and *Pex13* knockdown cells the ABCD3 protein amount was visibly decreased when the cells were treated with palmitate instead with vehicle. This agrees with the decreased ABCD3 staining seen during the IF analysis of PA-treated WT cells previously shown in this work (**Figure: 45**).

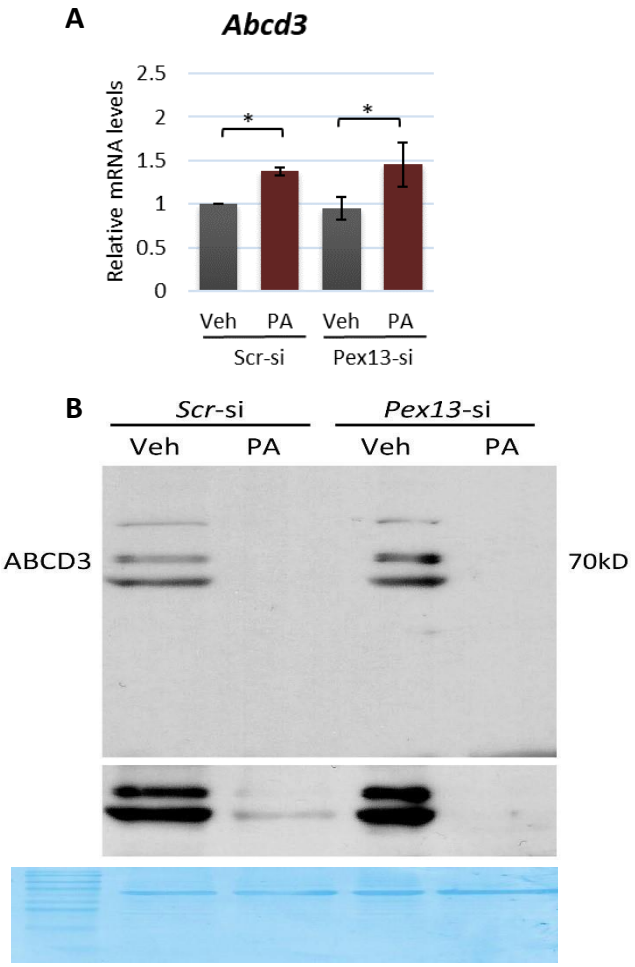

Figure: 54. *Abcd3* mRNA levels and protein abundance in *Pex13*-si transfected β-TC3 cells after palmitic acid treatment. β-TC3 cells were transfected with *Pex13*-si or *Scr*-siRNA and treated with PA (0.2 mM) for 48 h. **A:** The expression of *Abcd3* was analyzed by qRT-PCR. Total RNA was used for the analysis and *Abcd3* and *Actb* (β-Actin) expression levels were examined. The average threshold (Ct) values of at least three independent experiments were used to calculate the relative amounts of mRNA using the 2-ΔΔ CT method and data was normalized to *Actb* values. Results are presented as a fold over control. **B:** Western blot analysis of ABCD3. Total protein (20 µg) was used for the analysis and the Western blot was probed with an antibody against ABCD3. Equal loading of protein was controlled by Coomassie staining of the membrane after detection of antibodies. Statistics: ANOVA test for multi-paired values. * $p \leq 0.05$. Veh: vehicle; PA: palmitic acid; Abcd3: ATP-binding cassette, subfamily D, member 3.

5.14.4. Superoxide and hydrogen peroxide generation in the *Pex13* knockdown β-TC3 cells after palmitic acid exposure as an indicator of oxidative stress

To further assess the functional consequences of the *Pex13* knockdown in β-TC3 cells after PA exposure, we investigated the superoxide (O_2^-) and hydrogen peroxide (H_2O_2) production as an indicator of oxidative stress. As previously described in this thesis, the *Pex13* silencing

resulted in the mislocalization of catalase to the cytosol, an effect that potentially could surrender the β-cell to the adverse consequences of ROS accumulation. In addition, β-cells exposed to PA showed a high rate of apoptosis and impaired insulin secretion as result of the increased ROS accumulation [193, 194].

We used DHE to examine the amount of superoxide generated after *Pex13* silencing and exposure to 0.2 mM PA for 48h (**Figure: 55A-D**). In comparison with *Scr*-si transfected cells, we observed a significant ($p \leq 0.0001$) reduction of the DHE staining after the down-regulation of *Pex13* in cells treated with vehicle, suggesting a decrease in the superoxide accumulation (**Figure: 55A, C** and **I**). Similarly to the effect observed in WT cells (**Figure: 47**), the addition of PA to the culture medium of either *Scr*-si or *Pex13*-si transfected cells resulted in a significant ($p \leq 0.0001$) decrease of 0.5-fold and 0.75-fold respectively in the DHE fluorescence signal (**Figure: 55B, D** and **I**). Our results revealed that both the PA treatment and *Pex13* silencing caused independently of each other a decrease in the DHE fluorescence signal intensity. The combination of PA treatment and *Pex13* silencing resulted in a cumulative effect with cells displaying almost absent DHE staining (**Figure: 55D**). This suggests lowered intracellular superoxide levels in the *Pex13*-si + PA treated cells.

Next, we investigated the amount of H_2O_2 production by DCFDA staining. We observed that the *Pex13* silencing resulted in a significant ($p \leq 0.0001$) increase of H_2O_2 accumulation (1.9-fold) in those cells treated with the vehicle (**Figure: 55E, G,** and **J**). Also, the exposure to PA resulted in a statistically significant increase of the DCFDA signal intensity in both control and knockdown cells (3- and 2.7-fold respectively) (**Figure: 55F, H,** and **J**). Furthermore, a tendency of H_2O_2 to be less upregulated after PA treatment in the *Pex13*-si group was observed ($p \leq 0.064$) (**Figure: 55J**).

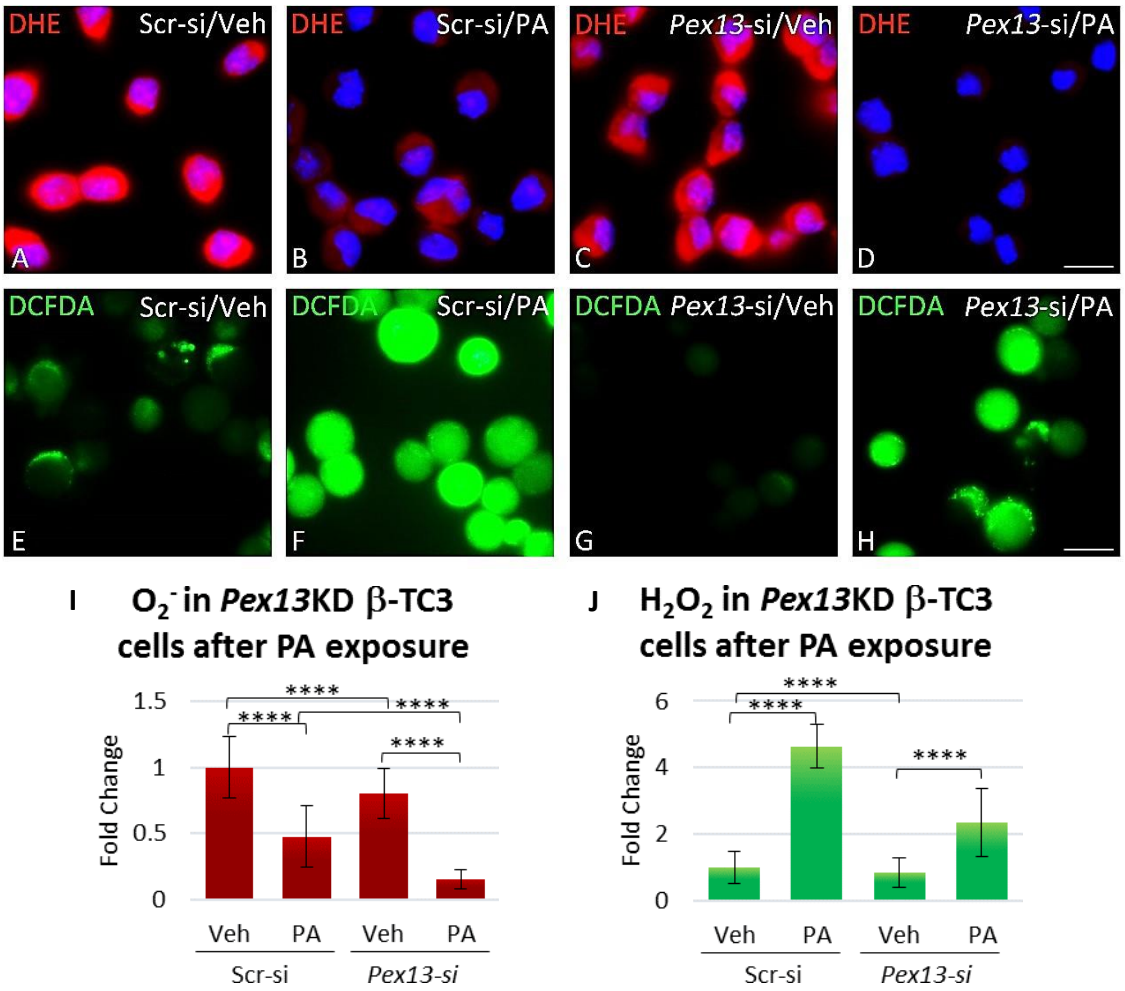

Figure: 55. Measurement of superoxide and hydrogen peroxide levels by relative quantification of DHE and DCFDA fluorescent signal in *Pex13* knockdown β-TC3 cells after PA exposure (see figure on page 98). β-TC3 cells were transfected with *Pex13*-si or *Scr*-siRNA, treated with PA, and stained with Dihydroethidium (DHE) or with 2´,7´-dichlorofluorescin diacetate (DCFDA) to visualize the accumulation of superoxide or H_2O_2 respectively. **A-D:** DHE staining of: **A:** *Scr*-siRNA transfected cells treated with vehicle or with **B:** 0.2 mM PA for 48h; **C:** *Pex13*-si transfected cells treated with vehicle or with **D:** 0.2 mM PA for 48h. Nuclei were counter stained with Hoechst 33342 dye. **E-H:** DCFDA staining of: **E:** *Scr*-siRNA transfected cells treated with vehicle or with **F:** 2 mM PA; **G:** *Pex13*-si transfected cells treated with vehicle or with **H:** 2 mM PA. The fluorescence measurement was done 6 h after treatment. **I:** Relative quantification of superoxide levels. At least 100 cells from 3 independent experiments were used for the measurements. **J:** Quantification of H_2O_2 production. 40 living cells from 3 independent experiments could be photographed to measure the fluorescence intensity due to the short-lived stability of the DCFDA staining. The quantification of the fluorescence intensity was done with the ImageJ software. Statistics: ANOVA test for multi-paired values. **** $p \leq 0.0001$. Veh: vehicle; PA: palmitic acid. Scale bar = 32 µm.

5.14.5. The protein abundances of the antioxidative enzymes Catalase and SOD2 are affected as a result of the PA exposure in transfected β-TC3 cells

As many normal metabolic processes within the cell produce ROS, antioxidative enzymes such as catalase or superoxide dismutase 2 (SOD2) are required to maintain the intracellular redox homeostasis to ensure cellular protection and health. As shown above, peroxisomal

dysfunction induced by the *Pex13* knockdown and PA exposure had opposite effects concerning the cellular accumulation of superoxide or hydrogen peroxide, which are both potentially toxic if not properly metabolized. Since the knockdown of *Pex13* led to a cytoplasmic mislocalization of *the* most important peroxisomal antioxidative enzyme, catalase (normally located within the peroxisomal matrix), we were interested to evaluate changes in the protein abundance and gene expression of this enzyme in response to *Pex13* silencing and PA treatment in β-TC3 cells. For this purpose, we treated the *Pex13*-si or *Scr*-siRNA transfected cells with 0.2 mM PA for 48 h. The extracted mRNA and obtained protein homogenates were analyzed by qRT-PCR and Western blotting respectively. Vehicle (BSA-NaOH) was used as a control treatment.

We observed a trend for the *Pex13* knockdown to induce a decrease in the *Cat* mRNA and protein levels in those cells exposed to vehicle ($p \leq 0.42$ and $p \leq 0.83$ respectively) (**Figure: 56A, C** and **D**). On the other hand, the addition of PA into the culture media resulted in a significant ($p \leq 0.05$) increase in the *Cat* expression and protein abundance in control cells treated with *Scr*-siRNA. Also, the PA treatment of the *Pex13* knockdown significantly increased the amount of both *Cat* mRNA expression and protein abundance ($p \leq 0.01$ and $p \leq 0.05$, respectively) (**Figure: 56A, C,** and **D**). However, the silencing of *Pex13*, in combination with PA did not further increase catalase mRNA and protein abundance in comparison to the *Scr*-si transfected group treated with PA.

SOD2 is an important mitochondrial antioxidative enzyme in living cells exposed to oxygen, playing a role in the regulation of the redox balance by catalyzing the dismutation of superoxide radicals produced as a by-product of the oxygen metabolism, into H_2O_2 and molecular oxygen. The *Sod2* mRNA expression and SOD2 protein abundance were analysed under the same experimental conditions used for the CAT analysis. Opposite to our catalase results, the amount of SOD2 (mRNA and protein) was strongly ($p \leq 0.01$) increased (> 2,2-fold) in cells lacking PEX13 (**Figure: 56B, C** and **E**). Furthermore, the addition of PA to the culture led in both groups, to a significant decrease ($p \leq 0.05$) of the SOD2 protein abundance whereas the addition of the FA to the *Scr*-si group showed a tendency ($p \leq 0.29$) to decrease the *Sod2* mRNA levels (**Figure: 56B, C,** and **E**). Interestingly, also here the value of SOD2 in the *Pex13*-si + PA treated group was higher as the one in the corresponding *Scr*-siRNA group.

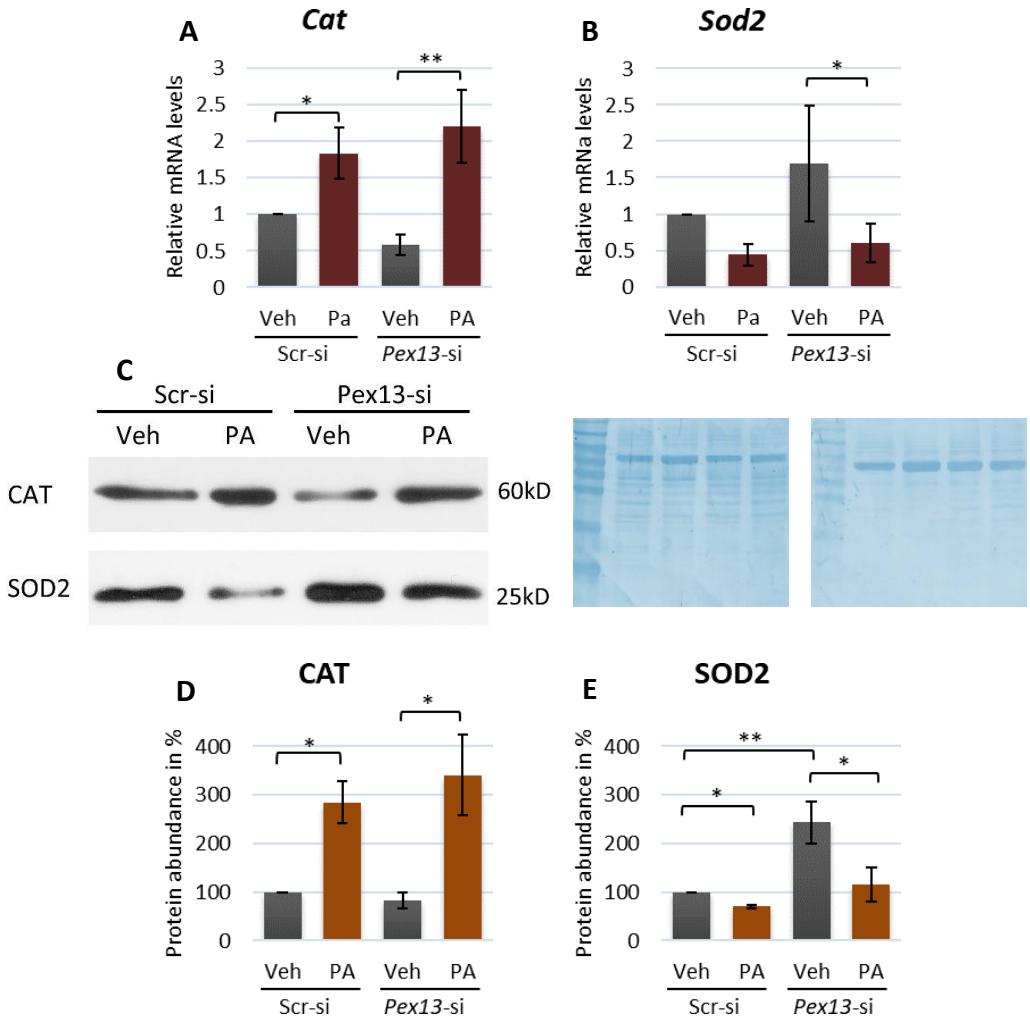

Figure: 56. mRNA levels and protein abundance of the peroxisomal antioxidant enzyme CAT and the mitochondrial antioxidant enzyme SOD2 in *Pex13*-si transfected β-TC3 cells after PA treatment. A-B: β-TC3 cells were transfected with *Pex13*-si or *Scr*-siRNA and treated with PA (0.2 mM). After 48 h the expression of *Cat* and *Sod2* were analyzed by qRT-PCR. Total RNA was used for the analysis and *Cat*, *Sod2* and *Actb* (β-Actin) expression levels were examined. The average threshold (Ct) values of at least three independent experiments were used to calculate the relative amounts of mRNA using the 2-ΔΔ CT method and data was normalized to *Actb* values. Results are presented as relative differences over control. **C:** Representative immunoblotting of CAT and SOD2 in transfected β-TC3 cells after 48 h of PA (0.2 mM) exposure. Total protein (20 µg) was used for the analysis and was sequentially probed with antibodies against CAT and SOD2. Equal loading of protein was controlled by Coomassie staining of the membrane after detection of antibodies. **D-E:** Western blot analysis of CAT and SOD2. Autoradiographic signals were visualized and quantified with the ImageJ software. Values ±SEM represent the protein abundance (in %) relative to *Scr*-si / vehicle sample normalized to total protein loaded from at least three independent experiments. Statistics: ANOVA test for multi-paired values. * $p \leq 0.05$; ** $p \leq 0.01$. Veh: vehicle; PA: palmitic acid; Cat: catalase; Sod2: superoxide dismutase 2.

5.14.6. The palmitic acid treatment in combination with the silencing of *Pex13* in β-TC3 was accompanied by an increase in the Catalase activity and H_2O_2 production.

To further assess the functional consequences of the *Pex13* knockdown on the H_2O_2 homeostasis in β-TC3 cells exposed to toxic concentrations of PA (0.2 mM), the catalase activity and the H_2O_2 production after 48 h of PA treatment was measured. As shown in IF-

experiments on pages 72 and 76, the peroxisome-deficient β-TC3 model exhibited a defective import of peroxisomal matrix proteins that led to a cytosolic accumulation of catalase. Although the protein is upregulated after PA exposure in the *Pex13*-si transfected cells (**Figure: 56C and D**), it might, however, not be enzymatically active due to the mistargeting of catalase. Therefore, we determined the catalase enzyme activity in an assay, based on its peroxidatic function to form formaldehyde from methanol and H_2O_2. Our experiments showed that the *Pex13* silencing (and consequently, the mistargeting of catalase) generally resulted in an increase of the enzymatic activity of catalase (**Figure: 57A**). Further, in both the control and the *Pex13* knockdown background the addition of PA led to a significant ($P<0.05$) increase in the catalase activity. This indicates that the mistargeting of the enzyme into the cytosol in *Pex13* knockdown cells did not abolish the activity of catalase, leading to a similar (~1.6-fold) upregulation in both PA-treated groups. Moreover, the highest induction of the catalase activity was observed in the *Pex13*-siRNA transfected group in combination with PA treatment.

Next, the H_2O_2 production was assessed in control or *Pex13*-si transfected cells, with higher catalase level, after the exposure to PA to corroborate the results previously obtained by the DCFDA dye staining. The highest amount of H_2O_2 was measured after exposing the *Scr*-si treated cells to PA (**Figure: 57B**). In agreement with the results obtained by the DCFDA analysis, the H_2O_2 level was less elevated ($p \leq 0.05$) in the *Pex13*-siRNA model when treated with PA in comparison to the *Scr*-si group exposed to PA.

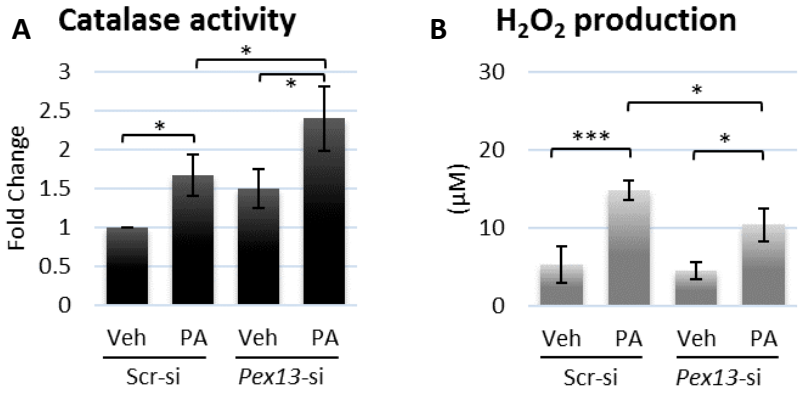

Figure: 57. Catalase enzymatic activity and H_2O_2 production after PA treatment in *Pex13*-si transfected cells. β-TC3 cells were transfected with *Pex13*-si or *Scr*-si RNA and treated with 0.2 mM PA for 48 h. **A:** The peroxidatic function of the antioxidative enzyme catalase was determined. Data were normalized to sample protein concentration determined with the Bradford assay. Values ±SEM represent the fold change relative to *Scr*-si / vehicle sample from three independent experiments. **B:** H_2O_2 production assayed from the sample supernatants. Values ±SEM represent the H_2O_2 in µM from three independent experiments. Data were normalized to sample protein concentration. Statistics: ANOVA test for multi-paired values. * $p \leq 0.05$; *** $p \leq 0.001$. Veh: vehicle; PA: palmitic acid; H_2O_2: hydrogen peroxide.

5.14.7. The insulin release and content were not affected in the *Pex13* knockdown β-TC3 cells exposed to palmitic acid

Because the presence and excretion of insulin is the most obvious evidence for the proper function of the β-cell, we further assessed the functional consequences of the combination of *Pex13* silencing and the PA exposure on insulin homeostasis. Transfected cells were cultured in the presence of 20 mM glucose and exposed to 0.2 mM PA for 48h and insulin biosynthesis and secretion were measured in the protein homogenate and culture medium by ELISA. The down-regulation of *Pex13* did not affect either insulin secretion or its intracellular content (**Figure: 58A** and **B**). Similarly, the exposure to PA in combination with the down-regulation of *Pex13* did not result in any significant change. However, we observed a slight elevation of insulin secretion and cell content after PA treatment only. However, due to the large standard deviation the results obtained from this experiment were not significant.

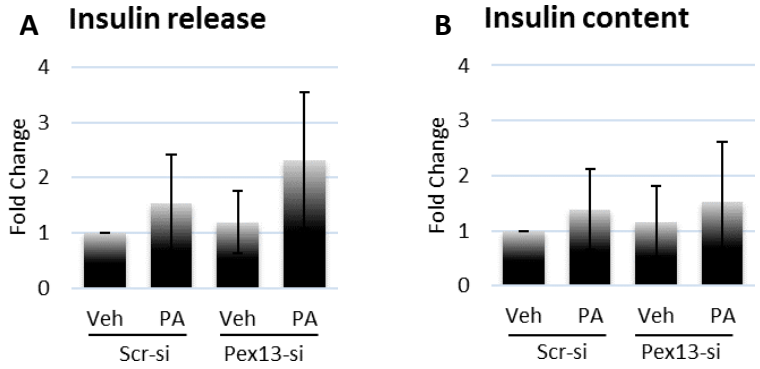

Figure: 58. Insulin release and content in *Pex13*-si transfected β-TC3 exposed to PA. β-TC3 cells were transfected with *Pex13*-si or *Scr*-si RNA and 24 h post transfection, treated with PA (0.2 mM) for 48 h under high glucose condition (20 mM). **A:** Insulin release was measured by ELISA in the harvested supernatant and corrected for protein concentration. **B:** Cell extracts were collected and assayed for insulin content. Data were normalized to sample protein concentration determined with Bradford assay. Values ±SEM represent the insulin fold change levels relative to *Scr*-si / vehicle sample from three independent experiments. Veh: vehicle; PA: palmitic acid.

5.14.8. Peroxisomal and β-cell specific markers regulation after *Pex13* silencing in β-TC3 cells exposed to palmitic acid

One of the main functions of peroxisomes is the β-oxidation of a variety of fatty acids (including long- and medium-chain length FA) playing a key role in their metabolism. For that reason, we were interested in determining whether PA in combination with the *Pex13* gene silencing had any effect on the mRNA expression as well as the protein abundance of peroxisomal enzymes involved in the β-oxidation pathway 1 (*Acox1* and *Acaa1*). qRT-PCR and Western blot were performed in our peroxisome-deficient model after the exposure to

0.2 mM PA for 48 h. As expected, the transient transfection with *Pex13*-siRNA led to a significant (p ≤0.0001) decrease in the *Pex13* mRNA and protein levels (85 %) independently of the addition of PA to the culture medium (**Figure: 59A, D** and **E**).

Surprisingly, the expression of *Acox1*, encoding for the first and rate-limiting enzyme of the β-oxidation pathway located in the peroxisome, was not affected by the *Pex13* silencing whereas the protein abundance of subunit B increased 2.8-fold under the same conditions (**Figure: 59B, D** and **F**). To our surprise the band pattern of ACOX1 in β-TC3 cells was different from the one that were regularly obtained in hepatocytes ((78) since the full enzyme (subunit A) of the ACOX1 was not detected, but only the cleaved subunit B, against which part the antibody was made. In hepatocytes, a clear band would be present at around 74 kD for the complete enzyme. Because of its function in the degradation of fatty acids, we expected an increased expression of *Acox1* in the presence of PA. While no changes were found in the protein levels of subunit B of ACOX1, we observed a slight increment of the mRNA expression of this enzyme after treatment of the cells with PA, which was however not significant (**Figure: 59B**).

Opposite to these observations, the down regulation of *Pex13* led to a significant (p≤ 0.01) decrease in the mRNA levels of *Acaa1,* the gene encoding for Thiolase, whereas its protein abundance was not affected (**Figure: 59C, D** and **G**). Thiolase is the enzyme in charge of the last step of the peroxisomal β-oxidation pathway. Additionally, the PA treatment led to a tendentially reduced expression of *Acaa1* and a significant (p≤ 0.001) decrease in its protein abundance.

Figure: 59. Regulation of peroxisomal genes and protein abundance after PA exposure in *Pex13*-si transfected β-TC3 cells (see figure on page 99). A-C: β-TC3 cells were transfected with *Pex13*-si or *Scr*-si RNA for 24 h and treated with PA (0.2 mM). After 48 h the expression of *Pex13*, *Acox1*, *Acaa1* and *Actb* (β-Actin) was analyzed by qRT-PCR. The efficiency of all primer pairs was ensured in advanced by running a qPCR on dilutions of the template cDNA. The average threshold (Ct) values of at least three independent experiments were used to calculate the relative amounts of mRNA using the 2-ΔΔ CT method and normalized to *Actb* values. Results are presented as a fold over control (*Scr*-si / Veh). **D-F**: Total protein (20 µg) was used for the analysis and was sequentially probed with antibodies against PEX13, ACOX1 and THIOLASE. Values ±SEM represent the protein abundance (in %) relative to *Scr*-si / vehicle sample normalized to total protein loaded from at least three independent experiments. **G**: Representative immunoblotting of PEX13, ACOX1 and THIOLASE after *Pex13*-siRNA transfection and PA treatment in β-TC3 cells. Statistics: ANOVA test for multi-paired values. ** $p \leq 0.01$; *** $p \leq 0.001$; ****$p \leq 0.0001$. *Pex13*: peroxisome biogenesis factor 13; *Acox1*: acyl-coenzyme A oxidase 1; *Acaa1*: acetyl-Coenzyme A acyltransferase 1; Veh: vehicle; PA: palmitic acid.

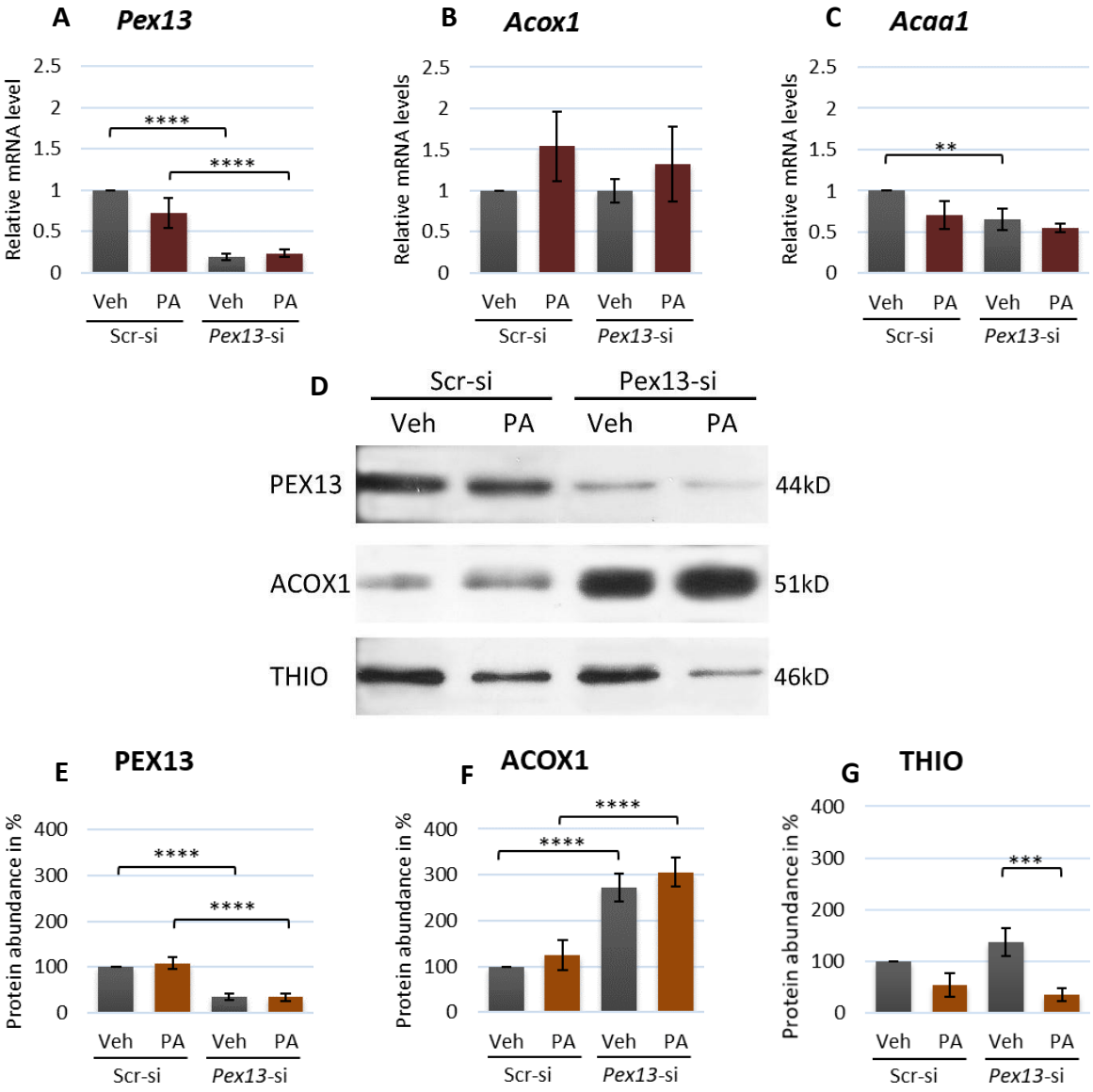

Figure: 59. For figure legend refer to page 98.

We next assessed the mRNA levels for *insulin* and other β-cell specific markers. Insulin, the prominent feature of β-cells and indicator of their differentiation-state, showed a significant decrease ($p \leq 0.05$) in its mRNA levels as a result of the *Pex13* silencing in those cells treated with the vehicle alone. Notably, the treatment of the PEX13 depleted β-TC3 cells with PA, led to an elevation of the insulin expression ($p \leq 0.05$) (**Figure: 60A**) up to levels even higher than the PA *Scr*-si values.

Furthermore, we investigated the *Pax6* expression level since this transcription factor is crucial for the control of key genes coding for proteins that are involved in insulin biosynthesis (*Ins*), secretion, and cell differentiation (*Pdx1*). It has also been shown that a *Pax6* KD leads to decreases in intracellular insulin content, insulin processing and defects in

glucose-induced insulin secretion [196]. Interestingly, the specific silencing of *Pex13* resulted in a significant decrease ($p \leq 0.0001$) of *Pax6* mRNA expression independently if the cells were exposed to PA or not (**Figure: 60B**).

Pdx1, a homeobox gene essential for pancreatic development and glucose homeostasis [197], showed a significant decrease in its mRNA levels as a result of the specific silencing of *Pex13* in the vehicle-treated group. Treatment of the β-TC3 cells with PA on the other hand led to an up-regulation of *Pdx1* without, however, reaching statistical significance ($p \leq 0.189$). Moreover, the response to PA showed a 1,5-fold increase in the *Scr*-si group compared to a > 2-fold increase of the value for the *Pex13*-si group (**Figure: 60C**). The overall *Pdx1* mRNA value of the PA stimulated *Scr*-si group was, however, not reached.

Pax4, a transcriptional factor involved in β-cell differentiation exhibited a non-significant ($p \leq 0.09$) reduction in its mRNA levels upon *Pex13* silencing in the vehicle-treated groups (**Figure: 60D**). PA treatment in the *Scr*-si transfected cells led to a significant ($p \leq 0.05$) decrease in the *Pax4* mRNA expression. In contrast, we observed the opposite effect in cells with the *Pex13* knockdown background where the PA exposure resulted in an ($p \leq 0.05$) increase in *Pax4* mRNA levels, suggesting a different regulation of the gene under peroxisome-deficient conditions.

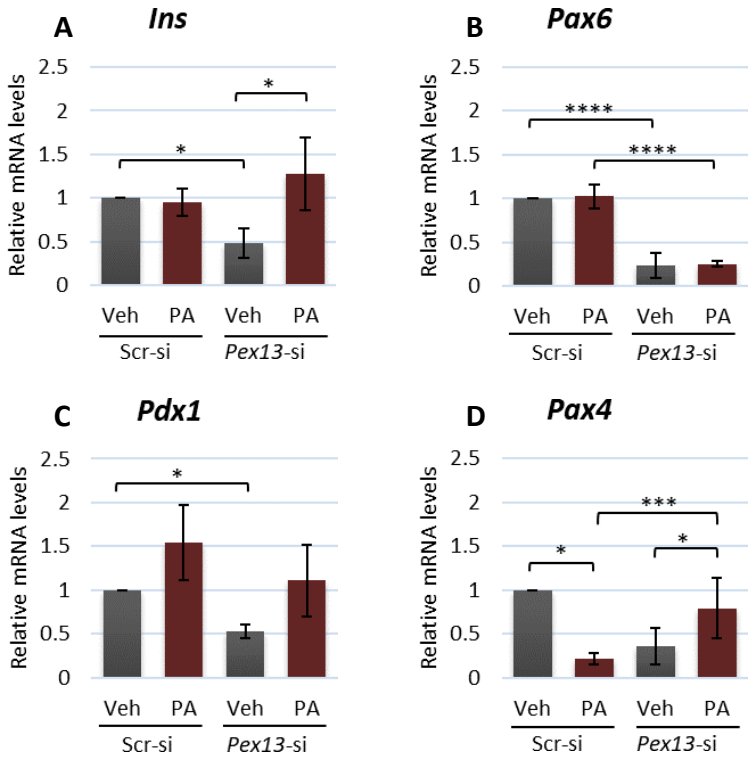

Figure: 60. Regulation of *insulin*, *Pax6*, *Pdx1* and *Pax4* mRNA levels after palmitic acid exposure in *Pex13*-si transfected β-TC3 cells. β-TC3 cells were transfected with *Pex13*-si or *Scr*-si RNA for 24 h and treated with PA (0.2 mM). After 48 h the expression of *Ins*, *Pdx1*, *Pax4*, *Pax6* and *Actb* (β-Actin) was analyzed by qRT-PCR. The average threshold (Ct) values of at least three independent experiments were used to calculate the relative amounts of mRNA using the 2-ΔΔ CT method and normalized to *Actb* values. Statistics: ANOVA test for multi-paired values. * $p \leq 0.05$; ** $p \leq 0.01$; **** $p \leq 0.0001$. *Ins*: insulin; *Pdx1*: pancreatic and duodenal homeobox 1; *Pax6*: paired box 6; *Pax4*: paired box 4; Veh: vehicle; PA: palmitic acid.

5.14.9. Analysis of the mRNA levels and protein abundance of PPARs in β-TC3 cells treated with either *Pex13*- or *Scr*-siRNA after palmitic acid exposure

PPARs represent one of the best-recognized sensor systems for fatty acids, responding to changes in the cell metabolic status and lipid fluxes [54]. Since their activation (by some fatty acids) results in the regulation of many peroxisomal enzymes involved in fatty acid oxidation as well as in peroxisomal division and proliferation [51], we analyzed the mRNA levels and protein abundance of the PPARs after the *Pex13* silencing in βTC3 cells exposed to PA. Our qPCR results indicated that all the treatments performed on the β-TC3 cells (PA exposure, *Pex13* knockdown and the combination of both) induced the expression of *Pparα* mRNA, whereas the treatment with PA caused a significant reduction ($p \leq 0.05$) of the PPARα protein abundance independently of the *Pex13* silencing (**Figure: 61A, D** and **E**).

The expression of *Pparβ* mRNA showed a significant ($p \leq 0.05$) decrease after silencing *Pex13* in the vehicle-treated cells. This effect was surprisingly counteracted following the PA exposure of the *Pex13* knockdown group, were a massive expression of the *Pparβ* mRNA was induced. The exposure of the *Scr*-si RNA transfected β-TC3 cells to PA alone did not affect the *Pparβ* expression (**Figure: 61B**).

The down regulation of *Pex13* induced a 1.8-fold increase of the *Pparγ* mRNA levels ($p \leq 0.001$) and did not affect its protein abundance. The addition of PA to the culture medium of the *Scr*-siRNA transfected group reduced the gene expression ($p \leq 0.05$) and protein abundance ($p \leq 0.01$) of *Pparγ*. Similarly, in the cells exhibiting the *Pex13* knockdown, the fatty acid treatment caused a 1.4-fold decrease in the PPARγ protein abundance ($p \leq 0.05$) (**Figure: 61C, D** and **F**).

Figure: 61. Regulation of PPARs gene and protein abundance after PA exposure in *Pex13*-si transfected β-TC3 cells (see figure on page 102). A-C: β-TC3 cells were transfected with *Pex13*-si or *Scr*-si RNA for 24 h and treated with PA (0.2 mM). After 48 h the expression of *Pparα, Pparβ, Pparγ* and *Actb* (β-Actin) was analyzed by qRT-PCR. The average threshold (Ct) values of at least three independent experiments were used to calculate the relative amounts of mRNA using the 2-ΔΔ CT method and normalized to *Actb* values. Results are presented as a fold-change of control values (*Scr*-si / Veh). **D:** Representative immunoblotting of PPARα and PPARγ in transfected β-TC3 cells after 48 h of PA (0.2 mM) exposure. Total protein (20 µg) was used for the analysis and was sequentially probed with antibodies against PPARα and PPARγ. Equal loading of protein was controlled by Coomassie staining of the membrane after detection of antibodies. **E-F**: Western blot analysis of PPARα and PPARγ. Autoradiographic signals were visualized and quantified with the ImageJ software. Values ±SEM represent the protein abundance (in %) relative to *Scr*-si / vehicle sample normalized to total protein loaded from at least three independent experiments. The bands on films were quantified with ImageJ Software. Statistics: ANOVA test for multi-paired values. * $p \leq 0.05$; ** $p \leq 0.01$; *** $p \leq 0.001$; ****$p \leq 0.0001$. PPARα / γ: peroxisome proliferator-activated receptor alpha / gamma; Veh: vehicle; PA: palmitic acid

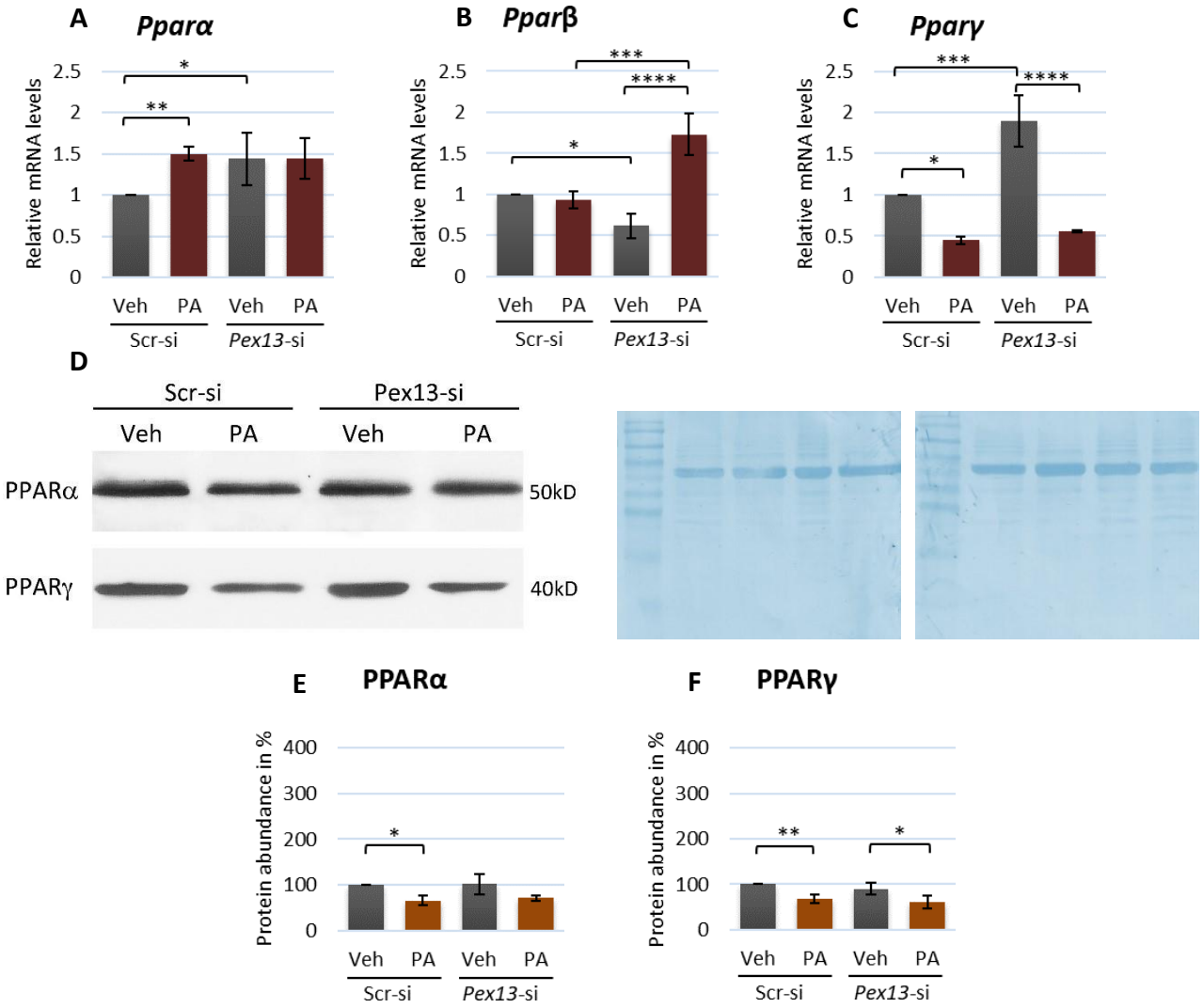

Figure: 61. For figure legend refer to page 101.

5.15. Influence of phytanic acid in β-TC3 cells displaying a *Pex13*-KD

5.15.1. The down-regulation of *Pex13* led to an increased lethality in β-TC3 cells after phytanic acid exposure

Since phytanic acid (PHY) depends completely on the peroxisomal β-oxidation for its degradation, we analyzed whether β-cells displaying a peroxisome-deficiency were more susceptible to lipotoxicity as a result of toxic PHY concentrations. To that end, we exposed our β-TC3 cell *Pex13* knockdown model to 60 µM Phy for 48 h in the background of hyperglycaemia (20 mM). The cell lethality was analyzed subsequently using the Trypan blue exclusion test. Parallel incubations were performed using the PHY solubilizing compound dimethyl sulfoxide (DMSO) as control. Similar to the experiments carried out with PA, we started the cell treatment 24 h after transfection adding the PHY solution every 24 h over a period of 2 days to ensure the down-regulation of *Pex13*. We observed that the treatment

with PHY led to a reduction of the cell viability in both, the Scr-si and Pex13-siRNA treated groups. However, cells exhibiting the *Pex13* knockdown showed higher susceptibility to PHY ($p<0.0001$) reaching more than 70 % lethality in comparison to the cells treated with DMSO only (**Figure: 62**).

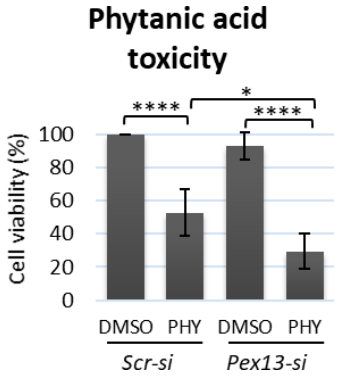

Figure: 62. Increased β-TC3 cell dead after PHY treatment. β-TC3 cells were prepared and transfected with *Pex13*-si and *Scr*-siRNA. Transfected cells were incubated with DMEM medium containing 60 μM phytanic acid (PHY) diluted in DMSO for 48 h. Trypan blue exclusion test was carried out for the determination of cell viability. The number of intact cells, which had no blue staining, was determined (eight fields per experiment) and percentage of living cells per group is given. Statistics: ANOVA test for multi-paired values. * $p \leq 0.05$; ****$p \leq 0.0001$. DMSO: dimethyl sulfoxide; PHY: phytanic acid.

5.15.2. The silencing of *Pex13* in β-TC3 cells led to an increased intracellular lipid accumulation after phytanic acid exposure

We analyzed whether the exposure to PHY modified the intracellular lipid accumulation in β-TC3 cells treated with *Pex13*-siRNA. The appearance of the lipid droplets was examined by light microscopy using the Oil red O staining method. Our results showed an increase in the lipid droplet abundance after the down-regulation of *Pex13* suggesting a rise in the cellular lipid storage. In both cases (*Scr*-si and *Pex13*-si) the droplets appeared as small and round bodies scattered heterogeneously across the cytoplasm of some cells (**Figure: 63A** and **C**). The introduction of 60μM PHY into the culture medium led to an increase in the droplet size (**Figure: 63A** and **B**), an effect, which was potentiate in the *Pex13* knockdown (**Figure: 63B** and **D**).

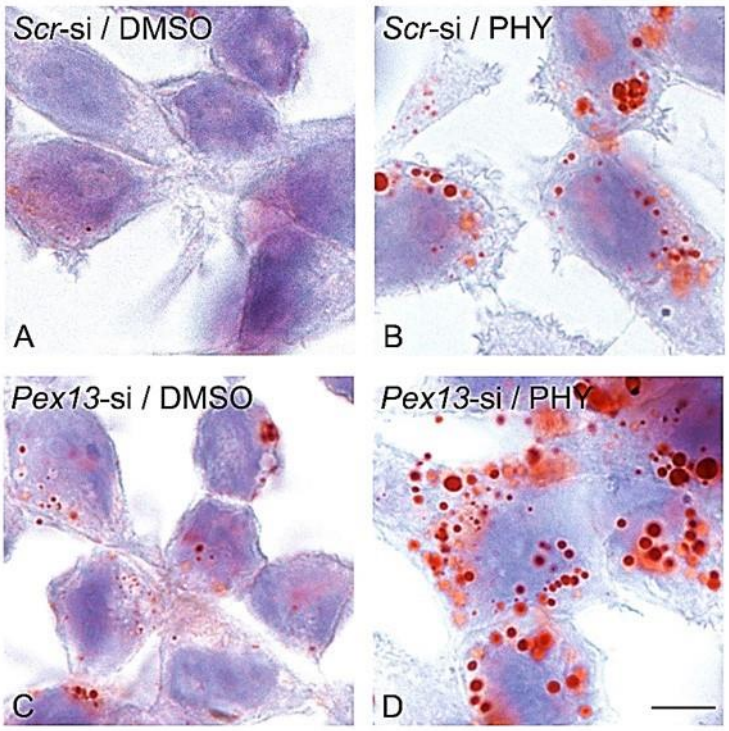

Figure: 63. Oil red O staining for detection of lipid droplet accumulation in *Pex13* KD β-TC3 cells after phytanic acid exposure. β-TC3 cells were transfected with *Pex13*-si and *Scr*-si RNA for 24 h before been exposed to PHY (60 µM) or DMSO/medium as a control for 48 h. The appearance of lipid droplets was observed after Oil red O staining. **A-B:** *Scr*-siRNA treated cells exposed to DMSO/medium (**A**) and PHY (**B**); **C-D:** *Pex13*-si transfected cells exposed to DMSO/medium (**C**) or PHY (**D**). Nucleoli were stained with Hematoxylin. Results were examined using a phase contrast microscope (LEICA DMRD equipped with a LEICA CD480 camera). Bar = 26 µm.

5.15.3. Regulation of peroxisomal lipid transporters *Abcd1* and *Abcd3* after *Pex13* silencing in β-TC3 cells exposed to phytanic acid

Following the same trend as the one observed after PA treatment, the exposure of β-TC3 cells lacking functional peroxisomes to PHY led to an increased lipid droplet accumulation. To further investigate the role of peroxisomes in this phenomenon we decided to analyze whether the import of fatty acids into the organelle was disturbed. For this purpose, we investigated *Abcd1* and *Abcd3* mRNA expressions as well as the ABCD3 protein abundance by qRT-PCR and Western blot respectively. Our results showed a trend for the *Pex13* knockdown to induce an increase in *Abcd1* mRNA levels ($p = 0.1$), while the exposure to PHY in the *Scr*-siRNA group did not alter the mRNA expression of the lipid transporter (**Figure: 64A**) whereas the combination of PHY with the Pex13 silencing exhibited a trend to reduce the Abcd1 mRNA to control levels again ($p = 0.29$). No changes in the *Abcd3* mRNA levels either after the down-regulation of *Pex13,* the treatment with PHY or the combination of both (fold change between 1.2 and 1.6) were observed (**Figure: 64B**). In contrast, the cell exposure to PHY did indeed increase the ABCD3 protein abundance in both, the Scr-si transfected cells and the *Pex13* silencing group (**Figure: 64C**), whereas the peroxisome-deficiency alone showed a tendency to decrease the ABCD3 protein amount.

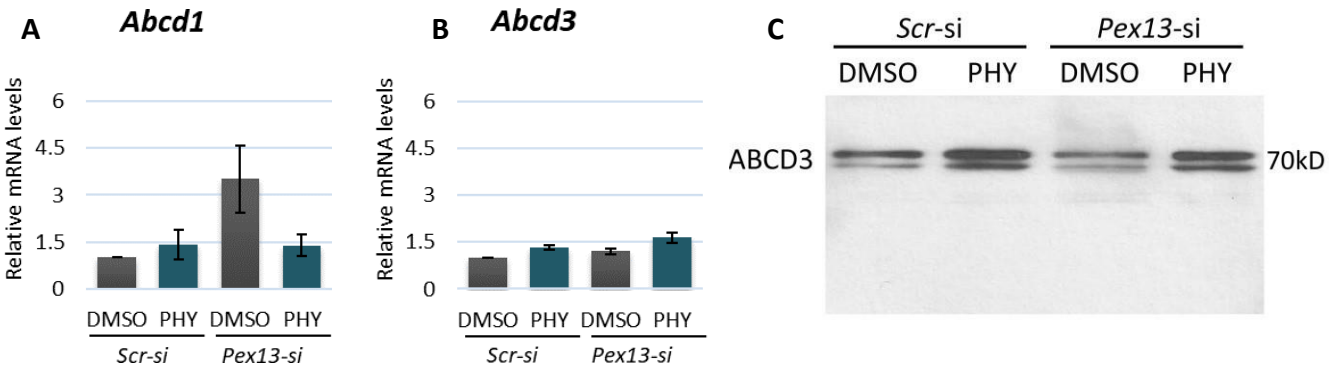

Figure: 64. Peroxisomal membrane lipid transporters *Abcd1* and *Abcd3* mRNA levels and ABCD3 protein abundance in *Pex13*-si transfected β-TC3 cells after phytanic acid treatment. β-TC3 cells were transfected with *Pex13*-si or *Scr*-si RNA and treated with PHY (60 µM) for 48 h. **A-B:** The expression of *Abcd1* and *Abcd3* was analyzed by qRT-PCR. The average threshold (Ct) values of three independent experiments were used to calculate the relative amounts of mRNA using the 2-ΔΔ CT method and data was normalized to *Actb* (β-Actin) values. Results are presented as a fold over control. **C:** Representative Western blot analysis of ABCD3. Total protein (20 µg) was used for the analysis and the Western blot was probed with an antibody against ABCD3. Equal loading of protein was controlled by Coomassie staining of the membrane after detection of antibodies. DMSO: dimethyl sulfoxide; Phy: phytanic acid; ABCD1/3: ATP binding cassette subfamily D member 1 and 3.

5.15.4. Superoxide and hydrogen peroxide generation in β-TC3 cells with *Pex13* knockdown after phytanic acid exposure as an indicator of oxidative stress

To further evaluate the functional consequences of the peroxisome dysfunction in β-TC3 cells after PHY exposure, we analyzed the generation of intracellular oxidative stress by analysing the production of superoxide (O^{2-}) and hydrogen peroxide (H_2O_2). Superoxide generation was monitored by the ROS-sensitive dye dihydroethidium (DHE) after *Pex13* silencing and the exposure to 60 µM PHY for 48 h. We observed no changes in the DHE fluorescence intensity either after the down-regulation of *Pex13*, the treatment with PHY or the combination of both (**Figure: 65**).

The amount of H_2O_2 produced was examined by DCFDA staining using 150 µM PHY for 6 h. In the *Scr*-siRNA group, the addition of PHY to the culture medium resulted in a significant 2.9-fold increase ($p \leq 0.0001$) in the DCFDA fluorescence signal (**Figure: 65J**). In contrast, already the *Pex13* silencing led to an accumulation of H_2O_2 (1.9-fold) in comparison to the *Scr*-siRNA group, however, the addition of PHY to the *Pex13*-si transfected group did not result in a significant H_2O_2 increase, suggesting that the cytoplasmic catalase result of the *Pex13* knockdown, protects the cells against further H_2O_2 accumulation. (**Figure: 65J**).

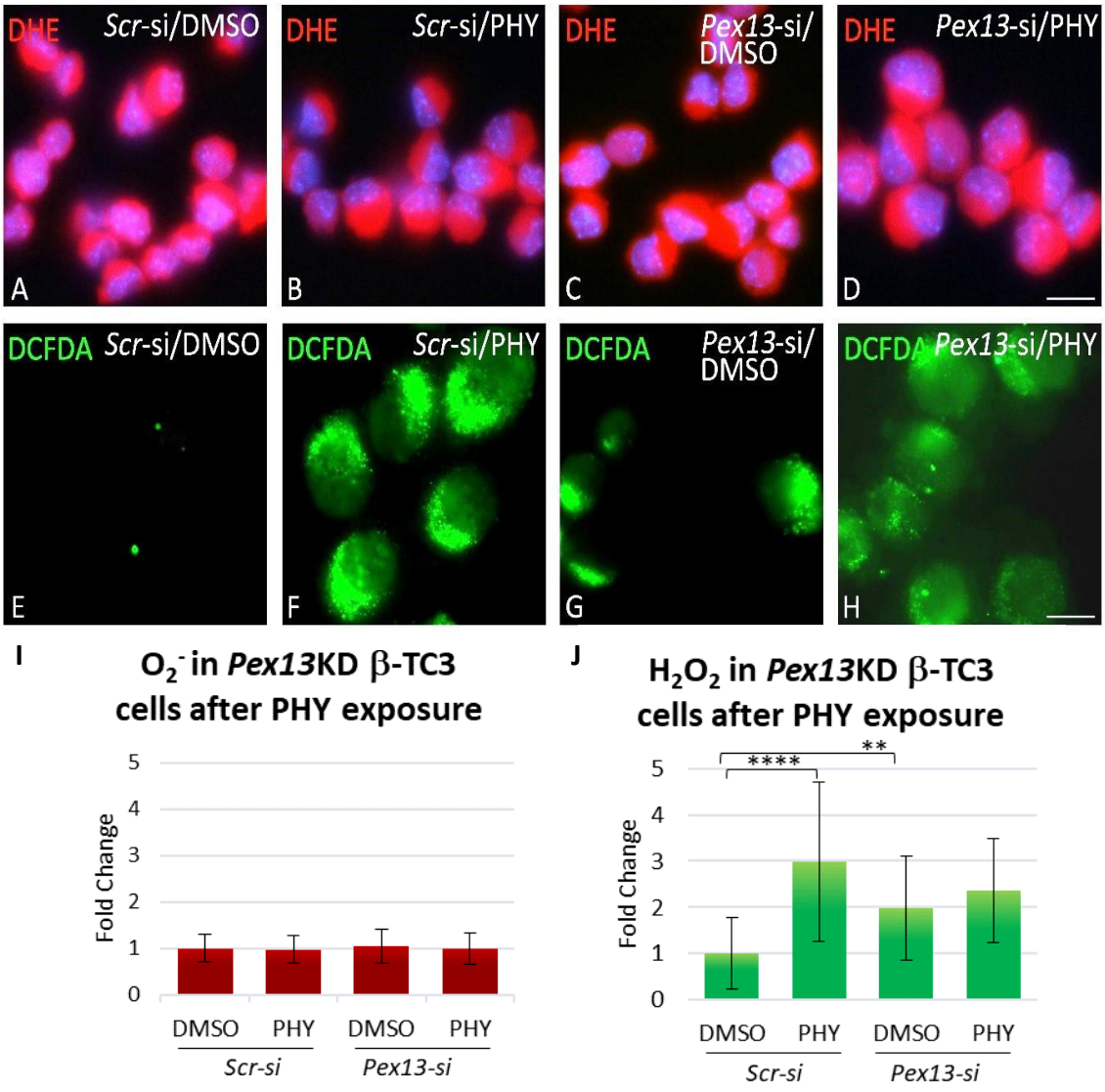

Figure: 65. Measurement of superoxide and hydrogen peroxide levels by relative quantification of DHE and DCFDA fluorescent signal in β-TC3 cells with *Pex13* knockdown after phytanic acid exposure. β-TC3 cells were transfected with *Pex13*-si or *Scr*-si RNA, treated with PHY, and stained with Dihydroethidium (DHE) (**A-D**) to visualize the accumulation of O^{2-} or with 2´,7´-dichlorofluorescin diacetate (DCFDA) to visualize the accumulation of H_2O_2 (**E-H**). **A-D:** DHE staining of: **A:** *Scr*-siRNA transfected cells treated with DMSO/medium or **B:** 60 µM PHY for 48h; **C:** *Pex13*-si transfected cells treated with DMSO/medium or **D:** 60 µM PHY for 48h. Nuclei were counterstained with Hoechst 33342 dye. **E-H:** DCFDA staining of: **A:** *Scr*-siRNA transfected cells treated with DMSO/medium or **B:** 150 µM PHY; **C:** *Pex13*-si transfected cells treated with DMSO/medium or **D:** 150 µM PHY. The fluorescence measurement was completed 6 h after treatment. **I:** Relative quantification of superoxide levels. At least 100 cells from 3 independent experiments were used for the measurements. **J:** Relative quantification of H_2O_2 production. 30 living cells could be photographed to measure the fluorescence intensity due to the short-lived stability of the DCFDA staining. The quantification of the fluorescence intensity was done with the ImageJ software. Statistics: ANOVA test for multi-paired values. **p≤0.01; **** p ≤ 0.0001. DMSO: dimethyl sulfoxide; Phy: phytanic acid. Scale bar = 32 µm in A-D and 24 µm in E-H.

5.15.5. Analysis of *Cat*, *Sod1* and *Sod2* mRNA expressions and protein abundances after phytanic acid exposure in transfected β-TC3 cells

As shown before in this thesis, the peroxisome import deficiency induced by the *Pex13* silencing in β-TC3 cells resulted in the cytoplasmic mislocalization of catalase. Therefore, we were interested in evaluating the influence of the *Pex13* knockdown together with the PHY

exposure in the protein abundance and gene expression of this and other antioxidative enzymes with the purpose of obtaining an overview of the regulation of ROS in our model. *Pex13*-si or *Scr*-siRNA treated cells were exposed to 60 μM PHY for 48 h and the extracted mRNA and obtained protein homogenates were analyzed by qRT-PCR and Western blot respectively. DMSO/medium was used as a control treatment.

Interestingly, neither the silencing of *Pex13* nor the introduction of PHY to both (*Scr*-si or *Pex13*-si) groups resulted in significant changes in the *cat* mRNA levels, although a tendency of PHY to decrease the *cat* mRNA levels was observed (**Figure: 66A**). No changes in the CAT protein abundance either after the down-regulation of *Pex13*, the treatment with PHY or the combination of both were observed (**Figure: 66A, D** and **E**). Interestingly, the transfection with *Pex13*-siRNA resulted in a 2.5-fold increase of *Sod2* gene expression ($p \leq 0.01$) (**Figure: 66C**) whereas the exposure of both groups (*Scr*-si and *Pex13*-si) to PHY showed a tendency to decrease the SOD2 protein abundance (**Figure: 66D** and **F**).

SOD1 (superoxide dismutase 1/ Cu-Zn) is an enzyme that converts superoxide radicals to molecular oxygen and H_2O_2 that is localized to several intracellular compartments (e.g. cytoplasm, mitochondria and peroxisomes). The transfection of β-TC3 cells with *Pex13*-siRNA led to a significant ($p \leq 0.001$) increase of *Sod1* mRNA levels. Moreover, the introduction of PHY to the *Scr*-siRNA transfected group resulted as well in an upregulation of the *Sod1* gene expression ($p \leq 0.01$) (**Figure: 66B**). Despite the elevated *Sod1* mRNA levels in the *Pex13* knockdown, the addition of PHY to the peroxisome-deficient group led to a small but significant reduction ($p \leq 0.05$) in its gene expression (**Figure: 66B**).

Figure: 66. mRNA levels and protein abundances of the antioxidative enzymes CAT, SOD2 and Sod1 in *Pex13*-si transfected β-TC3 cells after PHY treatment (see figure on page 108). A-C: β-TC3 cells were transfected with *Pex13*-si or *Scr*-siRNA and treated with PHY (60 μM). After 48 h the expression of *Cat*, *Sod1* and *Sod2* were analyzed by qRT-PCR. Total RNA was used for the analysis and *Cat*, *Sod1, Sod2* and *Actb* (β- Actin) expression levels were examined. The average threshold (Ct) values of at least three independent experiments were used to calculate the relative amounts of mRNA using the 2-ΔΔ CT method and data was normalized to *Actb* values. Results are presented as a fold over control. **D:** Representative immunoblotting of CAT and SOD2 after 48 h of PHY (60 μM) exposure. Total protein (20 μg) was used for the analysis and was sequentially probed with antibodies against CAT and SOD2. Equal loading of protein was controlled by Coomassie staining of the membrane after detection of antibodies. **E-F**: Western blot analysis of CAT and SOD2. Autoradiographic signals were visualized and quantified with the ImageJ software. Values ±SEM represent the protein abundance (in %) relative to *Scr*-si / DMSO sample normalized to total protein loaded from at least three independent experiments. Statistics: ANOVA test for multi-paired values. * $p \leq 0.05$; ** $p \leq 0.01$; *** $p \leq 0.001$. DMSO: dimethyl sulfoxide; Phy: phytanic acid; Cat: catalase; Sod1 and Sod2: superoxide dismutase 1 / 2.

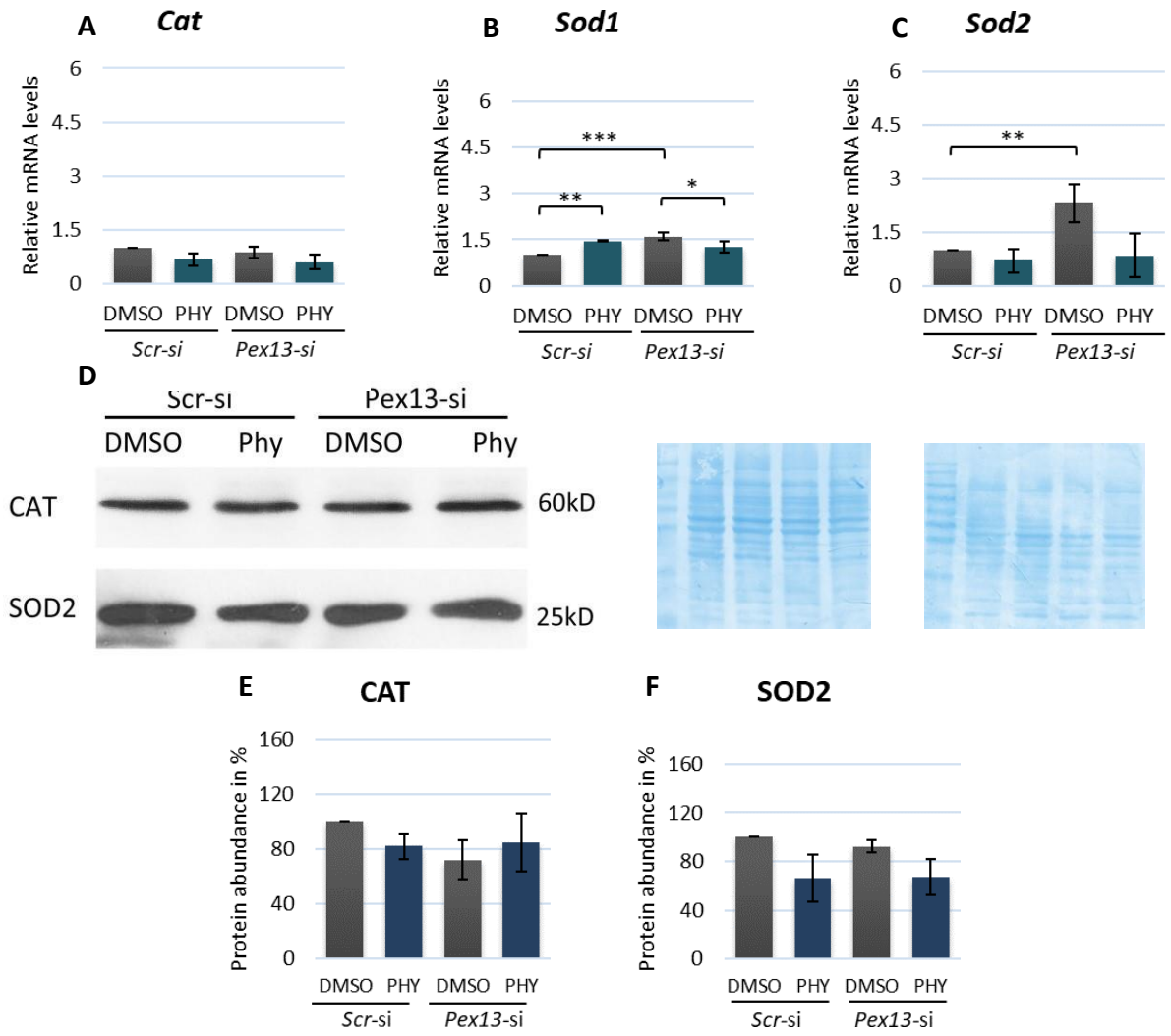

Figure: 66. For figure legend refer to page 107.

5.15.6. The phytanic acid treatment in β-TC3 led to an increase in the H_2O_2 production

To extend our overview of the functional consequences of the *Pex13* silencing together with the phytanic acid treatment on ROS homeostasis, we analysed the H_2O_2 production after 48 h of PHY (60 μM) treatment in peroxisome-deficient β-TC3 cells. This assay, as in the case of the PA experiments, helped us to ensure the DCFDA results as well as to understand the involvement of the cytoplasmic catalase (in the case of the *Pex13*-si transfected cells) or the peroxisomal one (for the *Scr*-si treated controls) in the H_2O_2 decomposition.

As shown in Fig. 76, the *Pex13* silencing induced a mild increase of H_2O_2 already in comparison to the *Scr*-siRNA group. However, the introduction of PHY to the culture medium resulted in the highest amount of H_2O_2 produced in the *Scr*-siRNA group (**Figure: 67**), while after the *Pex13* silencing, PHY induced only a very modest H_2O_2 increase.

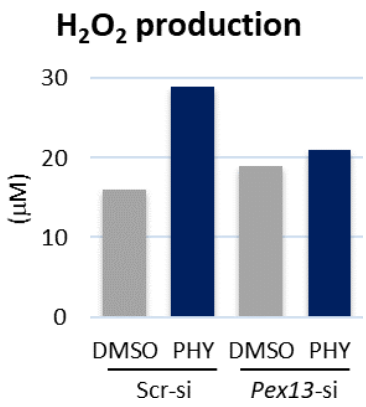

Figure: 67. H_2O_2 production after PHY treatment in *Pex13*-si transfected cells. β-TC3 cells were transfected with *Pex13*-si or *Scr*-si RNA and treated with 60 µM PHY for 48 h. H_2O_2 production was assayed from the sample supernatants. Values represent the H_2O_2 in µM from one experiment. Data were normalized to sample protein concentration. DMSO: dimethyl sulfoxide; Phy: phytanic acid; H_2O_2: hydrogen peroxide.

5.15.7. Insulin release and content in *Pex13* knockdown β-TC3 cells exposed to phytanic acid

Next, we evaluated insulin biosynthesis and secretory capacity in our model. *Pex13*si-transfected cells were cultured in the presence of 20 mM glucose and exposed to 60 µM phytanic acid for 48 h and insulin content and release were measured in the protein homogenate of cell pellet and culture medium by ELISA. Neither the silencing of *Pex13* nor the treatment with PHY in the control cells resulted in any change in the insulin release or in its intracellular content although we observed a slight trend for the insulin content (p = 0,16) to decrease after PHY treatment (**Figure: 68**). Moreover, we observed that in the group displaying a *Pex13* knockdown background the addition of PHY led to a significant ($p \leq 0.05$) increase in the insulin secreted as well as a decrease ($p \leq 0.01$) in the intracellular content of this protein (**Figure: 68A** and **B**).

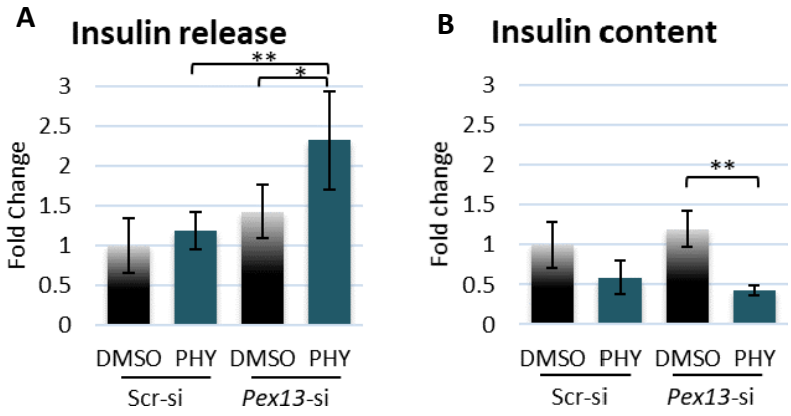

Figure: 68. Insulin release and content in *Pex13*-si transfected β-TC3 exposed to PHY. β-TC3 cells were transfected with *Pex13*-si or *Scr*-si RNA and treated with PHY (60 µM) for 48 h under high glucose condition (20 mM). **A:** Insulin release was measured by ELISA in the harvested supernatant and corrected for protein concentration. **B:** Cell pellet extracts were collected and assayed for insulin content. Data were normalized to sample protein concentration determined with the Bradford assay. Values ±SEM represent the insulin fold change levels relative to *Scr*-si / DMSO sample from three independent experiments. Statistics: ANOVA test for multi-paired values. * $p \leq 0.05$; ** $p \leq 0.01$. DMSO: dimethyl sulfoxide; Phy: phytanic acid.

5.15.8. Analysis of peroxisomal and β-cell specific marker regulation after *Pex13* silencing in β-TC3 cells exposed to phytanic acid

Phytanic acid is metabolised exclusively in the peroxisome. We were therefore interested to analyse whether the combination of PHY exposure with the *Pex13* silencing regulate the expression of genes involved in the peroxisomal α- and β-oxidation pathways. For this purpose, qRT-PCR was performed in the *Pex13*si-RNA treated β-TC3 cells after the exposure to 60 µM PHY for 48 h. As control and to assure that the *Pex13* knockdown was still active during our experiment, the mRNA levels and protein abundance of *Pex13* under the same experimental conditions were first analyzed. The transfection with *Pex13*-siRNA led to a significant decrease in the *Pex13* mRNA levels and protein amounts ($p \leq 0.0001$ and $p \leq 0.01$ respectively) independently of the exposure to PHY (**Figure: 69A-C**).

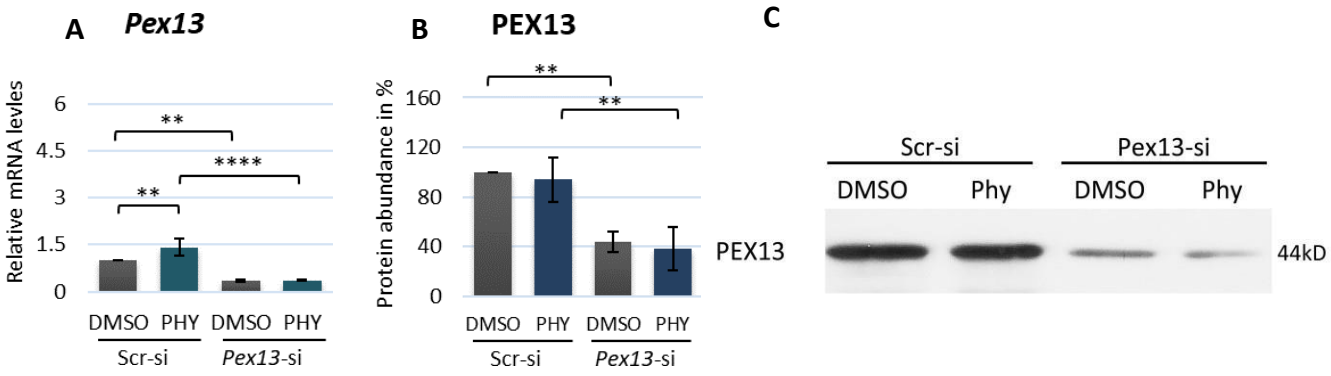

Figure: 69. Regulation of *Pex13* gene expression and protein abundance after PHY exposure in β-TC3 cells transfected with *Pex13*-siRNA. A: β-TC3 cells were transfected with *Pex13*-si or *Scr*-si RNA for 24 h and treated with PHY (60 µM). After 48 h the expression of *Pex13* and *Actb* (β-Actin) were analyzed by qRT-PCR. The average threshold (Ct) values of at least three independent experiments were used to calculate the relative amounts of mRNA using the 2-ΔΔ CT method and normalized to *Actb* values. Results are presented as a fold over control (*Scr*-si / DMSO). **B**: Total protein (20 µg) was used for the analysis and was sequentially probed with antibodies against PEX13. Values ±SEM represent the protein abundance (in %) relative to *Scr*-si / DMSO sample normalized to total protein loaded from at least three independent experiments. The bands on films were quantified with ImageJ Software. **C**: Representative immunoblotting of PEX13 after *Pex13*-siRNA transfection and PHY treatment in β-TC3 cells. Statistics: ANOVA test for multi-paired values. ** $p \leq 0.01$; ****$p \leq 0.0001$. *Pex13*: peroxisome biogenesis factor 13; DMSO: dimethyl sulfoxide; Phy: phytanic acid.

Further, our results showed a significant increase in the expression of *Phyh*, the gene encoding for phytanoyl-CoA hydroxylase (an enzyme required for the α-oxidation of phytanic acid), after *Pex13* silencing (1.7-fold) (**Figure: 70A**). Interestingly, the addition of PHY into the culture medium induce a strong *Phyh* increase (2.8-fold) only in the *Scr*-siRNa group. The PHY-induced upregulation was not present in the β-TC3 cells with *Pex13* deficiency.

In contrast to *Phyh* mRNA, the mRNA levels of *Acox3*, encoding for the first enzyme of the peroxisomal β-oxidation pathway involved in the desaturation of branched fatty acids, showed a significant ($p \leq 0.05$) increase of 2.2-fold only after PHY treatment in the *Scr*-siRNA group. No significant differences were observed between the non-treated groups (*Scr*-siRNA and *Pex13*-siRNA transfected) as well as between the *Pex13* deficient cells with and without the PHY exposure (**Figure: 70B**).

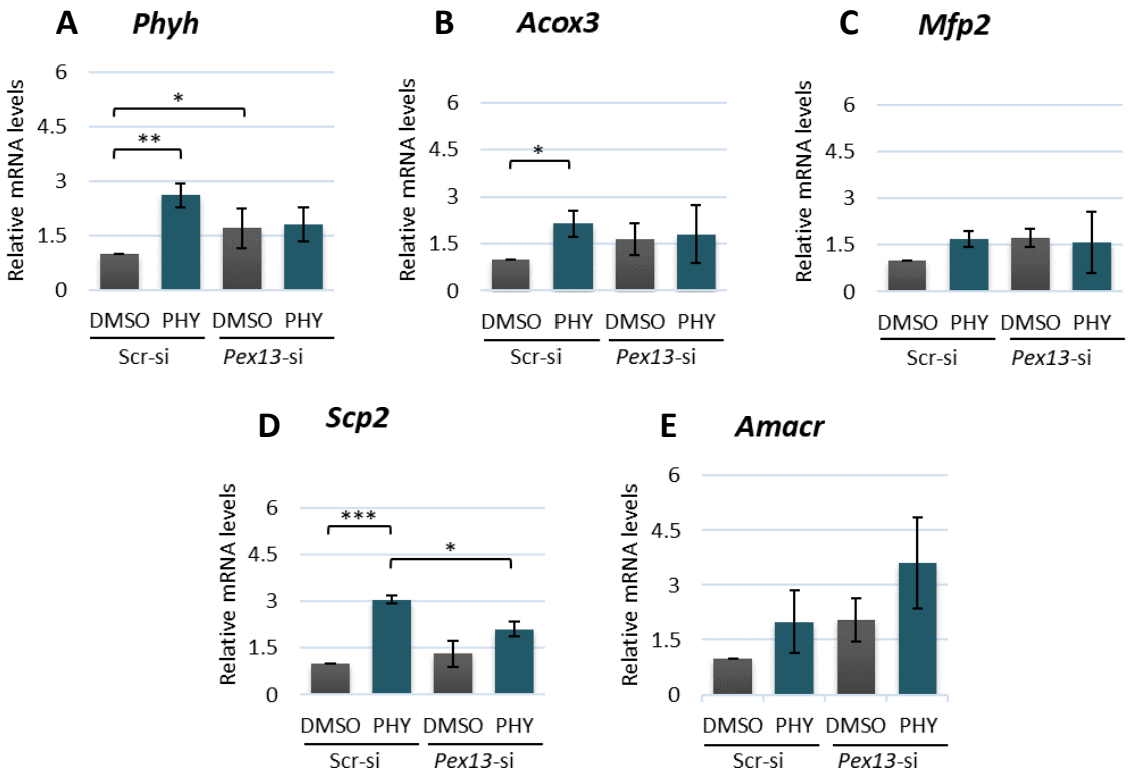

Figure: 70. Regulation of peroxisomal genes after PHY exposure in *Pex13*-si transfected β-TC3 cells. β-TC3 cells were transfected with *Pex13*-si or *Scr*-si RNA for 24 h and treated with PHY (60 μM). After 48 h the expression of *Phyh, Acox3*, *Mfp2*, *Scp2*, *Amacr* and *Actb* (β-Actin) was analyzed by qRT-PCR. The efficiency of all primer pairs was ensured in advanced by running a qPCR on dilutions of the template cDNA. The average threshold (Ct) values of three independent experiments were used to calculate the relative amounts of mRNA using the 2-ΔΔ CT method and normalized to *Actb* values. Results are presented as a fold over control (*Scr*-si / DMSO). Statistics: ANOVA test for multi-paired values. * $p \leq 0.05$; ** $p \leq 0.01$; *** $p \leq 0.001$. *Phyh*: phytanoyl-CoA hydroxylase; *Acox3*: acyl-coenzyme A oxidase 3; *Mfp2*: multifunctional protein 2; *Scp2:* sterol carrier protein X/2; *Amacr*: alpha-methylacyl-CoA racemase; DMSO: dimethyl sulfoxide; Phy: phytanic acid.

Surprisingly, neither the *Pex13* silencing, the PHY exposure or the combination of both affected the expression of *Mfp2* mRNA, encoding for the multifunctional protein 2, also involved in peroxisomal β-oxidation (**Figure: 70C**).

Scp2 is a gene that encodes 2 proteins: sterol carrier protein X (a peroxisome-associated thiolase involved in the last step of branched-chain fatty acids β-oxidation) and sterol carrier

protein 2 (an intracellular lipid transfer protein). The *Scp2* mRNA was not significantly altered after the *Pex13* silencing. However, a significant increase ($p \leq 0.001$) in the *Scp2* mRNA levels was noted following the introduction of PHY into the *Scr*-siRNA group (3-fold) which was attenuated in the *Pex13*-si treated cells (**Figure: 70D**).

Some derivatives from phytanic acid (e.g. CoA esters of pristanic acid) require the conversion from their 2R-methylacly-CoA ester to 2S-methylacyl-CoA epimers in order to be β-oxidized. The enzyme responsible of this catalysis is an alpha-methylacyl-CoA racemase, encoded by the *Amacr* gene. The *Amacr* mRNA level was increased 1.9-fold ($p = 0.09$) in the *Pex13* siRNA-treated cells in comparison to the *Scr*-siRNA control group. Moreover, the *Amacr* mRNA level exhibited a tendency to increase by 1.9-fold after the exposure to PHY in the *Scr*-siRNA group ($p = 0.18$) and the *Pex13* knockdown cells ($p = 0.14$) (**Figure: 70E**).

Additionally, the mRNA levels of *Ins*, the gene encoding for the precursor of insulin 1 and 2 were investigated. The results revealed a significant increase of *Ins* mRNA after the *Pex13* silencing ($p \leq 0.05$) whereas PHY treatment only led to an increase of *Ins* mRNA in the *Scr*-siRNA group ($p \leq 0.01$). The combination of the PHY treatment and the *Pex13* knockdown did not result in further upregulation of the *Ins* gene expression (**Figure: 71A**).

The *Pax6* mRNA level was strongly (4.4-fold) elevated ($p = 0.06$) in the *Pex13*-siRNA group, whereas the introduction of PHY led to an attenuation of this phenomenon (**Figure: 71B**). Similarly, also the expression of *Pdx1* was elevated (2.8-fold) as a consequence of the *Pex13* silencing and this upregulation was slightly attenuated by PHY treatment (**Figure: 71C**).

Pax4 expression behaved similar to the one of *Pdx1*, showing a strong increase after *Pex13* knockdown and exhibiting no further elevation after PHY treatment (**Figure: 71D**).

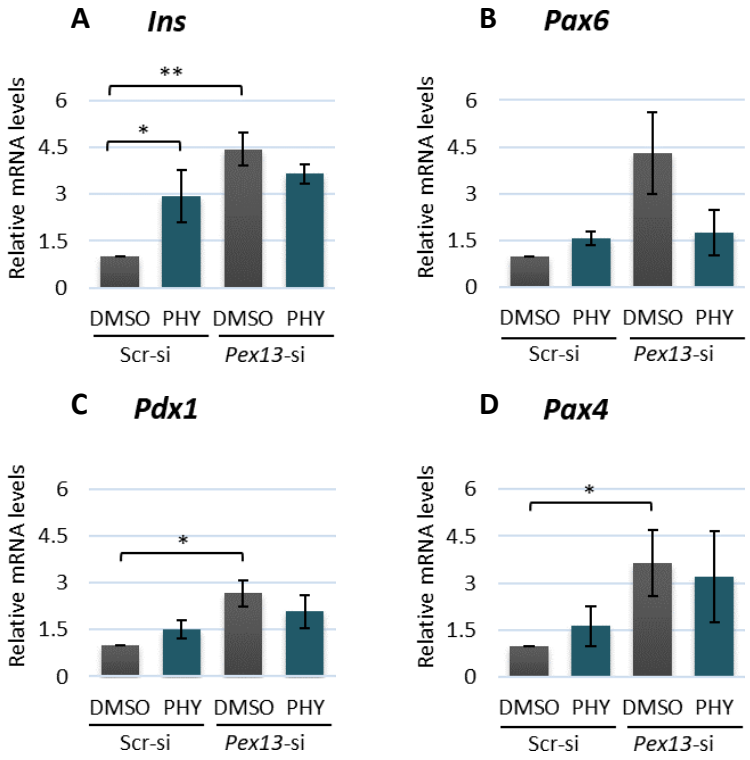

Figure: 71. Regulation of *insulin*, *Pax6*, *Pdx1* and *Pax4* mRNA levels after PHY exposure in *Pex13*-si transfected β-TC3 cells. β-TC3 cells were transfected with *Pex13*-si or *Scr*-si RNA for 24 h and treated with PHY (60 μM). After 48 h the expression of *Ins, Pdx1*, *Pax6*, *Pax4*, and *Actb* (β-Actin) was analyzed by qRT-PCR. The average threshold (Ct) values of three independent experiments were used to calculate the relative amounts of mRNA using the 2-ΔΔ CT method and normalized to *Actb* values. Results are presented as a fold over control (*Scr*-si / DMSO). Statistics: ANOVA test for multi-paired values. * $p \leq 0.05$; ** $p \leq 0.01$. *Ins:* insulin; *Pdx1:* pancreatic and duodenal homeobox1: *Pax6:* paired box6; *Pax4:* paired box 4; DMSO: dimethyl sulfoxide; Phy: phytanic acid.

5.15.9. Analysis of the mRNA levels of PPARs in β-TC3 cells treated with *Pex13*-siRNA after phytanic acid exposure

Numerous fatty acid–derived compounds including acyl-CoAs and phytanic acid (inter alia) have been shown to activate PPARs ((203). This phenomenon in turn results in the regulation of the expression of many peroxisomal genes. For this reason, we analyzed the mRNA expression and the protein abundance of the three PPAR subtypes, PPAR α, β and γ, after *Pex13* silencing in β-TC3 cells exposed to 60 μM PHY for 48 h.

Our results showed that the *Pparα*mRNA levels were not significantly affected by any of our treatments (*Pex13* silencing, PHY exposure, or the combination of both) (**Figure: 72A**). However, PPARα protein abundance increased 2.1-fold ($p \leq 0.01$) and 1.8-fold ($p \leq 0.01$) after the treatment with PHY in the *Scr*-si and *Pex13*-si transfected cells (**Figure: 72D** and **E**). Interestingly, our results showed no significant changes in *Pparβ* mRNA levels and protein amount following any of our treatments (**Figure: 72B, D** and **E**).

In contrast to the result of *PPARα* and *β* mRNAs, the expression for *PPARγ* mRNA was significantly increased after the *Pex13* knockdown (~4.5-fold). Moreover, PHY treatment induced a strong *PPARγ* upregulation (6.4-fold) in the *Scr*-siRNA group, whereas this upregulation was attenuated in the *Pex13*-si RNA group ($p = 0.05$) (**Figure: 72C**). The

silencing of *Pex13* in β-TC3 cells did result in an increase in PPARγ protein abundance. Furthermore, the introduction of PHY to the medium led to a massive increase of the PPARγ protein amount in both, the *Pex13*-si and the *Scr*-si mRNA transfected cells (2.2-fold) (**Figure: 72C, D** and **E**).

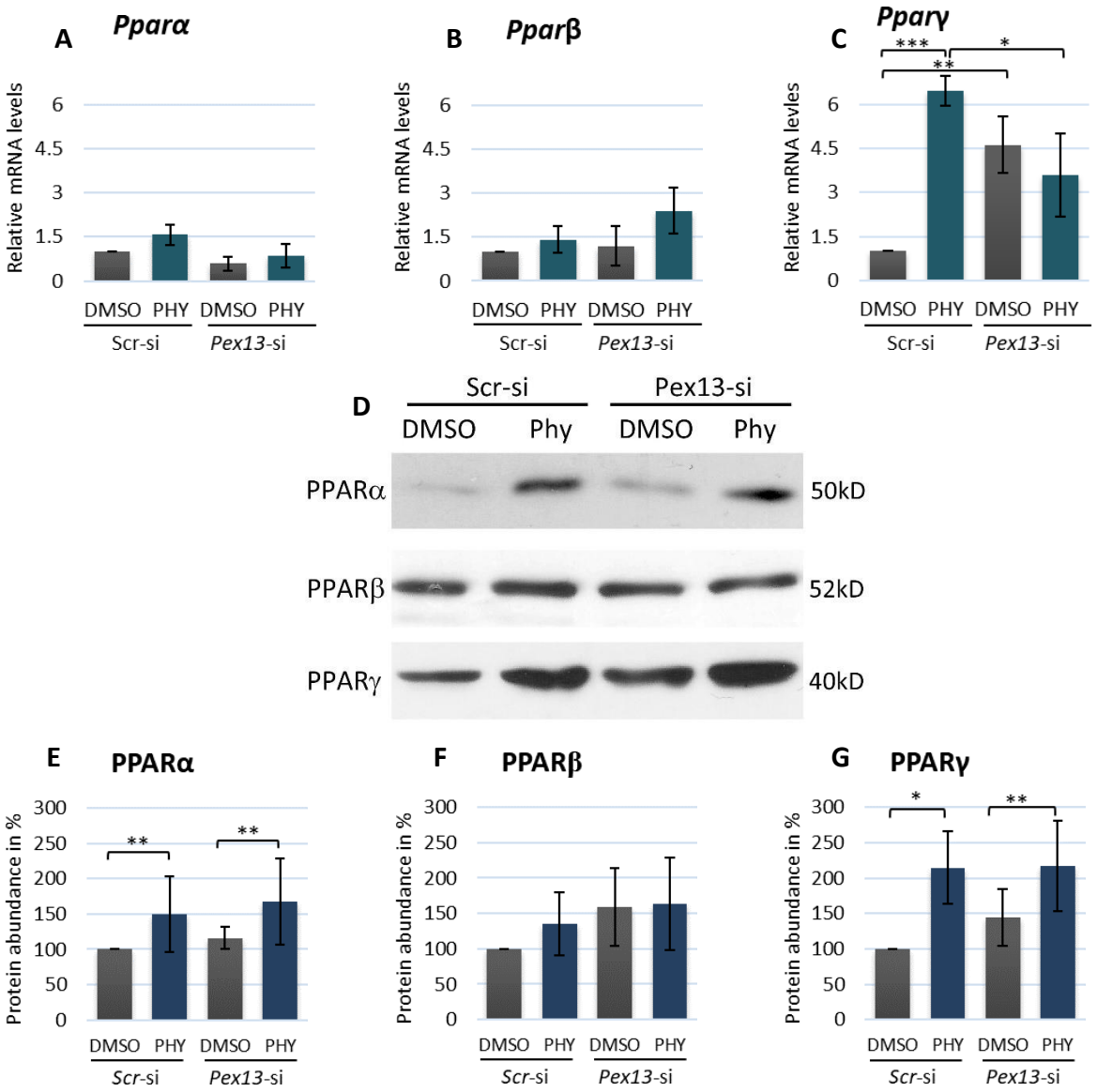

Figure: 72. Regulation of PPAR gene and protein abundances after PHY exposure in *Pex13*-si transfected β-TC3 cells. A-C: β-TC3 cells were transfected with *Pex13*-si or *Scr*-si RNA for 24 h and treated with PHY (60 μM). After 48 h the expression of *Pparα, Pparβ, Pparγ* and *Actb* (β-Actin) was analyzed by qRT-PCR. The average threshold (Ct) values of at least three independent experiments were used to calculate the relative amounts of mRNA using the 2-ΔΔ CT method and normalized to *Actb* values. Results are presented as a fold over control (*Scr*-si/DMSO). **D**: Representative immunoblotting of PPARα, PPARβ and PPARγ after *Pex13*-siRNA transfection and PHY treatment in β-TC3 cells. Total protein (20 μg) was used for the analysis. Equal loading of protein was controlled by Coomassie staining. **E-G**: Western blot analysis of PPARα, PPARβ and PPARγ. Values ±SEM represent the protein abundance (in %) relative to *Scr*-si/DMSO sample normalized to total protein loaded from at least three independent experiments. Statistics: ANOVA test for multi-paired values. * $p \leq 0.05$; ** $p \leq 0.01$; *** $p \leq 0.001$. PPARα, β, γ: peroxisome proliferator-activated receptor alpha/ beta or gamma; DMSO: dimethyl sulfoxide; Phy: phytanic acid.

6. DISCUSSION

The impact of defective peroxisomal metabolism on the development of diabetes mellitus type 2, particularly on pancreatic β-cell pathophysiology has been overlooked in the past decades. Increasing evidence suggests that the onset of this age-associated disease is linked to the accumulation of reactive oxygen species (ROS), resulting in oxidative stress and cellular damage [93, 198, 199], and to β-cell toxicity by excess plasma saturated long-chain fatty acids, commonly found in obesity [139]. Peroxisomes perform a wide range of important metabolic functions including the β-oxidation of very long-chain and branched-chain fatty acids and are actively involved in the metabolism of ROS. Interestingly, peroxisomes also metabolize long-chain FA through β-oxidation taking over the function of mitochondria when these are deficient or overloaded by fatty-acids [200]. Because of these properties, we hypothesized that peroxisomes could protect β-cells against lipotoxicity and oxidative stress damage. To investigate the molecular mechanisms underlying β-cell dysfunction in connection to peroxisomal dysfunction, a knockdown of the peroxisomal biogenesis protein gene *Pex13* in β-TC3 cells was generated.

6.1. Peroxisomes and peroxisomal dysfunction in pancreas

In former times, the study of catalase gene expression and protein level in pancreatic β-cells led to the notion that peroxisomes are rare organelles in this cell type [172, 201]. This was mainly due to the relatively low expression of catalase in pancreas when compared to liver. However, the use of different peroxisomal markers (e.g. PEX14) helped us to verify the presence of peroxisomes in the whole organ by IF analysis [173]. Further we demonstrated that in pancreas, peroxisomes exhibit a heterogeneous protein composition and intracellular localization, suggesting that they may adapt according to the specific metabolic needs of each distinct group of cells. PEX14 and ABCD3, both integral membrane proteins, resulted to be the best markers for the identification of peroxisomes in β-cells, and for the analysis of their distribution within the different regions of the tissue.

The results presented in this thesis revealed that β-cells express all genes related to peroxisomal β-oxidation pathways I and II and for the ABCD3 lipid transporter. This suggests that peroxisomal β-oxidation is particularly active in β-cells.

One of the aims of the present work was to achieve a knockdown of the peroxisomal membrane protein *Pex13*, a peroxin that is necessary for peroxisomal protein matrix import

(e.g. for β-oxidation enzymes) in β-TC3 cells. We successfully established a *Pex13* deficient β-TC3 cell model in which catalase was less abundant and mistargeted to the cytoplasm demonstrating the defective peroxisomal matrix protein import and partial degradation of the missorted protein. Within the cell, intact organelles are necessary to compartmentalize metabolic pathways and substrate flows. Similarly to catalase, also β-oxidation enzymes require PEX13 for their peroxisomal matrix import. Mistargeting to the cytoplasm as a consequence of the *Pex13* KD, could lead to the loss of the β-oxidation chain functionality decreasing lipid oxidation and causing steatosis.

In contrast to catalase, ABCD3 was not mistargeted since ABCD3 targeting does not involve the matrix protein import pathway through PEX13. In fibroblasts of *Pex13*$^{-/-}$ animals ABCD3 is indeed retained in empty membrane structures called peroxisomal membrane ghosts [40] without being degraded [38].

The *Pex13* knockdown did not only alter the subcellular localisation of proteins but also the expression of some peroxisome-related genes. For example, the expression of *Abcd3* and *Acox1* was substantially decreased. Furthermore, β-TC3 cells lacking functional peroxisomes exhibit an altered regulation of PPARβ and PPARγ gene expression, an effect that will be discussed later in this thesis.

6.2. Possible involvement of peroxisomes in the onset of type 2 diabetes.

In the last decades only few conditions have had as much medical, social and economical impact as diabetes mellitus type 2 (T2D). Representing the most common type of diabetes, T2D accounts for around 90% of all cases of diabetes [202]. This chronic condition is characterized by hyperglycaemia due to decreased or absent insulin production (β-cell failure) and/or the inability of the body to respond fully to this hormone. There is a strong link correlating T2D with genetic background, obesity, increasing age and lifestyle (physical inactivity, poor diet, prediabetes *inter alia*). However, despite all the efforts made so far, the precise mechanism of action behind T2D is not completely elucidated. Globally, the prevalence of T2D is rising, wherefore uncovering the molecular pathophysiology involved in the β-cell malfunction, the key feature of this condition, is of high importance.

T2D shows high prevalence in aged people older than 65 [203]. It has been shown that aging also compromises peroxisomal number [204] as well as peroxisomal protein import (particularly the import of PTS-1 containing proteins [205]). Catalase is particularly affected

since it contains a non-canonical PTS-1 (-KANL) [206], which interacts with PEX5 less efficiently than the normal PTS-1 (-SKL) [207]. This phenomenon has been observed not only in late-passage cells [205] but also under conditions of oxidative stress [208]. Catalase plays a critical role preventing oxidative stress, but it is low expressed in β-cells. This, coupled with the progressive mislocalization of catalase into the cytosol as cells age [207] has been directly correlated with the pathophysiology of T2D as observed in patients with hypocatalasaemia[209]. This implies that an imbalance in the ratio of ROS to catalase results in oxidative stress, cellular damage, aging and is probably involved in the onset of T2D. Several reports revealed the beneficial effect of catalase expression: In fibroblasts increased import of catalase specifically targeted to peroxisomes (SKL-catalase) dramatically reduced the cellular hydrogen peroxide levels [207] and in aging cells it delayed the appearance of senescence markers. Further, catalase protected peroxisomal β-oxidation, re-established mitochondrial membrane potential and reduced mitochondrial ROS production [210]. In contrast, it has been recently shown that the inefficient import of catalase, and in consequence its retention in the cytosol, could be a redox-regulated protective mechanism under conditions of elevated cellular oxidative stress [211]. Peroxisomal catalase can efficiently clear the internally-generated oxidative degradation products [101] but it only insufficiently degrades H_2O_2 produced in other subcellular compartments [95, 211]. So, cytosolic retention of catalase may indeed constitute a defense mechanism against cellular oxidative stress. The shuttling receptor for peroxisomal matrix proteins PEX5 thereby acts as a redox-regulated import receptor decreasing the import of PTS-1 proteins into the peroxisome under oxidizing conditions [212]. When the cellular redox states are re-established, the peroxisomal import machinery could then return to normal and import catalase into the peroxisomal matrix.

Also, when peroxisomes are deficient, medium-chain dicarboxylic acids (DCAs) are generated as a final product of the LCFA ω-oxidation (in the smooth endoplasmic reticulum) [213] as an alternative pathway to the β-oxidation. Under physiological conditions these ω-FA are degraded by peroxisomal β-oxidation, protecting cells against their toxicity and preventing the induction of inflammation and fibrosis [214]. When peroxisomes are depleted of PEX13, this protective function is inhibited, leading to medium-chain dicarboxylic acid toxicity.

These observations reinforced the notion that peroxisomes are particularly relevant for the β-cell wellbeing, however, as cells age and ROS levels increase, the protective mechanism performed by the peroxisome might be overwhelmed and the permanent mislocalization or inactivation of peroxisomal catalase result in β-cell damage and T2D.

6.3. Glucolipotoxicity in pancreatic β-cells

Obesity, (commonly accompanied by dyslipidaemia) is one of the main risk factors for the development of T2D [153] because increased levels of circulating FFA (non-esterified "free" fatty acids) in combination with hyperglycemia contribute to progressive β-cell loss [215]. In the search of the metabolic pathways associated with β-cell failure scientists have focused their attention on the effects of high glucose and FFA concentrations in β-cell metabolism, signal transduction pathways and viability.

As indicated by our results, the exposure of β-TC3 cells to different glucose concentrations (5 and 20 mM) for 72h did not result in any significant alteration in cell survival in agreement with previous results showing that an elevated glucose concentration alone is not toxic to pancreatic islets in normal or prediabetic stages [216]. Presumably, the duration of the exposure to the hyperglycaemic condition was insufficient to induce a toxic response since β-cells adaptative responses can counteract acute toxic effects [217]. Indeed, β-cells activate gene expression that induces the glycolytic pathway [218], which results in glucose degradation and detoxification [217]. Pinpointing the mechanisms by which β-cells fail is difficult because the experimental setups employed by different laboratories differ conspicuously. Depending on the genetic background of the used cell-lines [219–222], differences in the applied conditions for cell culture and glucose concentrations (alone or combined with FAs), a wide range of sometimes contradictory effects were obtained [222, 223]. As for glucose, the treatment with FFAs entails its owns challenges: contrasting, beneficial (likely short exposure) or detrimental (likely long exposure), effects for β-cell performance can be obtained when using FFAs depending on their concentration, the exposure time [156, 190, 224], and the level of concurrent hyperglycaemia [153, 193]. In primary rat β-cells, human β-cells or insulinoma cell lines, increasing the time of exposure to saturated fatty acids leads to cellular dysfunction causing reduced glucose-stimulated insulin secretion [225–227], decreased insulin gene expression [225] and apoptosis [139, 155, 169, 228, 229].

Furthermore, the FFA/BSA ratios [193] and the use of serum in the culture medium could lead

to different results.

The FAs concentrations and exposure times required to achieve a toxic effect in β-TC3 cells in this thesis were defined by the following criteria: (i) the doses at which 40-50 % of the cells were still viable, taking into account that some of the experiments required a si-RNA transfection treatment resulting in increased cell stress and higher susceptibility to the fatty acid treatment, and (ii) the need of sufficient material of viable cells for later analysis.

It is generally accepted that a causal relationship exists between chronically high FFA levels and pancreatic β-cell failure (lipotoxicity) [230, 231]. The metabolic interaction between glucose and palmitate and the resulting potentiated harmful effect on β-cells has led to the concept of glucolipotoxicity. Glucolipotoxicity is the combined deleterious effects of hyperglycaemia and high fatty acid levels on pancreatic β-cell function and survival [193].

In this thesis, it was shown that elevated PA concentrations *in vitro* are relatively benign to β-cells when glucose is not simultaneously elevated. Indeed, under physiological circumstances, long-chain fatty acids serve as regulators of β-cell function [153] and have been suggested as being beneficial during the hypersecretion of insulin by protecting against glucose intolerance in the early stages of obesity and diabetes [232]. Also, studies performed in INS-1E insulinoma cells by Barlow *et al.* [171] suggest that PA alone is non-toxic due to the capacity of β-cells to oxidize FFAs. These findings are supported by evidence that in animal models elevated FFAs *per se* function in the adaptation of the β-cell to insulin resistance through lipid-signaling molecules like PPARα and γ [144, 233].

Our results suggest a marked synergistic effect of high glucose and palmitate in inducing cell death in β-TC3 cells cultured for 3 days. This typical phenomenon was previously observed in experiments conducted in rat islets, INS 832/13 cells and human islet β-cells, and resulted in increased DNA fragmentation and decreased cell proliferation [144, 152, 156, 189, 234–237]. The cell death observed in the experimental set-up of this thesis might be caused by the influence of glucose on lipid metabolic pathways via alterations of substrate availability, changes in the activity and the expression of enzymes involved in glucose and lipid metabolism and of key transcription factors.

In this respect, it is of interest that the signaling molecule malonyl-CoA creates a metabolic link between the metabolism of glucose and the one of FFAs. Malonyl-CoA regulates lipid partitioning (FFA oxidation versus synthesis/esterification) in dependence of the

intracellular glucose concentration through the inhibition of carnitine palmitoyltransferase-1 (CPT-1), which catalyzes the rate-limiting step of the mitochondrial β-oxidation [144, 237]. Under condition of hyperglycaemia, malonyl-CoA accumulates in the cell, thereby lowering the oxidation-rate of FFA-derived long-chain acyl-CoA esters. As a result, FA-CoAs are directed towards their incorporation into complex lipids, some of which are cytotoxic (phosphatidic acid, lysophosphatidic acid, sphingolipids, ceramides, cyclo- and lipo-oxygenase products *inter alia*) [144, 155, 156, 228, 238] and accumulate in the cytoplasm causing β-cell apoptosis [226, 231] and insulin resistance in muscle tissue [239]. For the interpretation of the results presented in this thesis we have to consider that since our experiments are performed with high glucose concentration, mimicking a glucolipotoxic diabetes-like environment that promotes sustained formation of citrate and malonyl-CoA, this can result in the inhibition of FA oxidation with concomitant increased phospholipid and triglyceride deposition [240]. Further analysis of the intracellular fluctuations of malonyl-CoA could provide insight into how hyperglycemia impacts β-cells in our particular experimental setup and model and in correlation to peroxisome dysfunction. It is worth mentioning that acetyl-CoA, the final product of the peroxisomal β-oxidation is used as a substrate for the biosynthesis of fatty acids via its carboxylation to malonyl-CoA and be therefore responsible for the regulation of intracellular malonyl-CoA concentrations [24, 241].

It is unlikely that glucolipotoxicity acts alone in the failure of the β-cell in T2D. Other pathways and variables that could contribute to the loss of β-cell mass and function are ROS production and peroxisomal dysfunction, which will be discussed later in this thesis.

6.4. Alterations in peroxisomal protein patterns in pancreata from animal models of diabetes and dyslipidaemia

With the purpose of detecting alterations in peroxisome abundance and proteome caused by T2D, ob/ob and NZO animals, models for diabetes and hyperlipidaemia, were employed for IF analysis. The peroxisomal abundance was massively increased in the islets of NZO animals and in the ob/ob$^{(-/-)}$ group exposed to a high lipid diet. This phenomenon is comparable with the one observed in the liver of db/db mice, another model for obesity, diabetes and dyslipidaemia, where the expression of the peroxins PEX11α, PEX5 and PEX7 were elevated [242].

Presumably, the increase in peroxisome number in pancreatic islets that we have observed indicates a compensatory mechanism to decrease the accumulation of FFA (non-esterified "free" fatty acids) caused by the high-fat diet by increasing peroxisomal β-oxidation. Furthermore, an intriguing finding was the massive ABCD3 down-regulation in the pancreatic islets of both animal models after the exposure to the high lipid diet. Analogously, we observed a strong decrease of ABCD3 abundance in β-TC3 cells after PA treatment. Furthermore, preliminary experiments generated in β-TC3 cells with an *Abcd3* knockdown exposed to PA, showed a significant increase in cell death (data not shown) suggesting that the absence of ABCD3 causes β-cell toxicity. It has been shown that in rat glial cells the downregulation of *Abcd3* coupled with FA exposure (lignoceric and PA) caused a reduction of the rate of peroxisomal and mitochondrial β-oxidation activities [243]. Since ABCD3 is one of the most abundant peroxisomal membrane proteins [244] and is responsible of the transport of straight long- and very-long chain acyl-CoAs, as well of 2-methyl branched-chain acyl-CoAs, we could expect that the high lipid diet given to the animal models studied in this thesis, together with the observed ABCD3 downregulation could lead to an increased FA esterification and in consequence chronic pancreatic steatosis. Interestingly, after exposure of the β-TC3 cells to the fatty acid PHY, ABCD3 was upregulated. This suggests that the expression of this transporter might be differentially regulated by specific fatty acids.

In summary, our investigations show that, in these mouse models, peroxisomes are altered and their manipulation might be a key factor to neutralize pathophysiological alterations in pancreatic islets under diabetic or hyperlipidaemic conditions.

6.5. Pathophysiological consequences of peroxisomal deficiency in β-TC3 cells

6.5.1. Palmitic and phytanic acid lipotoxicity in *Pex13* KD β-TC3 cells

Intracellular accumulation of FA in non-adipose tissue (steatosis) has been associated with cellular dysfunction and death [243]. In β-cells, which are not a physiological site of lipid storage, *in vitro* and *in vivo* studies have clearly demonstrated that long-term exposure to FFAs and their accumulation induces apoptosis in cell culture and in isolated islets ultimately contributing to the pathogenesis of T2D [155, 156, 189, 243–245]. Cause of steatosis can be either increased import and synthesis or decreased catabolism of fatty acids. The latter is caused by dysfunction of pathways in different subcellular compartments controlling intracellular

lipid homeostasis such as: the cytosol, for synthesis and storage of lipid droplets, and mitochondria or peroxisomes, for lipid degradation [242]. In accordance with previous reports [246, 247], our study showed that long-term exposure to either PA or PHY induced β-cell death in a concentration dependent manner. Though some studies have already compared the steatogenic capacity of PA and unsaturated fatty acids (e.g. oleic acid) [248], to our knowledge, the experiments presented in this thesis are the first ones proving PHY toxicity in β-cells. PHY, a methyl-branched fatty acid found in ruminants fats, dairy products and beef with an estimated daily intake of 1 mg/kg body weight for an adult [83, 84], is solely oxidized in peroxisomes via one round of α-oxidation and subsequent β-oxidation [249]. PHY is a powerful ligand for PPARα, whose activation in pancreas enhances the transcription of genes implicated in peroxisomal and mitochondrial β-oxidation, lipid metabolism, and peroxisome proliferation, thereby protecting β-cells against lipotoxicity [250]. However, the accumulation of PHY due to a decrease or defect in peroxisomal metabolism has been proven toxic. This is exemplified by the peripheral neuropathy and demyelinisation observed in patients with Refsum´s disease [251]. Furthermore, the induction of oxidative stress by PHY has been also documented [252] resulting in ROS production, calcium deregulation and apoptosis [253, 254].

Several molecular mechanisms have been associated with β-cell PA-triggered apoptosis, including: (i) ER impaired function and stress [138, 178], (ii) *de novo* ceramide synthesis [155], (iii) generation of reactive oxygen species [255] and of NO [256], (iv) accumulation of LC-CoAs and lipid intermediate molecules [144], and (v) release of apoptogenic factors, such as cytochrome c, from the mitochondrial intermembrane space to the cytosol [257]. Furthermore, as already discussed, the metabolism of FFA can be shifted from their oxidation to their esterification, particularly when glucose is supplied like in our experiments, a process that promotes the accumulation of FFA. Less is known about the cytotoxic effect of PHY, although mitochondrial dysfunction and ROS production have been proposed to decrease cell viability in astrocytes and cardiomyocytes of wild type rats exposed to PHY [252, 254].

It is so far unclear to what extent peroxisomes contribute to fatty acid metabolism in β-cells. The involvement of the organelle is suggested by the decreased toxicity of PA after the stimulation of peroxisomal β-oxidation and proliferation [250] and by the dramatic pathogenic consequences observed in the inherited peroxisomal disorder, Refsum´s disease,

where the defective oxidation of PHY leads to its accumulation in the serum. However, to the best of our knowledge, in different general knockout mice with complete peroxisomal deficiency (e.g. PEX2, PEX5, PEX13), no development of T2D has been described [36, 38, 258]. This is due to the fact that these KO animals die shortly after birth, making the study of functional long-term pathologies with these animal models impossible.

In this thesis it was shown that peroxisome-dysfunction increased cell-death only after treatment with PHY but not with the PA concentrations used, suggesting that metabolically intact peroxisomes are important for the removal of high concentrations of PHY in β-cells. In the literature it has been demonstrated that the increase of either the activity of the peroxisomal matrix enzyme catalase or of the peroxisomal β-oxidation in rat β-cells and in the cell line INS-1 resulted in an improved β-cell resistance against PA-toxicity [178, 259–261]. By inducing peroxisomal activity, these cells channel PA towards initial degradation in the peroxisomes instead of performing the entire β-oxidation in the mitochondrion [250].

6.5.2. Lipid droplet accumulation in β-TC3 cells is incremented by peroxisomal deficiency: possible involvement of PPAR-mediated regulatory effects

We demonstrated that cytosolic lipid accumulation was proportional to the concentration of PA and PHY to which cells were exposed. Interestingly, at the concentration at which both FA reached toxic levels, cells treated with PA contained more and bigger lipid droplets than the ones treated with PHY. PA apparently induced greater steatosis suggesting that this FA might be more readily incorporated into TG (triglycerides)-storage droplets and therefore be less cytotoxic than PHY. Indeed, promoting lipid storage (and limiting lipolysis) can counteract lipotoxicity [224] to a certain extent. An emerging notion regarding lipotoxicity in pancreatic islets suggests that, when the availability of FFAs in the serum increases along with the concentration of toxic lipid intermediates, the sequestration of cytosolic FFAs into TG storage droplets [243] can have a cytoprotective effect. This is because toxic free fatty acyl moieties are removed from the cytoplasm and TGs are biologically inert and therefore non-toxic [224, 262, 263, 250].

Since peroxisomes degrade LCFA when mitochondrial β-oxidation is blocked or overloaded and because they are the only site for PHY degradation they might contribute to the protection of β-cells against intracellular lipid accumulation and lipotoxicity. In our peroxisome-deficient cell culture model we observed a massive increase in the number and

size of cytoplasmic lipid droplets after the treatment with either PA or PHY.

The increase in the lipid droplets after the incorporation of PA into our peroxisome-deficient model may be explained as a result of incomplete FA oxidation because of saturated mitochondrial CPT1-pathway and overload with cytosolic FFA.

The accumulation of lipid droplets in the *Pex13*-depleted cells treated with PHY was not as prominent as observed for PA and likely due to the fact that this branched-chain FA can exclusively be metabolized in intact peroxisomes.

PPARs are important regulators of lipid metabolism. In liver for example, the gene encoding for *Acox1*, which catalyzes the rate-limiting step in the peroxisomal fatty acid β-oxidation pathway, is strongly regulated by the activation of PPARα. Deficiency of PPARα therefore leads to the development of hepatic steatosis [(191)]. In pancreas this effect prevents fatty acid-induced β-cell dysfunction and apoptosis [(264)] and improves β-cell function in rodent models displaying an insulin resistant phenotype [(265)]. Therefore, PPARs have lately been the target for the development of drugs involved in the treatment of T2D.

It is important to mention at this point that metabolic derivatives of the peroxisomal FFA oxidation often serve as a PPAR ligands, which themselves in turn modulate FFA metabolism through a so-called peroxisome/PPAR-feedback loop [(24)]. Because of the peroxisomal defect non- or wrongly metabolized FFAs accumulate in the cell thereby potentially influencing the regulation of PPARs with repercussions on the entire cellular lipid metabolism.

Our studies showed that PPARα protein abundance was strongly induced by PHY independently of the peroxisomal dysfunction. In contrast to this and as described elsewhere [(250)], PA decreased PPARα mRNA expression. Previous *in vitro* studies reported that PHY activates several PPARs subtypes, predominantly PPARα [(266, 267)]. This results in enhanced β-oxidation, and as we observed, also in the upregulation of the mRNA levels of enzymes involved in peroxisomal α-oxidation such as *Phyh*, *Acox3* and *Scp2*. It has been recently shown that FALDH-V, an aldehyde dehydrogenase which oxidizes pristanal to pristanic acid in the last step of the α-oxidation pathway, is induced by PPARα agonists resulting in cell protection against phytanic acid-induced damage [(268)], probably as a peroxisome-PPAR feedback loop.

Also PPARγ was strongly induced by the peroxisomal dysfunction and further upregulated by the addition of PHY but not by PA. Apart from polyunsaturated fatty acids, phytanic acid is also a natural PPARγ agonist and increases glucose uptake and insulin sensitivity [(266)].

Opposite to the conventional lipogenic role of PPARγ as the key transcriptional factor for adipogenesis [144], it has been suggested that the activation of PPARγ is also beneficial to the pancreatic β-cell, preventing lipotoxicity by increasing the capacity of the β-cell lipid-buffering and by enhancing the proliferative response of β-cells to insulin resistance [238, 269]. The role of PPARγ in pancreatic β-cells, however, remains to be fully clarified primarily due to its low expression under physiological conditions [270, 271] and secondly because ablation of both PPARγ isoforms in β-cells did not result in a metabolic phenotype.

PPARβ, the PPAR subtype expressed at the highest level in insulinoma cells and rat pancreatic islets, was also activated by PHY and increased lipid oxidation capacity (as shown in INS-1E β-cells) [272].

However, a cautious interpretation should be made concerning the effects of PPARs due to the species-specific (rodents vs. humans) regulatory effects leading to contradictory results [280]. Also, it is important to notice that PPARs and PPAR-binding synthetic ligands often display overlapping specificity resulting in the activation of the same subsets of genes. Indeed, our results show that despite the upregulation of PPARs the treatment of β-TC3 cells with PHY resulted in increased apoptosis.

Even if the accumulation of lipid droplets may initially be just a cellular defense mechanism against FFA, their chronic and massive accumulation, along with a decreased oxidative capacity, causes β-cell steatosis and cell death [144]. Indeed, the apoptotic effect of FFA on β-cells is related to elevated islet fat content, deposited after a chronic increase of FFA in the serum [155]. Since the *Pex13* knockdown is only active for a short period of time, longer FA treatment periods with the purpose of mimicking the effects of chronic steatosis in the background of peroxisome deficiency could not be performed at the moment under our experimental conditions. However, the use of the CRISPR/Cas9-gRNA complex-technology for genome editing could potentially be used in future experiments of our group to overcome this obstacle.

In conclusion, our results suggest that peroxisome deficiency in combination with lipotoxicity, alter the lipid storage capability of β-cells. Additionally, when β-cells face an accumulation of FAs like PHY that are exclusively metabolised by peroxisomes, this causes an increase of apoptosis as a consequence of highly elevated amount of FFA in the cytoplasm that cannot be oxidised. This pinpoints to the importance of intact peroxisomes

for the protection of the cell against excess FAs that cannot be metabolised by mitochondria in β-cells.

6.6. Alterations in reactive oxygen species (ROS) metabolism induced by peroxisome deficiency in β-TC3 cells

The level of oxidative stress exerted on β-cells depends on their capacity to scavenge ROS generated under conditions of glucolipotoxicity. Disruptions of oxidative stress homeostasis either by the exposure to high FA concentrations or by the decrease of the oxidative capacity such as when peroxisomes are dysfunctional, has dramatic physiological consequences. In this thesis, the levels of two reactive intermediates (H_2O_2 and superoxide) were quantified in the peroxisome-deficient cell culture model. As indicate by the results, the *Pex13* knockdown and the associated peroxisomal dysfunction, resulted in a strong increase of intracellular H_2O_2 production. In neuronal cultures of PEX13 knockout animals no significant differences in H_2O_2 could be detected in comparison to wildtype animals [186]. Most likely neuronal tissue has a different susceptibility to the peroxisomal dysfunction or possesses other defence mechanisms catalysed by other antioxidative enzymes.

Since the H_2O_2 levels increased after the knockdown of *Pex13,* it was not surprising to find that superoxide levels were significantly lower. A plausible explanation could be the up-regulation of the SOD2 protein abundance shown in the peroxisome-deficient model. Since inside the mitochondrion superoxide is dismutated to H_2O_2 by SOD2, its upregulation might result in an increased inactivation of superoxide radicals, resulting in an increase in H_2O_2. These results also suggest a close interaction between the mitochondrial and the peroxisomal oxidative stress metabolism. It has been reported that the absence of functional peroxisomes in the *Pex5*- and *Pex13*-deficient mice can compromise mitochondrial integrity and lead to severe mitochondrial alterations including a marked increase of SOD2 suggesting that peroxisomal defects can cause secondary mitochondrial pathologies [37, 99, 186].

Results from other groups concerning the involvement of FFA induced ROS in apoptosis are contradictory [139, 252, 255]. Previous works have demonstrated that treatments with antioxidative enzymes (e.g. SOD and CAT) exert beneficial effects on β-cells such as significantly inducing cell proliferation through decreased apoptosis and higher levels of insulin secretion [256]. On the other hand, it is well established that at physiological low levels, ROS, particularly H_2O_2, [274, 275] serve as signalling messengers to mediate various

biological responses, including inflammation, immunity, differentiation, cell growth, tumorigenesis, and apoptosis [276]. Also insulin-related signal transduction pathways are regulated by the presence of ROS [277–279]. After PA and PHY supplementation we observed an increase in β-cell death as well as an increase in H_2O_2 production. The generation of superoxide by PHY has been linked to cell cytotoxicity in cardiomyocytes and brain cells [252]. However, in our experience, the β-cell death after PHY supplementation was not accompanied by any changes in superoxide levels. There is evidence that in isolated rat heart and liver mitochondria, PHY increases ROS generation by partly inhibiting the electron transport and, most likely, by changing membrane fluidity [280]. Pancreatic β-cells exposed to high concentrations of FFAs at non-lethal concentrations showed an elevated generation of ROS and NO [281]. Similar observations were made in tumor cell lines and in rat pancreatic islets as well as in myocytes, where the overexpression of catalase abolished the rise of H_2O_2 after PA supplementation [282]. Accordingly, our results show that the PA- and PHY- induced increase in H_2O_2 was accompanied by a rise in CAT protein abundance and enzymatic activity very likely as a stress response. It has been shown that PPARγ is an activator of the catalase gene transcription [283], explaining the increased catalase expression after PHY treatment observed in this thesis. PA instead activates the transcription of Nrf2 (NF-E2-related factor 2) target genes [284] that is involved in cellular defenses against oxidative stress and increases the expression of catalase [285]. NADPH oxidase activation could also be a source of PA mediated superoxide radical generation [286] causing lipotoxicity in β-cells [287].

Interestingly, the treatment of *Pex13*-deficient β-cells with PA did not increase cytotoxicity. Until now, the source of H_2O_2 after FFAs supplementation is not clear. It is often assumed that mitochondria are the primary source of ROS production in the β-cell after FFA exposure [252, 288–290]. During aging, when the peroxisomal catalase abundance is reduced due to its cytosolic mislocalization [204], peroxisomes may become a source of toxic ROS [99], increasing the risk of developing age- related diseases including diabetes [209]. The considerable clinical heterogeneity of T2D, and the large number of pathways that are involved in the pathophysiology of this disease, clearly show that the pathogenesis of type 2 diabetes is not simple. Our studies suggest that the saturated FFA palmitate and the branched- chain FA phytanic acid induce the formation of reactive intermediates (H_2O_2) in β-TC3 cells that independently lead to cell death. Furthermore, our findings suggest that the PEX13

knockdown causes secondary mitochondrial oxidative stress, since it massively increased SOD2 protein abundance and mRNA levels. However, the elevated cell toxicity observed after PHY exposure in our peroxisomal dysfunction model did not correlated with an increase in ROS production.

6.7. Functional significance of peroxisomes in insulin production and secretion in β-TC3 cells exposed to palmitic and phytanic acid

Insulin secretion can be regulated by several cooperative signalling pathways [291]. Glucose constitutes the primary extracellular signal triggering insulin secretion. Secondary signals augmenting insulin secretion are lipid-derived intracellular signals (e.g. long-chain acyl-CoAs) [292, 293]. Externally added FFAs can induce enhanced insulin secretion as well [145].

Our study showed that, when pancreatic β-TC3 cells were exposed to toxic concentrations of PA under hyperglycaemic condition, the insulin secretion and biosynthesis was stimulated. In this thesis, 48 h of toxic concentrations of PA (limited by the necessity to sustain the *Pex13* silencing) were used. Under these conditions β-cells retained their functionality. Stronger, irreversible or deleterious alterations in β-cell gene expression and signalling, which are necessary to provoke β-cell failure, might be obtained by longer treatment periods. An alternative explanation for the conserved functionality of the β-cells after the introduction of PA is the upregulation of *Pdx1* expression, a transcription factor necessary for β-cell maturation and for the maintenance of insulin production. Other studies showed that a typical symptom for islet lipotoxicity is an initially increased basal insulin secretion [220] followed by β-cell apoptosis [155].

Interestingly, opposite to what we observed for PA, elevated concentration of PHY, decreased the biosynthesis of insulin, an effect that was stronger in the peroxisome deficient β-TC3 cells. This effect could be caused by the PHY-mediated activation of PPARα. It was indeed demonstrated that PPARα has a direct effect on islet function suppressing insulin secretion in insulinoma cells [260].

6.8. Effect of peroxisomal dysfunction and fatty acid exposure on β-cell identity

6.8.1. *Ins* gene regulation

On a purely functional level β-cell-identity defines a cell that is capable of synthesizing, processing and secreting mature insulin in response to metabolic, hormonal and neurological stimuli. On this base, a new concept evolved namely the “loss of β-cell

identity". This notion proposes that β-cells in T2D lose their differentiated specialization through the inhibition of key β-cell transcription factors such as *Pdx1* (pancreatic and duodenal homeobox 1) and *Pax6* (paired box protein 6) *inter alia*, thereby silencing β-cell-specific genes associated with basal and regulated insulin production. Overall, β-cell differentiation and function result from an interrelated network of transcription factors, including apart from those already mentioned, also *Pax4* (paired box protein 4) [197, 294–296]. To our knowledge, the present study is the first one attempting to determine whether peroxisomal dysfunction and FFA exposure trigger changes in β-cell identity.

The PAX6 transcription factor is crucial for β-cell differentiation and function [297]. As indicated by our results, the peroxisome deficiency drastically decreased *Pax6* expression independently of the addition of PA. This phenomenon was associated with a decline in *Pdx1*, *Pax4*, and *ins* gene expression. This is in accordance with previous results carried out in rat primary β-cells and β-TC3 cells revealing that silencing of *Pax6* controlled the mRNA levels of the *ins* and *Pdx1* genes [196]. When the peroxisome-deficient model was exposed to PA, not only *ins*, but also *Pdx1* and *Pax4* were induced, while the mRNA levels of *Pax6* were not affected. This allows us to hypothesize that other mechanisms play a role in the regulation of these genes. However, a cautious interpretation concerning mRNA expression should be made, since the protein levels or binding activities of the involved transcription factors were not measured in these experiments.

The results obtained from the experiments carried out with PHY are inconclusive since the addition of DMSO alone, which is used to solubilize PHY as is used as a control, affected the expression of *Pax6*, *Pdx1*, *Pax4* and *ins*. This specific effect of DMSO needs to be elucidated in future experiments.

Emerging evidence from multiple lines of research is suggesting how metabolic stress, in particular hyperglycaemia, may lead to compromised β-cell identity [298]. Despite some researchers reported that glucolipotoxicity decreased both insulin mRNA synthesis and secretion of insulin [140, 152, 299], we did not observe changes in the *ins* gene expression after PA exposure in the presence of high glucose. Similar results were found in another β-cell line (INS-1), which displayed no changes in *ins* expression after 2 days of PA treatment [300]. While it appears that the PA/glucose exposure time is primarily responsible for this

discrepancy, the used cells or organism type and the fatty acid preparation also strongly influence the obtained results.

6.8.2. Insulin secretion

The mechanisms through which fatty acids affect insulin gene expression are distinct from those by which they impair insulin secretion. The transcriptional mechanisms by which PA inhibits insulin gene expression do not involve changes in insulin mRNA stability but, rather, inhibition of glucose- induced insulin promoter activity [(226)]. This is associated with decreased binding activity of PDX1, which is affected in its ability to translocate to the nucleus [(301)]. Alone, high glucose concentrations (25 mM) chronically decrease the expression of *Pdx1* and therefore the insulin content in β-cells [(302)].

As indicated by our results, the changes in *Pax6* found after the *Pex13* did not correlated with any significant changes in insulin content/release at least after 72 h post transfection despite its influence on other β-cell specific markers. PAX6 regulates insulin biosynthesis [(303)] but is not interfering with the insulin secretory process.

Our results provide evidence that functional peroxisomes are required for the normal expression of β-cell-specific genes including *ins*, *Pax6*, *Pax4* and *Pdx1*. Thus, *Pex13* silencing influenced β-cell identity by modifying the expression of genes essential for β-cell function and maturation.

7. SUMMARY

Type 2 diabetes is characterized by impaired insulin secretion paralleled by a progressive decline in β-cell function and chronic insulin resistance. The failure in β-cell function has been attributed to the deleterious effect of chronically elevated levels of glucose and fatty acids. These processes, known as glucolipotoxicity, are related to the generation of chronic oxidative stress and the alteration of the intracellular energy metabolism in pancreatic β-cells.

Peroxisomes are organelles involved in the degradation of a variety of lipid derivatives and in the metabolism of reactive oxygen species. To date, scarce information is available concerning the function of peroxisomes in pancreatic β-cells, however, the abundance of this organelle in the pancreatic endocrine region suggests that the metabolic function of peroxisomes might be particularly relevant to β-cell function. Therefore, we investigated whether the dysfunction of peroxisomes is involved in oxidative stress and intracellular lipid accumulation which in turn results in β-cell dysfunction and death.

Therefore, the main goal of this thesis was to analyse the role of peroxisomes in maintaining normal β-cell physiology and protecting β-cells against glucolipotoxicity induced by palmitic and phytanic acid.

To this end, a peroxisomal dysfunction was induced in β-TC3 cells by siRNA-mediated *Pex13* and *Abcd3* knockdown. To obtain an integral overview on the peroxisomal compartment and its enzyme composition and to analyse the molecular consequences of peroxisome deficiency as well as the induced glucolipotoxicity in the pathology of β cells, total RNA isolation, qRT-PCR, Western blot, immunofluorescence analysis, catalase-assay, reactive oxygen species indirect measurements, laser capture microdissection and lipid droplet accumulation analysis were carried out. Further, we also assessed the capability of the β-TC3 cells to store/secrete insulin after the induced peroxisomal defect and lipid overload.

The results in this thesis stress the importance of functional peroxisomal metabolism for the detoxification of excess FA in β-cells. Our findings support the notion that peroxisomal dysfunction, here achieved by the silencing of *Pex13*, leads to an increased intracellular H_2O_2 production and causes mitochondrial alterations in β-TC3 cells. Furthermore, the

peroxisomal dysfunction (alone or in combination with toxic lipid concentrations) alters the lipid storage capability of β-cells.

Novel evidence of the toxicity of PHY for the β-cell (which was exacerbated by the *Pex13* knockdown) was presented, which was accompanied by a decrease in insulin biosynthesis. We showed a rise in the formation of H_2O_2 production after PA treatment together with an increase in catalase expression and activity suggesting a positive-feedback to re-establish the redox homeostasis that was disturbed by the addition of the FA. Moreover, the treatment with PA and the *Pex13* silencing (but not PHY treatment) resulted in alterations of β-cell-specific genes involved in β-cell function and identity *(Pax6, Pax4 and Pdx1*).

Further elucidation of the role of this organelle in β-cell function and disease might bring new research opportunities to find new targets and strategies in the treatment and prevention of diabetes.

8. ZUSAMMENFASSUNG

Typ 2 Diabetes ist durch eine beeinträchtigte Insulinsektetion mit einem kombinierten Verlust der β-Zellen und einer chronischen Insulinresistenz charakterisiert. Dieser Verlust der Funktionalität von β-Zellen wird einer chronisch erhöhten Konzentration von Glucose und Fettsäuren zugeschrieben. Dieser Prozess, bekannt als Glucolipotoxizität, steht im Zusammenhang mit oxidativem Stress und verändertem Energie-Metabolismus in pankreatischen β-Zellen.

Peroxisomen sind Organellen, die beim Abbau von Fettsäureabkömmlingen und oxidativem Stress beteiligt sind. Bis heute stehen nur wenige Informationen über die Funktion der Peroxisome in pankreatischen β-Zellen zur Verfügung, obwohl die hohe Anzahl dieser Organellen im endokrinen Pankreas eine wichtige Rolle in deren Funktionalität nahelegt. Daher untersuchten wir, ob eine beeinträchtige Funktion von Peroxisomen zu verändertem oxidativem Stress und intrazellulärer Fettakkumulation führt, welche wiederum zu Schädigungen der Zellphysiologie bzw. Zelltod führt.

Daher war das Hauptziel dieser Arbeit die Rolle von Peroxisomen in der Aufrechterhaltung eines normalen Stoffwechsels in der β-Zelle und dem Schutz vor oxidativem Stress von Glucolipotoxizität, induziert durch Phytansäure und Palmitinsäure, zu analysieren.

Um dies zu untersuchen, haben wir eine peroxisomale Fehlfunktion durch ein siRNA-induziertes Knockdown der Gene für *Pex13* und *Abcd3* herbeigeführt. Um sowohl eine Übersicht über die Verteilung und die Enzymfunktion von Peroxisomen, als auch eine Analyse über die molekulären Konsequenzen einer Fehlfunktion und der Glucolipotoxizität zu erhalten, haben wir zum einen RNA isoliert, Western blots, Immunofluoreszenzen und Katalase analysiert, und zum anderen ROS indirekt gemessen, Laser-Mikrodissektionen durchgeführt und die Verteilung von Fetttröpfchen in der β-Zelle untersucht. Darüber hinaus haben wir die Fähigkeit der β-Zelle zur Speicherung und Sekretion von Insulin, nach vorrausgegangener induzierter Fehlfunktion von Peroxisomen bzw. Fettüberladung, untersucht.

Die Ergebnisse dieser Arbeit unterstreichen die wichtige Rolle der korrekten Funktion des peroxisomalen Metabolismus für die Detoxifizierung von überschüssigen Fettsäuren in β -Zellen.

Unsere Resultate unterstützen weiterhin die Auffassung, dass peroxisomale Fehlfunktion, die hier durch das beeinträchtigen des *Pex13*-Gens herbeigeführt wurde, zu einer erhöhten intrazellulären H_2O_2 Produktion führt und dadurch die Mitochondrien in β-TC3 Zellen beeinflusst. Außerdem führt die Fehlfunktion von Peroxisomen (alleine oder in Kombination mit toxischen Fettsäurekonzentrationen) zu einer veränderten Speicherfähigkeit von Fett in β-Zellen.

Neue Evidenz für die Toxizität von PHY für die β -Zelle (welche durch ein *Pex13* Knockdown verstärkt werden konnte) mit einer einhergehenden Reduktion der Insulinsynthese konnte erzeugt werden. Wir zeigten einen Anstieg in der H_2O_2 Produktion, gefolgt von einer erhöhten Katalase Expression und Aktivität nach Behandlung der Zellen mit PA, was auf ein positives Feedback hinweist, dass wahrscheinlich die durch Fettsäuren veränderte Redox-Homeostase wiederherstellen soll. Abschließend zeigten wir, dass eine Behandlung mit PA (aber nicht mit PHY) und ein Knock-Down des *Pex13* Gens in einer veränderten Expression in β -Zell spezifisches Genen für peroxisomale Funktion bzw. Integrität *(Pax6, Pax4 and Pdx1*) mündet.

Weitere Untersuchungen über die Rolle dieses Organells in der Funktion von β-Zellen, wie auch dessen Krankheiten könnten zu neuen Forschungsansätzen, und damit zu neuen Strategien in der Bekämpfung bzw. der Prävention von Diabetes, führen.

9. LITERATURE CITED

1. De Duve C, Baudhuin P. Peroxisomes microbodies and related particles. Physiol. Rev. 1966; 46:323–57.
2. Schrader M, Fahimi H. The peroxisome: still a mysterious organelle. Histochem. Cell Biol. 2008; 129(4):421–40.
3. Titorenko V, Rachubinski R. Dynamics of peroxisome assembly and function. Trends Cell Biol. 2001; 11(1):22–9.
4. Fahimi H. Cytochemical localization of peroxidatic activity of catalase in rat hepatic microbodies (peroxisomes). J. Cell Biol. 1969; 43:275–88.
5. Fahimi H, Reich D, Völkl A, Baumgart E. Contributions of the immunogold technique to investigation of the biology of peroxisomes. Histochem. Cell Biol. 1996; 106(1):105–14.
6. Mi J, Kirchner E, Cristobal S. Quantitative proteomic comparison of mouse peroxisomes from liver and kidney. Proteomics. 2007; 7(11):1916–28.
7. Wiese S, Gronemeyer T, Ofman R, Kunze M, Grou C, Almeida A et al. Proteomics characterization of mouse kidney peroxisomes by tandem mass spectrometry and protein correlation profiling. Mol. Cel. Proteomics. 2007; 6(12):2045–57.
8. Islinger M, Grille S, Fahimi H, Schrader M. The peroxisome: an update on mysteries. Histochem. Cell Biol. 2012; 137(5):547–74.
9. Francisco T, Rodrigues T, Dias A, Barros-Barbosa A, Bicho D, Azevedo J. Protein transport into peroxisomes: Knowns and unknowns. Bioessays. 2017; 39(10):1-7.
10. Distel B, Erdmann R, Gould S, Blobel G, Crane D, Cregg J et al. A unified nomenclature for peroxisome biogenesis factors. J. Cell Biol. 1996; 135(1):1–3.
11. Schrader M, Costello J, Godinho L, Azadi A, Islinger M. Proliferation and fission of peroxisomes - An update. Biochem. Biophys. Acta. 2016; 1863(5):971–83.
12. Dimitrov L, Lam S, Schekman R. The role of the endoplasmic reticulum in peroxisome biogenesis. Cold Spring Harb. Perspect. Biol. 2013; 5(5):1-12.
13. Fujiki Y, Okumoto K, Mukai S, Honsho M, Tamura S. Peroxisome biogenesis in mammalian cells. Front. Physiol. 2014; 5(307):1-8.
14. Matsuzaki T, Fujiki Y. The peroxisomal membrane protein import receptor Pex3p is directly transported to peroxisomes by a novel Pex19p- and Pex16p-dependent pathway. J. Cell Biol. 2008; 183(7):1275–86.
15. Soukupova M, Sprenger C, Gorgas K, Kunau W, Dodt G. Identification and characterization of the human peroxin PEX3. Eur. J. Cell Biol. 1999; 78(6):357–74.
16. Muntau A, Roscher A, Kunau W, Dodt G. The interaction between human PEX3 and PEX19 characterized by fluorescence resonance energy transfer (FRET) analysis. Eur. J. Cell Biol. 2003; 82(7):333–42.
17. Kashiwayama Y, Asahina K, Shibata H, Morita M, Muntau A, Roscher A et al. Role of Pex19p in the targeting of PMP70 to peroxisome. Biochim. Biophys. Acta 2005; 1746(2):116–28.
18. Morita M, Imanaka T. Peroxisomal ABC transporters: structure, function and role in disease. Biochim. Biophys. Acta. 2012; 1822(9):1387–96.
19. Jones J, Morrell J, Gould S. Multiple distinct targeting signals in integral peroxisomal membrane proteins. J. Cell Biol. 2001; 153(3):1141–9.
20. Halbach A, Lorenzen S, Landgraf C, Volkmer-Engert R, Erdmann R, Rottensteiner H. Function of the PEX19-binding site of human adrenoleukodystrophy protein as targeting motif in man and yeast. PMP targeting is evolutionarily conserved. J. Biol. Chem. 2005; 280(22):21176–82.
21. Sato Y, Shibata H, Nakatsu T, Nakano H, Kashiwayama Y, Imanaka T et al. Structural basis for docking of peroxisomal membrane protein carrier Pex19p onto its receptor Pex3p. EMBO J. 2010; 29(24):4083–93.
22. Shibata H, Kashiwayama Y, Imanaka T, Kato H. Domain architecture and activity of human Pex19p, a chaperone-like protein for intracellular trafficking of peroxisomal membrane proteins. J. Biol. Chem. 2004; 279(37):38486–94.
23. Lazarow P, Fujiki Y. Biogenesis of peroxisomes. Ann. Rev. Cell Biol. 1985; (1):489–530.
24. Colasante C, Chen J, Ahlemeyer B, Baumgart-Vogt E. Peroxisomes in cardiomyocytes and the peroxisome / peroxisome proliferator-activated receptor-loop. Thromb. Haemost. 2015; 113(3):452–63.
25. Rucktäschel R, Girzalsky W, Erdmann R. Protein import machineries of peroxisomes. Biochim. Biophys. Acta. 2011; 1808(3):892–900.
26. Gould S, Keller G, Subramani S. Identification of a peroxisomal targeting signal at the carboxy terminus of firefly luciferase. J. Cell Biol. 1987; 105(6):2923–31.
27. Gould S, Keller G, Hosken N, Wilkinson J, Subramani S. A conserved tripeptide sorts proteins to peroxisomes. J. Cell Biol. 1989; 108(5):1657–64.

28. de Hoop M, Ab G. Import of proteins into peroxisomes and other microbodies. Biochem. J. 1992; 286:657–69.
29. Otera H, Harano T, Honsho M, Ghaedi K, Mukai S, Tanaka A et al. The mammalian peroxin Pex5pL, the longer isoform of the mobile peroxisome targeting signal (PTS) type 1 transporter, translocates the Pex7p.PTS2 protein complex into peroxisomes via its initial docking site, Pex14p. J. Biol. Chem. 2000; 275(28):21703–14.
30. Subramani S. Components involved in peroxisome import, biogenesis, proliferation, turnover, and movement. Physiol. Rev. 1998; 78(171-188).
31. Erdmann R, Blobel G. Identification of Pex13p a peroxisomal membrane receptor for the PTS1 recognition factor. J. Cell Biol. 1996; 135(1):111–21.
32. Gould S, Kalish J, Morrell J, Bjorkman J, Urquhart A, Crane D. Pex13p is an SH3 protein of the peroxisome membrane and a docking factor for the predominantly cytoplasmic PTS1 receptor. J. Cell Biol. 1996; 135(1):85–95.
33. Elgersma Y, Kwast L, Klein A, Voorn-Brouwer T, van den Berg M, Metzig B et al. The SH3 domain of the Saccharomyces cerevisiae peroxisomal membrane protein Pex13p functions as a docking site for Pex5p, a mobile receptor for the import PTS1-containing proteins. J. Cell Biol. 1996; 135(1):97–109.
34. Barnett P, Bottger G, Klein A, Tabak H, Distel B. The peroxisomal membrane protein Pex13p shows a novel mode of SH3 interaction. EMBO J. 2000; 19(23):6382–91.
35. Liu Y, Björkman J, Vamecq J, Wanders R, Crane D, Gould S. PEX13 Is Mutated in Complementation Group 13 of the Peroxisome. Am. J. Hum. Genet. 1999:621–34.
36. Baes M, Gressens P, Baumgart E, Casteels M, Evrard P, Fahimi D et al. A mouse model for Zellweger syndrome. Nat. Genet. 1997; 17(1):49–57.
37. Baumgart E, Vanhorebeek I, Grabenbauer M, Borgers M, Declercq P, Fahimi D et al. Mitochondrial alterations caused by defective peroxisomal biogenesis in a mouse model for Zellweger syndrome (PEX5 knockout mouse). Am. J. Pathol. 2001; 159(4):1477–94.
38. Maxwell M, Bjorkman J, Nguyen T, Sharp P, Finnie J, Paterson C et al. Pex13 inactivation in the mouse disrupts peroxisome biogenesis and leads to a Zellweger syndrome phenotype. Mol. Cell Biol. 2003; 23(16):5947–57.
39. Ahlemeyer B, Gottwald M, Baumgart-Vogt E. Deletion of a single allele of the Pex11β gene is sufficient to cause oxidative stress, delayed differentiation and neuronal death in mouse brain. Dis. Model Mech. 2012; 5(1):125–40.
40. Santos M, Imanaka T, Shio H, Small G, Lazarow P. Peroxisomal membrane ghosts in Zellweger syndrome--aberrant organelle assembly. Science 1988; 239(4847):1536–8.
41. Thoms S, Erdmann R. Dynamin-related proteins and Pex11 proteins in peroxisome division and proliferation. FEBS J. 2005; 272(20):5169–81.
42. Schrader M, Fahimi H. Growth and division of peroxisomes. Int. Rev. Cytol. 2006; 255:237–90.
43. Hettema E, Motley A. How peroxisomes multiply. J. Cell Sci. 2009; 122(Pt 14):2331–6.
44. Kim P, Mullen R, Shumann U, Lippincott-Schwartz J. The origin and maintenance of mammalian peroxisomes involves a de novo PEX16-dependent pathway from the ER. J. Cell Biol. 2006;173(4):521–32.
45. Schrader M, Reubers B, Morrell J, Jimenez-Sanchez G, Obie C, Stroh T et al. Expression of PEX11 β mediates peroxisome proliferation in the absence of extracellular stimuli. J. Biol. Chem. 1998; 273(45):29607–14.
46. Li X, Gould S. PEX11 promotes peroxisome division independently of peroxisome metabolism. J. Cell Biol. 2002; 156(4):643–51.
47. Li X, Baumgart E, Morrell J, Jimenez-Sanchez G, Valle D, Gould S. PEX11 deficiency is lethal and impairs neuronal migration but does not abrogate peroxisome function. Mol. Cell Biol. 2002; 22(12):4358–65.
48. Li X, Baumgart E, Dong G, Morrell J, Jimenez-Sanchez G, Valle D et al. PEX11 is required for peroxisome proliferation in response to 4-phenylbutyrate but is dispensable for peroxisome proliferator-activated receptor alpha-mediated peroxisome proliferation. Mol. Cell. Biol. 2002; 22(23):8226–40.
49. Issemann I, Green S. Activation of a member of the steroid hormone receptor superfamily by peroxisome proliferators. Nature. 1990; 347(6294):645–50.
50. Berger J, Moller D. The mechanisms of action of PPARs. Annu. Rev. Med. 2002; 53:409–35.
51. Contreras A, Torres N, Tovar A. PPAR-alpha as a key nutritional and environmental sensor for metabolic adaptation. Adv. Nutr. 2013; 4(4):439–52.
52. Fruchart J, Staels B, Duriez P. Ppars, metabolic disease and atherosclerosis. Pharm. Res. 2001; 44(5):345–52.
53. Evans J, Goldfine I, Maddux B, Grodsky G. Are oxidative stress-activated signaling pathways mediators of insulin resistance and beta-cell dysfunction? Diabetes. 2003; 52(1):1–8.

54. Evans R, Grant D, Wang Y. PPARs and the complex journey to obesity. Nat. Med. 2004; 10(4):355–61.
55. Jay M, Ren J. Peroxisome proliferator-activated receptor (PPAR) in metabolic syndrome and type 2 diabetes mellitus. Diabetes. 2007; 3:33–9.
56. Rogue A, Renaud M, Claude N, Guillouzo A, Spire C. Comparative gene expression profiles induced by PPARgamma and PPARalpha/gamma agonists in rat hepatocytes. Toxicol. Appl. Pharmacol. 2011; 254(1):18–31.
57. Bernlohr D, Simpson M, Hertzel A, Banaszak L. Intracellular lipid-binding proteins and their genes. Annu. Rev. Nutr. 1997; 17:277–303.
58. Ellinghaus P, Wolfrum C, Assmann G, Spener F, Seedorf U. Phytanic acid activates the peroxisome proliferator-activated receptor alpha (PPARa) in sterol carrier protein 2-/sterol carrier protein x-deficient mice. J. Biol. Chem. 1999; 274(5):2766–72.
59. Delille H, Bonekamp N, Schrader M. Peroxisomes and disease- An overview. Int. J. Biomed. Sci. 2006; 2(4):308–14.
60. Waterham HR, Ferdinandusse S, Wanders R. Human disorders of peroxisome metabolism and biogenesis. Biochem. Biophys. Acta 2016; 1863(5):922–33.
61. Theodoulou F, Holdsworth M, Baker A. Peroxisomal ABC transporters. FEBS Lett. 2006; 580(4):1139–55.
62. Angermüller S, Bruder G, Völkl A, Wesch H, Fahimi D. Localization of xanthine oxidase in crystalline cores of peroxisomes. A cytochemical and biochemical study. Eur. J. Cell Biol. 1987; 45(1):137–44.
63. Vujcic S, Liang P, Diegelman P, Kramer D, Porter C. Genomic identification and biochemical characterization of the mammalian polyamine oxidase involved in polyamine back-conversion. Biochem. J. 2003; 370(Pt 1):19–28.
64. Diano S, Liu Z, Jeong J, Dietrich M, Ruan H, Kim E et al. Peroxisome proliferation-associated control of reactive oxygen species sets melanocortin tone and feeding in diet-induced obesity. Nat. Med. 2011; 17(9):1121–7.
65. Dixit E, Boulant S, Zhang Y, Lee A, Odendall C, Shum B et al. Peroxisomes are signaling platforms for antiviral innate immunity. Cell. 2010; 141(4):668–81.
66. Lazarow P, De Duve C. A fatty acyl-CoA oxidizing system in rat liver peroxisomes; enhancement by clofibrate, a hypolipidemic drug. Proc. Natl. Acad. Sci. 1976; 73(6):2043–6.
67. Wanders R, Waterham H, Ferdinandusse S. Metabolic interplay between peroxisomes and other subcellular organelles including mitochondria and the endoplasmic reticulum. Front. Cell Dev. Biol. 2015; 3:1–15.
68. Van Veldhoven P. Biochemistry and genetics of inherited disorders of peroxisomal fatty acid metabolism. J. Lipid Res. 2010; 51(10):2863–95.
69. Vamecq J, Draye JP. Peroxisomal and mitochondrial b-oxidation of monocarboxylyl-CoA, omega-hyroxymonocarboxylyl-CoA and dicarboxylyl-CoA esters in tissues from untreated and clofibrate-treated rats. J. Biochem. 1989; 106:216–22.
70. Watkins P, Ellis J. Peroxisomal acyl-CoA synthetases. Biochem. Biophys. Acta 2012; 1822(9):1411–20.
71. Van Veldhoven P, Casteels M, Mannaerts G, Baes M. Further insights into peroxisomal lipid breakdown via alpha- and beta-oxidation. Biochem. Soc. Trans. 2001; 29:292–8.
72. Schrader M, Yoon Y. Mitochondria and peroxisomes: are the 'big brother' and the 'little sister' closer than assumed? BioEssays. 2007; 29(11):1105–14.
73. Uchida Y, Kondo N, Orii T, Hashimoto T. Purification and properties of rat liver peroxisomal very-long-chain Acyl-CoA synthetase. J. Biochem. 1996; 119:555–71.
74. Wanders R, Ferdinandusse S, Brites P, Kemp S. Peroxisomes, lipid metabolism and lipotoxicity. Biochim. Biophys. Acta 2010; 1801(3):272–80.
75. Vanhooren J, Baumgart E, Fransen M, Mannaerts G, Van Veldhoven P. Mammalian peroxisomal acyl-CoA oxidases. I. Molecular characterization of rat pristanoyl-CoA oxidase. Ann. N.Y. Acad. Sci. 1996;804:674–5.
76. Baumgart E, Vanhooren J, Fransen M, Van Veldhoven P, Mannaerts G. Mammalian peroxisomal acyl-CoA oxidases. II. Molecular characterization of rat trihydroxycoprostanoyl-CoA oxidase. Ann. N.Y. Acad. Sci. 1996; 804:676–7.
77. Baumgart E, Vanhooren J, Fransen M, Mannaerts G, Van Veldhoven P. Mammalian peroxisomal acyl-CoA oxidases. III. Molecular characterization of human branched chain fatty acyl-CoA oxidase. Ann. N.Y. Acad. Sci. 1996; 804:678–9.
78. Lemaitre R, Fretts A, Sitlani C, Biggs M, Mukamal K, King I et al. Plasma phospholipid very-long-chain saturated fatty acids and incident diabetes in older adults: The Cardiovascular Health Study. Am. J. Clin. Nutr. 2015; 101(5):1047–54.

79. Vanhooren J, Van Veldhoven V. Rat Pristanoyl-CoA Oxidase: cDNA cloning and recognition of its C-terminal (SQL) by the peroxisomal-targeting signal 1 receptor. Eur. J. Biochem. 1996;239:302-309.
80. Ferdinandusse S, Denis S, van Roermund C, Wanders R, Dacremont G. Identification of the peroxisomal beta-oxidation enzymes involved in the degradation of long-chain dicarboxylic acids. J. Lipid Res. 2004; 45(6):1104–11.
81. Wanders R, Waterham H. Biochemistry of mammalian peroxisomes revisited. Annu. Rev. Biochem. 2006; 75:295–332.
82. Lloyd M, Darley D, Wierzbicki A, Threadgill M. Alpha-methylacyl-CoA racemase-an 'obscure' metabolic enzyme takes centre stage. FEBS J. 2008; 275(6):1089–102.
83. Westin M, Hunt M, Alexson S. Peroxisomes contain a specific phytanoyl-CoA/pristanoyl-CoA thioesterase acting as a novel auxiliary enzyme in alpha- and beta-oxidation of methyl-branched fatty acids in mouse. J. Biol. Chem. 2007;282(37):26707-716.
84. Wierzbicki A. Peroxisomal disorders affecting phytanic acid α-oxidation: a review. Biochem. Soc. Trans. 2007; 35(5):881–6.
85. Mukherji M, Schonfeld P, Wierzbicky A, Jansen G, Wanders R, Lloyd M. The chemical biology of branched-chain lipid metabolism. Prog. Lipid. Res. 2003; 42:359–76.
86. Van Veldhoven P, Huang S, Eyssen H, Mannaerts G. The deficient degradation of synthetic 2- and 3-methyl-branched fatty acids in fibroblasts from patients with peroxisomal disorders. J. Inherit Metab. Dis. 1993; 16(2):381–91.
87. Holzinger A, Kammerer S, Berger J, Roscher A. cDNA cloning and mRNA expression of the human adrenoleukodystrophy related protein (ALDRP), a peroxisomal ABC transporter. Biochem. Biophys. Res. Commun. 1997:261–4.
88. Kawaguchi K, Morita M. ABC Transporter subfamily D: distinct differences in behavior between ABCD1-3 and ABCD4 in subcellular localization, function, and human disease. BioMed Res. Int. 2016; 1-11.
89. Contreras M, Sengupta K, Sheikh F, Aubourg P, Sinhg I. Topology of ATP-binding domain of adrenoleukodystrophy gene product in peroxisomes. Arch. Biochem. Biophys. 1996; 334(2):369–79.
90. Salmon A, Richardson A, Pérez V. Update on the oxidative stress theory of aging: does oxidative stress play a role in aging or healthy aging? Free Radic. Biol. Med. 2010; 48(5):642–55.
91. Terlecky S, Koepke J, Walton P. Peroxisomes and aging. Biochim. Biophys. Acta. 2006; 1763(12):1749–54.
92. Nathan C, Ding A. SnapShot: Reactive oxygen intermediates (ROI). Cell. 2010; 140(6):951–2.
93. Antonenkov V, Grunau S, Ohlmeier S, Hiltunen K. Peroxisomes are oxidative organelles. Antiox. Redox Signal. 2010; 13(4):525–37.
94. Dansen T, Wirtz K. The peroxisome in oxidative stress. Life. 2001; 51:223–30.
95. Fritz R, Bol J, Hebling U, Angermüller S, Völkl A, Fahimi H et al. Compartment-dependent management of H_2O_2 by peroxisomes. Free Radic. Biol. Med. 2007; 42(7):1119–29.
96. Nordgren M, Fransen M. Peroxisomal metabolism and oxidative stress. Biochimie. 2014; 98:56–62.
97. Moldovan L, Moldovan N. Oxygen free radicals and redox biology of organelles. Histochem. Cell Biol. 2004; 122(4):395–412.
98. Yin H, Xu L, Porter N. Free radical lipid peroxidation: mechanisms and analysis. Chem. Rev. 2011; 111(10):5944–72.
99. Schrader M, Fahimi H. Peroxisomes and oxidative stress. Biochim. Biophys. Acta 2006; 1763(12):1755–66.
100. del Río L, Sandalio L, Corpas F, Palma J, Barroso J. Reactive oxygen species and reactive nitrogen species in peroxisomes. Production, scavenging, and role in cell signaling. Plant Physiol. 2006; 141(2):330–5.
101. Siraki A, Pourahmad J, Chan T, Khan S, O´Brien P. Endogenous and endobiotic induced reactive oxygen species formation by isolated hepatocytes. Free Radic. Biol. Med. 2002; 32(1):2–10.
102. Hashimoto F, Hayashi H. Significance of catalase in peroxisomal fatty acyl-CoA beta-oxidation: NADH oxidation by acetoacetyl-CoA and H2O2. J. Biochem. 1990;108(3):426–31.
103. Singh A, Dobashi K, Gupta M, Asayama K, Singh I, Orak J. Manganese superoxide dismutase in rat liver peroxisomes: biochemical and immunochemical evidence. Mol. Cell. Biochem. 1999; 197(1-2):7–12.
104. Karnati S, Lüers G, Pfreimer S, Baumgart-Vogt E. Mammalian SOD2 is exclusively located in mitochondria and not present in peroxisomes. Histochem. Cell Biol. 2013; 140(2):105–17.
105. Singh A, Dhaunsi G, Gupta M, Orak J, Asayama K, Singh I. Demonstration of glutathione peroxidase in rat liver peroxisomes and its intraorganellar distribution. Arch. Biochem. Biophys. 1994; 315(2):331–8.
106. Keller G, Warner T, Steimer K, Hallewell R. Cu,Zn superoxide dismutase is a peroxisomal enzyme in human fibroblasts and hepatoma cells. Proc. Natl. Acad. Sci. U.S.A. 1991; 88:7381–5.
107. Dhaunsi G, Gulati S, Singh A, Orak J, Asayama K, Singh I. Demonstration of Cu–Zn superoxide dismutase in rat liver peroxisomes: Biochemical and immunochemical evidence. J. Biol. Chem. 1992; 267:6870–3.

108. Waechter F, Bentley P, Bieri F, Stäubli W, Völkl A, Fahimi H. Epoxide hydrolase activity in isolated peroxisomes of mouse liver. FEBS Lett. 1983; 158(2):225–8.
109. Immenschuh S, Baumgart-Vogt E, Tan M, Iwahara S, Ramadori G, Fahimi H. Differential cellular and subcellular localization of heme-binding protein 23/peroxiredoxin I and heme oxygenase-1 in rat liver. J. Histochem. Cytochem. 2003; 51(12):1621–31.
110. Yamashita H, Avraham S, Jiang S, London R, Van Veldhoven P, Subramani S et al. Characterization of human and murine PMP20 peroxisomal proteins that exhibit antioxidant activity in vitro. J. Biol. Chem. 1999; 274(42):29897–904.
111. van der Valk P, Gilie J, Oostra A, Roubos E, Sminina T, Joenje H. Characterization of an oxygen-tolerant cell line derived from Chinese hamster ovary. Antioxygenic enzyme levels and ultrastructural morphometry of peroxisomes and mitochondria. Cell. Tissue Res. 1985; 239(1):61–8.
112. Schrader M, Wodopia R, Fahimi H. Induction of tubular peroxisomes by UV irradiation and reactive oxigen species in HepG2 cells. J. Histochem. Cytochem. 1999; 47:1141–8.
113. Schrader M, Fahimi H. Mammalian peroxisomes and reactive oxygen species. Histochem. Cell Biol. 2004; 122(4):383–93.
114. Santos M, Quintanilla R, Toro A, Grandy R, Dinamarca M, Godoy J et al. Peroxisomal proliferation protects from beta-amyloid neurodegeneration. J. Biol. Chem. 2005; 280(49):41057–68.
115. Fransen M, Nordgren M, Wang B, Apanasets O. Role of peroxisomes in ROS/RNS-metabolism: implications for human disease. Biochim. Biophys. Acta. 2012; 1822(9):1363–73.
116. Rani V, Deep G, Singh R, Palle K, Yadav U. Oxidative stress and metabolic disorders: Pathogenesis and therapeutic strategies. Life Sci. 2016; 148:183–93.
117. Camões F, Bonekamp N, Delille H, Schrader M. Organelle dynamics and dysfunction: A closer link between peroxisomes and mitochondria. J. Inherit Metab. Dis. 2009; 32(2):163–80.
118. Wanders R. Peroxisomes, lipid metabolism, and peroxisomal disorders. Mol. Genet. Metab. 2004; 83(1-2):16–27.
119. Poirier Y, Antonenkov V, Glumoff T, Hiltunen K. Peroxisomal beta-oxidation-a metabolic pathway with multiple functions. Biochem. Biophys. Acta. 2006; 1763(12):1413–26.
120. Antonenkov V, Hiltunen J. Peroxisomal membrane permeability and solute transfer. Biochim. Biophys. Acta. 2006; 1763(12):1697–706.
121. Antonenkov V, Hiltunen J. Transfer of metabolites across the peroxisomal membrane. Biochim. Biophys. Acta. 2012; 1822(9):1374–86.
122. Jezek P, Hlavata L. Mitochondria in homeostasis of reactive oxygen species in cell, tissues, and organism. Int. J. Biochem. Cell Biol. 2005; 37(12):2478–503.
123. Koepke J, Wood C, Terlecky L, Walton P, Terlecky S. Progeric effects of catalase inactivation in human cells. Toxicol. Appl. Pharmacol. 2008; 232(1):99–108.
124. Ivashchenko O, Van Veldhoven P, Brees C, Ho Y, Terlecky S, Fransen M. Intraperoxisomal redox balance in mammalian cells: oxidative stress and interorganellar cross-talk. Mol. Biol. Cell. 2011; 22(9):1440–51.
125. Hwang I, Lee J, Huh J, Park J, Lee H, Ho Y et al. Catalase deficiency accelerates diabetic renal injury through peroxisomal dysfunction. Diabetes 2012; 61(3):728–38.
126. Wanders R, Waterham H. Peroxisomal disorders I: biochemistry and genetics of peroxisome biogenesis disorders. Clin. Genet. 2005; 67(2):107–33.
127. Steinberg S, Dodt G, Raymond G, Braverman N, Moser A, Moser H. Peroxisome biogenesis disorders. Biochim. Biophys. Acta. 2006; 1763(12):1733–48.
128. Weller S, Gould S, Valle D. Peroxisome biogenesis disorders. Annu. Rev. Genomics Hum. Genet. 2003; 4:165–211.
129. Wanders R, Komen J. Peroxisomes, Refsum´s disease and the alpha- and omega-oxidation of phytanic acid. Biochem. Soc. Trans. 2007; 35:865–9.
130. Wanders R. Refsum disease, peroxisomes and phytanic acid oxidation: a review. J. Neuropathol. Exp. Neurol. 2001;60(11)1021.31.
131. Baumgart-Vogt E. Lipidstoffwechsel in Peroxisomen und dessen experimentelle Beeinflussung. Habilitationsschrift 1998:97.
132. Murtaugh L, Melton D. Genes, signals, and lineages in pancreas development. Annu. Rev. Cell Dev. Biol. 2003; 19:71–89.
133. International Diabetes Federation. IDF Atlas 2015.
134. Goldberg R, Mather K. Targeting the consequences of the metabolic syndrome in the Diabetes Prevention Program. Arterioscler. Thromb. Vasc. Biol. 2012; 32(9):2077–90.
135. Yki-Järvinen H. Glucose Toxicity. Endocr. Rev. 1992; 13(3):415–31.

136. Lee Y, Hirose H, Ohneda M, Johnson J, McGarry D, Unger R. Beta-cell lipotoxicity in the pathogenesis of non-insulin-dependent diabetes mellitus of obese rats impairment in adipocyte beta cell relationships. Proc. Natl. Acad. Sci. 1994; 91(23):10878–82.
137. Unger R. Minireview: weapons of lean body mass destruction: the role of ectopic lipids in the metabolic syndrome. Endocrinology. 2003; 144(12):5159–65.
138. Cnop M, Welsh N, Jonas J, Jörns A, Lenzen S, Eizirik D. Mechanisms of pancreatic beta-cell death in type 1 and type 2 diabetes: Many Differences, Few Similarities. Diabetes. 2005; 54:97–107.
139. Cnop M, Hannaert J, Hoorens A, Eizirik D, Pipeleers D. Inverse relationship between cytotoxicity of free fatty acids in pancreatic islet cells and cellular triglyceride accumulation. Diabetes. 2001; 50(8):1771–7.
140. Robertson R, Harmon J, Tran P, Tanaka Y, Takahashi H. Glucose toxicity in beta-cells: type 2 diabetes, good radicals gone bad, and the glutathione connection. Diabetes. 2003; 52:581–7.
141. Poitout V, Amyot J, Semache M, Zarrouki B, Hagman D, Fontés G. Glucolipotoxicity of the pancreatic beta cell. Biochim. Biophys. Acta. 2010; 1801(3):289–98.
142. Robertson R, Harmon J, Oanh P, Poitout V. Beta-cell glucose toxicity, lipotoxicity, and chronic oxidative stress in type 2 diabetes. Diabetes. 2004; 53:119–24.
143. Matsuzawa-Nagata N, Takamura T, Ando H, Nakamura S, Kurita S, Misu H et al. Increased oxidative stress precedes the onset of high-fat diet-induced insulin resistance and obesity. Metabolism. 2008; 57(8):1071–7.
144. Prentki M, Joly E, El-Assaad W, Roduit R. Malonyl-CoA signaling, lipid partitioning, and glucolipotoxicity: Role in b-cell adaptation and failure in the etiology of diabetes. Diabetes. 2002; 51(3).
145. Warnotte C, Gilon P, Nenquin M, Henquin J. Mechanisms of the stimulation of insulin release by saturated fatty acids: A study of palmitate effects in mouse beta-cells. Diabetes. 1994; 43(5):703–11.
146. Parker S, Moore P, Johnson L, Poitout V. Palmitate potentiation of glucose-induced insulin release: A study using 2-bromopalmitate. Metabolism. 2003; 52(10):1367–71.
147. Dobbins R, Chester M, Stevenson B, Daniels M, Stein D, McGarry D. A fatty acid- dependent step is critically important for both glucose- and non-glucose-stimulated insulin secretion. J. Clin. Invest. 1998; 101(11):2370–6.
148. Haber E, Procópio J, Carvalho C, Carpinelli A, Nwsholme P, Curi R. New insights into fatty acid modulation of pancreatic beta-cell function. Int. Rev. Cytol. 2006; 248:1–41.
149. Poitout V, Olson L, Robertson P. Chronic exposure of betaTC-6 cells to supraphysiologic concentrations of glucose decreases binding of the RIPE3b1 insulin gene transcription activator. J. Clin. Invest. 1996; 97(4):1041–6.
150. Pick A, Clark J, Kubstrup C, Levisetti M, Pugh W, Bonner-Weir S et al. Role of apoptosis in failure of beta-cell mass compensation for insulin resistance and beta-cell defects in the male Zucker Diabetic fatty rat. Diabetes 199847(3):358–61.
151. Kaneto H, Matsuoka T. Involvement of oxidative stress in suppression of insulin biosynthesis under diabetic conditions. Int. J. Mol. Sci. 2012; 13(10):13680–90.
152. Jacqueminet S, Briaud I, Rouault C, Reach G, Poitout V. Inhibition of insulin gene expression by long-term exposure of pancreatic β cells to palmitate is dependent on the presence of a stimulatory glucose concentration. Metabolism. 2000; 49(4):532–6.
153. Donath M, Ehses J, Maedler K, Schumann D, Ellingsgaard H, Eppler E et al. Mechanism of beta-cell death in type 2 diabetes. Diabetes. 2005; 54:108–13.
154. Rutter G, Parton L. The beta-cell in type 2 diabetes and in obesity. Front. Horm. Res. 2008; 36:118–34.
155. Shimabukuro M, Zhou Y, Levi M, Unger R. Fatty acid-induced beta cell apoptosis: a link between obesity and diabetes. Proc. Natl. Acad. Sci. 1998; 95:2498–502.
156. Maedler K, Oberholzer J, Bucher P, Spinas G, Donath M. Monounsaturated fatty acids prevent the deleterious effects of palmitate and high glucose on human pancreatic beta-cell turnover and function. Diabetes. 2003; 52(3):726–33.
157. Lupi R, Del Prato S. β-cell apoptosis in type 2 diabetes: quantitative and functional consequences. Diabetes Metab. J. 2008; 34:S56-S64.
158. Mancini A, Imperlini E, Nigro E, Montagnese C, Daniele A, Orru S et al. Biological and nutritional properties of palm oil and palmitic acid: effects on health. Molecules. 2015; 20(9):17339–61.
159. Liu K, Czaja M. Regulation of lipid stores and metabolism by lipophagy. Cell Death Differ. 2013; 20(1):3–11.
160. Unger R, Zhou Y. Lipotoxicity of beta-cells in obesity and in other causes of fatty acid spillover. Diabetes. 2001; 50:118–21.

161. Ye G, Metreveil S, Donthi R, Xia S, Xu M, Carlson E et al. Catalase protects cardiomyocyte function in models of type 1 and type 2 diabetes. Diabetes. 2004; 53:1336–43.
162. Brookheart R, Michel C, Listenberger L, Ory D, Schaffer J. The non-coding RNA gadd7 is a regulator of lipid-induced oxidative and endoplasmic reticulum stress. J. Biol. Chem. 2009; 284(12):7446–54.
163. Efrat S, Linde S, Kofod H, Spector D, Delannoy M, Grant S et al. Beta-cell lines derived from transgenic mice expressing a hybrid insulin gene-oncogene. Proc. Natl. Acad. Sci. U.S.A. 1988; 85(23):9037–41.
164. D'Ambra R, Surana M, Efrat S, Starr R, Fleischer N. Regulation of insulin secretion from β-Cell lines derived from transgenic mice insulinomas resembles that of normal β-cells. Endocrinology. 1989; 126(6):2815–22.
165. Kozak J, Logothetis D. A calcium-dependent chloride current in insulin-secreting beta TC-3 cells. Pflugers. Arch. 1997; 433(6):679–90.
166. Ortlepp, Kluge, Giesen, Plum, Radke, Hanrath et al. A metabolic syndrome of hypertension, hyperinsulinaemia and hypercholesterolaemia in the New Zealand obese mouse. Eur.J Clin. Invest. 2000; 30(3):195–202.
167. Jurgens J. Hyperphagia, lower body temperature, and reduced running wheel activity precede development of morbid obesity in New Zealand obese mice. Physiol. Genomics. 2006; 25(2):234–41.
168. Brennan A, Mantzoros C. Drug insight: the role of leptin in human physiology and pathophysiology--emerging clinical applications. Nat. Rev. Endocrinol. 2006; 2(6):318–27.
169. Kharroub I, Ladriere L, Cardozo A, Dogusan Z, Cnop M, Eizirik D. Free fatty acids and cytokines induce pancreatic beta-cell apoptosis by different mechanisms: role of nuclear factor-kappaB and endoplasmic reticulum stress. Endocrinology. 2004; 145(11):5087–96.
170. Eizirik D, Cardozo A, Cnop M. The role for endoplasmic reticulum stress in diabetes mellitus. Endocr. Rev. 2008; 29(1):42–61.
171. Barlow J, Affourtit C. Novel insights into pancreatic beta-cell glucolipotoxicity from real-time functional analysis of mitochondrial energy metabolism in INS-1E insulinoma cells. Biochem. J. 2013; 456(3):417–26.
172. Morikawa S, Harada T. Immunohistochemical localization of catalase in mammalian tissues. J. Histochem. Cytochem. 1969:30–5.
173. Grant P, Ahlemeyer B, Karnati S, Berg T, Stelzig I, Nenicu A et al. The biogenesis protein PEX14 is an optimal marker for the identification and localization of peroxisomes in different cell types, tissues, and species in morphological studies. Histochem. Cell Biol. 2013; 140(4):423–42.
174. Colasante C, Chen J, Ahlemeyer B, Bonilla-Martinez R, Karnati S, Baumgart-Vogt E. New insights into the distribution, protein abundance and subcellular localisation of the endogenous peroxisomal biogenesis proteins PEX3 and PEX19 in different organs and cell types of the adult mouse. PLoS ONE. 2017; 12(8):1-35.
175. Crane D, Holmes R, Masters C. On the synthesis and incorporation of catalase and urate oxidase into the peroxisomes of mouse liver. Int. J. Biomed. Sci. 1983; 15:1429–37.
176. Björkman J, Gould S, Crane D. Pex13, the mouse ortholog of the human peroxisome biogenesis disorder PEX13 gene: gene structure, tissue expression, and localization of the protein to peroxisomes. Genomics. 2002; 79(2):162–8.
177. Nguyen T, Bjorkman J, Paton B, Crane D. Failure of microtubule-mediated peroxisome division and trafficking in disorders with reduced peroxisome abundance. J. Cell Sci. 2006; 119(Pt 4):636–45.
178. Choi S, Ik-Rak J, Lee Y, Lee S, Lee J, Kim Y et al. Stimulation of lipogenesis as well as fatty acid oxidation protects against palmitate-induced INS-1 beta-cell death. Endocrinology. 2011; 152(3):816–27.
179. Bradford M. A rapid and sensitive method for the quantitation of microgram quantities of protein utilizing the principle of protein-dye binding. Anal. Biochem. 1976; 72:248–54.
180. Marselli L, Thorne J, Ahn Y, Omer A, Sgroi D, Libermann T et al. Gene expression of purified beta-cell tissue obtained from human pancreas with laser capture microdissection. J. Clin. Endocrinol. Metab. 2008; 93(3):1046–53.
181. Krosting J, Latham G. AMBION, Inc.
182. Grabenbauer M, Fahimi H, Baumgart E. Detection of peroxisomal proteins and their mRNAs in serial sections of fetal and newborn mouse organs. J. Histochem. Cytochem. 2001; 49(2):155–64.
183. Karnati S, Baumgart-Vogt E. Peroxisomes in mouse and human lung: their involvement in pulmonary lipid metabolism. Histochem. Cell Biol. 2008; 130(4):719–40.
184. Nenicu A, Lüers G, Kovacs W, David M, Zimmer A, Bergmann M et al. Peroxisomes in human and mouse testis: differential expression of peroxisomal proteins in germ cells and distinct somatic cell types of the testis. Biol. Reprod. 2007; 77(6):1060–72.
185. Roderigo-Milne H, Hauge-Evans A, Persaud S, Jones P. Differential expression of insulin genes 1 and 2 in MIN6 cells and pseudoislets. Biochem. Biophys. Res. Commun. 2002; 296(3):589–95.

186. Müller C, Nguyen T, Ahlemeyer B, Meshram M, Santrampurwala N, Cao S et al. PEX13 deficiency in mouse brain as a model of Zellweger syndrome: abnormal cerebellum formation, reactive gliosis and oxidative stress. Dis. Model. Mech. 2011; 4(1):104–19.
187. Itoh Y, Kawamata Y, Harada M, Kobayashi M, Fuji R, Fukusumi S et al. Free fatty acids regulate insulin secretion from pancreatic beta cells through GPR40. Nature. 2003; 422(6928):173–6.
188. Roduit R, Nolan C, Alarcon C, Moore P, Barbeau A, Delghingaro-Augusto V et al. A Role for the Malonyl-CoA/Long-Chain Acyl-CoA Pathway of Lipid Signaling in the Regulation of Insulin Secretion in Response to Both Fuel and Nonfuel Stimuli. Diabetes. 2004; 53(4):1007–19.
189. El-Assaad W, Buteau J, Peyot M, Nolan C, Roduit R, Hardy S et al. Saturated fatty acids synergize with elevated glucose to cause pancreatic beta-cell death. Endocrinology. 2003; 144(9):4154–63.
190. Maedler K, Spinas G, Dyntar D, Moritz W, Kaiser N, Donath M. Distinct effects of saturated and monounsaturated fatty acids on beta-cell turnover and function. Diabetes. 2001; 50:69–76.
191. Reddy J, Hashimoto T. Peroxisomal b-oxidation and peroxisome proliferator-activated receptor alpha: An adaptive metabolic system. Annu. Rev. Nutr. 2001; (21):193–230.
192. Gong J, Dong H, Jiang S, Wang D, Fang K, Yang D et al. Fenugreek lactone attenuates palmitate-induced apoptosis and dysfunction in pancreatic beta-cells. World J. Gastroenterol. 2015; 21(48):13457–65.
193. Poitout V. Glucolipotoxicity of the pancreatic beta-cell: myth or reality? Biochem. Soc. Trans. 2008; 36(5):901–4.
194. Graciano M, Valle M, Kowluru A, Curi R, Carpinelli A. Regulation of insulin secretion and reactive oxygen species production by free fatty acids in pancreatic islets. Islets. 2014; 3(5):213–23.
195. Lenzen S, Drinkgern J, Tiedge M. Low antioxidant enzyme gene expression in pancreatic islets compared with various other mouse tissues. Free Radic. Biol. Med. 1996; 20(3):463–6.
196. Gosmain Y, Katz L, Heddad M, Cheyssac C, Poisson C, Philippe J. Pax6 is crucial for beta-cell function, insulin biosynthesis, and glucose-induced insulin secretion. Mol. Endocrin. 2012; 26(4):696–709.
197. Iype T, Francis J, Garmey J, Schisler J, Nesher R, Weir G et al. Mechanism of insulin gene regulation by the pancreatic transcription factor Pdx-1. J. Biol. Chem. 2005;280(17):16798–807.
198. Góth L, Vitai M. The effects of hydrogen peroxide promoted by homocysteine and inherited catalase deficiency on human hypocatalasemic patients. Free Radic. Biol. Med. 2003; 35(8):882–8.
199. Giordano C, Terlecky S. Peroxisomes, cell senescence, and rates of aging. Biochem. Biophys. Acta. 2012; 1822(9):1358–62.
200. Kunau W, Dommes V, Schulz H. β-Oxidation of fatty acids in mitochondria, peroxisomes, and bacteria: A century of continued progress. Prog. Lipid. Res. 1995; 34(4):267–342.
201. Tiedge M, Lortz S, Drinkgern J, Lenzen S. Relation between antioxidant enzyme gene expression and antioxidative defense status of insulin-producing cells. Diabetes. 1997; 46(11):1733–42.
202. Evans J, Newton R, Ruta D, MacDonald T, Morris A. Socio-economic status, obesity and prevalence of Type 1 and Type 2 diabetes mellitus. Diabet. Med. 2000; 17(6):478–80.
203. Aschner P. New IDF clinical practice recommendations for managing type 2 diabetes in primary care. Diab. Res. Clin. Pract. 2017; 132:169–70.
204. Beier K, Völkl A, Fahimi H. The impact of aging on enzyme proteins of rat liver peroxisomes: quantitative analysis by immunoblotting and immunoelectron microscopy. Virchows Arch. B. Cell Pathol. Incl. Mol. Pathol. 1993; 63(3):139–46.
205. Legakis J, Koepke J, Jedeszko C, Barlaskar F, Terlecky L, Edwards H et al. Peroxisome senescence in human fibroblasts. Mol. Biol. Cell. 2002; 13(12):4243–55.
206. Purdue E, Lazarow P. Targeting of human catalase to peroxisomes is dependent upon a novel COOH-terminal peroxisomal targeting sequence. J. Cell Biol. 1996; 134(4):849–62.
207. Koepke J, Nakrieko K, Wood C, Boucher K, Terlecky L, Walton P, Terlecky S. Restoration of peroxisomal catalase import in a model of human cellular aging. Traffic. 2007; 8(11):1590–600.
208. Murakami K, Ichinohe Y, Koike M, Sasaoka N, Iemura S, Natsume T et al. VCP Is an integral component of a novel feedback mechanism that controls intracellular localization of catalase and H_2O_2 Levels. PLoS ONE. 2013; 8(2):1–7.
209. Goth L, Eaton J. Hereditary catalase deficiencies and increased risk of diabetes. Lancet. 2000; 356(9244):1820–1.
210. Hagen T, Yowe D, Bartholomew J, Wehr C, Do K, Park J et al. Mitochondrial decay in hepatocytes from old rats: Membrane potential declines, heterogeneity and oxidants increase. Proc. Natl. Acad. Sci. U.S.A. 1997; 94:3064–9.

211. Walton PA, Brees C, Lismont C, Apanasets O, Fransen M. The peroxisomal import receptor PEX5 functions as a stress sensor, retaining catalase in the cytosol in times of oxidative stress. Biochem. Biophys. Acta. 2017; 1864(10):1833–43.
212. Apanasets O, Grou CP, Van Veldhoven, Paul P., Brees C, Wang B, Nordgren M et al. PEX5, the shuttling import receptor for peroxisomal matrix proteins, is a redox-sensitive protein. Traffic. 2014; 15(1):94–103.
213. Houten S, Denis S, Argmann C, Jia Y, Ferdinandusse S, Reddy J et al. Peroxisomal L-bifunctional enzyme (Ehhadh) is essential for the production of medium-chain dicarboxylic acids. J. Lipid Res. 2012; 53(7):1296–303.
214. Ding J, Loizides-Mangold U, Rando G, Zoete V, Michielin O, Reddy J et al. The peroxisomal enzyme L-PBE is required to prevent the dietary toxicity of medium-chain fatty acids. Cell Rep. 2013; 5(1):248–58.
215. Kahn S. The relative contributions of insulin resistance and beta-cell dysfunction to the pathophysiology of Type 2 diabetes. Diabetologia. 2003; 46(1):3–19.
216. Kim J, Yoon K. Glucolipotoxicity in pancreatic beta-cells. Diabetes Metab. J. 2011; 35(5):444–50.
217. Farfari S, Schulz V, Corkey B, Prentki M. Glucose-regulated anaplerosis and cataplerosis in pancreatic beta-cells. Diabetes. 2000; 49:718–26.
218. Roche E, Assimacopoulos F, Witters L, Perruchoud B, Yaney G, Corkey B et al. Induction by glucose of genes coding for glycolytic enzymes in a pancreatic beta-cell line (INS-1). J. Biol. Chem. 1997; 272(5):3091–8.
219. Federici M, Hribal M, Pergo L, Ranalli M, Caradonna Z, Prego C, et al. High Glucose Causes Apoptosis in Cultured Human Pancreatic Islets of Langerhans: a potential role for regulation of specific Bcl family genes toward an apoptotic cell death program. Diabetes. 2001;50(6):1290-301.
220. Maedler K, Spinas G, Lehmann R, Sergeev P, Weber M, Fontana A et al. Glucose induces beta-cell apoptosis via upregulation of the Fas receptor in human islets. Diabetes. 2001; 50(8):1683–90.
221. Maedler K, Fontana A, Ris F, Sergeev P, Toso C, Oberholzer J et al. FLIP switches Fas-mediated glucose signaling in human pancreatic beta cells from apoptosis to cell replication. Proc. Natl. Acad. Sci. U.S.A. 2002; 99(12):8236–41.
222. Maedler K, Sergeev P, Ris F, Oberholzer J, Joller-Jemelka H, Spinas G et al. Glucose-induced beta cell production of IL-1β contributes to glucotoxicity in human pancreatic islets. J. Clin. Invest. 2002; 110(6):851–60.
223. Efanova I, Zaitsev S, Zhivotovsky B, Köhler M, Efendié S, Orrenius S et al. Glucose and tolbutamide induce apoptosis in pancreatic beta cells. J. Biol. Chem. 1998;273(50):33501–7.
224. Borg J, Klint C, Wierup N, Ström K, Larsson S, Sundler F et al. Perilipin is present in islets of Langerhans and protects against lipotoxicity when overexpressed in the beta-cell line INS-1. Endocrinology. 2009; 150(7):3049–57.
225. Bollheimer L, Skelly R, Chester M, McGarry D, Rhodes C. Chronic exposure to free fatty acid reduces pancreatic beta cell insulin content by increasing basal insulin secretion that is not compensated for by a corresponding increase in proinsulin biosynthesis translation. J. Clin. Invest. 1998; 101(5):1094–101.
226. Kelpe C, Moore P, Parazzoli S, Wicksteed B, Rhodes C, Poitout V. Palmitate inhibition of insulin gene expression is mediated at the transcriptional level via ceramide synthesis. J. Biol. Chem. 2003; 278(32):30015–21.
227. Zhou Y, Grill V. Long-term exposure of rat pancreatic islets to fatty acids inhibits glucose-induced insulin secretion and biosynthesis through a glucose fatty acid cycle. J. Clin. Invest. 1994; 93(2):870–6.
228. Lupi R, Dotta F, Marselli L, Del Guerra S, Masini M, Santangelo C, Patané G et al. Prolonged exposure to free fatty acids has cytostatic and pro-apoptotic effects on human pancreatic islets: Evidence that beta-cell death is caspase mediated, partially dependent on ceramide pathway, and Bcl-2 regulated. Diabetes. 2002; 51:1437–42.
229. Piro S, Anello M, Di Pietro C, Lizzio M, Patane G, Rabuazzo A et al. Chronic exposure to free fatty acids or high glucose induces apoptosis in rat pancreatic islets: possible role of oxidative stress. Metabolism 2002; 51(10):1340–7.
230. Unger R, Zhou Y. Lipotoxicity of beta cells in obesity and in other causes of fatty acid spillover. Diabetes. 2001;50(1):118–21.
231. Prentki M, Nolan C. Islet beta cell failure in type 2 diabetes. J. Clin. Invest. 2006; 116(7):1802–12.
232. Amery C, Nattrass M. Fatty acids and insulin secretion. Diabetes Obes. Metab. 2000; 2(4):213–21.
233. Nolan C, Leahy J, Delghingaro-Augusto V, Moibi J, Soni K, Peyot M et al. Beta cell compensation for insulin resistance in Zucker fatty rats: increased lipolysis and fatty acid signalling. Diabetologia. 2006; 49(9):2120–30.

234. Briaud I, Harmon J, Kelpe C, Segu V, Poitout V. Lipotoxicity of the pancreatic beta-cell is associated with glucose-dependent esterification of fatty acids into neutral lipids. Diabetes. 2001; 50(2):315–21.
235. Briaud I, Kelpe C, Johnson L, Tran P, Poitout V. Differential effects of hyperlipidemia on insulin secretion in islets of langerhans from hyperglycemic versus normoglycemic rats. Diabetes. 2002; 51(3):662–8.
236. Maestre I, Jordán J, Calvo S, Reig J, Cena V, Soria B et al. Mitochondrial dysfunction is involved in apoptosis induced by serum withdrawal and fatty acids in the beta-cell line INS-1. Endocrinology. 2003; 144(1):335–45.
237. Sol E, Sargsyan E, Akusjärvi G, Bergsten P. Glucolipotoxicity in INS-1E cells is counteracted by carnitine palmitoyltransferase 1 over-expression. Biochem. Biophys. Res. Commun. 2008; 375(4):517–21.
238. Shimabukuro M, Zhou Y, Lee Y, Unger R. Troglitazone Lowers Islet Fat and Restores Beta Cell Function of Zucker Diabetic Fatty Rats. J. Biol. Chem. 1998; 237(6).
239. Kraegen E, Saha A, Preston E, Wilks D, Hoy A, Cooney G et al. Increased malonyl-CoA and diacylglycerol content and reduced AMPK activity accompany insulin resistance induced by glucose infusion in muscle and liver of rats. Am. J. Physiol. Endocrinol. Metab. 2006; 290(3):471–9.
240. Roche E, Farfari S, Witters L, Assimacopoulos F, Thumelin S, Brun T et al. Long-term exposure of beta-INS cells to high glucose concentrations increases anaplerosis, lipogenesis, and lipogenic gene expression. Diabetes. 1998; 47(7):1086–94.
241. Tong L. Acetyl-coenzyme A carboxylase: crucial metabolic enzyme and attractive target for drug discovery. Cell. Mol. Life Sci. 2005; 62(16):1784–803.
242. Knebel B, Hartwig S, Haas J, Lehr S, Goeddeke S, Susanto F et al. Peroxisomes compensate hepatic lipid overflow in mice with fatty liver. Biochim. Biophys. Acta. 2015; 1851(7):965–76.
243. Unger R, Orci L. Lipoapoptosis: its mechanism and its diseases. Biochim. Biophys. Acta. 2002; 1585(2-3):202–12.
244. Gwiazda K, Yang T, Lin Y, Johnson J. Effects of palmitate on ER and cytosolic Ca2+ homeostasis in beta-cells. Am. J. Physiol. 2009; 296(4):690–701.
245. Johnson J. Proteomic identification of carboxypeptidase E connects lipid-induced beta-cell apoptosis and dysfunction in type 2 diabetes. Cell cycle. 2009; 8(1):38–42.
246. Karaskov E, Scott C, Zhang L, Teodoro T, Ravazzola M, Volchuk A. Chronic palmitate but not oleate exposure induces endoplasmic reticulum stress, which may contribute to INS-1 pancreatic beta-cell apoptosis. Endocrinology. 2006; 147(7):3398–407.
247. Yuan H, Zhang X, Huang X, Lu Y, Tang W, Man Y et al. NADPH oxidase 2-derived reactive oxygen species mediate FFAs-induced dysfunction and apoptosis of beta-cells via JNK, p38 MAPK and p53 pathways. PLoS ONE. 2010; 5(12):1–9.
248. Ricchi M, Odoardi M, Carulli L, Anzivino C, Ballestri S, Pinetti A et al. Differential effect of oleic and palmitic acid on lipid accumulation and apoptosis in cultured hepatocytes. J. Gastroenterol. Hepatol. 2009; 24(5):830–40.
249. del Río L. Peroxisomes and their key role in cellular signaling and metabolism. Springer Netherlands; 2013. (vol 69).
250. Helleman K, Kerckhofs K, Hannaert J, Martens G, Van Veldhoven P, Pipeleers D. Peroxisome proliferator-activated receptor alpha-retinoid X receptor agonists induce beta-cell protection against palmitate toxicity. FEBS J. 2007; 274(23):6094–105.
251. MacBrinn M, O´Brien S. Lipid composition of the nervous system in Refsum´s disease. J. Lipid Res. 1968; 9:552–61.
252. Schönfeld P, Reiser G. Rotenone-like action of the branched-chain phytanic acid induces oxidative stress in mitochondria. J. Biol. Chem. 2006; 281(11):7136–42.
253. Ronicke S, Kruska N, Kahlert S, Reiser G. The influence of the branched-chain fatty acids pristanic acid and Refsum disease-associated phytanic acid on mitochondrial functions and calcium regulation of hippocampal neurons, astrocytes, and oligodendrocytes. Neurobiol. Dis. 2009; 36(2):401–10.
254. Kahlert S, Schönfeld P, Reiser G. The Refsum disease marker phytanic acid, a branched chain fatty acid, affects Ca2+ homeostasis and mitochondria, and reduces cell viability in rat hippocampal astrocytes. Neurobiol. Dis. 2005; 18(1):110–8.
255. Listenberger L, Ory D, Schaffer J. Palmitate-induced apoptosis can occur through a ceramide-independent pathway. J. Biol. Chem. 2001; 276(18):14890–5.
256. Michalska M, Wolf G, Walther R, Newsholme P. Effects of pharmacological inhibition of NADPH oxidase or iNOS on pro-inflammatory cytokine, palmitic acid or H_2O_2-induced mouse islet or clonal pancreatic beta-cell dysfunction. Biosci. Rep. 2010; 30(6):445–53.
257. Kroemer G, Reed J. Mitochondrial control of cell death. Nat. Med. 2000; 6(5):513–9.

258. Phyllis L, Hatten F, Hatten M. Targeted deletion of the PEX2 peroxisome assembly gene in mice provides a model for Zellweger syndrome, a human neuronal migration disorder. J. Cell Biol. 1997; 139(5):1293–12305.
259. Xu B, Moritz J, Epstein P. Overexpression of catalase provides partial protection to transgenic mouse beta cells. Free Radic. Biol. Med. 1999; 27(7-8):830–7.
260. Tordjman K, Standley K, Bernal-Mizrachi C, Leone T, Coleman T, Kelly D et al. PPAR alpha suppresses insulin secretion and induces UCP2 in insulinoma cells. J. Lipid Res. 2002; 43:936–43.
261. Hellemans K, Hannaert J, Denys B, Steffensen K, Raemdonck C, Martens G et al. Susceptibility of pancreatic beta cells to fatty acids is regulated by LXR/PPARalpha-dependent stearoyl-coenzyme A desaturase. PLoS ONE. 2009; 4(9):1–14.
262. Listenberger L, Han X, Lewis S, Cases S, Farese R, Ory D et al. Triglyceride accumulation protects against fatty acid-induced lipotoxicity. Proc. Natl. Acad. Sci. 2003; 100(6):3077–82.
263. Wanten J, Naber A. Cellular and physiological effects of medium-chain triglycerides. Mini Rev. Med. Chem. 2004; 4(8):847–57.
264. Lalloyer F, Vandewalle B, Percevault F, Torpier G, Kerr-Conte J, Oosterveer M et al. Peroxisome proliferator-activated receptor alpha improves pancreatic adaptation to insulin resistance in obese mice and reduces lipotoxicity in human islets. Diabetes 2006; 55(6):1605–13.
265. Koh E et al. Peroxisome Proliferator–Activated Receptor (PPAR)-alpha Activation Prevents Diabetes in OLETF Rats. Diabetes. 2003;52(9)2331-7.
266. Heim M, Johnson J, Boess F, Bendik I, Weber P, Hunziker W et al. Phytanic acid, a natural peroxisome proliferator-activated receptor (PPAR) agonist, regulates glucose metabolism in rat primary hepatocytes. FASEB J. 2002; 16(7):718–20.
267. Gloerich J, Van den Brink D, Ruiter J, van Vlies N, Vaz F, Wanders R et al. Metabolism of phytol to phytanic acid in the mouse, and the role of PPARalpha in its regulation. J. Lipid Res. 2007; 48(1):77–85.
268. Ashibe B, Hirai T, Kigashi Kyoichiro, Sekimizu K, Motojima K. Dual subcellular localization in the endoplasmic reticulum and peroxisomes and a vital role in protecting against oxidative stress of fatty aldehyde dehydrogenase are achieved by alternative splicing. J. Biol. Chem. 2007; 282(28):20763–73.
269. Medina-Gomez G, Gray SL, Yetukuri L, Shimomura K, Virtue S, Campbell M et al. PPAR gamma 2 prevents lipotoxicity by controlling adipose tissue expandability and peripheral lipid metabolism. PLoS Genet. 2007; 3(4):634-474.
270. Braissant O, Foufelle F, Scotto C, Dauca M, Wahli W. Differential expression of peroxisome proliferator-activated receptors (PPARs): tissue distribution of PPAR-alpha, -beta, and -gamma in the adult rat. Endocrinology. 1996; 137(1):354–66.
271. Dubois M, Pattou F, Kerr-Conte J, Gmyr V, Vandewalle B, Desreumaux P et al. Expression of peroxisome proliferator-activated receptor gamma (PPARgamma) in normal human pancreatic islet cells. Diabetologia. 2000; 43(9):1165–9.
272. Ravnskjaer K, Frigerio F, Boergesen M, Nielsen T, Maechler P, Mandrup S. PPARdelta is a fatty acid sensor that enhances mitochondrial oxidation in insulin-secreting cells and protects against fatty acid-induced dysfunction. J. Lipid Res. 2010; 51(6):1370–9.
273. Tugwood J, Aldridge T, Lambe K, Macdonald N, Woodyatt N. Peroxisome proliferator-activated receptors: structures and function. Ann. N.Y. Acad. Sci. 1996; 804:252–65.
274. Finkel T. Oxidant signals and oxidative stress. Curr. Opin. Cell Biol. 2003; 15(2):247–54.
275. Zielonka J, Kalyanaraman B. Hydroethidine- and MitoSOX-derived red fluorescence is not a reliable indicator of intracellular superoxide formation: another inconvenient truth. Free Radic. Biol. Med. 2010; 48(8):983–1001.
276. Morgan M, Liu Z. Crosstalk of reactive oxygen species and NF-kappaB signaling. Cell Res. 2011; 21(1):103–15.
277. Sundaresan M, Yu Z, Ferrans V, Irani K, Finkel T. Requirement for generation of H2O2 for platelet-derived growth factor signal transduction. Science 1995; 270(5234):296–9.
278. Rao G. Hydrogen peroxide induces complex formation of SHC-Grb2-SOS with receptor tyrosine kinase and activates Ras and extracellular signal-regulated protein kinases group of mitogen-activated protein kinases. Oncogene. 1996; 13(4):713–9.
279. Pi J, Bai Y, Zhang Q, Wong V, Floering L, Daniel K et al. Reactive oxygen species as a signal in glucose-stimulated insulin secretion. Diabetes. 2007; 56(7):1783–91.
280. Reiser G, Schönfeld P, Kahlert S. Mechanism of toxicity of the branched-chain fatty acid phytanic acid, a marker of Refsum disease, in astrocytes involves mitochondrial impairment. Int. J. Devl. Neuroscience. 2006; 24(2-3):113–22.

281. Newsholme C, Haber E, Hirabara S, Rebelato E, Procopio J, Morgan D et al. Diabetes associated cell stress and dysfunction: role of mitochondrial and non-mitochondrial ROS production and activity. J. Physiol. 2007; 583(Pt 1):9–24.
282. Barbosa M, Sampaio I, Teodoro B, Sousa T, Zoppi C, Queiroz A et al. Hydrogen peroxide production regulates the mitochondrial function in insulin resistant muscle cells: effect of catalase overexpression. Biochim. Biophys. Acta. 2013; 1832(10):1591–604.
283. Glorieux C, Zamocky M, Sandoval J, Verrax J, Calderon P. Regulation of catalase expression in healthy and cancerous cells. Free Radic. Biol. Med. 2015; 87:84–97.
284. Park J, Kang D, Lee D, Bae S. Concerted action of p62 and Nrf2 protects cells from palmitic acid-induced lipotoxicity. Biochem. Biophys. Res. Commun. 2015; 466(1):131–7.
285. Venugopal R, Jaiswal A. Nrf2 and Nrf1 in association with Jun proteins regulate antioxidant response element-mediated expression and coordinated induction of genes encoding detoxifying enzymes. Oncogene. 1998; 17(24):3145–56.
286. Schönfeld P, Wojtczak L. Fatty acids as modulators of the cellular production of reactive oxigen species. Free Radic. Biol. Med. 2008; 45(3)231-41.
287. Morgan D, Oliveira-Emilio H, Keane D, Hirata A, Santos da Rocha M, Bordin S, et al. Glucose, palmitate and pro-inflammatory cytokines modulate production and activity of a phagocyte-like NADPH oxidase in rat pancreatic islets and a clonal beta cell line. Diabetologia. 2007; 50(2):359-69.
288. Gurgul E, Lortz S, Tiedge M, Jörns A, Lenzen S. Mitochondrial catalase overexpression protects insulin-producing cells against toxicity of reactive oxygen species and proinflammatory cytokines. Diabetes. 2004; 53(9):2271–80.
289. Lowell B, Shulman G. Mitochondrial dysfunction and type 2 diabetes. Science. 2005; 307(5708):384–7.
290. Starkov A. The role of mitochondria in reactive oxygen species metabolism and signaling. Ann. N.Y. Acad. Sci. 2008; 1147:37–52.
291. Henequin J. Triggering and Amplifying Pathways of Regulation of Insulin Secretion by Glucose. Diabetes. 2000; 49:1751–60.
292. Masiello P, Novelli M, Bombara M, Fierabracci V, Vittorini S, Prentki M et al. The antilipolytic agent 3,5-dimethylpyrazole inhibits insulin release in response to both nutrient secretagogues and cyclic adenosine monophosphate agonists in isolated rat islets. Metabolism. 2002; 51(1):110–4.
293. Mulder H, Yang S, Sörhede M, Holm C, Ahrén B. Inhibition of lipase activity and lipolysis in rat islets reduces insulin secretion. Diabetes. 2004; 53:112–28.
294. Lee C, Sund N, Vatamaniuk M, Matschinsky F, Stoffers D, Kaestner K. Foxa2 controls Pdx1 gene expression in pancreatic beta-cells in vivo. Diabetes. 2002; 51(8):2546–51.
295. Zhang C, Moriguchi T, Kajihara M, Esaki R, Harada A, Shimohata H et al. MafA is a key regulator of glucose-stimulated insulin secretion. Mol. Cell. Biol. 2005; 25(12):4969–76.
296. Gao T, McKenna B, Li C, Reichert M, Nguyen J, Singh T et al. Pdx1 maintains beta cell identity and function by repressing an alpha cell program. Cell Metab. 2014; 19(2):259–71.
297. Mitchell R, Nguyen M, Chabosseau P, Callingham R, Pullen T, Cheung R et al. The transcription factor Pax6 is required for pancreatic beta cell identity, glucose-regulated ATP synthesis and Ca2+ dynamics in adult mice. J. Biol. Chem. 2017; 292(21):8892-8906.
298. Swisa A, Glaser B, Dor Y. Metabolic stress and compromised identity of pancreatic beta cells. Front. Genet. 2017; 8:1–11.
299. Moore P, Ugas M, Hagman D, Parazzoli S, Poitout V. Evidence against the involvement of oxidative stress in fatty acid inhibition of insulin secretion. Diabetes. 2004; 53:2610–6.
300. Xiao J, Gregersen S, Pedersen S, Hermansen K. Differential impact of acute and chronic lipotoxicity on gene expression in INS-1 cells. Metabolism. 2002; 51(2):155–62.
301. Hagman D, Hays L, Parazzoil S, Poitout V. Palmitate inhibits insulin gene expression by altering Pdx-1 nuclear localization and reducing MafA expression in isolated rat islets of Langerhans. J. Biol. Chem. 2005; 280(37):32413–8.
302. Brun T, Scarcia P, Li N, Gaudet P, Duhamel D, Palmieri F et al. Changes in mitochondrial carriers exhibit stress-specific signatures in INS-1Eβ-cells exposed to glucose versus fatty acids. PLoS ONE. 2013; 8(12):1–13.
303. Samaras S, Cissell M, Gerrish K, Wright C, Gannon M, Stein R. Conserved Sequences in a Tissue-Specific Regulatory Region of the pdx-1 Gene Mediate Transcription in Pancreatic Cells: Role for Hepatocyte Nuclear Factor 3 and Pax6. Mol. Cell. Biol. 2002; 22(13):4702–13.

APENDIX

X. Techniques used for catalase over-expression in *E.coli* and antibody generation

X. 1. Preparation of chemocompetent DH5α bacteria

DH5α cells were streaked out on a LB plate without antibiotics and incubated overnight at 37°C. Two clones were selected the next day and grown overnight in a 5 ml culture in fresh LB medium. Subsequently, the culture was diluted 1:20 into 50 ml of LB medium and shaken at 300 rpm and 37°C in an incubator shaker until the solution reached an OD_{600} of 0.45-0.5. Thereafter, the culture was incubated on ice for 5 min. All subsequent steps were carried out at 4°C and under sterile conditions. The cells were harvested by centrifugation for 15 min at 3,000 x *g* in a pre-cooled centrifuge. After removing the supernatant, the cell pellet was resuspended in chilled TfbI buffer in 40 % of the culture original volume. Later, the cells were incubated on ice for 10 min and centrifuged again at 3,000 x *g* for 15 min. Following the removal of the supernatant, the pellet was resuspended in 4 ml TfbII cold buffer and incubated on ice for 15 min more. Finally, 50 µl aliquots of the competent cells were immediately frozen using a dry ice chamber and stored at -80°C.

X.2. Transformation of competent DH5α cells for plasmid replication and preparation of agarose LB-ampicillin plates

A 50 µl aliquot of frozen competent cells was thawed on ice and then gently mixed with 100 ng plasmid DNA. After 20 min incubation on ice, the bacteria were heat shocked in a water bath for 90 s at 42°C and transferred back on ice for 2 min. Thereafter, 200 µl of LB medium without antibiotics were added and the cells were allowed to grow in a 37°C incubator for 30 min. Finally, the transformation was spread onto a 10 cm LB agar plate containing ampicillin and incubated overnight at 37°C.

For the preparation of agarose LB-ampicillin plates, 500 ml Agar-LB solution was microwaved at 350 W until dissolved and then allowed to cool to 50°C for 1 h in a water bath. The process of preparing the plates was carried out in a fume hood keeping the area sterile. Ampicillin (100 µg / ml) was then added to the solution and mixed. Subsequently ~20 ml of Agar-LB solution was slowly poured into 10 cm polystyrene Petri dishes. After cooling the plates for 30-60 min until solidified, they were stored inverted and sealed with parafilm at 4°C.

X.3. Isolation of plasmid DNA

X.3.1. Mini preparation for DNA isolation

After transformation, one single clone was selected from the LB/ampicillin-agar plates to inoculate 3 ml of LB medium containing ampicillin (50 μg/ml). The bacterial culture was incubated at 37°C with constant shaking (300 rpm) overnight. The next day 1 ml of the saturated DH5α cells culture was harvested by centrifugation for 30 s at 11,000 x *g*. The supernatant was discarded, and the pellet resuspended in 250 µl Buffer A1 (NucleoSpin plasmid QuickPure). After vortexing, 250 µl Buffer A2 was added, gently mixed and incubated at RT for 5 min. After the addition of 300 µl Buffer A3 the sample was centrifuged again for 5 min at 11,000 x *g* at RT. Once the supernatant appeared clear, 750 µl were transferred onto a NucleoSpin plasmid column and centrifuged for 1 min at 11,000 x *g* to bind the DNA to the matrix. The previous step was repeated with the remaining lysate. Thereafter, the silica membrane was washed and centrifuged (1 min at 11,000 x *g*) first with 500 µl prewarmed Buffer AW (50°C) and then with 600 µl Buffer A4 at RT. The flow-through was discarded and the column was centrifuged for 2 min at 11,000 x *g*. Finally, the DNA was eluted with 50 µl Buffer AE after 1 min incubation at RT followed by 1 min centrifugation at 11,000 x *g*.

X.3.2. Midi preparation for DNA isolation

After bacterial transformation, a starter culture was prepared inoculating a 3 ml culture of LB medium containing ampicillin with a single clone picked from a freshly streaked LB/ampicillin-agar plate. The culture was shaken at 37°C and 300 rpm for 8 h. To provide enough plasmid DNA for purification, a large culture was set up diluting the pre-culture 1:1,000 into 200 ml of LB medium containing ampicillin (50 μg/ml). The culture was allowed to grow overnight at 37°C. The bacteria were then harvested by centrifugation at 6,000 x *g* for 15 min at 4°C. The OD_{600} allowed the determination of the right culture volume to be used for the isolation as follows: Volume (ml) = $800/OD_{600}$. After centrifugation, the cell pellet was resuspended in 8 ml Resuspension Buffer (RES) containing RNase A (NucleoBond Xtra MidiEF). Thereafter, 16 ml of Buffer LYS was added to the suspension and mixed by inverting the tube 5 times to lysate the cells. The mixture was incubated at RT for 5 min. Subsequently, 16 ml of Buffer NEU was added and the lysate was gently mixed. The precipitate formed in the last step was removed by centrifugation at 10,000 x *g* for 20 min at 4°C. The resulting cleared lysate was then loaded onto a pre-equilibrated NucleoBond

Xtra Column. For equilibration, 12 ml Buffer EQU were applied onto the rim of the column filter and then allowed to empty by gravity flow. The loading of the column was followed by two washing steps, the first one with 15 ml Buffer EQU and after the removal of the column filter the second one with 25 ml Buffer WASH. Finally, the plasmid DNA was eluted with 15 ml prewarmed Buffer ELU (50°C), precipitated with 10.5 ml isopropanol at RT, and centrifuged at 10,000 x *g* for 30 min at 4°C. The DNA pellet was washed with 70 % ethanol and centrifuged at 10,000 x *g* for 5 min at RT. The pellet was allowed to air dry for 5 min after the complete removal of ethanol and subsequently resuspended in 200 µl TE buffer.

X.3.3. DNA quantification

The purity and concentration of the DNA was measured using a NanoDrop 2000 spectrophotometer (Thermo Scientific). The A_{260}/A_{280} ratio was ~1.8 and the $A_{260}/_{230}$ ratio was higher than 2.0-2.2. Both ratios are accepted as a measurement for DNA purity.

X.4. Catalase coding sequence amplification by polymerase chain reaction (PCR)

The bacterial plasmid cloning vector pCMV-Sport 6 containing the full-length open reading frame (ORF) encoding for mouse catalase was used as a template to amplify the coding region of catalase via PCR in order to add the restriction sites to both 3´and 5´ends of the piece of DNA. The amplification was carried out using self-designed gene-specific cloning primers containing the restriction enzymes sites for Sac I / Hind III or Nde I / Nde I. Three nucleotides were added upstream of the restriction sites to improve restriction enzymes cleaving and cutting efficiency.

The reaction mix was set using 1-5 ng of template DNA, 1 µl forward primer (equivalent to 100 pmol), 1 µl reverse primer (100 pmol), 5 µl of 10x PCR reaction buffer, 1 µl of 10 mM dNTPs mix (0.2 mM) and 1 U of Taq DNA polymerase. The reaction mix was adjusted with dH_2O to a final volume of 50 µl.

Table X.1.: Primers used for the amplification of catalase open reading frame (ORF).
The restriction sites for Sac I / Hind III and Nde I / Nde I were added (indicated in bold letters)

Name	Sequence (5´→3´)	Laboratory storage no.
MmCAT-Sac I (forward)	ATA**GAGCTC**ATGTCGGACAGTCGGGACCCAGC	AZ53
MmCAT-Hind III (reverse)	ATA**AAGCTT**TTACAGGTTAGCTTTTCCCTTC	AZ54
MmCAT-Nde I (forward)	ATA**CATATG**TCGGACAGTCGGGACCCAGCCAG	BA43
MmCAT-Nde I (reverse)	ATA**CATATG**TTACAGGTTAGCTTTTCCCTTC	AZ56

The PCR reaction was carried out in a Bio-Rad iCycler C1000 using the following parameters: initial denaturation at 95°C for 1 min, followed by 30 cycles of denaturation at 95°C for 30 s, annealing at 60°C for 30 s, extension at 72°C for 30 s, and a final extension at 72°C for 7 min.

X.5. Purification of DNA fragments from agarose gels

Fragments of DNA that were separated by 1 % agarose gel electrophoresis were excise with a clean scalpel and weighed. The PCR products were then purified using a QIAquick Gel Extraction kit. Three volumes of Buffer QG were added to 1 volume of gel (300 µl /100 mg) and incubated at 50°C for 10 min until the gel slice was completely dissolved. During the incubation time the sample was vortexed every 2 min. Subsequently, 100 µl of isopropanol were added to the sample, mixed and loaded onto a QIAquick spin column. To bind the DNA to the column, the last one was centrifuged twice, each time for 1 min at 9,600 x *g* discarding the flow-through in between. Thereafter, 750 µl Buffer PE were added to wash the column and then centrifuged for 1 min at 9,600 x *g*. After discarding the flow-through, the column was allowed to stand 5 min and it was centrifuged again for 1 min at 17,900 x *g* in order to remove residual wash buffer. The DNA was eluted in 30 µl Buffer EB and applied directly into the center of the membrane with 2 subsequent centrifugation steps (1 min, 17,900 x *g*, RT).

X.6. Subcloning of the catalase constructs into pGEM-T Easy vector

To improve the efficiency of ligation of the catalase constructs into the expression plasmids, *Cat*-Sac I / Hind III and *Cat*-Nde I / Nde I were sub-cloned into the pGEM-T Easy vector (Promega). The sub-cloning helped to prevent recircularization of the vector and provided a compatible overhang for the catalase-PCR products.

A molar ratio of 1:5 (vector: insert) was used to set up the reaction on ice as follows: 5 µl of 2x rapid ligation buffer, 1 µl of pGEM-T Easy vector (equivalent to 50 ng), 5 µl of insert DNA (PCR product) and 1 µl of DNA ligase. The reaction was incubated overnight at 16°C.

X.6.1. Restriction digestion of plasmid DNA

After selecting the adequate restriction enzymes (Sac I / Hind III or Nde I / Nde I) a double digestion of the expression vectors or the Cat-pGEM-T Easy vector construct was carried out. The appropriate buffer used in the reaction was determined according to the compatibility with both enzymes (or in the case of Pet16b, just for Nde I). The restriction digestion reaction was set on ice as follows: 5 µg of DNA, 1 µl of each restriction enzyme

(equivalent to 5 U), 3 µl of 10x Buffer and adjusted with dH_2O to a final volume of 50 µl. The reaction was incubated for 3 h at 37°C. The results were visualized by agarose gel electrophoresis and the digested vectors were then extracted and purified.

X.7. Dephosphorylation of 5´overhangs from Pet16b after Nde I / Nde I digestion

In the case of Pet16b a single restriction enzyme (Nde I) was used to digest the vector, therefore the hydrolysis of 5´-phosphate groups from the DNA was needed to prevent re-circularization and re-ligation of the vector during cloning. Calf intestinal alkaline phosphatase (CIAP) was used to remove the phosphate groups from both 5´-termini. The purified Pet16b DNA was resuspended in 40 µl of Tris-HCl (10 mM, pH 8.0) and incubated at 37°C for 30 min. The reaction was set up as follows: 40 µl of DNA (equivalent to maximum 10 pmol of 5´-ends), 5 µl of CIAP 10x reaction buffer and 2.5 µl of diluted CIAP (0.01 U/µl). After adding another 2.5 µl of diluted CIAP, the solution was incubated at 37°C for an additional 30 min. Finally, 300 µl of CIAP stop buffer were added prior to sample purification.

X.8. DNA ligation

To clone both catalase inserts into the compatible expression vector backbone (pTrcHis A or Pet16b), a ligation reaction was set on ice using a T4 DNA ligase as follows: 20-40 ng of vector DNA, 5 µl of insert DNA, 2 µl of 10x ligation buffer, 1 µl of T4 DNA ligase (equivalent to 4 U) and adjusted to a final volume of 20 µl using dH_2O. The reaction was incubated at 16°C overnight.

X.9. Blue-white screening

To identify correctly generated recombinant plasmids, the ligation reaction was transformed into competent DH5α cells. One hundred µl of transformants were then spread onto an X-Gal (5-bromo-4-chloro-indolyl-β-galactopyranoside) plate. Previously, 100 µl LB medium, 40 µl X-Gal and 20 µl IPTG (isopropyl β-D-1-thiogalactopyranoside) were spread onto an LB/ampicillin agar plate and allowed to dry in a laminar flow chamber before use. The cells were incubated overnight at 37°C. The next day the recombinant cells in the white colonies were selected for PCR and agarose gel electrophoresis screening.

X.10. Catalase expression

The plasmid constructs were transformed into BL21(DE3) Rosetta (Novagen) competent cells, plated on LB/ampicillin agar plates and incubated overnight at 37°C. The next day a single clone was selected and resuspended in 5 ml LB medium supplemented with 100 µg/ml ampicillin to produce a starter culture. Subsequently, the overnight culture was used to inoculate 50 ml of fresh LB medium supplemented with ampicillin at a 1:50 dilution. The culture was incubated at 37°C with shaking until OD_{600} reached 0.45. The catalase expression was then induced by the addition of IPTG to a final concentration of 1 mM. After induction, the culture was maintained at 20°C with constant shaking (300 rpm) for a period of 250 min. Finally, the bacteria were harvested by centrifugation at 20,000 x *g* for 1 min. The bacterial pellet was stored at 20°C until catalase isolation.

X.11. Catalase affinity purification via His-Tag isolation

The isolation of the recombinant catalase after its expression was carried out using the Dynabeads His-Tag isolation & pulldown system (Life Technologies). To prepare a cell lysate, the bacterial pellet expressing histidine-tagged catalase was resuspended in Lysate buffer (4 ml/bacterial pellet from 50 ml culture) containing lysozyme (to increase the lysis efficiency) and incubated on ice for 30 min. The lysates were subsequently disrupted and homogenized using five 10 s pulses (10 s in between pulses) with a probe sonicator. Samples were kept in an ice bath all the time. Cell debris were removed by centrifugation at 5,000 x g for 10 min at 4°C. Two mg Dynabeads were added to the lysate supernatant after bead equilibration and incubated at 4°C for 1 h on a roller. After magnet attraction, the supernatant was discarded and the beads were washed 4 times with 1 ml cold binding/washing buffer discarding the supernatant in between. Subsequently the protein was eluted adding 1.5 ml elution buffer to the beads and incubating the suspension on a roller for 1 h at 4°C. Finally, the beads were resuspended in 1.5 ml binding/washing buffer and were stored at -20°C as well as the suspension containing isolated catalase.

X.12. Chicken antibody (IgY) purification

X.12.1. Precipitation of IgY

The egg yolk was diluted 1:5 (v/v) with dH_2O and frozen at -20°C overnight. The next day the diluted egg yolk was allowed to thaw at RT and then frozen for a second time at -20°C overnight. After thawing, the aggregated egg yolk granules were sedimented by

centrifugation at 13,500 x *g* for 5 min at 4°C. The water-soluble fraction was then collected to precipitate the IgY and 0.67 volume of saturated ammonium sulfate solution (pH 7.5) was slowly added. After centrifugation at 10,000 x *g* for 5 min at 4°C the supernatant was discarded and the pellet dissolved in 1/10 volume dH_2O. Thereafter, 0.67 volume of saturated ammonium sulfate solution was added and the mixture centrifuged (10,000 x *g* for 5 min). The pellet was dissolved in dH_2O and dialyzed in PBS (see below).

X.12.2. Dialysis of IgY sample

To remove the ammonium sulfate from the IgY sample after precipitation, a dialysis procedure using PBS as a dialysate was performed. A Fisherbrand regenerated cellulose tubing was placed for 30 min in dH_2O to remove storage solutions and rinsed. The sample was carefully loaded into a one-end closed dialysis tube. After removing the air from the tube, it was completely closed and placed in a beaker filled with PBS (100 times the sample volume). The sample was dialyzed at 4°C for 2 h under constant movement and then the dialysate was changed. Subsequently, the sample was allowed to dialyze overnight at 4°C. The next day the dialysate was changed again and after 2 more h of dialysis the antibody was removed, aliquoted and stored at -20°C.

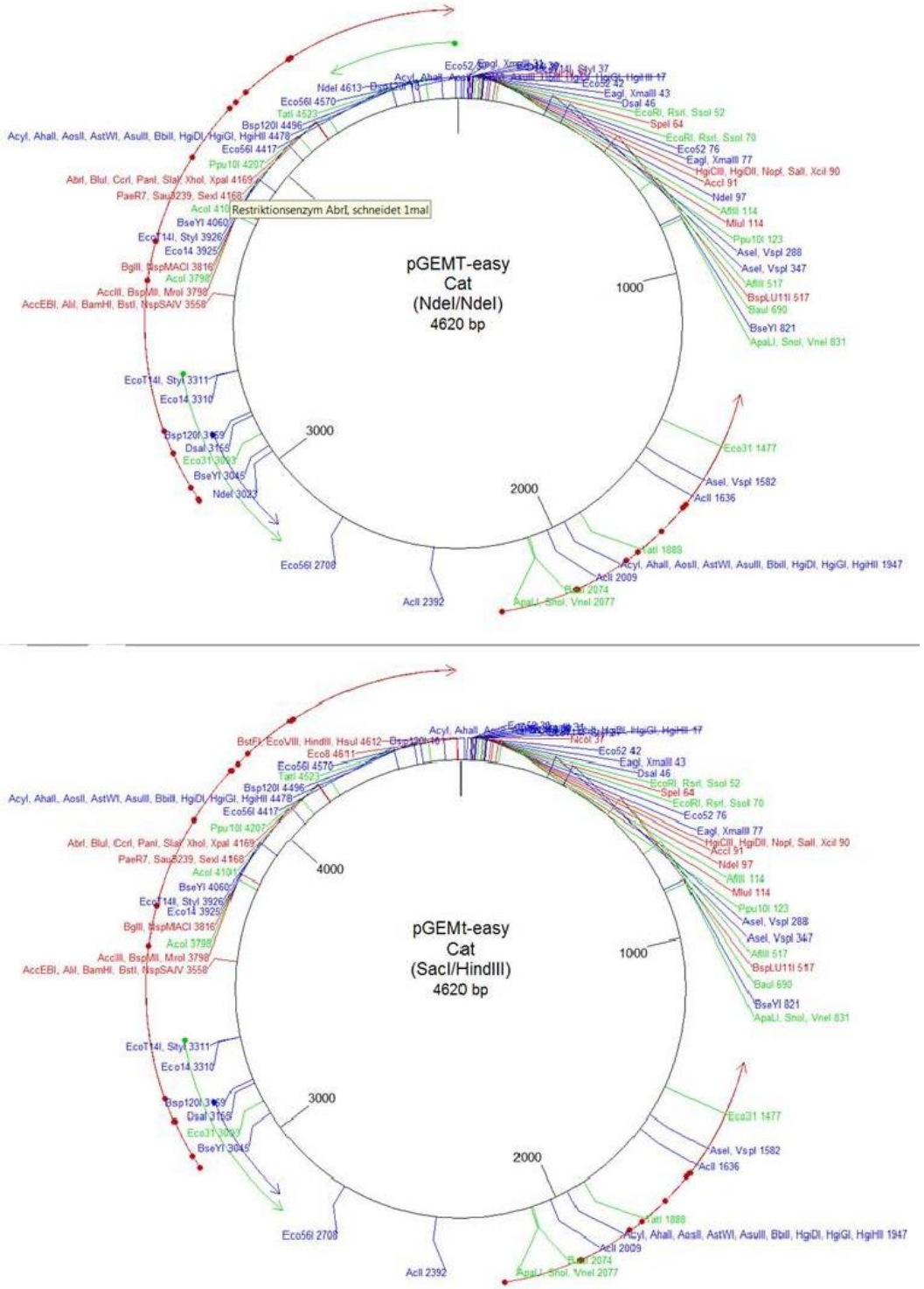

Figure: X.1. Construct maps of catalase containing Sac I/Hind III or Nde I/Nde I restriction enzymes sites sub-cloned into the pGEM-T Easy vector

Acknowledgments

Firstly, I would like to express my deepest gratitude to Prof. Dr. Baumgart-Vogt for having placed her confidence in me, for her continuous advice and encouragement through the course of this PhD, her patience, and knowledge, which led us to interesting discussions. I am very grateful for her support and help, not only with issues related to this work but also on a personal level.

A very special thank goes to my postdoc and dear friend, Dr. Claudia Colasante, who offered her unconditional and continuous advice and encouragement during all these years. I thank her for her guidance and great effort, that she put into training me in the scientific field, for all the countless laughs and tears and unforgettable hours we spent having fun together.

My sincere thanks also go to Dr. Barbara Ahlemeyer for being always open to any question and for her constructive and valuable recommendations.

I would also like to extend my thanks to Andrea Textor, Susanne Pfreimer, Bianca Pfeiffer, Petra Hahn-Kohlberger, Elke Rodenberg Frank and Silvia Heller for their patience, technical support, and knowledge so kindly offered during all this time. Was a pleasure to work side by side constantly learning in the coziest and at the same time professional atmosphere.

Last but not the least, I would like to express the profound gratitude to my beloved parents, whose love and guidance are with me even when they are so far away. Most importantly, I wish to thank my loving and supportive husband, Sascha, who with patience and humor helps me every day to find the way. And finally, to Elizabeth, who provides me with sleepless nights but also with immense satisfactions.